To the Graduate Council:

I am submitting herewith a thesis written by John A. Henning entitled "Transformation and Postweld Heat Treatment Cracking in Modified Chromium-Molybdenum Steels." I have examined the final copy of this thesis for form and content and recommend that it be accepted in partial fulfillment of the requirements for the degree of Master of Science, with a major in Metallurgical Engineering.

Carl D. Lundin, Major Professor

We have read this thesis
and recommend its acceptance:

E. E. Stansbury

L. C. Cuthrell

Accepted for the Council:

Vice Provost
and Dean of The Graduate School

STATEMENT OF PERMISSION TO USE

In presenting this thesis in partial fulfillment of the requirements for a Master's degree at The University of Tennessee, Knoxville, I agree that the Library shall make it available to borrowers under rules of the Library. Brief quotations from this thesis are allowable without special permission, provided that accurate acknowledgement of the source is made.

Permission for extensive quotation from or reproduction of this thesis may be granted by my major professor, or in his absence, by the Head of Interlibrary Services when, in the opinion of either, the proposed use of the material is for scholarly purposes. Any copying or use of the material in this thesis for financial gain shall not be allowed without my written permission.

Signature John A. Kenney

Date May 30, 1986

TRANSFORMATION AND POSTWELD HEAT TREATMENT CRACKING IN MODIFIED CHROMIUM-MOLYBDENUM STEELS

A Thesis

Presented for the

Master of Science

Degree

The University of Tennessee, Knoxville

John A. Henning

June 1986

DEDICATION

This thesis is dedicated to

Erna Bertha Whilhelmina Luebke

whose love, strength and faith was unbounded

ACKNOWLEDGEMENTS

This thesis and the work that made it possible could not have been accomplished without the continued effort, support and dedication of the author's advisor, Dr. Carl Lundin. Sincere appreciation is also extended to the committee members, Dr. E. E. Stansbury and Dr. D. A. Canonico.

The financial support provided through research grants from the Advanced Research and Technology Development Fossil Energy Materials Program, Oak Ridge National Laboratory is gratefully acknowledged.

The assistance of the staff of the Metallurgical Laboratory of Combustion Engineering, Chattanooga, Tennessee in providing chemical analyses and for use of the library facilities which have been used extensively in the preparation of this thesis are gratefully acknowledged.

Last, but not least, the author sincerely appreciates the help and initial guidence of Mr. Mark Richey and the support of his fellow graduate students.

ABSTRACT

This research program was undertaken to evaluate the postweld heat treatment cracking susceptibility of the new generation of Cr-Mo steels for pressure vessel applications. Mechanical testing was performed to determine the relative susceptibility of the modified alloys in comparison with standard, unmodified materials. Extensive optical, scanning electron and transmission electron microscopy were utilized to evaluate the role of carbide morphology on susceptibility to cracking. The kinetics of carbide formation and the effect of residual elements on cracking susceptibility were related to alloy composition.

The test methods were varied to investigate the effects of postweld heat treatment temperature and restraint (externally applied) on cracking susceptibility. Stress rupture testing of the Gleeble simulated heat affected zone and an adaptation of the C-ring test (normally employed for stress-corrosion cracking evaluation) which included an actual weld and notch in the coarse grained heat affected zone were employed to evaluate susceptibility to cracking. The Gleeble was also employed to determine the continuous cooling transformation behavior of the coarse grained heat affected zone under simulated welding conditions.

The literature review provides a concise historical review, an overview of the theoretical aspects, and a thorough discussion of the effects of composition on post weld heat treatment cracking. This

investigation has brought together and clarified many of the individual aspects previously investigated by other researchers.

The continuous cooling transformation determinations for the coarse grained heat affected region in the 9Cr-1Mo-V-Nb materials showed that the primary microstructural constituents were martensite and auto tempered martensite although the Timken alloy, with a chromium equivalent of 13.4, also exhibited some delta ferrite. The minor variations in chemical composition had no observable effect on the M_s or M_f temperatures which were in substantial agreement with those obtained under standard continuous cooling transformation conditions.

The continuous cooling transformation investigation of the coarse grained heat affected region in the modified 3Cr-Mo and 2 1/4Cr-1Mo materials showed that the microstructures were cooling rate dependent but were similar for all materials tested. With rapid cooling (low energy inputs), the microstructures consisted of martensite and auto-tempered martensite. With intermediate cooling rates, the microstructures consisted of auto-tempered martensite and lower bainite. With the slowest cooling conditions (highest energy input) the on-cooling microstructure consisted of lower bainite and granular bainite. The transformation temperatures were depressed approximately 45F° (25C°) below those determined for standard continuous cooling transformation diagrams.

Gleeble simulation of the weld thermal cycle and postweld heat treatment of the 9Cr-1Mo-V-Nb alloys resulted in significantly lower rupture ductilities than were observed in unmodified 9Cr-1Mo. The

lower rupture ductility of the modified alloys may be related to increased matrix strengthening as a result of precipitation of fine V/Nb carbo-nitrides, nucleation of $M_{23}C_6$ on the V/Nb carbo-nitrides in a fine dispersed form and a reduction in the rate of growth of $M_{23}C_6$ due to a lowering of chromium mobility by vanadium. Grain boundary embrittlement due to phosphorous segregation may be the primary factor in the relatively low rupture ductility of the Sumitomo heat. However, the macroscopic and microscopic ductility of the 9Cr-1Mo-V-Nb alloys is considered sufficient to preclude postweld heat treatment cracking as a problem in fabrication.

Gleeble simulation testing and C-ring testing of the modified 3Cr-Mo and 2 1/4Cr-1Mo materials for postweld heat treatment cracking showed that the vanadium modified alloys are susceptible to postweld heat treatment cracking while the Berkeley alloy with 0.5% Ni and no additional carbide forming elements was not susceptible to postweld heat treatment cracking. Transmission electron microscopy coupled with convergent beam diffraction techniques and energy dispersive X-ray analysis on carbide extraction replicas showed the carbide evolution in the vanadium modified alloys to be retarded in comparison to the Berkeley alloy. The retarded evolution of the grain boundary carbides is probably accompanied by a concomitant slow growth of M_2C type carbides in the grain matrix. Slower growth of the M_2C type carbides in the matrix will be associated with longer times of coherency and matrix strengthening resulting in greater susceptibility to cracking. The transmission electron microscopy examination showed a greater volume fraction of matrix precipitates

in the vanadium modified alloys and the scanning electron microscopy examination showed the carbides to be coarser in the Berkeley alloy thus supporting the hypothesis of slower development of the matrix carbides in the vanadium modified alloys.

Indirect evidence indicates that the low rupture ductility of AMAX (Climax) 3Cr-1 1/2Mo-0.1V alloy in comparison to the other vanadium modified materials is the result of grain boundary embrittlement by phosphorous. The high phosphorous content (0.012%) combined with the relatively high silicon content (0.26%), which tends to promote phosphorous segregation by enhancing Mo_2C formation, form the basis for this assessment.

Experimental evidence employing Gleeble simulation has been obtained to demonstrate that superposition of a grain refining thermal cycle on a grain coarsening thermal cycle improves the rupture ductility of the vanadium modified materials from less than 5% to more than 12% which results in substantial resistance to cracking. Pragmatically, this suggests that welding techniques which result in refinement of the coarse grained heat affected zone may prevent postweld heat treatment cracking in highly susceptible materials.

The modified C-ring test, which incorporates all the factors for an ideal test to evaluate postweld heat treatment cracking, appears to be a valid, simple test for determining susceptibility to cracking. Substantial agreement was obtained between the results of the C-ring test and those obtained by the commonly employed stress-rupture testing performed on the Gleeble. In particular the

C-ring test and Gleeble simulation test both predict that the vanadium modified materials will be susceptible to cracking while the Berkeley 3Cr-1 1/2Mo-1/2Ni and stamdard 2 1/4Cr-1Mo-0.10C materials will not be susceptible.

TABLE OF CONTENTS

CHAPTER		PAGE
I.	INTRODUCTION	1
II.	LITERATURE REVIEW	4
	Phase transformations	4
	Postweld heat treatment cracking	18
III.	MATERIALS	56
IV.	EXPERIMENTAL PROCEDURES	65
	Phase transformations	66
	Postweld heat treatment cracking	70
V.	RESULTS AND DISCUSSION	80
	Transformation behavior	80
	Postweld heat treatment cracking behavior	115
VI.	CONCLUSIONS	191
VII.	FUTURE WORK	200
LIST OF REFERENCES		202
VITA		214

LIST OF TABLES

TABLE		PAGE
1.	As received material condition	62
2.	Chemical compositions of materials studied	64
3.	Summary of the on-heating transformation temperatures for the 9Cr-1Mo-V-Nb alloys.	83
4.	Summary of the on-cooling transformation temperatures for the 9Cr-1Mo-V-Nb alloys.	83
5.	Summary of the on-heating transformation temperatures for the modified 3Cr and 2 1/4Cr alloys.	96
6.	Summary of the on-cooling transformation temperatures for the modified 3Cr and 2 1/4Cr alloys.	97
7.	Stress-rupture parameter and stress rupture index for the modified 3Cr and 2 1/4Cr alloys.	130
8.	Carbide analysis for the modified 3Cr and 2 1/4Cr alloys; Gleeble simulated PWHT at 1250°F (680°C) for 100 minutes	158
9.	Weld parameters and heat input utilized in C-ring specimen preparation.	167
10.	PWHT cracking results for the C-ring test.	171

LIST OF FIGURES

FIGURE PAGE

1. Schematic diagram of the various regions of the HAZ approximately corresponding to the 0.15w/o carbon indicated on the $Fe-Fe_3C$ equilibrium diagram 6

2. CCT diagram for 2 1/4Cr-1Mo. 7

3. CCT diagram for 2 1/4Cr-1Mo under simulated welding conditions 8

4. Continuous cooling transformation diagrams for V-Ti-B-modified 2 1/4Cr-1Mo steel and standard 2 1/4Cr-1Mo steel. . 10

5. CCT diagrams of a 3Cr-1Mo and a 3Cr-1Mo-1/4V-Ti-B steels . . 11

6. CCT diagram for commercial heat of 3Cr-1.5Mo steel (Heat A9394) Austenite grain size: ASTM No. 5/6. 12

7. CCT diagram of heat XA 3619, 9Cr-1Mo-0.2V-0.1Nb steel. Austenite grain size: ASTM No. 9 13

8. Effect of chromium on the critical restraint stress, $\sigma_{AW-crit}$. 29

9. Contour lines of critical restraint stress ($\sigma_{AW-crit}$) shown on the Cr-Mo content diagram 30

10. Comparison between the critical restraint stress ($\sigma_{AW-crit}$) and cracking sensitivity indexes, P_{SR} and ΔG. . 32

11. Carbides present in Cr-Mo steels tempered at 600°C for 24 hours. 34

12. Weight fraction of M_2C shown on the $\sigma_{AW-crit}$ diagram. . . . 35

13. Hot hardness and hardness at room temperature versus tempering temperature. 36

14. Schematic representation of demonstrating Tamaki's mechanism of reheat cracking 38

15. Block diagram showing factors involved in stress relief cracking 55

16. Schematic representation of dilatometric output for the determination of transformation temperatures 68

17. Thermal cycles employed in the determination of transformation temperations for welding conditions 69

18. Groove geometry for 1/8" (3.2mm) shielded metal arc electrodes 74

19. Successive steps in the making of C-rings specimens. 77

20. NKK 9Cr-1Mo-V-Nb CCT specimen, 18KJ/in. Modified Wazu's etch, OLM 200X 85

21. NKK 9Cr-1Mo-V-Nb CCT specimen, 150KJ/in. Modified Wazu's etch, OLM 200X 85

22. Sumitomo 9Cr-1Mo-V-Nb CCT specimen, 18KJ/in. Modified Wazu's etch, OLM 200X 86

23. Sumitomo 9Cr-1Mo-V-Nb CCT specimen, 150KJ/in. Modified Wazu's etch, OLM 200X 86

24. Timken 9Cr-1Mo-V-Nb CCT specimen, 18KJ/in. Modified Wazu's etch, OLM 200X 87

25. Timken 9Cr-1Mo-V-Nb CCT specimen 150KJ/in. Modified Wazu's etch, OLM 200X 87

26. NKK 9Cr-1Mo-V-Nb CCT specimen, 150KJ/in. 88

27. Sumitomo 9Cr-1Mo-V-Nb CCT specimen, 150KJ/in 89

28. Timken 9Cr-1Mo-V-Nb CCT Specimen, 150KJ/in 90

29. Timken 9Cr-1Mo-V-Nb CCT specimen, 150KJ/in. Modified Wazu's etch. SEM 10,000X. 91

30. CCT diagram for AMAX (climax) 3Cr-1 1/2Mo-0.1V, determined for welding conditions 98

31. CCT diagram for Berkeley composition 3Cr-1 1/2Mo-1/2Ni, determined for welding conditions. 99

32. CCT diagram for JSW 3Cr-1Mo-V-Ti-B, determined for welding conditions 100

33. CCT diagram for JSW 2 1/4Cr-1Mo-V-Ti-B, determined for welding conditions 101

34. JSW 3Cr-1Mo-V-Ti-B, CCT specimen, helium quenched. 105

35. JSW 3Cr-1Mo-V-Ti-B, CCT specimen, 35KJ/in. 106

36. JSW 3Cr-1Mo-V-Ti-B, CCT specimen 60KJ/in 107

37. JSW 3Cr-1Mo-V-Ti-B, CCT specimen, 150KJ/in 108

38. AMAX (Climax) 3Cr-1 1/2Mo-0.1V, CCT specimen, 60KJ/in. . . . 109

39. Berkeley 3Cr-1 1/2Mo-1/2Ni CCT Specimen, 60KJ/in 110

40. JSW 2 1/4Cr-1Mo-V-Ti-B, CCT specimen, 60KJ/in. 111

41. 9Cr-1Mo-V-Nb alloys' Gleeble stress-rupture behavior for simulated PWHT at 1350°F (732°C) 118

42. Fractograph of NKK 9Cr-1Mo-V-Nb. 121

43. Fractograph of Timken 9Cr-1Mo-V-Nb 121

44. Fractograph of Sumitomo 9Cr-1Mo-V-Nb 122

45. Modified 3Cr and 2 1/4Cr alloys' Gleeble stress-rupture behavior for simulated PWHT at 1250°F (680°C). 124

46. Modified 3Cr and 2 1/4Cr alloys' Gleeble stress-rupture behavior for simulated PWHT at 1150°F (620°C). 125

47. Fractograph of AMAX (Climax) 3Cr-1 1/2Mo-0.1V, 1250°F (680°C) PWHT 134

48. Fractograph of AMAX (Climax) 3Cr-1 1/2Mo-0.1V, 1150°F (620°C) PWHT 134

49. Fractograph of Berkeley 3Cr-1 1/2Mo-1/2Ni, 1250°F (680°C) PWHT 135

50. Fractograph of Berkeley 3Cr-1 1/2Mo-1/2Ni, 1150°F (620°C) PWHT 135

51. Fractograph of JSW 2 1/4Cr-1Mo-V-Ti-B, 1250°F (680°C) PWHT . 136

52. Fractograph of JSW 2 1/4Cr-1Mo-V-Ti-B, 1150°F (620°C) PWHT . 136

53. Fractographs of JSW 3Cr-1Mo-V-Ti-B, 1250°F (680°C) PWHT. . . 137

54. Fractographs of JSW 3Cr-1Mo-V-Ti-B, 1150°F (620°C) PWHT. . . 138

55. Fractographs of Berkeley 3Cr-1 1/2Mo-1/2Ni, 1150°F (620°C) PWHT. 64.2ksi (442MPa), 2.7 min. to fracture, 11% RA, a) SEM 500X, b) SEM 2000x. 141

56. Energy dispersive X-ray analysis (EDAX) of; a) inclusion, b) region A, c) region B vs. inclusion shown in Figure 58. . 142

57. Fractographs of JSW 3Cr-1Mo-V-Ti-B, 1250°F (680°C) PWHT. 34.6ksi (239MPa), 16.3 min. to fracture, 7.7%RA, a) SEM 2000X, b) EDAX of grain boundary particle, c) EDAX of area immediately adjacent to the particle 144

58. Fractographs of JSW 3Cr-1Mo-V-Ti-B, 1150°F (620°C) PWHT. 64.8ksi (446MPa), 8.6 min. to fracture, 1.8% RA, a) SEM 500X, b) SEM 1000X 145

59. EDAX analysis of grain boundary particles initiating cavitation in JSW 3Cr-1Mo-V-Ti-B (Figure 58) 146

60. AMAX (Climax) 3Cr-1 1/2Mo-0.1V Gleeble simulated PWHT cracking specimen, 1250°F (680°C) PWHT 148

61. Berkeley 3Cr-1 1/2Mo-1/2Ni Gleeble simulated PWHT cracking specimen, 1250°F (680°C) PWHT. 149

62. JSW 3Cr-1Mo-V-Ti-B Gleeble simulated PWHT cracking specimen, 1250°F (680°C) PWHT. 150

63. JSW 2 1/4Cr-1Mo-V-Ti-B Gleeble simulated PWHT cracking specimen, 1250°F (680°C) PWHT. 151

64. Transmission electron micrographs of AMAX (Climax) 3Cr-1 1/2Mo-0.1V, thermal cycled and PWHT at 1250°F (680°C) for 100 min. 154

65. Transmission electron micrographs of Berkeley 3Cr-1 1/2Mo-1/2Ni, thermal cycled and PWHT at 1250°F (680°C) for 100 min. 155

66. Transmission electron micrographs of JSW 3Cr-1Mo-V-Ti-B, thermal cycled and PWHT at 1250°F (680°C) for 100 min. . . . 156

67. Transmission electron micrographs of JSW 2 1/4Cr-1Mo-V-Ti-B, thermal cycled and PWHT at 1250°F (680°C) for 100 min. . . . 157

68. PWHT cracking results for the C-ring test. 170

69. AMAX (Climax) 3Cr-1 1/2Mo-0.1V C-ring specimen 177

70. JSW 3Cr-1Mo-V-Ti-B C-ring specimen 178

71. JSW 2 1/4Cr-1Mo-V-Ti-B C-ring specimen 179

72. Higher magnification fractograph of the JSW 2 1/4Cr-1Mo-V-Ti-B C-ring specimen 180

73. Grain boundary cavitation at the intergranular-cleavage fracture interface in the AMAX (Climax) 3Cr-1 1/2Mo-0.1V C-ring specimen. 180

74. Unequal, non-linear HAZ's as a result of welding in a C-ring specimen 182

75. Schematic of ideal notch placement and two sites of notch misplacement in the C-ring test specimen 182

76. Notch displaced into the fusion zone in a AMAX (Climax) 3Cr-1 1/2Mo-0.1V C-ring specimen 183

77. Notch displaced towards the fine grained HAZ in a JSW 2 1/4Cr-1Mo-V-Ti-B C-ring specimen 184

CHAPTER I

INTRODUCTION

Ferritic steels alloyed with chromium and molybdenum are utilized in applications where creep behavior or corrosion/oxidation resistance are necessary factors in materials selection. The principle use of these alloys has been in the power generation and process industries. With the advent of the nuclear power industry[1,2] and synfuels development programs[3,4] a world wide effort was initiated to develop materials with improved properties. Further, those industries historically using Cr-Mo alloys seek to employ higher operating temperatures and pressures or larger pressure vessels which would result in increased economy and efficiency.[5,6]

Development of modified alloys with 2 1/4%Cr and 3%Cr have had the following criteria of principal concern:

1. resistance to high temperature hydrogen attack,
2. minimum variation in hardenability with small changes in composition,
3. a broad range of tempering conditions which will result in a fine bainitic microstructure possessing both strength and toughness,
4. weldability must be as good as or superior to standard 2 1/4Cr-1Mo.[7]

In response to these criteria, Climax Molybdenum Company developed a 3Cr-1Mo-0.1V alloy,[8,9] the University of California-Berkeley

proposed a 3Cr-1 1/2Mo alloy with 0.5% Ni added,[10] Japan Steel Works (JSW) developed both 2 1/4Cr-1Mo and 3Cr-1Mo alloys with additions of 1/4% V, 0.02% Ti, and 0.002% B,[11] Nippon Kokan's modified 2 1/4Cr-1Mo and 3Cr-1Mo alloys have additions of 0.5% Ni, 0.3%V, 0.009% Ti and 0.007%B,[12] while Kawasaki's modified 3Cr-1Mo has additions of 0.02%Nb and 0.2%V.[13]

Development of the 9Cr alloys was undertaken to eliminate ferritic to austenitic transition joints, to utilize the increased corrosion resistance compared to 2 1/4Cr and 3Cr materials, to obtain increased resistance to stress-corrosion cracking in caustic and chloride environments compared to type 304 stainless steel, and to reduce the use of strategic materials compared to 304 stainless steel, in particular chromium. The principle criteria for alloy modification were to achieve creep properties that equalled or exceeded those of type 304 austenitic stainless steel up to 1100°F (590°C) and to maintain adequate weldability.[2] These criteria have been addressed by the development of a V-Nb modified 9Cr-1Mo at Oak Ridge National Laboratory (ORNL)[1] and by Sumitomo Metal Industries duplex, low C 9Cr-2Mo material.[14,15]

The use of these modified alloys for pressure vessel applications requires that they be approved in the appropriate codes and standards. (9Cr-1Mo-V-Nb has recently been approved for use by ASTM, A213-T91 for pipe and ASTM A387-Gr91 for plate.) Therefore the mechanical and fabrication properties must be fully documented. As can be seen from the foregoing criteria, weldability is a

significant factor in the acceptance of the these materials for use in pressure vessel fabrication.

Weldability has been defined as "the capacity of a material to be welded under fabrication conditions imposed into a specific, suitably designed structure and to perform satisfactorily in the intended service."[16] In practice, weldability is mainly associated with a materials resistance to various types of cracking.[17] In Cr-Mo steels susceptibility to postweld heat treatment cracking and hydrogen assisted cracking are most often considered.

Work undertaken in the following described research was primarily concerned with the evaluation of susceptibility to postweld heat treatment (stress-relief or reheat) cracking for the modified, enhanced properties, 9Cr-1Mo, 3Cr-Mo and 2 1/4Cr-1Mo alloys. Also, work performed to determine the heat affected zone transformation temperatures and microstructures is presented.

CHAPTER II

LITERATURE REVIEW

Phase Transformations

The metallurgical transformations that occur during welding affect the final microstructure and therefore influence many of the potential problems that may develop during and after welding. The coarse grained heat affected zone (HAZ) is the location of maximum susceptibility for postweld heat treatment (PWHT) cracking. It is also the primary region for hydrogen assisted cracking.

The discussion of hydrogen assisted cracking by Linnert[17] indicates that susceptibility increases with increasing hardness of the microstructure. Therefore a martensitic microstructure is more susceptible to hydrogen assisted cracking than a mixed martensitic-bainitic one which, in turn, is more susceptible than an entirely bainitic microstructure. Ito and Nakanishi[18] showed in a study of 1Cr-1/2Mo alloys that a HAZ microstructure consisting of martensite or lower bainite was more susceptible to PWHT cracking than upper bainite. In temper embrittlement, a related materials problem, it was found that a martensitic microstructure is more prone to a loss of ductility and toughness than a bainitic microstructure.[19,20] Thus, the determination of (HAZ) transformation characteristics is a first step in determining the weldability of a material and which may, in turn, provide the key to reducing or eliminating weld HAZ problems.

Easterling[21] has compared the microstructural regions of a weld with the equilibrium phase diagram (Figure 1). However, such a representation is overly simplistic in that it ignores major differences between the weld thermal cycle and the conditions that are utilized in establishing the equilibrium phase diagram. Welding can induce rapid heating (3000F°/sec) and cooling (500F°/sec) rates resulting in conditions far from equilibrium. Futhermore, complete homogenization, required for equilibrium, never exists during welding. Also equilibrium considerations do not include such non-equilibrium constituents such as martensite or bainite.

Many of the objections to the use of the equilibrium diagram to predict weld HAZ transformations also extend to the use of standard continuous cooling transformation diagrams. These diagrams are developed starting with homogeneous austenite. However, in welding the inhomogeneity occurs due to the inability of alloying elements to diffuse uniformly throughout the austinitic microstructure and the incomplete solution of carbides or nitrides as a result of the rapidity of the welding thermal cycle and the concommitant short austenitizing times. In order to accurately predict the on-cooling transformation temperatures and microstructures, weld HAZ continuous cooling transformation diagrams must be derived using the heating and cooling conditions attendent upon welding.[22,23,24]

Figure 2 shows a conventional continuous cooling transformation diagram for 2 1/4Cr-1Mo and Figure 3 illustrates a diagram determined under simulated welding conditions for the coarse grained HAZ in 2 1/4Cr-1Mo.[25] As may be seen by comparing Figures 2 and 3 the

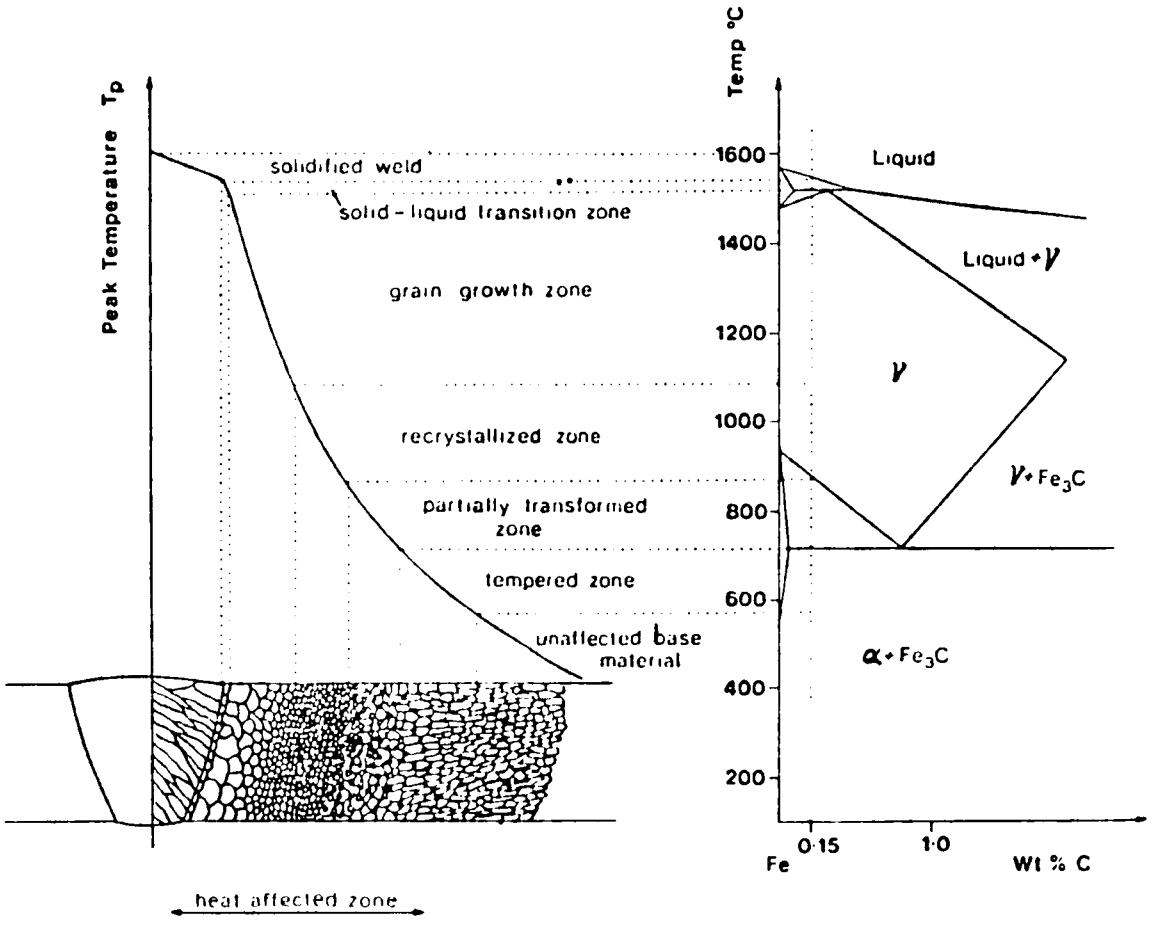


Figure 1. Schematic diagram of the various regions of the HAZ approximately corresponding to the 0.15w/o carbon indicated on the Fe-Fe_3C equilibrium diagram.

Source: Easterling, K., Introduction to the Physical Metallurgy of Welding, Butterworths, 1983.

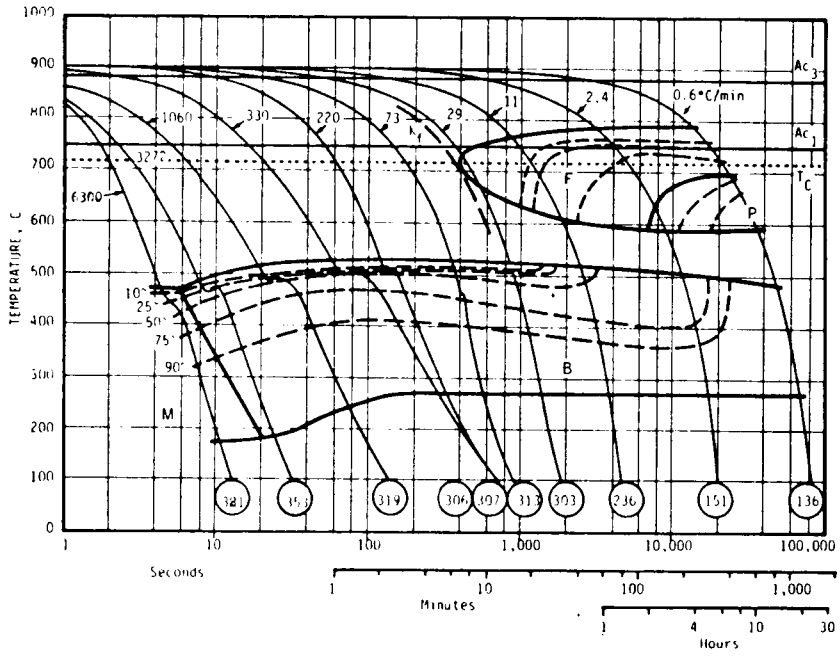


Figure 2. CCT diagram for 2 1/4Cr-1Mo.

Source: Wada, T. and Eldis, Transformation Characteristics of 2 1/4Cr-1Mo Steel, ASTM-STP 755, Applications of 2 1/4Cr-1Mo Steel for Thick Wall Pressure Vessels, Sengdohl and Semehysen, eds., American Society for Testing and Materials, Philadelphia, 1982.

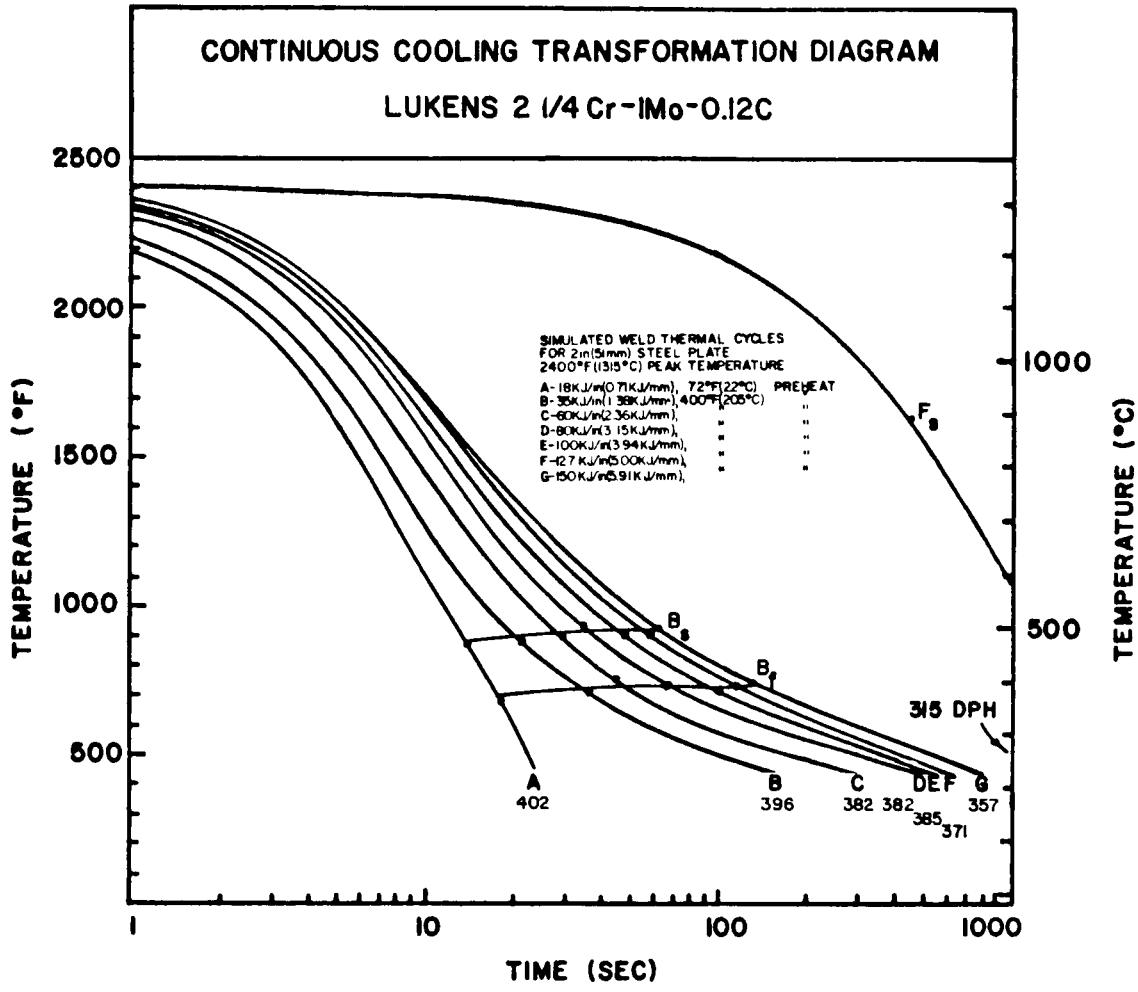


Figure 3. CCT diagram for 2 1/4Cr-1Mo under simulated welding conditions.

Source: Richey, M.W., The Weldability of Cr-Mo Steels for Fossil Energy Applications, M.S. Thesis - University of Tennessee, 1984.

depression of the on-cooling transformation temperatures (principally bainite), under welding conditions is approximately 90°F (50°C) due to the rapid heating and cooling rates and short austenitizing times.

The literature review by Richey[25] reveals that only a few continuous cooling transformation diagrams have been determined under welding conditions for the Cr-Mo materials. However, conventional continuous cooling transformation diagrams are available for many of the modified Cr-Mo alloys. Continuous cooling transformation diagrams for various Cr-Mo steels are shown in Figures 4, 5, 6, and 7. The effects of the additions of vanadium, titanium, and boron to the 2 1/4Cr-1Mo and 3Cr-1Mo alloys on the continuous cooling transformation behavior are shown in Figures 4 and 5 by the superposition of the continuous cooling transformation diagrams for the unmodified and modified materials.

The 2 1/4Cr and 3Cr continuous cooling transformation diagrams, Figures 4, 5 and 6, give clues to the fact that the resulting microstructures under various welding conditions may be complex. Depending on the degree of homogenization and cooling rate (related to the heat input and preheat for a given process and material thickness), the on-cooling transformation microstructures in the weld HAZ may consist of martensite, mixed martensite and bainite, or bainite coupled with retained austenite. However, the continuous cooling transformation diagram for the V-Nb modified 9Cr, Figure 7, indicates that the transformation microstructure will be primarily

	C	Si	Mn	P	S	Cr	Mo	V	Ti	B	Austenitizing Temperature
$2\frac{1}{4}$Cr-1Mo-V-Ti-B	10	.02	.51	.005	.005	2.20	.94	.30	.022	.0023	950°C (1742°F)
$2\frac{1}{4}$Cr-1Mo	10	.34	.48	.017	.013	2.16	.96	-	-	-	920°C (1688°F)

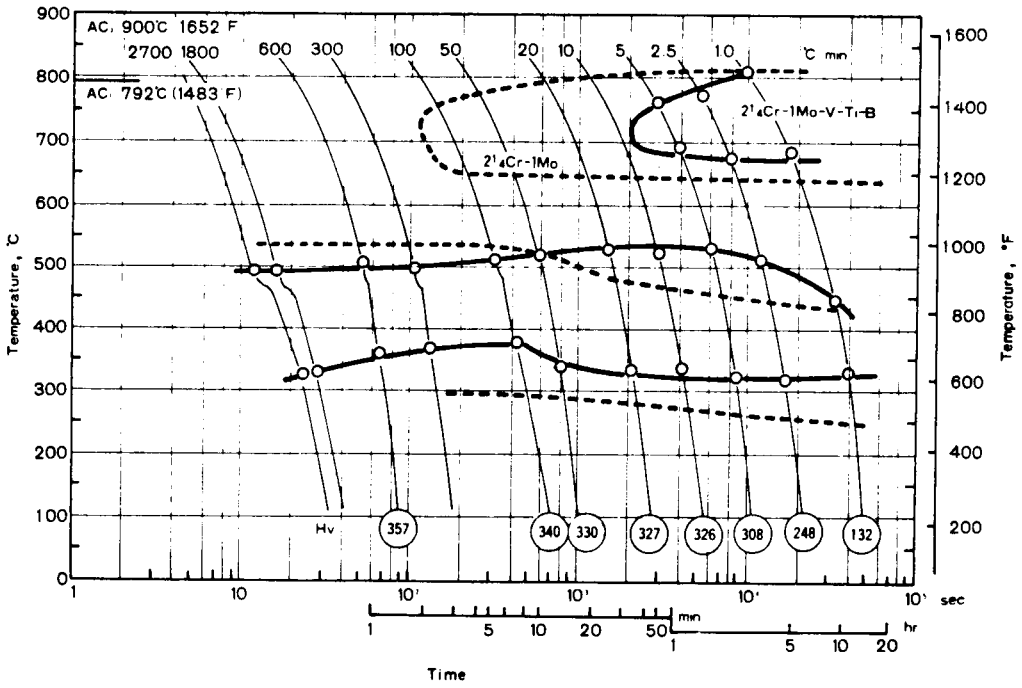


Figure 4. Continuous cooling transformation diagrams for V-Ti-B-modified 2 1/4Cr-1Mo steel and standard 2 1/4Cr-1Mo steel.

Source: T. Ishiguro, et al., A 2 1/4Cr-1Mo Pressure Vessel Steel with Improved Creep Rupture Strength, ASTM-STP 755, Application of 2 1/4Cr-1Mo Steel for Thick Wall Pressure Vessels, Sengdahl and Semechysen, eds., American Society for Testing and Materials, Philadelphia, 1982.

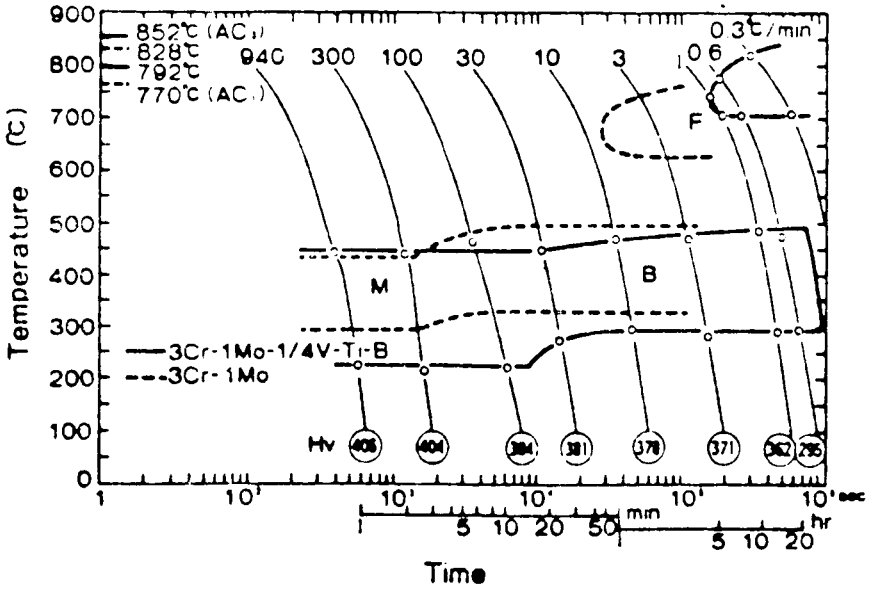


Figure 5. CCT diagrams of a 3Cr-1Mo and a 3Cr-1Mo-1/4V-Ti-B steels.

Source: Ishiguro, T., Murakawi, Y., Ohnishi, K. and Watanabe, J. A 2 1/4Cr-1Mo Pressure Vessel Steel with Improved Creep Rupture Strength, ASTM-STP 755, Application of 2 1/4Cr-1Mo Steel for Thick Wall Pressure Vessels, Sengdahl and Semechysen, eds., American Society for Testing and Materials, Philadelphia, 1982.

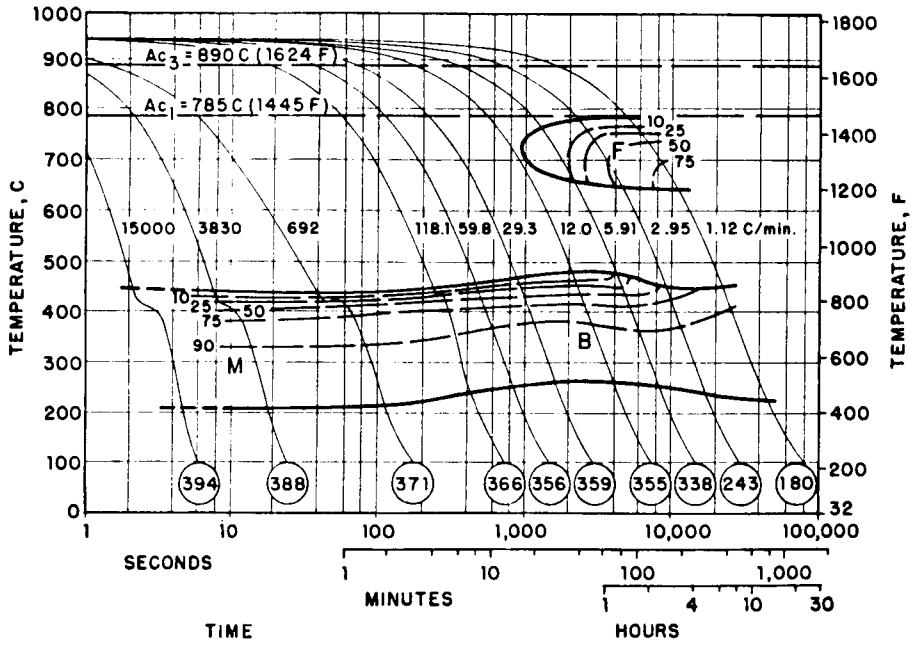


Figure 6. CCT diagram for commercial heat of 3Cr-1.5Mo steel (Heat A9394) Austenite grain size: ASTM No. 5/6.

Source: Wada, T. and Cox, T.B., A New 3Cr-1.5Mo Steel for Pressure Vessel Applications, MPC-21 Research on Chrome-Moly Steels, American Society of Mechanical Engineers, 1984, pp. 77-94.

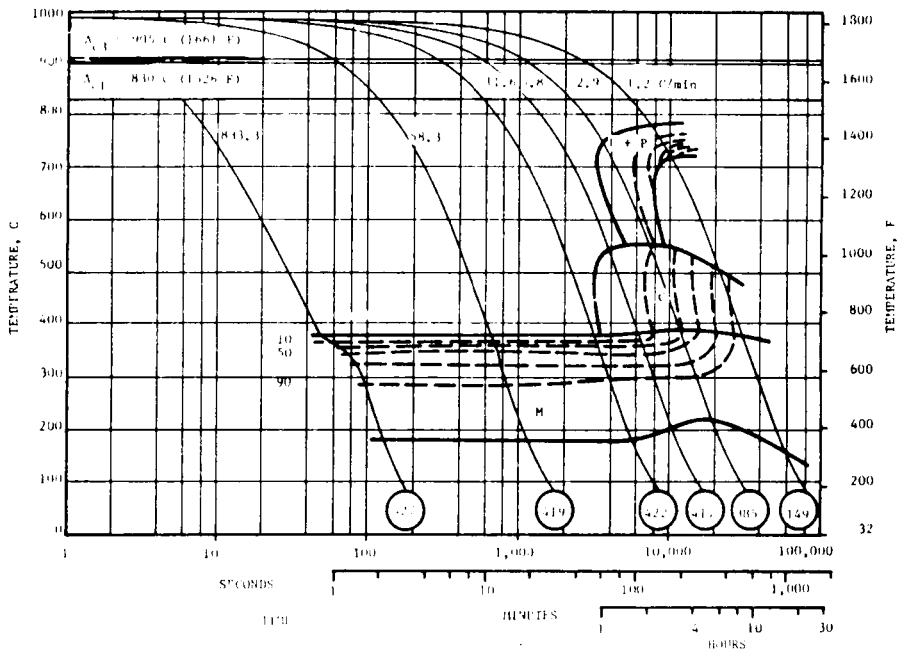


Figure 7. CCT diagram of heat XA 3619, 9Cr-1Mo-0.2V-0.1Nb steel. Austenite grain size: ASTM No. 9.

Source: Wada, T., Climax Molybdenum Company Report J-4617, Climax Molybdenum Company, 1980.

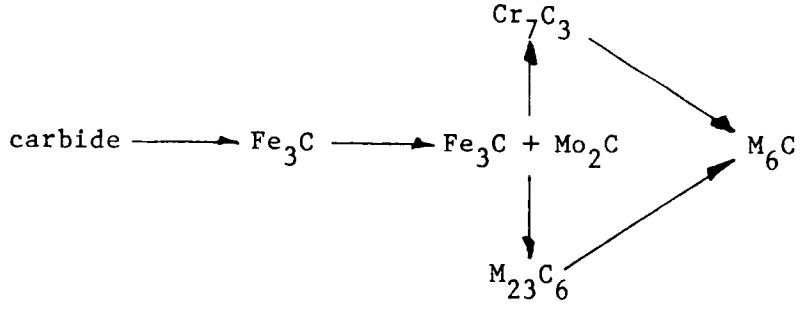
martensite, martensite + austenite, or martensite + austenite + carbide for cooling rates faster than 11C°/min. (20F°/min.) which is slower than that expected for the usual welding conditions employed in pressure vessel construction.

The microstructure of the 2 1/4Cr and 3Cr steels may be further complicated by the formation of martensite-austenite islands (a martensite-austenite constituent). The formation of a martensite-austenite constituent is due to the partitioning of carbon to the austenite during the bainite transformation reaction resulting in locking of dislocations which prevents the shear transformation from occurring[26] or the stabilization of the austenite.[27,28] The last austenite present can be highly enriched in carbon. Carbon contents of the martensite-austenite constituent have been reported by Biss and Cryderman[28] to exceed 0.5 wt%C in a nominal 0.15%C alloy and to be approximately 3 at%C (approximately 0.7 wt%C) in a series of 0.3%C-3Cr-0.5Mo as shown by Thomas et al.[28]

Biss and Cryderman[27] found that slow cooling rates enhanced formation of the martensite-austenite constituent by allowing carbon to diffuse away from the ferrite-austenite interface into the austenite. However rapid cooling rates resulted in higher ferrite-austenite interface carbon content due to carbon diffusion being slower than interface advancement. This results in enhanced cementite precipitation and suppression of the martensite-austenite constituent. Economopoulos and Habraken[26] found that the presence of the martensite-austenite constituent was associated particularly with massive, or granular, bainitic structures formed at slow cooling

rates. The cooling rate dependence of martensite-austenite constituent formation probably accounts for the inability of Richey[25] to detect any martensite-austenite constituent in his study of the transformation characteristics of 2 1/4Cr-1Mo steels under simulated welding conditions. However, it is to be noted that Thomas et al.[28] detected thin films of retained austenite along martensite laths by TEM examination. It was claimed that the retention of austenite was due to carbon redistribution during the martensite reaction and that this diffusion of C was possible due to the high M_s temperature, 300°C (572°F) or higher, and the time to cool through the temperature range for martensite formation.

The as welded HAZ transformation microstructures may undergo significant changes during subsequent heat treatment. Baker and Nutting[29] have shown that the types of carbides present in 2 1/4Cr-1Mo are dependent on starting microstructure, heat treatment and time at the heat treatment temperature. For bainite and martensite the general sequence for carbide precipitation was found to be:



However, in proeutectoid (polygonal) ferrite, formed during slow cooling from the austenitizing temperature, the precipitation

sequence during tempering was significantly different. The precipitation sequence in ferrite was found to be:

$$Mo_2C \longrightarrow M_6C$$

Mo_2C, the carbide conferring the greatest resistance to creep deformation, was found to be more stable in ferrite than in the initial microstructures consisting of martensite or bainite. In the martensitic and bainitic microstructures $M_{23}C_6$ grew at the expense of Mo_2C resulting in a degradation of the creep properties with increasing tempering temperature or time at a tempering temperature.

Because of the stability of Mo_2C within the ferrite, Baker and Nutting recommended the use of normalized and tempered 2 1/4Cr-1Mo rather than quenced and tempered 2 1/4Cr-1Mo. However, the presence of proeutectoid ferrite is generally regarded as unfavorable due to its low strength and poor toughness. Current alloy development reflects the need to avoid the formation of ferrite in the microstructure during cooling by making increased hardenability one of the principle criteria in alloy design.[3]

Modification of the 2 1/4Cr and 3Cr alloys by the addition of vanadium results in the precipitation of finely dispersed, slow growing V_4C_3 upon tempering or post weld heat treatment.[30] The precipitation of V_4C_3 occurs directly from the matrix and, unlike Mo_2C, is not dependent on the formation of any other carbides. Vanadium has also been reported to be present in Mo_2C with a metal atom ratio of up to 0.3 in alloys containing more than 0.1%V. Vanadium in Mo_2C results in stabilization of the Mo_2C.[31] The combined effects of precipitation and stabilization result in

vanadium being one of the most potent elements in promoting creep resistance.

The nature of carbide formation in the 9Cr-1Mo alloys is substantially different. The general sequence of carbide formation is:[32]

$$Fe_3C \longrightarrow M_7C_3 \longrightarrow M_{23}C_6$$

The addition of niobium and vanadium may alter the kinetics of precipitation and growth of carbides in the 9Cr-1Mo alloys. The presence of niobium and vanadium results in the precipitation of both niobium and vanadium rich MC type carbides.[32] These MC type precipitates, present in a fine, dispersed, form may act as nucleation sites for the precipitation of $M_{23}C_6$ in a fine, dispersed form.[33] The presence of vanadium carbides of the V_4C_3 or VC type was not found in 9%Cr-0.2%C steels with 0.4%V and 0.97%V by Seal and Honeycombe[34], but it was shown that the presence of vanadium in the alloy restricts the diffusion of chromium in ferrite reducing the rate of carbide growth. This results in a lower rate of softening and minimizes the loss of strength upon tempering or post weld heat treatment.

The effect of vanadium in restricting the mobility of chromium may be an important factor in HAZ softening that occurs in the vanadium-niobium modified 9Cr-1Mo materials. If, during temperature excursions into the intercritical range, chromium mobility in the austenite is restricted while carbon partitions to the austenite, a more rapid rate of tempering may occur during PWHT in the subsequently transformed martensite.

Two factors should be evident from the above discussion of transformation characteristics and resulting microstructure. Since the continuous cooling transformation diagrams are important to the understanding of properties and potential cracking susceptibility, there exists a need to determine the continuous cooling transformation diagrams for welding conditions as the development of the Cr-Mo alloys continues. Also, since the possible role of partial austenite transformation, due to temperature excursions into the intercritical temperature region, on HAZ softening has not been previously addressed, a need exists to evaluate the effect of partial transformation on HAZ softening.

Postweld Heat Treatment Cracking

Post weld heat treatment (PWHT) cracking, also referred to as reheat or stress-relief cracking, is a problem that occurs in Cr-Mo steels containing less than 3% chromium.[35,36] Cracking is manifested by low rupture ductility and intergranular fracture along prior austenite grain boundaries, typically occurring in the coarse grained HAZ and occasionally in the weld metal, after an initially sound weldment has been subjected to a stress-relief heat treatment.[37] Heat-to-heat variations in stress-relief cracking, indicating a dependence on residual elements, add to the worrisome nature of this problem as bulk chemistry of an alloy may not be a reliable predictor of cracking susceptibility.[38] This type of cracking, if undetected prior to service, may lead to failure of pressure vessels and piping in service.[39]

Through 1975 the mechanism of PWHT cracking was thought to be related solely to the precipitation of alloy carbides and the plastic flow due to stress relaxation at the post weld heat treatment temperature. Temperature excursions experienced in the HAZ above 1200°C (2192°F) result in the rapid solution of carbides and grain growth. The rapid cooling associated with welding results in alloying elements and carbon being retained in martensitic or lower bainitic transformation products above the saturation limit. Subsequent reheating leads to precipitation of intragranular alloy carbides, particularly Mo_2C and V_4C_3, causing an increase in grain matrix strength. Thus, the ratio of the grain matrix strength to the grain boundary strength increases. The relaxation of stress at the post weld heat treatment temperature is accomplished primarily by creep induced plastic flow involving grain boundary sliding which must be accompanied by general grain deformation if grain boundary cavitation or cracking is be avoided. However, when the grain matrix strength is increased by precipitation, deformation is restricted to the grain boundaries, the area of which has been minimized by grain growth. Although the total strain is small, the locally high strain concentration in the grain boundaries exceeds the ductility of the grain boundaries resulting in cavitation and rupture.[37,39-43]

The type and morphology of precipitates has been a topic of considerable research. Several investigators have contended that the most critical time in PWHT is during the formation of coherent or pre-precipitate clusters at about 500 to 550°C (932 to 1022°F) which corresponds to the maximum in secondary hardening.[42,44-48] Orr et

al.[47] have noted that due to the strong lattice correpondance of Mo_2C with bainite or martensite, the nucleation energy is relatively low and therefore Mo_2C forms quickly as a finely divided slow growing precipitate. Swift et al.[42,44-46] have proposed that coherent precipitates, Mo_2C and/or V_4C_3, nucleate in the matrix and at dislocation jogs and intersections. Coherent Mo_2C yields a nonuniform, highly strained matrix with decreased dislocation mobility and dislocation locking and results in a reduction of the ability of the grain interiors in the coarse grained HAZ to plastically deform upon stress-relief.

Temperature is an important factor in that Mo_2C persists for more than 500 hours at 590°C (1100°F) without decomposition to more complex carbides and has a correspondingly long coherency duration. However, at 680°C (1250°F) coherency is quickly lost as evidenced by the formation of visible Mo_2C within one-half hour at temperature.[46] Another factor is the presence of notches, either surface irregularities or internal defects, at which "stress relief cracking is almost invariably initiated."[40] The notches in the coarse grained HAZ are particularly detrimental, as they act as intense stress concentrators in the very region of the weld already under a high tensile stress and with a low ductility microstructure.[40,43,49,50] The notch acuity further inhibits deformation by the creation of a triaxial stress state.[46]

A carbide denuded zone has also been reported to exist adjacent to the grain boundaries.[31,40,43,51,52] These zones are apparently a result of depletion of alloying elements due to carbide precipitation

in the grain boundaries. Several researchers have considered the carbide denuded zones to be detrimental as they provide a narrow soft region in which strain can accumulate preferentially.[52,30] However, Meitzner and Pense[50] found the presence of denuded zones did not contribute to stress-relief cracking and Swift[46] found that although denuded zones were present they formed only at times beyond those corresponding to the minimum in ductility.

After 1975, interest in the heat-to-heat variability and the development of new techniques, particularly Auger spectroscopy, to study grain boundary compositions led to intense evaluation of residual element effects on stress-relief cracking.[40,41] Segregation of residual elements; phosphorous, sulfur, tin, and antimony, was found to play a critical role by causing embrittlement of grain boundaries.[53-55] The effects of grain boundary embrittlement due to impurity segregation and impurity interactions during precipitation are superposed on the matrix strengthening effects of coherent precipitation.[42] Hippsley et al.[56] have noted that grain boundary segregation of impurities can be due to equilibrium segregation from the grain matrix or may be due to solute rejection from growing grain boundary carbides, the solubility of impurities being higher in the matrix material than in the carbides. Vinckier and Dhooge[53,55] state that loss of ductility caused by segregation during stress relief heat treatment is certainly a major factor in cracking but "that the true mechanism is almost certainly a combination of these two ideas (segregation and precipitation strengthening) and is more complex."

Other researchers have proposed additional factors that increase the intricacy of the previous PWHT cracking mechanisms. Vinckier[39] proposed that "the decomposition of martensite needles" during heating creates high localized strains at the grain boundary interfaces. These strains plus external restrain can result in the formation of microcavities, particularly when the matrix is strengthened by intragranular precipitation. Hippsley et al.[57] have proposed that segregation of less mobile, embrittling elements, such as phosphorous, tin, and antimony, occurs at elevated temperatures in a fashion similar to that proposed by Troiano[58] for hydrogen. Segregation is locally enhanced in regions of maximum triaxial stresses, such as at the root of a notch or in the region of a crack tip, by diffusion along the strain gradient. Dislocation pile ups at grain boundaries and grain boundary carbides plus the strain induced segregation of impurities reduce the cohesive strength of the grain boundaries and carbide-matrix interfaces sufficiently to allow the development of microcracks. Thus, according to Hippsley et al.[57], the factors involved in cracking are not only segregation and precipitation but also the amount of plastic strain, which for a given load increases as the yield strength falls with increasing temperature.

The necessary factors for stress-relief cracking to occur were summarized by Ito and Nakanishi[18]:

1. the material must have undergone a thermal cycle that results in solution of alloying elements and that retains the elements in solid solution after cooling,

2. grain growth must have occurred as a result of thermal cycling,
3. heat treatment between 450°C and 700°C (850°F and 1300°F) resulting in significant precipitation hardening,
4. grain strength and internal stress must exceed the strength of the grain boundaries,
5. a stress riser must be present to initiate cracking.

In addition to these five the material must be one that has a composition that is susceptible to reheat cracking in alloy content and residual or impurity elements.

Origin of Residual Stresses[17,22]

Residual stresses are developed in the weld HAZ and fusion zone during cooling due to restrained shrinkage and transformation volume changes as a result of austenite decomposition. On-cooling, those areas of the base metal that experienced thermal expansion due to heating must contract or plastically flow. The bulk of the base metal which has experienced no significant heating (and therefore no decrease in strength) prevents or restrains the contraction of the cooling material. Above approximately 1200°F (650°C) the weld fusion zone and those regions immediately adjacent to the weld accomodate the thermal contraction by plastic deformation without developing any significant stress as the yield strength is low above this temperature. Cooling below 1200°F (650°C) results in significant increases in yield strength with decreasing temperature. Plastic deformation only occurs when the stresses due to thermal contraction

exceed the yield stress and therefore cooling to the preheat temperature results in increasing residual tensile stress concomitant with the increased yield strength in the fusion zone and HAZ. The resultant residual tensile stress occuring in the HAZ and fusion zone are in equilibrium with compressive stresses in the bulk of the base material.

Transformation stresses are a result of the volumetric expansion that occurs during the decomposition of austenite. The material being transformed attempts to expand but expansion is hindered by the cooler material not undergoing transformation. The material being transformed therefore experiences a compressive stress and the cooler material a tensile stress. If the transformation temperature is high the transformation stress will be overridden by the effects of subsequent bulk shrinkage. However, if the transformation temperature is low, the transformation stress will lower the overall tensile stress in the HAZ and fusion zone.

Superposition of the components of the residual stress developed during welding leads to an extremely complex final residual stress state. The coarse grained HAZ, that portion of the HAZ adjacent to the fusion zone, is under a significant tensile stress both in the direction of and perpendicular to the weld. This biaxial residual stress state as well as the unfavorable metallurgical characteristics of the grain coarsened zone helps explain the susceptibility of this region to PWHT cracking.

Microstructural Effects

Meitzner and Pense[51] have found that martensite and lower bainite are more susceptible to stress-relief cracking than upper bainite although the authors state that the difference is probably due to precipitation processes rather than optically resolved microstructure. Ito and Nakanishi[18] also found that martensitic and lower bainitic microstructures are more susceptible than upper bainite. They related the increased susceptibility to the supersaturation of the bainitic and martensitic microstructures with alloying elements and carbon which results in intense secondary hardening. Debiez and Granjon[59] found that a "bainitic structure seems to be a little more susceptible to cracking than the martensitic" structure under implant testing. However, they do not state whether the bainitic microstructure obtained is upper or lower bainite.

Effects of Composition

Meitzner[40] and Dhooge et al.[53], in extensive literature reviews indicate the effects of specific alloying elements. The elements generally considered to be detrimental to PWHT cracking are: carbon, vanadium, molybdenum (in concert with vanadium), columbium, aluminum and the residual elements: tin, antimony, arsenic and phosphorus. The effects of chromium, boron and titanium are not clearly defined. Nickel was found to be the one element that appears to have no effect on cracking. In general, the elements found to be deleterious are either those which promote the formation of carbides of the M_2C or

M_4C_3 type or which are known to have general grain boundary embrittling effects.

In 1965 Nakamura et al.[60] attempted to determine the effect of alloy additions on cracking susceptibility in Cr-Mo steels. Variations in the levels of chromium (0.1-1.5%), molybdenum (0.3-0.6%), nickel (0-3%), and vanadium (0-0.08%) resulted in the ΔG parameter:

$$\Delta G = \%Cr + 3.3(\%Mo) + 8.1(\%V) \qquad (1\text{-}1)$$

When ΔG is greater than zero the material is determined to be susceptible to PWHT cracking. In 1972, Ito and Nakanishi[18] extended the work of Nakamura. The alloying elements; manganese (0.5-1.4%), nickel (0.5-1.5%), chromium (0.5-1%), and vanadium (0.05-0.12%), were varied and additions of copper (0.15% and 0.26%), niobium (0.06%) and titanium (0.02% and 0.07%) were made to steels containing nominally 0.3% silicon and 0.5% molybdenum. This work resulted in the development of the cracking parameter, P_{SR}:

$$P_{SR} = \%Cr + \%Cu + 2(\%Mo) + 10(\%V) + 7(\%Nb) + 5(\%Ti) - 2 \qquad (1\text{-}2)$$

When P_{SR} is greater than zero the material is deemed to be susceptible to cracking. The applicable range of the P_{SR} parameter is limited to alloys containing less than: 2%Mo, 1.5%Cr, 1%Cu, and 0.15% V, Nb and Ti. Ito and Nakanishi found that chromium contents in excess of 2% eliminated cracking.

Subsequent to development of the P_{SR} and ΔG parameters several investigators have found poor correlation with the parameters and actual susceptibility of different alloys. Pense et al.[61] found that ΔG was a poor predictor of cracking in A535-A, A517-F, and A543

steels. McMahon et al.[62] found that both P_{SR} and ΔG did not accurately predict cracking susceptibility in multiple heats of SA 533-B and SA 508-2. Also, many investigators[35,44-46,57,63-67] have found that 2 1/4Cr-1Mo alloys are susceptible to PWHT cracking although a chromium content of 2% or greater was considered to eliminate stress-relief cracking susceptibility by Ito and Nakanishi.[18]

McMahon et al.[62] have suggested using the CERL parameter with the addition of the percentage chromium in the alloy:

$$CERL = 0.2(\%Cu) + 0.44(\%S) + \%P + 1.8(\%As) + 1.9(\%Sn) + 2.79(\%Sb) + \%Cr \quad (1\text{-}3)$$

The greater the CERL+Cr value the greater the cracking susceptibility. This parameter clearly emphasizes the effects of embrittling elements over the effect of carbide formers. The authors state that individual alloy content will affect the necessary parameters and that increasing the carbide former content may necessitate their inclusion in a manner similar to that of the P_{SR} parameter. Similarly, in reviewing results of cracking susceptibility tests of 2 1/4Cr-1Mo weld metal, Boniszewski[68] recommended use of the MCF (metal composition factor) to rank cracking susceptibility. The MCF factor :

$$MCF = \%Si + \%Cu + 2(\%P) + 10(\%As) + 15(\%Sn) + 20(\%Sb) \quad (1\text{-}4)$$

combines the relative overall potency of grain boundary embrittling elements present in a material. An increase in the MCF factor was found to correlate with a decrease in rupture ductility as measured by elongation in hot tensile tests.

The recent work of Tamaki[36,69-71] attempts to determine the seperate effects of chromium and molybdenum on PWHT cracking. His papers represent extensive work on materials of varying chromium (0-5%) and molybdenum (0.3-1.5%) contents. The effects of chromium and molybdenum, independently and in concert, were studied using a modified implant test. The modified implant test was employed to determine the minimum stress which would cause the specimen to fracture within 20 hours while postweld heat treating the specimen at a temperature of 600°C. The susceptibility to reheat cracking was related to the magnitude of the critical stress to rupture ($\sigma_{AW-crit}$). The lower the minimum critical stress to cause rupture, the greater is the susceptibility to reheat cracking.

Alloys containing chromium over the range tested but low in molybdenum (0.25%) were found to be susceptible to cracking. The 1%Cr-0.25%Mo alloy showed the lowest critical stress for failure and therefore the greatest susceptibility to cracking. Increasing molybdenum at any level of chromium increased susceptibility, but the lowest critical stress for any particular molybdenum level occurred for alloys containing 1% chromium. These data from his studies are shown in Figure 8. Note that for low molybdenum contents (0.25% and 0.5%) when no chromium is present, no cracking occurred over the range of stresses employed indicating that these materials are not susceptible to stress relief cracking.

When the results are expressed as a function of chromium and molybdenum for differrent stress levels the evaluation shown in Figure 9 results. Susceptibility to PWHT cracking with a change in

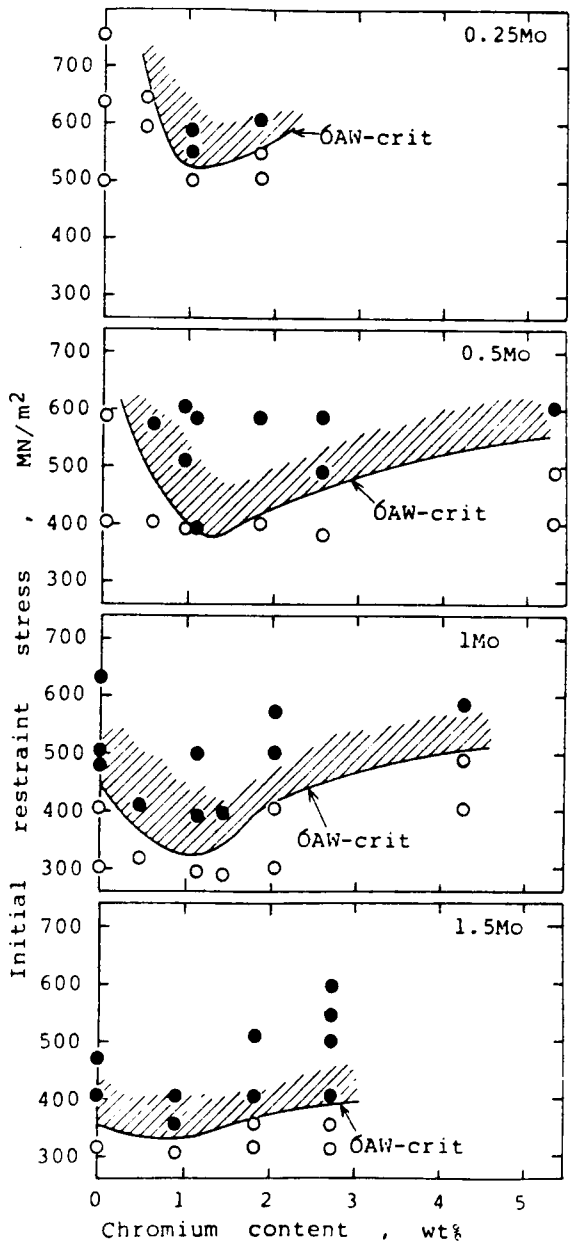


Figure 8. Effect of chromium on the critical restraint stress, $\sigma_{AW\text{-}crit}$.

Source: Tamaki, K., and Suzuki, J., Effect of Chromium and Molybdenum on Reheat Cracking Sensitivity of Steels, Transactions of the Japan Welding Society, 15(1), 1984.

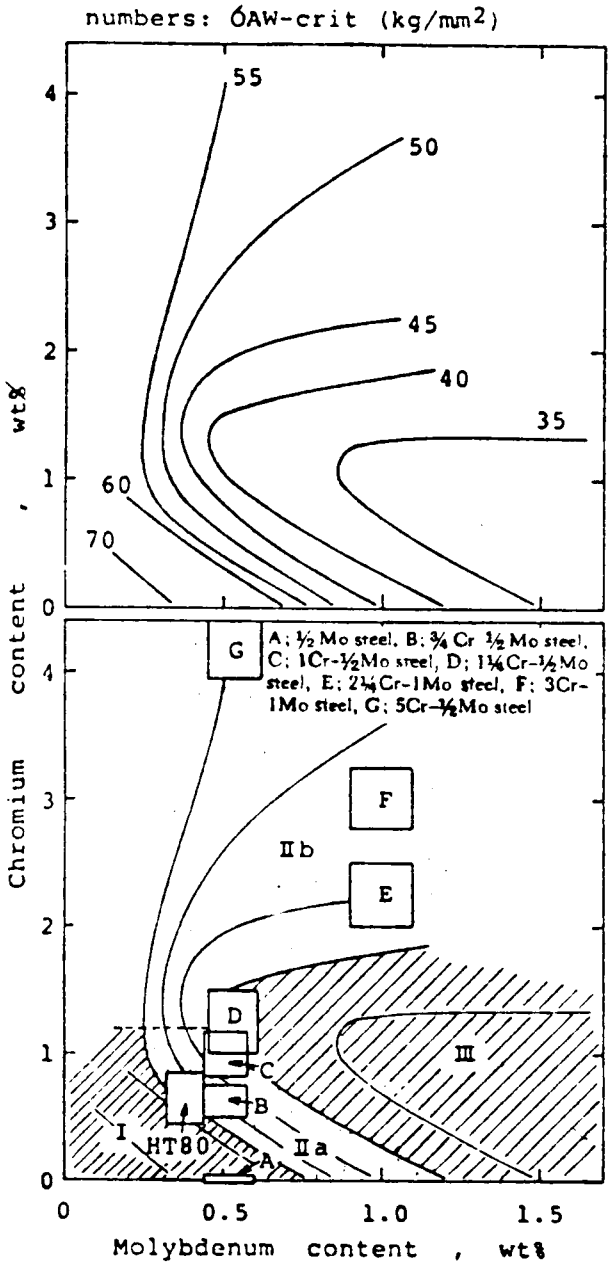


Figure 9. Contour lines of critical restraint stress ($\sigma_{AW\text{-}crit}$) shown on the Cr-Mo content diagram.

Source: Tamaki, K., and Suzuki, J., "Effect of Chromium and Molybdenum on Reheat Cracking Sensitivity of Steels," Transactions of the Japan Welding Society, 15(1), 1983.

alloying element content is a maximum on these diagrams where the stress contours are closest together. Susceptibility for a particular alloy may be judged by the magnitude of the critical stress to failure ($\sigma_{AW-crit}$). The ploted data is divided into four regions labeled I, IIa, IIb and III (Figure 9). The materials in region I, those with less than 1%Cr and less than 0.5%Mo, are relatively insensitive to cracking. Materials in region IIa, comprised of alloys with 0-1%Cr and 0.5-1%Mo, have rapidly increasing sensitivity to cracking with increasing chromium or molybdenum content based on the relatively large decreases in the critical stress with small changes in alloy content. Region IIb, comprised of alloys with greater than 2%Cr and 0.5-1%Mo, characterizes behavior of decreasing sensitivity with increasing chromium content. Region III, comprised of alloys with approximately 1%Cr and greater than 1%Mo, represents the highest sensitivity to cracking. The Nakamura parameter[60] for PWHT cracking susceptibility, ($\Delta G>0$), was found to predict cracking principally in fields IIa and III extending somewhat in field IIb. The cracking parameter due to Ito[18] predicted cracking, ($P_{SR}>0$), principally in field IIa. (Note: these parameters are limited to chromium contents less than 1.5%.) Since fields IIa and III indicate the alloys of maximum reheat cracking sensitivity, the agreement is excellent, with Tamaki's diagrams being more discriminating than either index (fig. 10).

In order to discern the microstructural causes for the differences in cracking susceptibility for the various materials, Tamaki[71] undertook an extensive study of the carbides in the alloys

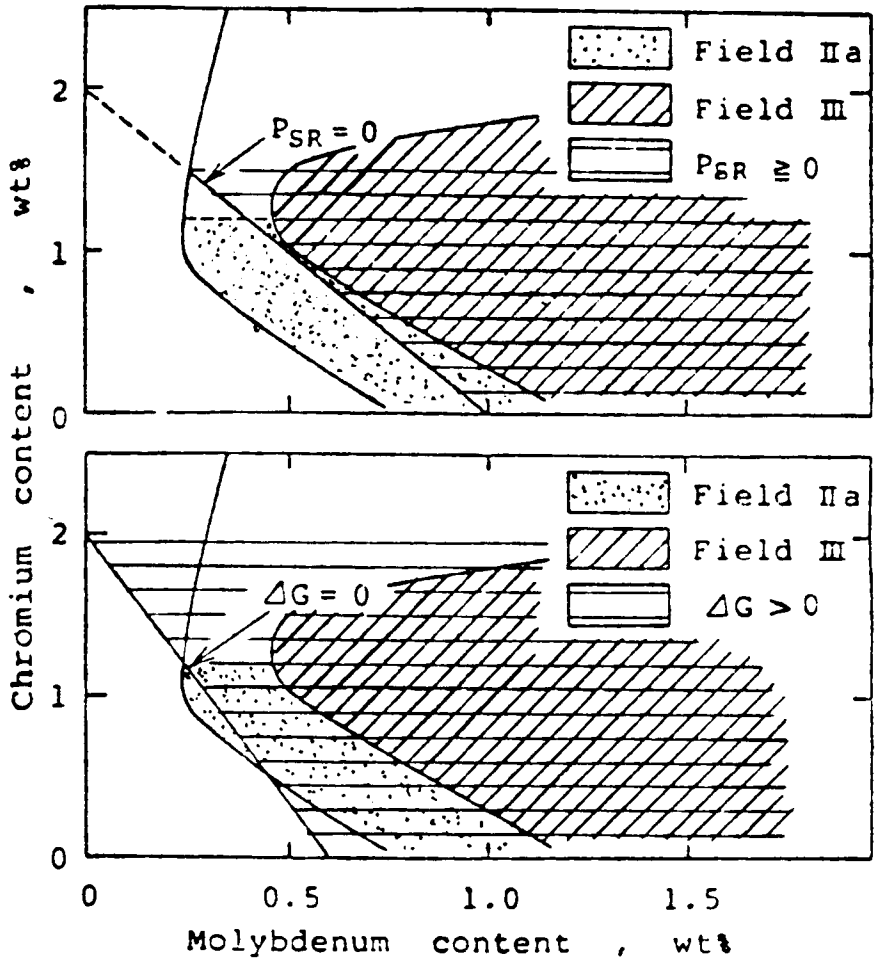


Figure 10. Comparison between the critical restraint stress ($\sigma_{AW-crit}$) and cracking sensitivity indexes, P_{SR} and ΔG.

Source: Tamaki, K., and Suzuki, J., Effect of Chromium and Molybdenum on Reheat cracking Sensitivity of Steels, Transactions of the Japan Welding Society, 14(2), 1983.

using x-ray diffraction techniques of extracted carbides and transmission electron microscopy of carbide extraction replicas. It was found that the materials most susceptible to PWHT cracking showed the greatest fraction of M_2C type carbides after post weld heat treatment. With a smaller amount of M_2C, (or a larger amount of M_7C_3 and/or $M_{23}C_6$), the susceptibility to cracking decreased.

Figures 11 and 12 depict these results graphically. Figure 11 shows the relative amounts of carbides present for different alloys on a chromium vs. molybdenum content diagram with the curved lines being constant weight percent M_2C. Figure 12 superimposes these constant weight percent M_2C lines (solid lines-fig. 12) on the chromium vs. molybdenum content diagram of Figure 9. Figures 11 and 12 thus show that the greatest susceptibility to cracking coincides with the largest fraction of M_2C. The only exception noted is confined to below the a-a[1] line in Figure 12, where, according to Tamaki, in alloys with less than 1%Cr and less than 1%Mo, phosphorus segregation is inhibited.

Since both M_2C and M_7C_3 strengthen the matrix by precipitation, Tamaki investigated the effects of secondary hardening and high temperature hardness by making hardness measurements on samples held at temperature for one hour both at the holding temperature and at room temperature after cooling. While secondary hardening is manifested by an increase in hardness at room temperature, Tamaki found at high temperature the phenomenon is represented only in a delay of softening, ie. softening continues to occur but at a lower rate than that which occurs at lower temperatures. Figure 13

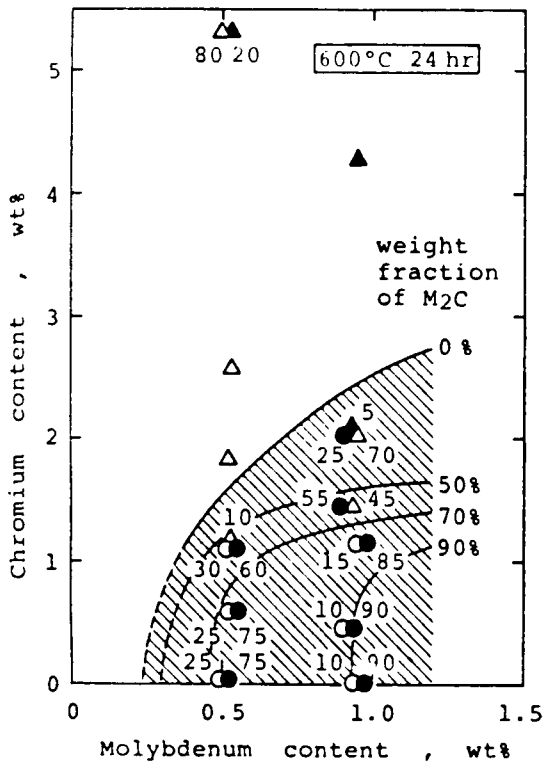


Figure 11. Carbides present in Cr-Mo steels tempered at 600°C for 24 hours. (○ M_3C, ● M_2C, △ M_7C_3, ▲ $M_{23}C_6$)

Source: Tamaki, K., Suzuki, J., Nakaseko, Y., and Tajiri, M., Effect of Carbides on Reheat Cracking Sensitivity, Transactions of the Japan Welding Society, 15(1), 1984.

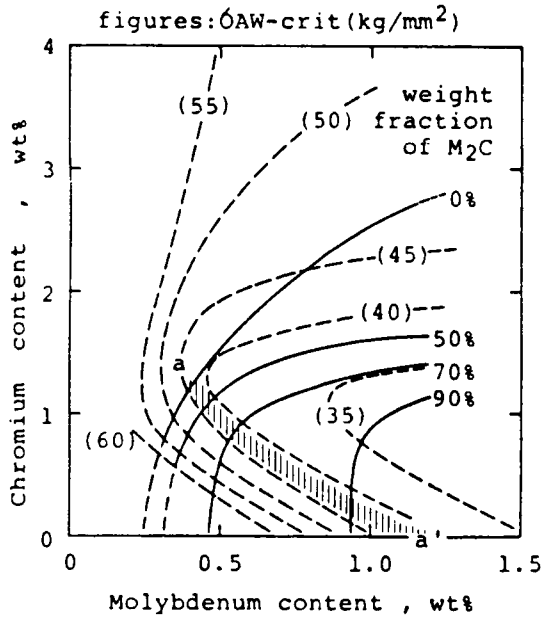


Figure 12. Weight fraction of M_2C shown on the $\sigma_{AW-crit}$ diagram.

Source: Tamaki, K., Suzuki, J., Nakaseko, Y., and Tajiri, M., Effect of Carbides on Reheat Cracking Sensitivity, Transactions of the Japan Welding Society, 15(1), 1984.

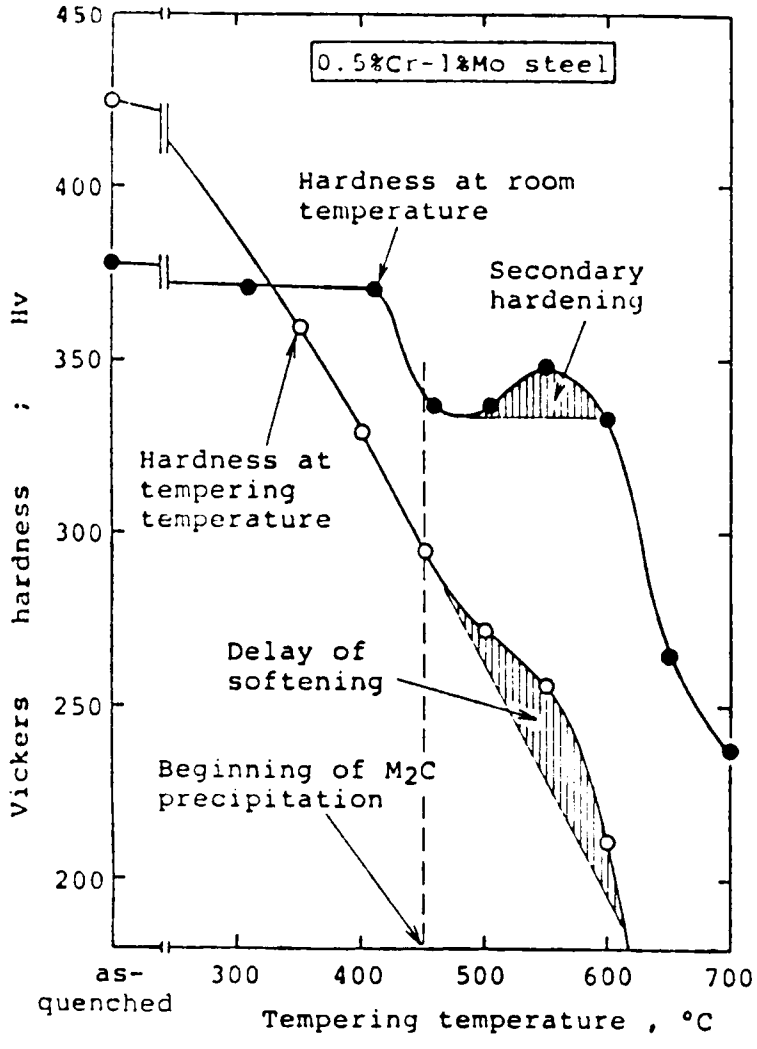


Figure 13. Hot hardness and hardness at room temperature versus tempering temperature.

Source: Tamaki, K., Suzuki, J., Nakaseko, Y., and Tajiri, M., Effect of Carbides on Reheat Cracking Senesitivity, Transactions of the Japan Welding Society, 15(1), 1984.

illustrates these results with the room temperature hardness shown as filled circles and the elevated temperature hardness as open circles. This agrees with the findings of Bauford[72]. In hot tensile tests Bauford found that at temperature there is no increase in strength with time but yield strength remains constant over a long period followed by a slow loss in strength.

It was found that in alloys in which the principle precipitate is M_7C_3, the delay in softening occurred at lower temperatures than for those alloys in which the precipitate consists of large fractions of M_2C. Tamaki[70] postulated that the grain boundary embrittlement would be of a similar nature in either type of alloy and therefore embrittlement of the grain boundaries would initiate at the same temperature and proceed in a similar fashion for both types of alloys. As shown schematically in Figure 14a, if a delay in softening occurs at higher temperatures, as for M_2C type precipitation, the embrittlement of the grain boundary may cause the intercrystalline flow stress to be less than the intracrystalline flow stress resulting in fracture. However, as shown in Figure 14b, if a delay in softening occurs at lower temperatures, as with M_7C_3 precipitation, the intercrystalline flow stress exceeds the intracrystalline flow stress at all temperatures and thus intercrystalline fracture does not occur.

In the Cr-Mo alloys vanadium additions dramatically increase the elevated temperature strength. Unfortunately the addition of vanadium to Cr-Mo steels almost universally has been found to

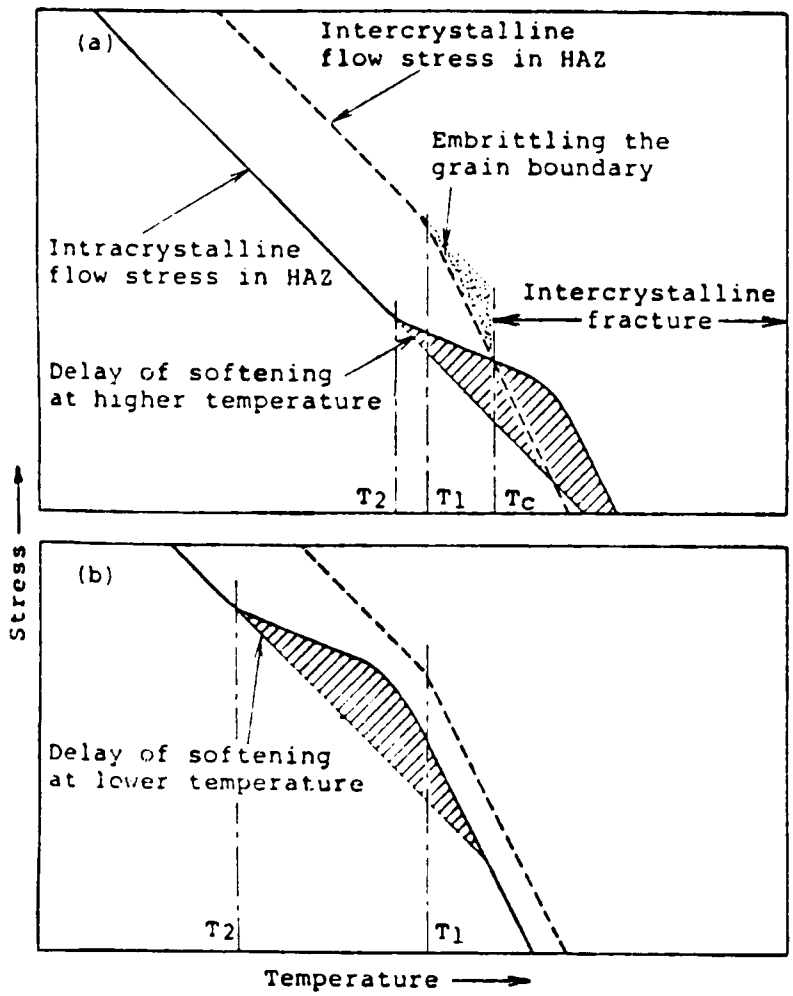


Figure 14. Schematic representation of demonstrating Tamaki's mechanism of reheat cracking.

Source: Tamaki, K., Suzuki, J., Nakaseko, Y., and Tajiri, M., Effect of Carbides on Reheat Cracking Sensitivity, Transactions of the Japan Welding Society, 15(1), 1984.

result in an equally dramatic increase in PWHT cracking susceptibility.[18, 35,39,43,46,48,49,51,59,73,74] The importance of vanadium in increasing cracking susceptibility can be seen in the P_{SR} and ΔG parameters in that the multipliers for vanadium are the largest.[60,18]

The addition of vanadium results, as has been previously indicated, in a uniform and fine precipitation of V_4C_3 in the matrix resulting in significant grain matrix strengthening and accumulation of strain in the grain boundaries.[33,49,73] Bently[48] has noted that early in the heat treatment cycle, intense V_4C_3 precipitation occurs at the ferrite-bainite interfaces due to segregation effects; the bainite having a higher carbon content and the ferrite having a higher vanadium content. At temperatures between 500°C and 550°C (930°F and 1020°F) coherent precipitation of V_4C_3 occurs in the ferrite lattice similar to Mo_2C formation and is concurrent with the development of maximum hardness and strength. At higher temperatures, 700°C (1300°F), and longer time, 10 hours, carbide precipitation is transferred to the grain boundaries and large carbides with a grain boundary denuded zone are formed.

Meyers[75], in a study of 1/2Cr-1/2Mo with varying vanadium content, determined that vanadium content below 0.22% to 0.27% did not appreciably increase cracking susceptibility. It was speculated that vanadium content could be increased if residual elements were restricted in order to limit grain boundary embrittlement. However, Meyers noted attention must also be paid to the effects of chromium, manganese, and nickel, which increase initial hardness, and the

effect of molybdenum, which increases secondary hardening, and that restrictions may have to be placed on them as well as vanadium.

Jones[76] noted that the vanadium to carbon ratio must be considered. In a study of actual welds in 1Cr-1/2Mo-1/2V materials with a vanadium to carbon ratios between 3.5 and 4.5, a high susceptibility to cracking was found. Stone and Murray[77] noted that a minimum in creep ductility was apparent at vanadium to carbon ratios of 3 to 4 and the reduction of this ratio to 1.5 markedly increased ductility. Thus, a vanadium to carbon ratio of 1.5 to 2 was recommended to prevent PWHT cracking.

Tamaki et al.[71] found that small additions of vanadium (0.06%) reduced the critical stress to fracture in the implant test. The maximum effect was found to occur in low chromium, low to high molybdenum alloys. The increase in cracking susceptibility was said to be related to a decrease in the rate of stress relaxation in a similar fashion to that experienced in the Cr-Mo alloys previously studied.

Nickel is the one element that appears to have the least detrimental effect on the Cr-Mo alloys with respect to PWHT cracking susceptibility. In establishment of the ΔG parameter nickel was varied between 0% and 3.4% without increasing susceptibility to cracking.[60] The same is true of the P_{SR} parameter where nickel was varied between 0% and 1.5%.[18] Thus nickel does not appear in either cracking susceptibility parameter. Tamaki and Suzuki[69] found that nickel content below 1.5% had no effect on the critical stress to

fracture but that above 1.5% increasing nickel content greatly increased cracking susceptibility.

The effect of nickel is probably related to the fact that nickel alters the kinetics of carbide precipitation. In a study of the tempering characteristics of 3Cr-1 1/2Mo-Ni alloys Ritchie et al.[10] found that $M_{23}C_6$ replaces M_2C, M_3C and M_7C_3 after only one hour at 700°C (1290°F) as compared to 400 hours for 2 1/4Cr-1Mo. In accordance with Tamaki's model[70], carbides which cause the greatest strengthening of the matrix would form while the overall strength of the grain boundaries is high and before significant embrittlement could occur. The rapid formation of carbides at lower temperatures and the probable very short times of coherency would result in the lowering of PWHT cracking susceptibility.

Boniszewski[68] states the effect of silicon reduction is an increase in ductility and a lower cracking susceptibility. Vinckier[78] found that silicon in excess of 0.5% caused cracking in 2 1/4Cr-1Mo. Increased silicon has been reported to enhance Mo_2C formation in Cr-Mo materials.[74,79] Ratliff and Brown[80] state that increased silicon appears to enhance cementite dissolution and thereby precipitation of alloy carbides containing chromium, molybdenum, and vanadium resulting in increased secondary hardening which "ultimately impairs stress-rupture ductility."

Research on the effects of titanium on PWHT cracking susceptibility have had mixed results. When titanium has been added for deoxidation purposes (Meyers[81] - 0.016% to 0.055% and Harris and Jones[82] - 0.021% to 0.030%) cracking susceptibility was reported to

be diminished in comparison to the same materials deoxidized with other elements, particularly aluminum. Spaeder and Plodder[83] found that addition of 0.048% titanium to T-1 steel did not increase susceptibility while Ito and Nakanishi[18] found that additions of 0.03% to 0.07% titanium in 1Cr-1/2Mo alloys increased susceptibility slightly. Tamaki and Suzuki[71] found that the addition of a small amount of titanium, 0.07%, increased the critical stress to fracture in low chromium high molybdenum alloys. Harris[84] pointed out that, while small amounts of titanium may appear beneficial, larger amounts as deliberate alloying additions may increase cracking susceptibility due to matrix strengthening.

The presence of aluminum, used as a deoxidizer in Cr-Mo steels, has been found to enhance PWHT cracking susceptibility.[54,82] Meyers[81] found that increasing amounts of aluminum, up to 0.035%, used for deoxidation progressively lowered resistance to cracking in a 1/2Cr-1/2Mo-1/4V alloy. Aluminum was thought to prevent grain boundary mobility by the presence of aluminum-nitrogen precipitate clusters rendering the grain boundaries unable to "recrystallize" local regions of strain induced shear. Ratliff and Brown[80] found that when aluminum content exceeded 0.010% in a 1Cr-1/2Mo-1/4V alloy a marked degradation in stress rupture properties occurred. Aluminum was proposed to reduce the stability of cementite thereby enhancing the formation of Mo_2C and V_4C_3. Edwards et al.[52] found segregation of aluminum, silicon, and nitrogen to have occurred at the grain boundaries by Auger spectroscopy. They speculated that if the combined aluminum and silicon concentration exceeded the austenite

loop concentration, the formation of ferrite at the grain boundaries could result causing the rejection of carbon and the creation of a soft, carbide denuded region.

Several researchers have found that the combination of boron and aluminum was particularly detrimental, ie. promoting cracking.[38,52,54] Presser and McPherson[54] speculated that aluminum scavenges nitrogen allowing boron to remain in solution and segregate to the grain boundaries. Boron, segregated to the grain boundaries, forms $M_{23}(C,B)_6$ when held between 1100°F and 1650°F (600°C and 900°C) during cooling or upon reheating above 1200°F (650°C) resulting in deembrittlement. Presser and McPherson[85] also speculated that other strong nitride formers such as titanium or zirconium could enhance embrittlement due to boron. Boron alone has been reported to cause a slight increase in cracking susceptibility.[38,51,54]

Tramp elements have also been reported to affect PWHT cracking susceptibility. Copper and tin were reported to increase susceptibility in 1/2Cr-1/2Mo-1/4V.[82] Copper additions to 2 1/4Cr-1Mo weld metal have been reported by Hunter[86,87] to increase cracking susceptibility. The addition of tin to 1/2Cr-1/2Mo-1/4V was reported by Townsend[84] to significantly lower ductility in weld simulated specimens. However, Meyers[81] determined that tin additions decreased susceptibility in 1/2Cr-1/2Mo-1/4V while both copper and antimony additions increased cracking susceptibility.

Among the residual elements, phosphorous is the most potent in embrittling the grain boundaries and therefore in enhancing PWHT cracking susceptibility. Auger analysis of fracture surfaces has

provided significant evidence of phosphorous segregation in many studies.[57,64,79,88-91] Phosphorous segregation has been reported to be affected by carbide formation and element interaction,[19,57,79,91-93] microstructure,[19,93] and grain size.[19]

Phosphorous has been reported by Yu and McMahon[79,91], Hippsley et al.[92,57] and Eyre et al.[19] to interact with molybdenum in solution in the matrix. Molybdenum in solution scavenges or ties up phosphorous in the form of Mo-P clusters or compounds preventing the segregation of phosphorous to the grain boundaries. Precipitation of Mo_2C during heat treatment releases phosphorous allowing segregation to the grain boundaries to occur.

Silicon enhances the formation of Mo_2C and has been reported to have a repulsive interaction with phosphorous similar to that which occurs with carbon. Silicon content was also shown by Auger analysis to be lower at the grain boundaries than within the grains.[79,91] Thus silicon would appear to enhance grain boundary embrittlement by phosphorous.

Precipitation of alloy carbides has also been reported to decrease the activity of carbon in solution thus allowing greater phosphorous segregation.[19,90] The precipitation of molybdenum rich carbides increases the relative amount of chromium in solution and appears to enhance phosphorous segregation through Cr-P cosegregation.[79,91,93] Also, the formation of carbides in the grain boundaries results in the rejection of phosphorous in to the grain boundaries as phosphorous solubility in the carbides is less than the solubility in the matrix.[19,57,92]

Viswanathan and Joshi[20] and Eyre et al.[19] have found that phosphorous segregation is greater in martensitic microstructures than in bainitic microstructures. Viswanathan and Joshi[20] also reported that segregation increased with increasing hardness for a given microstructure in a 1 1/4Cr-1 1/4Mo-0.3V material. Eyre et al.[19] demonstrated that grain size also affected embrittlement in that increased grain size decreases the area available for segregation.

Tamaki also undertook a study of the effect of phosphorus in Cr-Mo alloys[57]. Several notable results were obtained with Tamaki's study:

(1) Plots similar to those of Figure 12 but made for alloys low in phosphorus (0.010%-0.013%) and higher in phosphorus (0.016%-0.020%) showed that increased phosphorus moved the critical stress curves to lower molybdenum contents.

(2) Phosphorus had already segregated to some extent in the HAZ during the weld thermal cycle.

(3) For a particular alloy there exists a critical phosphorus level below which embrittlement is apparent. The minimum critical value of phosphorus coincides with the 1% Chromium content.

(4) For the range of alloys tested, (0-2%Cr, 0.5%Mo), as long as the phosphorus content was below a critical value for a particular alloy, the critical stress level remained approximately the same.

Thus, phosphorus did indeed adversely affect the cracking susceptibility of the Cr-Mo alloys.

Since phosphorus did not segregate in materials subjected to heat treatments below the A_1 but did segregate when heated above the A_1, Tamaki surmised that the transformation to austenite played a vigorous role in the segregation of phosphorus. It was assumed that the equilibrium distribution of phosphorus was established at the ferrite/austenite interface during the course of transformation and that "the diffusion rate is so small that it (phosphorus) diffuses little from the ferrite/austenite interface to the original ferrite phase."[57] These assumptions combined with the knowledge that the solubility of phosphorus is approximately 2 1/2 times larger in the ferrite than in the austenite, led Tamaki to conclude that phosphorus was carried along on the ferrite/austenite interface. This interface, which is the prior austenite grain boundary on cooling, is therefore enriched with the phosphorus. The welding cycle thus initiates the segregation and embrittling processes.

Sulphur is another residual element that has been found to segregate to fracture surfaces by Auger analysis.[89,90] Imanaka et al.[67] in a study on the effects of sulphur, rare earth metal (REM) and calcium additions in 2 1/4Cr-1Mo found that if "free sulphur" exceeded 25ppm the material showed a high sensitivity to PWHT cracking but below 25ppm exhibited no susceptibility. Free sulphur was calculated by the equation:

$$(S) = [\%S - (32/40)\%Ca - (32/140)\%REM] \times 10^4 ppm \qquad (1\text{-}5)$$

Sulphur in the form of grain boundary sulphides has been linked with the initiation of cavitation on the grain boundaries.[64,94,95]

Hippsley et al.[64,96] have shown that at PWHT temperatures in excess of 600°C (1110°F) materials susceptible to cracking exhibit a change from smooth intergranular fracture surfaces to fracture surfaces with extensive intergranular microvoid coalescence. The microvoids were said to have nucleated on sulphides which were thought to have low interfacial strength with the matrix. The presence of sulphides was thought to be the result of solution of MnS during the thermal cycle and subsequent preferential reprecipitation at grain boundary sites during cooling.

However, Dolby[95] reports that the relationship between grain boundary particles and PWHT cracking is unclear in that some researchers have found that grain boundary particles have no effect on cracking. Further, both Horn and Kunze[90] and Kikuchi and Nakao[89] have found that even in relatively high sulphur materials a reduction in the phosphorous content eliminated cracking in susceptible materials. Thus the effect of sulphur is minor in comparison to that of phosphorous.

In summary, composition is probably the most significant factor in PWHT cracking of the Cr-Mo alloys. Of the alloying elements, molybdenum and vanadium have the greatest effect due to the preferential formation of coherent or fine precipitates in the grain matrix which significantly increase the flow strength of the grain matrix over the that of the grain boundaries. Of the residual elements phosphorous has the greatest effect due to segregation to

and embrittlement of the grain boundaries. The effect of composition is complicated by precipitation kinetics, element interactions and the superposition of the effects of other elements such as titanium, tin and copper.

Testing Techniques.

Baker[84] has enumerated some of the factors that should be included for the ideal PWHT cracking test. The specimen should include some defect or notch in a microstructure representative of the actual HAZ. The HAZ should be strained, particularly when testing austenitic materials, in a manner similar to that experienced in an actual weld. Finally, the test method employed should preferably incorporate stress relaxation since constant load testing may introduce misleading factors into the evaluation. Dhooge et al.[53] note that the incorporation of all the factors involved in an actual weld into a small specimen would be "difficult".

A common theme among papers reviewing PWHT cracking is that there exists a multitude of tests that have been employed and therefore comparison of test results is difficult and confusing.[40,41,53,78] Dhooge et al[53] cite the use of 26 different testing techniques prior to 1978. In order to simplify the overall number of tests three categories were proposed:

1. Tests on complete weldments
2. Tests on specimens containing a weld
3. Tests on specimens containing thermally simulated heat affected zones

Meitzner[40] in 1975 separated tests into only two categories; direct weldment tests (those containing an actual weld or potions of an actual weld) and simulated weld tests. Vinckier[41,78] in 1974 used three categories to divide some 17 different testing techniques:

1. Tests of a welded specimen
2. Tensile tests at high temperatures on welded or simulated specimens
3. simulation of the PWHT cycle on simulated specimens.

The use of tests on complete weldments or direct weldment tests have the obvious advantage of being directly related to the actual weld and PWHT conditions as well as joint geometry. However, both Meitzner[40] and Dhooge et al[53] note that reproducibility is a significant problem with Meitzner citing erratic results in which one specimen may crack extensively while another may not crack at all. Also a small test specimen will experience a significantly smaller amount of creep strain than a large welded structure.[40,78]

Weld simulation tests have the advantages of reproducibility, known stress level and control of microstructure.[40] The disadvantages are that the strains associated with weld contractural stresses are not duplicated, in general only one region of the HAZ is tested and the effects of adjacent weld metal and base metal are not present.[40,53] Therefore the results of simulation tests must be carefully evaluated before being directly applied to full scale weldments.

The most popular type of tests, although no standard exists, is the tensile or stress rupture test.[53] Several means of evaluating

this type of test have been proposed. Vinckier[39] suggested that in hot tensile tests the minimum acceptable reduction in area for an alloy to be considered not susceptible to cracking was 20%. Meyers and Price[97] suggested that, in constant load stress rupture testing, HAZ, base metal and weld metal rupture strengths be compared. If the HAZ rupture strength was lower than the base metal and weld metal strengths the material was to be considered susceptible and the greater the difference the greater the susceptibility. Spaeder and Plodder[83] have proposed a stress rupture parameter in which the reduction in area was multiplied by the stress to rupture. If the stress rupture parameter was less than 15×10^4 the material was determined to be susceptible to cracking. Vinckier and Pense[53,78] in extensive Gleeble simulation have determined the following criteria for simulated PWHT at 600°C (1110°F):

1. Extremely susceptible if the reduction in area is less than 5% and peak temperature of the weld simulation exceeds 1200°C (2190°F)
2. Highly susceptible if the reduction in area is below 10% and the peak temperature exceeds 1300°C (2370°F)
3. Slightly susceptible if the reduction in area is below 15% and the peak temperature exceeds 1350°C (2460°F)
4. Not susceptible if the reduction in area exceeds 20% at all peak temperatures.

Thus tensile type or stress rupture tests have been shown to yield a general determination as to the susceptibility of a material to PWHT cracking and allow a ranking of various materials to be determined.[40]

The ideal test previously described can perhaps be accomplished by the use of two or more tests making more efficient use of materials and funds. Utilizing Gleeble simulation to make an initial ranking of a material's stress-relief cracking susceptibility will determine if further testing is indicated. If the material is deemed susceptible to stress relief cracking further testing may be employed with specimens incorporating a weld or full scale weldments to determine if the material is susceptible under welding conditions or in the actual weldment to be fabricated.

Prevention of Postweld Heat Treament Cracking.

The most obvious remedy for PWHT cracking, as suggested by Stout[98], is to avoid the use of susceptible alloys. Murray[35] has recommended the use of alloys with limited molybdenum and vanadium. Mullery and Cadman[49] have recommended the use of materials in which the sulphur, phosphorous, and vanadium contents are minimized and manganese content is increased.

When the avoidance of susceptible alloys is not practical process changes may be beneficial. Murray[35] and Pense et al.[61] have recommended using a low strength weld metal with high strength base metals to allow deformation to occur in the fusion zone rather than in the HAZ. Mullery and Cadman[49] have proposed buttering of susceptible alloys to promote the formation of coarser carbides in the coarse grained HAZ of the parent metal. Muraki et al.[66] have suggested preferential welding of the larger side of unsymetric, double V-groove butt joints.

Increasing heat input and/or preheat has been seen to bring about favorable microstructural changes in the HAZ.[84,66] Higher energy inputs and preheating result in slower cooling rates and softer transformation products,[98] overaging of carbides in the HAZ during cooling,[18] or an "autostress relief".[44] Preheating may also be beneficial in decreasing the temperature range over which internal stresses build up.[99] However, Vinckier[39] reported that higher heat input yielded mixed results. Higher heat input causes two competing effects to occur: a coarser grain structure results which increases intergranular embrittlement and a softer HAZ is formed which decreases intergranular embrittlement.

An alternative to increasing heat input is to decrease heat input in multiple pass welds. Miller and Batte[65] found that using small gas tungsten arc weld beads in a multipass weld increased the amount of grain refinement due to overlapping of the heat affected zones and that even highly susceptible materials could be welded with this technique with no evidence of cracking after PWHT. Similarly, the use of temper beads, small stringer beads placed over the last pass to refine the grain structure of the HAZ, have been found to be beneficial in eliminating stress-relief cracking.[39]

Complete austenitization after welding[39] or normalizing[59] has been seen to increase the HAZ toughness and prevent cracking. Bentley[48] recommended using low PWHT temperatures and high heating rates to avoid prolonged coherent precipitate formation. However Granjon and Debiez[61] found increasing the heating rate is ineffectual in reducing cracking. Hippsley[101] found high heating rates produced

marginal benefit in reducing cracking but speculated that high heating rates might exacerbate cracking in actual weldments due to increased thermal stresses.

Weld dressing to remove discontinuities at weld toes has been found effective in reducing cracking by elimination of crack initiation sites.[35,49,66,98] Peening has also been suggested to eliminate residual tensile stresses at the surface of the weld.[98] Weld stresses can also be reduced by attention to weld sequencing, the use of techniques such as backstepping, the use of interstage stress relief heat treatments, and simplification of the design of weldments to lower overall levels of restraint.[35]

Thus it may be possible to mitigate PWHT cracking in susceptible alloys by utilizing the techniques described above. Perhaps the most economical means is to eliminate stress risers through careful dressing of the surface of the weld. Temper beading, if correctly performed, combined with weld dressing should provide a microstructure and surface unfavorable to the initiation and propagation of cracks. One important factor however is that oxidation during PWHT may provide initiation sites by oxide penetration and wedging along grain boundaries.[59] Therefore inherently susceptible materials may not be prevented from cracking by simple measures and it becomes necessary to know the susceptibility of individual alloys to PWHT cracking in order to ascertain the usefulness of preventative measures.

Summation

Figure 15 is a block diagram of the factors affecting the development of PWHT cracking in a material. The complexity of PWHT cracking is demonstrated by the interrelationship of the many factors. As has been shown previously the superposition of several factors may result in the occurrence of cracking but when the same factors are considered alone cracking may not occur.

As vanadium, titanium, and boron are being utilized in the new generation of 3Cr-1 1/2Mo and 2 1/4Cr-1Mo alloys, with vanadium known to increase PWHT cracking susceptibility and the effects of titanium and boron uncertain, it is evident that the susceptibility of these alloys to cracking needs to be investigated. The effect of nickel on PWHT cracking in the Berkeley 3Cr-1 1/2Mo-1/2Ni material needs to be fully documented. Also additional information on the effect of phosphorous in the 3% chromium alloys needs to be determined.

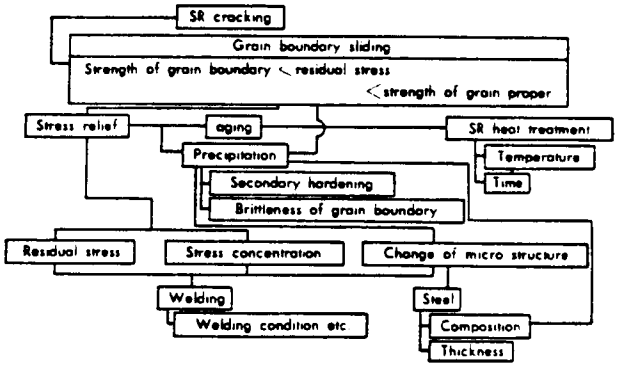


Figure 15. Block diagram showing factors involved in stress relief cracking.

Source: Ito, Y., and Nakanishi, M., Study of Stress Relief Cracking in Welded Low Alloy Steels, The Sumitomo Search, No. 7, 1972.

CHAPTER III

MATERIALS

The impetus for development of substitute alloys for 2 1/4Cr-1Mo primarily has been to provide resistance to high temperature and pressure hydrogen attack in synthetic fuels and refining applications and for increased high temperature strength which will permit the production of larger pressure vessels and/or operation at higher temperatures and pressures.[9,102,103] The interest in the modified 9Cr-1Mo alloys is primarily due to the increased corrosion resistance and the possibility of using the material as a substitute for austenitic stainless steel which would eliminate austenitic to ferritic transition joints and result in significant savings both economic and in strategic materials.

The materials that have been studied represent several of the proposed substitutes for 2 1/4Cr-1Mo and several commercial heats of the modified 9Cr-1Mo. Two of the candidate replacement alloys for 2 1/4Cr-1Mo have originated in the United States. The 3Cr-1Mo-0.1V material was conceived by the AMAX (Climax Molybdenum) Materials Research Center[9] and the 3Cr-1 1/2Mo-1/2Ni alloy originated at the University of California, Berkeley.[10,104] The remaining two 2 1/4Cr-1Mo substitutes that were examined, 2 1/4Cr-1Mo-V-Ti-B and 3Cr-1Mo-V-Ti-B, were the result of research performed at the Japan Steel Works (JSW).[4,105]

The alloy developed at the AMAX Materials Research Center has a chromium content of 3% to reduce hydrogen attack susceptibility. Molybdenum and vanadium contents are nominally 1.5% and 0.09% respectively in order to obtain elevated temperature strength. Manganese content of approximately 1% with a small addition of nickel (approximately 0.2%) is utilized to obtain increased hardenability. Carbon content is limited to 0.1% to promote weldability and prevent any degradation in toughness.[8,9]

The Berkeley alloy, 3Cr-1 1/2Mo-1/2Ni, has higher levels of chromium and molybdenum with respect to 2 1/4Cr-1Mo for the same reasons as the AMAX material. The increased chromium and molybdenum contents are also considered to improve the oxidation resistance in comparison to 2 1/4Cr-1Mo. Nickel is added to increase hardenability and to promote early formation, during tempering, of more stable alloy carbides thus increasing hydrogen attack resistance. However, unlike the AMAX material, manganese is limited to approximately 0.5% in order to prevent temper embrittlement, minimize the amount of retained austenite and prevent banding. Retained austenite and banding are thought to increase susceptibility to hydrogen attack due to non-uniform distributions of unstable alloy carbides. Carbon content is held to a maximum of 0.15% to eliminate the possibility of welding related problems.[10,104]

Development by JSW of the 3Cr-1Mo-V-Ti-B alloy[4,102] followed directly from research performed in the design of the 2 1/4Cr-1Mo-V-Ti-B alloy.[105] The major difference between the two alloys is the chromium content which is increased to provide better

resistance to hydrogen attack. Carbon content in the 2 1/4Cr material is 0.10% while the 3Cr material had a maximum content of 0.15%. Silicon content is restricted to a maximum 0.10% in the 3Cr alloy (0.02% - 2 1/4Cr) to minimize temper embrittlement. The addition of 0.25% vanadium is made to increase both tensile and creep strength through the formation of a fine dispersion of vanadium carbides. Boron, 0.001% to 0.003%, is included to increase hardenability and assure uniformity of mechanical properties throughout thick sections. Titanium additions, 0.015% to 0.035%, are utilized to scavenge nitrogen in order to prevent boron nitride formation and secondarily for grain refinement.

Nippon Kokan (NKK) and Kawasaki, two Japanese steel makers, have also proposed alloys for replacement of 2 1/4Cr-1Mo. Although these steels were not tested, the reasoning behind the alloy modifications provides some background in the different approaches taken in the design of the 2 1/4Cr-1Mo substitutes. Kawasaki[13] obtains the necessary strength and resistance to hydrogen attack with additions of niobium (0.023%) and vanadium (0.20%) to 3Cr-1Mo. Titanium and boron additions are specifically not included due to the degradation of toughness and because adequate hardenability is thought to be obtained by the niobium and vanadium additions. Kawasaki further lowered silicon to 0.08% and sulphur to 0.001% to control hydrogen attack, temper embrittlement and stress-relief cracking. NKK,[5,12] on the other hand, employed low titanium, 0.01% maximum, low boron, 0.0010% maximum, and low nitrogen, 0.004% maximum, to obtain adequate hardenability and toughness and maintain

weldability. Although vanadium improves resistance to hydrogen attack and increased creep rupture strength, Nippon Kokan limits additions of vanadium to approximately 0.08%. Vanadium in excess of 0.08% is thought to decrease hardenability substantially. Lower phosphorous, 0.004% maximum, is maintained rather than lowering the silicon content to reduce temper embrittlement. (The proposed silicon level is 0.25%.) Nickel content is 0.15% for the Kawasaki material and 0.5% for the NKK alloy. No discussion of the level of nickel employed was given by either steel maker.

Thus a variety of developmental approaches have been taken. Common among all the materials is the limitation of carbon content to promote weldability. However, beyond that there exists little agreement between the various developers. Weldability and temper embrittlement resistance are thought to be promoted by very lower sulfur content (0.001%) by one steelmaker while temper embrittlement control has been attempted through limiting silicon (below 0.010%) or phosphorous (0.004%) by others. Hardenability has been increased by the addition of boron, high manganese, manganese and nickel additions or niobium and vanadium additions. Manganese has been increased in one instance to between 1% and 1.2% in order to increase hardenability while in another it has been limited to approximately 0.5% to mitigate hydrogen attack. On the one hand, vanadium additions are limited to 0.08% and niobium not added due to the possible loss of toughness and hardenability while on the other hand, 0.25% vanadium is utilized in one case and 0.20% vanadium plus 0.023% niobium in another. In one alloy nickel is used as the primary

alloying addition (other than chromium and molybdenum) to increase both hardenability and eliminate hydrogen attack.

The four alloys that have been studied are representative of those proposed to replace 2 1/4Cr-1Mo. The Berkeley alloy has no additional carbide formers (beyond chromium and molybdenum) and utilizes nickel and a moderate amount of manganese to achieve adequate hardenability. The AMAX (Climax) alloy utilizes high manganese to obtain hardenability and a modest addition of vanadium to increase high temperature strength. The two JSW materials, both the 2 1/4Cr-1Mo and 3Cr-1Mo, utilize B to increase hardenability and relatively high vanadium content to increase high temperature strength.

In addition to the four modified materials, a standard 2 1/4Cr-1Mo alloy, Lukens 2 1/4Cr-1Mo-0.10C, has been employed in portions of this work. This material has been extensively studied by Richey[25] and the transformation characteristics and sensitivity to PWHT cracking, as determined by Gleeble simulation, has been reported.

This study has also employed three commercial heats of the modified 9Cr-1Mo alloy. The NKK, Sumitomo and Timken commercial heats of 9Cr-1Mo-V-Nb are quite similar in composition. The NKK heat has very low levels of phosphorous, 0.004%, sulphur, 0.004%, aluminum, 0.006%, and nickel, 0.01%. The Sumitomo heat has the highest phosphorous, 0.014%, and nickel, 0.10%, and the lowest vanadium, 0.20%, contents. The Timken material had the highest

levels of vanadium, 0.31%, aluminum, 0.027%, and sulphur, 0.007%, with an intermediate amount of phosphorous, 0.010%.

The chromium equivalents of the 9Cr-1Mo-V-Nb materials ranges from 9.59 for ORNL heat 176 (an experimental heat tested by Richey[25]) to a high of 13.42 for the Timken material. The chromium equivalent was determined by the equation:[106]

$$CrE = Cr + 6Si + 4Mo + 1.5W + 11V + 5Nb + 8Ti + 12Al - 40C - 30N - 4Ni - 2Mn - Cu \quad (3\text{-}1)$$

where all elements are in weight percent. The chromium equivalent can be used as a predictor of the degree of delta ferrite present on cooling after welding. For chromium equivalents above 12, substantial amounts of delta ferrite may be formed in the coarse grained heat affected zone, between 10 and 12, some delta ferrite may be formed and below 10, no delta ferrite is expected.[106] Thus, for ORNL heat 176 no delta ferrite would be expected while substantial amounts of delta ferrite may be present in the heat affected zone of the Timken alloy after welding.

The as received material form and heat treatment appears in Table 1. With the exception of the Berkeley 3cr-1Mo-1/2Ni alloy all materials were tested in the as-received condition. The as-received Berkeley material was given a low temperature, 1125°F (607°C), stress-relief following normalizing and as a result was in a hardened condition. Therefore some of the Berkeley 3cr-1 1/2Mo-1/2Ni material was subsequently heat treated for 24 1/2 hours at 1175°F (635°C) inorder to obtain a tensile strength within the limits of those proposed for the new SA 387 grade 22 class 3 classification.

Table 1. As received material condition.

MATERIAL	DESIGNATION	HEAT NO.	FORM	HEAT TREATMENT °F(°C)
9Cr-1Mo-V-Nb	NKK	HT-A-231001	1in (25mm) plate	Normalized 1900 (1040) Tempered 1400 (760)
9Cr-1Mo-V-Nb	Sumitomo	OYYC-9082	2in (50mm) OD tube	Normalized 1740 (950) Tempered 1440 (780)
9Cr-1Mo-V-Nb	Timken	82631	3 in (76mm) dia. bar	Normalized 1900 (1040) Tempered 1400 (760)
9Cr 1Mo-V-Nb	ORNL	176	3/8 in (9.5mm) plate	Normalized 1900 (1040) Tempered 1400 (760)
3Cr-1½Mo-V	AMAX (Climax)	A9349	4 in (102 mm) plate	Austenitized 1750 (955) Water Quenched Tempered 1050 (565)
3Cr-1½Mo-¼Ni	Berkeley	A9749	4 in (102 mm) plate 1 in (25 mm) plate	Normalized 1750 (955) Tempered 1125 (607)
3Cr-1Mo-V-Ti-B	JSW	---	18 in (450 mm) ring Forging Section	Normalized 1850 (1010) Tempered 1220 (660)
2¼Cr-1Mo-V-Ti-B	JSW	---	10 in (250 mm) forging 1 in (25mm) plate	Normalized 1830 (1000) Tempered 1200 (650)
2¼Cr-1Mo-0.10C	Lukens	3443	16 in (400 mm) ring	Austenitized 1960 (1070) Water Quenched Tempered 1200 (650)
2¼Cr-1Mo-0.12C	Lukens	BP3	13 in (150mm) plate	Austenitized 1780 (955) Water Quenched Tempered 1225 (655)

Although this classification applies to 2 1/4Cr-1Mo, it was felt that the requirements of this new classification could reasonably be extended to include the alloys proposed to replace 2 1/4Cr-1Mo. It will be noted throughout the following discussions whether the material was in the as received or heat treated condition.

Table 2 shows the chemical compositions of the alloys examined in this study. With the exception of the JSW 2 1/4Cr-1Mo-V-ti-B material, the analyses were performed by the Metallurgical Laboratory of Combustion Engineering in Chattanooga, Tennessee. The modified JSW 2 1/4Cr-1Mo material was analyzed at ORNL and the values reported in Table 2 represents an average composition for the forged section.

Table 2. Chemical compositions of materials studied.

			Composition (Weight %)																					
Heat	Designation	Supplier	C	Mn	P	S	Si	Ni	Cr	Mo	V	Nb	Ti	Co	Cu	Al	B	W	As	Sn	Zr	N	O	Cr.E
176	9Cr 1Mo V Nb	ORNL	0.081	0.37	0.010	0.003	0.11	0.09	8.61	0.89	0.21	0.07	<0.01	0.010	0.04	0.007	0.001	0.01	0.001	0.001	0.001	0.055		9.59
HCA 231001	9Cr 1Mo V Nb	NKK	0.10	0.41	0.004	0.004	0.41	0.01	8.36	0.98	0.22	0.07	<0.01	0.011	0.02	0.008	0.001	0.02	<0.001	0.002	<0.001	0.038	0.007	11.7
82631	9Cr 1Mo V Nb	Timken	0.095	0.41	0.010	0.007	0.42	0.09	8.76	1.00	0.21	0.08	<0.01	0.017	0.09	0.027	0.001	0.02	0.007	0.006	<0.001	0.036	0.003	13.42
OYYC 9082	9Cr 1Mo V Nb	Sumitomo	0.10	0.43	0.014	0.006	0.40	0.10	8.50	0.98	0.20	0.07	<0.01	0.010	0.04	0.011	<0.001	0.02	0.003	0.002	0.001	0.045	0.003	10.96
P2904	3Cr 1Mo 0.1V	AMAX	0.082	0.86	0.006	0.009	0.16	0.21	3.02	1.43	0.12	<0.01	<0.01	0.005	0.02	0.005	<0.001	0.01	0.001	0.001	0.001	0.010		
A9349 1A	3Cr 1Mo 0.1V	Lukens	0.11	0.86	0.012	0.001	0.26	0.11	2.94	1.42	0.09	0.01	<0.01	0.008	0.07	0.004	0.001	0.01	0.003	0.002	<0.001	0.013	0.003	
	3Cr 1Mo V Ti B	JSW	0.14	0.46	0.007	0.008	0.06	0.20	3.11	0.97	0.28	<0.01	0.02	0.014	0.09	0.003	0.003	0.01	0.008	0.006	<0.001	0.011		
9749	3Cr 1Mo 1Ni	Berkeley	0.16	0.52	0.010	0.003	0.28	0.51	3.05	1.48	0.007	<0.01	<0.01	0.010	0.11	0.005	<0.001	0.01	0.007	0.003	<0.001	0.033		
	2¼Cr 1Mo V Ti B*	JSW	0.12	0.48	0.007	0.008	0.06	0.15	2.31	0.98	0.26	-	0.033	-	0.08	0.016	0.0022	-	0.008	0.007	-	0.001	-	-
3443	2¼Cr 1Mo 0.12C	Lukens	0.12	0.41	0.006	0.003	0.22	0.02	2.27	1.05	0.01	<0.01	<0.01	0.008	0.08	0.008	<0.001	0.01	0.002	0.003	<0.001	0.015	0.004	
3PJ	2¼Cr 1Mo 0.10C	Lukens	0.10	0.44	0.006	0.026	0.19	0.16	2.18	1.02	0.01	<0.01	<0.01	0.014	0.15	0.003	0001	0.01	0.006	0.011	0.001	0.007	0.007	

CHAPTER IV

EXPERIMENTAL PROCEDURES

This investigation incorporated two areas of research: a determination of transformation temperatures and microstructures under welding conditions (for the coarse grained HAZ), an assessment of the susceptibility of the modified alloys to PWHT cracking. In each of these of these areas an essential research tool has been the Gleeble.

The Gleeble is a device that was developed at Rensselaer Polytechnic Institute[107] which allows simulation of the actual thermal cycles experienced at any particular point adjacent to a weld. While a region in the weld HAZ is small, use of the Gleeble permits expansion of the region of interest to a larger volume so that testing may be accomplished on that region alone.

Samples are mounted on the Gleeble in water cooled jaws, one fixed and the other free to move, which function as both electrical contact points and heat sinks. Electric current is passed between the jaws through the sample resulting in resistance heating of the sample. A maximum heating rate of 3000F°/sec (1650C°/sec) may be attained in this manner. Extraction of heat longitudinally by conduction to the copper jaws can result in cooling rates up to 350F°/sec (175C°/sec) at 1000°F (540°C). Temperature control is achieved by a high speed, time temperature control device which utilizes thermocouple potential for feedback. The thermocouple is

percussion welded to the surface of the sample midway between the copper jaws. The programmed reference signal and thermocouple potential are compared 120 times per second resulting in temperature control to within $\pm$ 15F° ($\pm$8C°). The thermocouple provides not only feedback to the controller but also an output signal for either a multi-channel light beam oscillograph or an X-Y chart recorder. The input impedance of either recording device is sufficiently high to prevent any significant perturbation of the the thermocouple voltage sampled by the controller.

The Gleeble is also capable of applying a tensile load up to 10,000 pounds (44.5kN) at any point in the thermal cycle. At the selected point, the controller energizes a solenoid valve supplying pressure regulated air to a pneumatic cylinder which is affixed to the moveable jaw. The load applied is determined from the output of an electrical resistance, strain gauge type of load cell attached to the ram of the pneumatic cylinder. The load cell output is recorded by the light beam oscillograph.

Phase Transformations

On-heating and on-cooling transformation temperatures are determined with the Gleeble utilizing a high speed dilatometer. The dilatometer employs a precision rectilinear potentiometer connected by a mechanical linkage to quartz rods in contact with opposite sides of the specimen mounted in the Gleeble. Changes in specimen diameter due to thermal expansion/contraction and phase changes result in a change in position of the potentiometer slider and therefore a change

in output voltage. The dilatometer is connected to the Gleeble and becomes one leg of a precision bridge circuit.

The output of the bridge circuit is fed to an X-Y chart recorder as the Y input. The voltage of the thermocouple percussion welded to the sample is utilized as the X input to the chart recorder. Thus, a plot of relative dilation versus temperature is obtained from the chart recorder. Figure 16 shows a schematic representation of such a dilation versus temperature plot. As indicated in Figure 16 the duration of transformation is determined by the points at which the trace deviates from linearity with the end points being the start and finish temperatures.

The transformation characteristics of the coarse grained HAZ are determined for welding heat inputs varying from those associated with shielded metal arc welding to submerged arc welding. A peak temperature of 2400°F (1315°C) is utilized with all thermal cycles in order to achieve a microstructure similar to that which occurs immediately adjacent to weld fusion zone. Figure 17 shows the six welding thermal cycles employed to determine the transformation temperatures. These six thermal cycles simulate weld heat inputs ranging from 18KJ/in (0.7KJ/mm), preheat 72°F (22°C) for a 2in (51mm) thick plate, to 150 KJ/in (59KJ/mm), preheat 400°F (205°C) for a 2in (51mm) thick plate. The 18KJ/in (0.7KJ/mm) thermal cycle is only approximate as the Gleeble is turned off upon reaching the peak temperature allowing cooling to occur as fast as heat could be extracted from the sample by conduction.

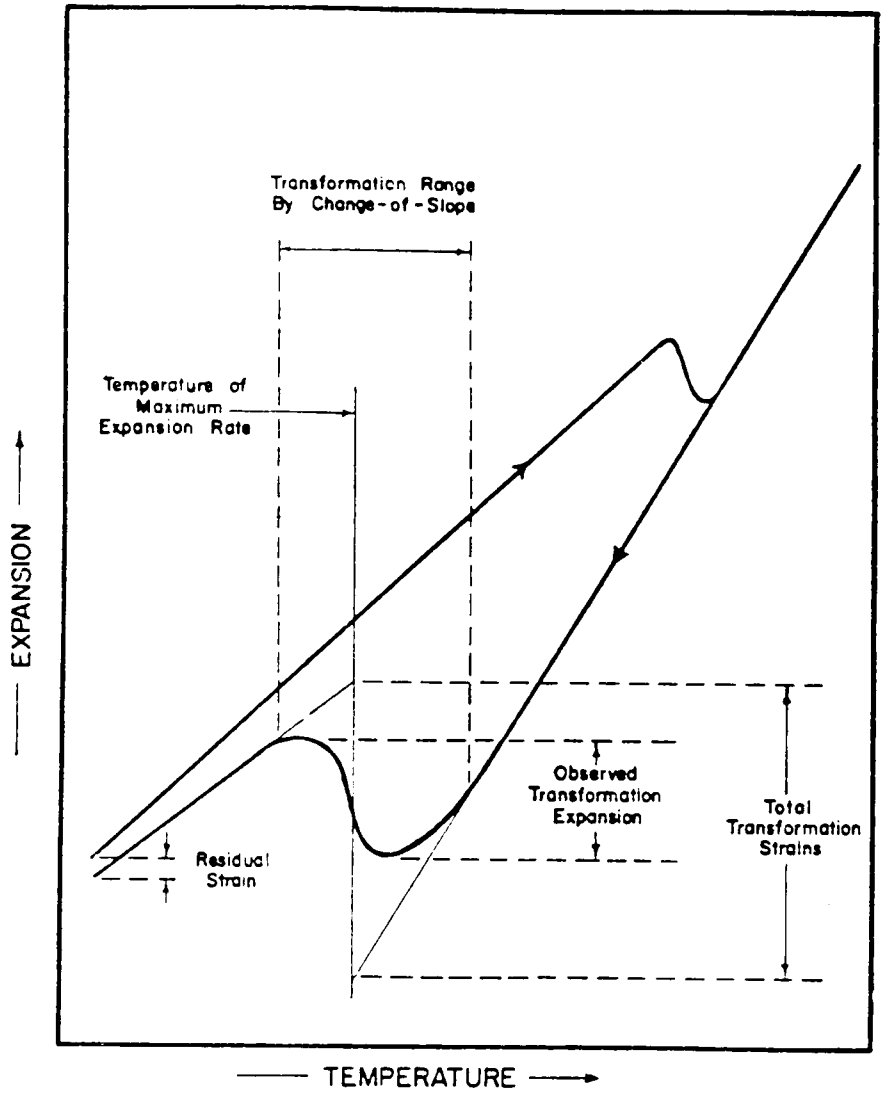


Figure 16. Schematic representation of dilatometric output for the determination of transformation temperatures.

Source: Torok, T.E. and Stout, R.D., Relation of Dilatometric Characteristics of Steels to Delayed Cracking in Welds, Welding Journal, 44(12), 1965.

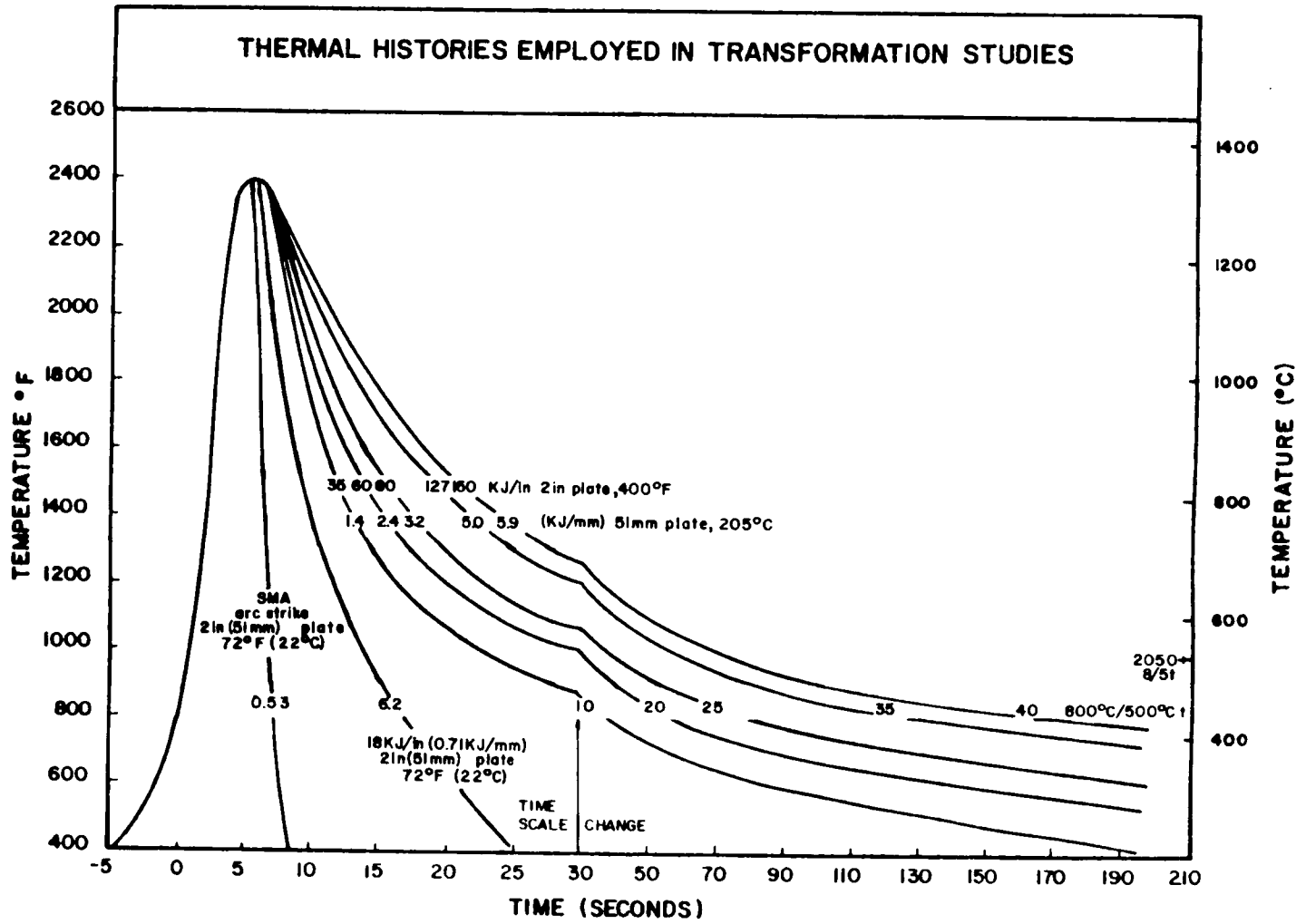


Figure 17. Thermal cycles employed in the determination of transformation temperations for welding conditions.

The seventh thermal cycle, indicated in Figure 17 as an arc strike, is simulated by turning off the Gleeble as the specimen reaches the peak temperature and simultaneously blasting the specimen with helium to achieve high radial heat loss as well as longitudinal conduction heat loss. This cycle is only employed to give a baseline, fastest possible cooling rate microstructure, for comparison with the microstructures obtained with the other six thermal cycles.

The samples employed in determination of the transformation temperatures are 0.250 inches (6.4mm) in diameter and 4 inches in length. Jaw separation is approximately 3/4 of an inch (19mm) thereby allowing three thermal cycles to be run on virgin material per sample. A minimum sample population of three thermal cycle runs is used for the determination of the on-cooling transformation temperatures for a particular thermal cycle. Since the on heating portion of each thermal cycle is the same, the on-heating transformation temperatures, A_{R1} and A_{R3}, for a particular material represent an average of a minimum of 18 values (from the six thermal cycles).

Postweld Heat Treatment Cracking

PWHT cracking is intergranular cracking that usually occurs in the coarse grained HAZ of a weld during PWHT or during service at elevated temperatures. This type of cracking is caused by a combination of matrix strengthening as a result of carbide precipitation, embrittlement of the grain boundaries as a result of

residual element segregation and both internal residual stress due to welding and externally applied stress.

The Gleeble was utilized to make an initial assessment of cracking susceptibility for all modified materials. Samples are initially subjected to a 60KJ/in (2.4KJ/mm) thermal cycle with a peak temperature of 2400°F (1315°C). This peak temperature was selected to obtain a microstructure similar to that in the coarse grained HAZ in an actual weld. Subsequent to thermal cycling, the sample is simultaneously loaded in tension to simulate the restraint stress experienced by the coarse grained HAZ and heated to the post weld heat treatment temperature. While the stress is held constant for an individual specimen, a range of stress levels is employed during the testing of a material in order to obtain various times to fracture.

The PWHT temperatures employed in this investigation are 1350°F (730°C) for the modified 9Cr-1Mo materials and both 1250°F (680°C) and 1150°F (620°C) for the 2 1/4Cr and 3Cr modified materials. The lower temperature employed for the 2 1/4Cr and 3Cr materials is representative of the trend to lower post weld heat treatment temperatures and higher strengths for these materials.

The duration of the hold at the PWHT temperature is a maximum of 200 minutes. If the sample does not fracture within the 200 minute period the test is terminated. The reduction in area of the fractured specimens is determined and selected sample fracture surfaces examined for microstructure features in with the scanning electron microscope.

In order to facilitate fractographic examination, several samples of each of the modified 2 1/4Cr and 3Cr materials were tested in an argon atmosphere. An atmosphere chamber was mounted between the Gleeble jaws and alternate evacuation and argon backfilling is undertaken to provide a suitable oxygen free atmosphere. After four cycles of evacuation and argon backfill the chamber is filled with argon and maintained at a slight positive pressure and the test sequence initiated. This technique resulted in fracture surfaces essentially free of oxidation.

Samples of the modified 3Cr-Mo and 2 1/4Cr-1Mo were prepared for transmission electron microscopy examination on the Gleeble by thermal cycling to 2400°F (1315°C) to produce a grain coarsened microstructure followed by a 100 minute simulated PWHT at 1250°F (680°C) with an applied load. The load employed was the highest possible that would not cause fracture or necking of the specimen within the 100 minute hold at the PWHT temperature. The specimens were sectioned at the point of thermocouple attachment with one half mounted and polished for utilization in the replica studies. Four 0.025 inch (0.64mm) thick sections were cut from the thermocouple end of the opposite half of the sample for use as thin foil specimen blanks. The mounted specimens and the thin sections were submitted to Dr. Judith Todd of the University of Southern California, Los Angeles, for final preparation and transmission electron microscopy evaluation.

Several objections may be raised to the Gleeble technique employed in the determination of PWHT susceptibility. A major

objection is that the Gleeble simulation does not represent the conditions present during PWHT, in that a constant load rather than a time dependent decreasing load is used. Also the effects of surrounding base metal and weld metal on the HAZ are not present in the Gleeble simulation which reproduces only a single portion of the HAZ. Finally, the samples employed were smooth 0.250 inch (6.4mm) round samples although stress-relief cracking is known to be associated with the presence notches at the surface or discontinuities in the interior of the weld.

With these objections in a mind the C-ring test, normally employed in testing for stress corrosion cracking tendency, was selected as a suitable small scale test specimen for verification of the results obtained from the Gleeble testing program. ASTM standard G-38[108] was followed for design of the C-ring specimens and for determination of the deflection necessary to achieve the initial stress state.

To incorporate a weld in the C-ring specimens a 1 inch by 1 inch (25mm x 25mm) square bar is machined with a flat bottomed groove parallel to the rolling direction at the plate surface. Groove geometry is modified in order to accommodate different diameter shielded metal arc welding electrodes. For 5/32 inch (4.0mm) diameter electrodes the groove walls are machined at a 40° angle radial from the center of the bar. For 1/8 inch (3.2mm) diameter electrodes the angle is 30°. In all cases the depth of the groove is 5/32 inch (4.0mm). Figure 18 is a drawing of the cross section

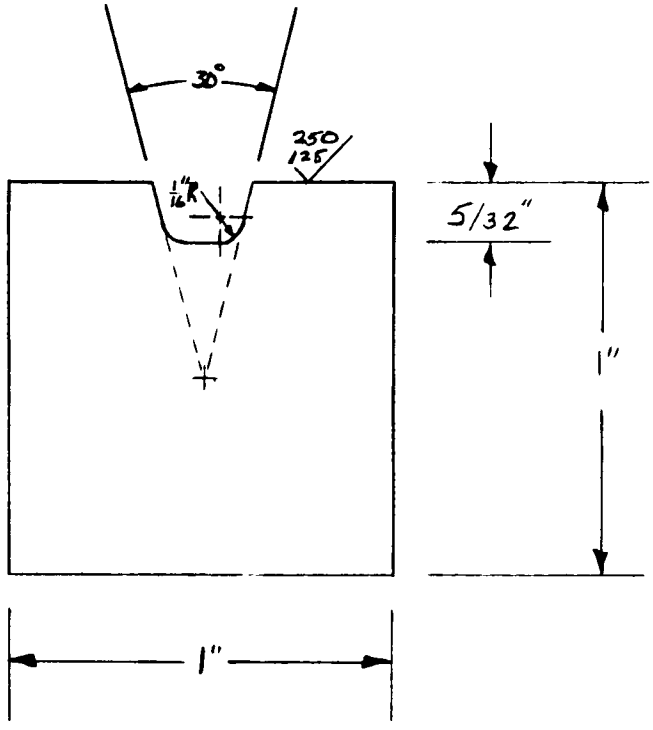


Figure 18. Groove geometry for 1/8" (3.2mm) shielded metal arc electrodes.

of a bar with a 30° angle groove for use with 1/8 inch (3.2mm) diameter electrodes.

A single pass shielded metal arc weld deposit is used to fill the groove (using matching chemistry electrodes whenever possible). The Berkeley 3Cr-1 1/2Mo-1/2Ni material is welded with matching chemistry 1/8 inch (3.2mm) shielded metal arc electrodes. The AMAX (Climax) 3Cr-1 1/2Mo-0.1V material is welded with matching chemistry 5/32 inch (4.0mm) electrodes. These electrodes were manufactured on a special lot basis by Combustion Engineering in Chattanooga, Tennessee. The JSW 3Cr-1Mo-V-Ti-B material is welded with the same electrodes as those used for the AMAX (Climax) 3Cr-1 1/2Mo-0.1V material. The JSW 2 1/4Cr-1Mo-V-Ti-B material and Lukens 2 1/4Cr-1Mo-0.10C material, used for baseline comparison, are welded with 5/32 inch (4.0mm) E9018-B3 electrodes.

The welded bars are machined into cylinders and surface ground to a fine, 32 RMS, finish. The cylinders have a nominal 1 inch outside diameter and 0.125 inch wall thickness. Rings, 0.750 inches long, are sectioned from the cylinders. The rings are etched with a 2% solution of hydrofluoric acid in 30% hydrogen peroxide in order to reveal the heat affected and fusion zones. A charpy V type notch, 0.035 inches (0.90mm) deep, is broached into one of the coarse grained heat affected zones and a hole drilled through the ring 90 degrees from the axis of the notch. The back of the ring, away from the notch, is removed in order to allow compression of the ring by

tightening of a bolt placed through the drilled holes. Figure 19 schematically shows the successive steps in production of the C-ring specimen from the welded bar to the finished C-ring.

The bolts employed for stressing the C-rings are machined from the Berkeley 3cr-1Mo-1/2Ni material. This is done so that the thermal expansion and stress relaxation properties in the bolts would be similar to those of the tested materials. Stress relaxation in the bolts is not found to be a significant factor since elongation of the bolt is only approximately 0.0005 inches (0.01mm) when the C-ring is loaded to a nominal stress of 100ksi (690MPa). This elongation corresponds to approximately 15ksi (103MPa) in the bolt which is not great enough to cause significant stress relaxation in the bolt during PWHT.

Tightening of the bolt through the C-ring results in a constant strain specimen with tensile stresses produced on the exterior of the ring. The amount of deflection of the outside diameter (OD) necessary to produce the desired stress is determined by the equation:[108]

$$\Delta = (f\pi D^2) \,/\, (4EtZ) \qquad (4\text{-}1)$$

where: f = the desired stress, D = the mean diameter (OD - t), t = the wall thickness, E = the modulus of elasticity, and Z = a correction factor for curved beams determined from a graph included in ASTM standard G38. This equation is modified for the presence of the notch by considering the outer fiber of the ring to be at the root of the notch rather than the outside surface. This results in the OD of the ring and thickness of the ring (t) being reduced by the

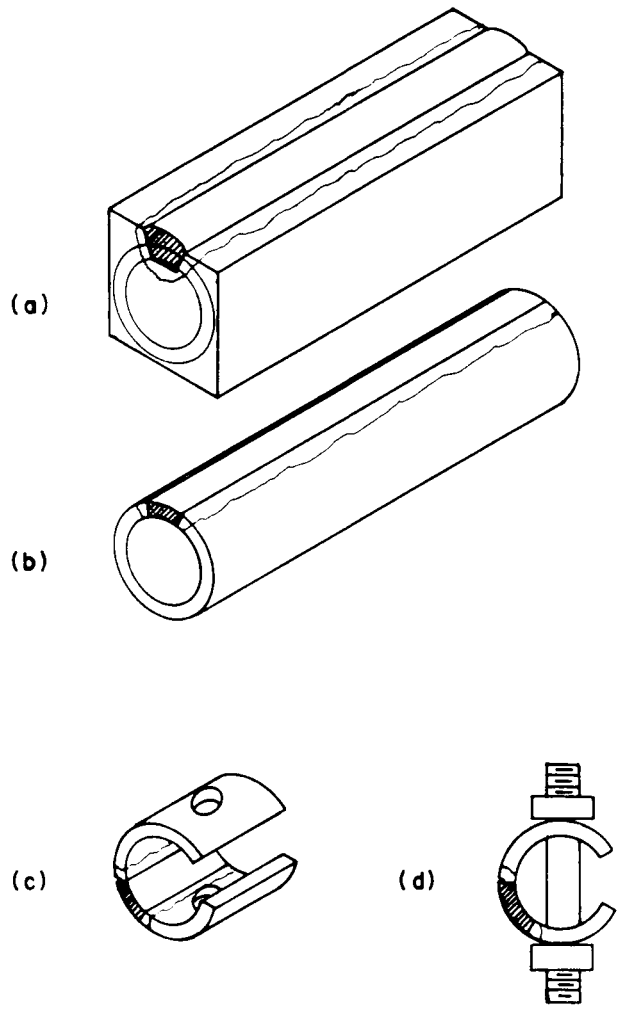


Figure 19. Successive steps in the making of C-rings specimens. (a)bar with weld filled groove, (b)tube machined from square bar stock, (c)portion of the tube notched in the heat affected zone with hole drilled through ring and back removed, and (d) finished C-ring with loading bolt in place.

depth of the notch. The deflection thus calculated is subtracted from the "true" OD to obtain the OD, parallel to the bolt, to which the ring has to be deformed to obtain the nominal stress level desired at the root of the notch.

The stress at the root of the charpy V type notch is considerably higher than the nominal outer fiber stress calculated above due to the induced stress concentration. Utilizing Peterson's[109] curves for the stress concentration factor resulting from bending of a flat bar with a U-shaped notch on one side, the stress concentration factor, K_t, is determined to be approximately 1.7. Thus the stress at the root of the notch for a nominal outer fiber stress of 100ksi (690MPa) would be approximately 170ksi (1200MPa). Based on an average hardness of 400DPH (approximately 380BHN) obtained in the transformation studies for the modified 2 1/4 and 3Cr materials, the coarse grained HAZ has an ultimate strength of approximately 190ksi (1300MPa). A 100ksi (690MPa) applied load should therefore not exceed the ultimate strength of the coarse grained HAZ.

A nominal stress of 100ksi (690MPa) is employed at PWHT temperatures of 1150°F (620°C) and 1250°F (680°C). The initial stress of 100ksi (690MPa) was chosen to insure that plastic deformation had occurred at the root of the notch and therefore that the stress level is of yield stress magnitude. Additional testing is performed at 1150°F (620°C) at stress levels of 80ksi (550MPa) and 60ksi (410MPa) in order to attempt to discern differences in

susceptibility of materials that exhibit cracks at the 100ksi (690MPa) stress level.

C-ring specimens are PWHT in air and under vacuum. The specimens heat treated in vacuum are placed in quartz tubes and the tubes evacuated and sealed. Selected specimens heat treated in vacuum are broken open after being cooled in liquid nitrogen and examined in the scanning electron microscope. The remaining specimens heat treated in vacuum are sectioned into six pieces, mounted, and examined metallographically. The maximum extent (depth) of cracking in the sections is noted. The samples post weld heat treated in air are cooled in liquid nitrogen and broken open. Oxidation of the C-rings heat treated in air simplifies evaluation of the extent cracking as the intergranular fracture surface is darkened while the cleavage fracture surface is bright. The maximum depth of intergranular fracture is determined and used as the parameter for evaluation of PWHT cracking susceptibility.

CHAPTER V

RESULTS AND DISCUSSION

Transformation Behavior

The formation of cracks in weldments fabricated from the Cr-Mo steels is most often found to occur in the coarse grained heat affected zone. The types of cracking most often associated with welds in these alloys, PWHT cracking hydrogen and assisted cracking, result from the high residual tensile stress state in and metallurgical condition of this region. Therefore, the first step in determining the weldability of these materials is the determination of the transformation characteristics and microstructure of the coarse grained heat affected zone.

The coarse grained heat affected zone in actual welds is a narrow region adjacent to the fusion zone that experiences a gradient of peak temperatures associated with the upper temperature regimes of the austenite region in the equilibrium phase diagram. The limited extent of the coarse grained HAZ and temperature the steep gradient experienced over this region make characterization of the coarse grained heat affected zone in actual welds difficult. Gleeble simulation permits the expansion of this portion of the heat affected zone associated with a single peak temperature to a volume sufficient for mechanical testing and facilitates metallographic examination.

Gleeble simulation of the coarse grained heat affected zone was achieved in the transformation studies by employing a peak

temperature of 2400°F (1320°C) and thermal cycles representative of a variety of welding conditions. The transformation temperatures associated with welding conditions were determined by the use of a high speed dilatometer in contact with the specimen during the thermal cycle. When the dilatometer output is coupled by the appropriate electronic circuitry to an X-Y chart recorder, a relative dilation versus temperature plot is obtained from which the transformation temperatures may be determined. Selected thermal cycled samples were sectioned at the point of thermocouple attachment, mounted, polished, and examined by both optical microscopy and scanning electron microscopy to determine the on-cooling transformation microstructures over the range of simulated welding conditions employed.

Transformation Results for the 9Cr-1Mo-V-Nb Materials.

The V-Nb modified 9Cr-1Mo alloys have been shown to possess high hardenability in Jominy tests, exhibiting uniform hardness over the length of the Jominy bar.[94] Bodine et al.[117] have shown that the modified 9Cr-1Mo alloys "invariably transform to martensite on cooling after normalization, irrespective of the cooling rate used." Based on these observations and the continuous cooling transformation diagram for a 9Cr-1Mo-V-Nb alloy (Figure 7, page 14), it was anticipated that a martensitic microstructure would result in the coarse grained heat affected zone for all thermal cycles employed in the transformation investigation. Therefore, only three weld thermal cycles were utilized to characterize the transformation behavior of

the three commercial 9Cr-1Mo-V-Nb heats. The three thermal cycles employed were the nominal 18KJ/in (0.71KJ/mm), 35KJ/in (1.4KJ/mm), and 150KJ/in (5.9KJ/mm) heat input weld simulations.

The on-heating transformation temperatures, A_{C1} and A_{C3}, for the NKK 9Cr-1Mo-V-Nb, Sumitomo 9Cr-1Mo-V-Nb, and Timken 9Cr-1Mo-V-Nb are shown in Table 3. For these materials the A_{C1} temperatures range from 1620° to 1640°F (880 to 895°C) and the A_{C3} temperatures range from 1750 to 1770°F (940 to 950°C). A comparison of the A_{C1} and A_{C3} temperatures obtained for the three commercial heats with the A_{C1} and A_{C3} temperatures (1526°F (830°C) and 1661°F (905°C) respectively) shown on the continuous cooling transformation diagram (Figure 7, page 14) shows that the fast heating rate associated with welding has resulted in an increase of the on-heating transformation temperatures. The A_{C1} temperatures have been increased between 94 and 124F° (50 and 65C°) and the A_{C3} temperatures have been increased between 89 and 109F° (35 and 45C°).

The on-cooling transformation temperatures, M_s and M_f, for the NKK, Timken, and Sumitomo 9Cr-1Mo-V-Nb materials are shown in Table 4. The M_s temperatures range from 755 to 710°F (400 to 375°C) and the M_f temperatures range from 540 to 495°F (280 to 260°C). The M_s and M_{f90} temperatures obtained from the continuous cooling transformation diagram (Figure 7, page 14) are 716°F (380°C) and 545°F (285°C) respectively. Thus, the M_s and M_f temperatures obtained for the NKK, Timken, and Sumitomo under welding conditions agree reasonably well with those from the conventional continuous cooling transformation diagram. The M_s temperatures are within +36

Table 3. Summary of the on-heating transformation temperatures for the 9Cr-1Mo-V-Nb alloys.

Material	Supplier	A_{C1}		A_{C3}	
		°F	(°C)	°F	(°C)
9Cr-1Mo-V-Nb-0.10C	NKK	1640	(895)	1750	(950)
9Cr-1Mo-V-Nb 0.095C	Timken	1620	(880)	1750	(950)
9Cr-1Mo-V-Nb-0.10C	Sumitomo	1630	(890)	1770	(940)

Table 4. Summary of the on-cooling transformation temperatures for the 9Cr-1Mo-V-Nb alloys.

Material	Supplier	18KJ/in		35 KJ/in		150 KJ/in	
		M_S °F (°C)	M_f °F (°C)	M_S °F (°C)	M_f °F (°C)	M_S °F (°C)	M_f °F (°C)
9Cr-1Mo-V-Nb	NKK	755 (400)	520 (270)	710 (375)	495 (260)	730 (390)	530 (275)
9Cr-1Mo-V-Nb	Timken	720 (380)	530 (275)	735 (390)	540 (280)	740 (395)	535 (280)
9Cr-1Mo-V-Nb	Sumitomo	735 (390)	535 (280)	715 (380)	515 (270)	730 (390)	520 (270)

to -9F° (+20 to -5C°) and the M_f temperatures are within +9 to -45F° (+5 to -25C°) of the M_s and M_{f90} temperatures shown in Figure 7 (page 14).

Figure 7 (page 14) shows that the last 10% of the austenite to martensite transformation occurs between 716°F (380°C), the M_{f90} temperature, and 536°F (280°C), the M_f temperature. This small amount of transformation over a relatively large temperature range is not likely to have been detected in the Gleeble transformation studies. System sensitivity, electronic noise and small variations that occur in the slope of the dilation versus temperature trace combine to obscure a minor amount of transformation over a wide temperature range. However, in a practical sense, the M_f for the modified materials obtained by Gleeble simulation is sufficiently accurate for the purpose of weldability assessment.

9Cr-1Mo-V-Nb Microstructures. Optical micrographs of the Gleeble simulated 18KJ/in (0.71KJ/mm) and 150KJ/in (5.9KJ/mm) weld thermal cycle specimens of the NKK 9Cr-1Mo-V-Nb, Sumitomo 9Cr-1Mo-V-Nb, and Timken 9Cr-1Mo-V-Nb are shown in Figures 20 through 25. Scanning electron micrographs of the 150KJ/in (5.9KJ/mm) for the three 9Cr-1Mo-V-Nb heats are shown in Figures 26 through 29.

The optical micrographs (Figures 20-25) reveal little about the microstructure of the 9Cr-1Mo-V-Nb materials. A comparison of the 150KJ/in micrographs (Figures 20, 22, and 24) with the 18KJ/in (0.71KJ/mm) micrographs (Figures 21, 23, and 25) shows a modest amount of grain coarsening which would be anticipated with the longer

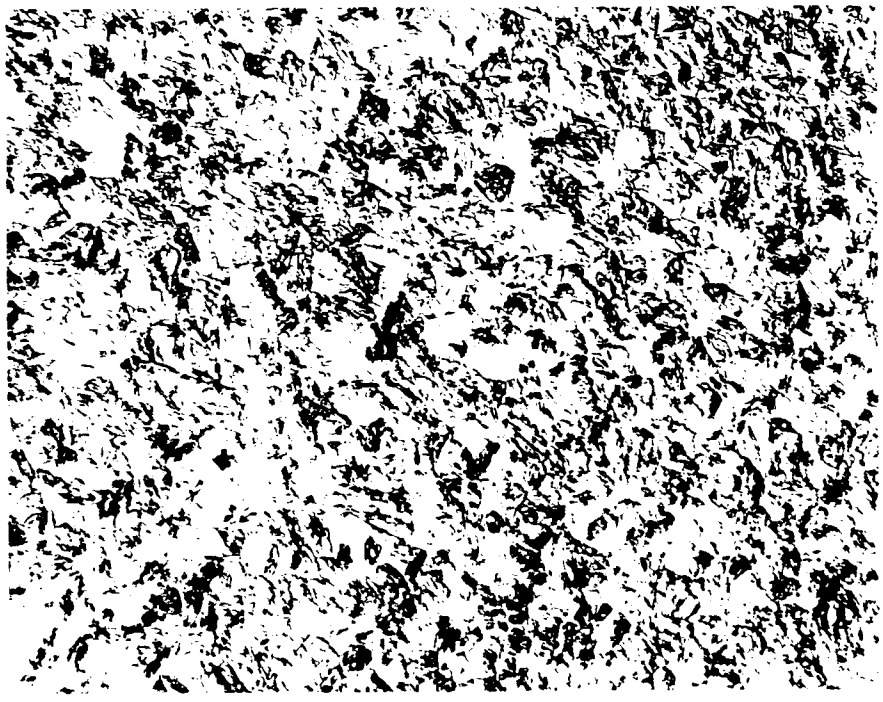


Figure 20. NKK 9Cr-1Mo-V-Nb CCT specimen, 18KJ/in. Modified Wazu's etch, OLM 200X.

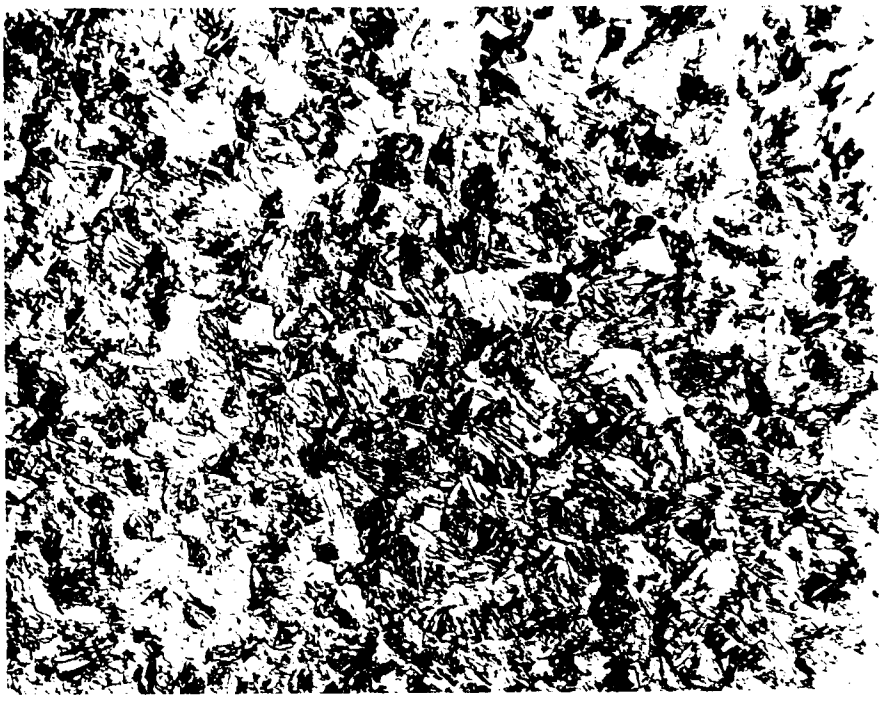


Figure 21. NKK 9Cr-1Mo-V-Nb CCT specimen, 150KJ/in. Modified Wazu's etch, OLM 200X.

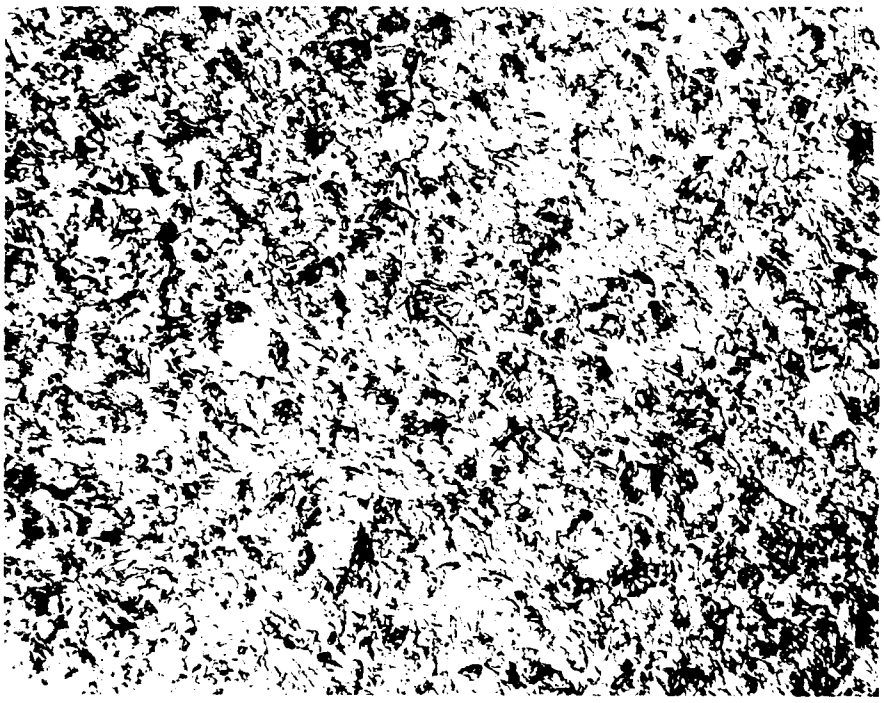


Figure 22. Sumitomo 9Cr-1Mo-V-Nb CCT specimen, 18KJ/in. Modified Wazu's etch, OLM 200X.

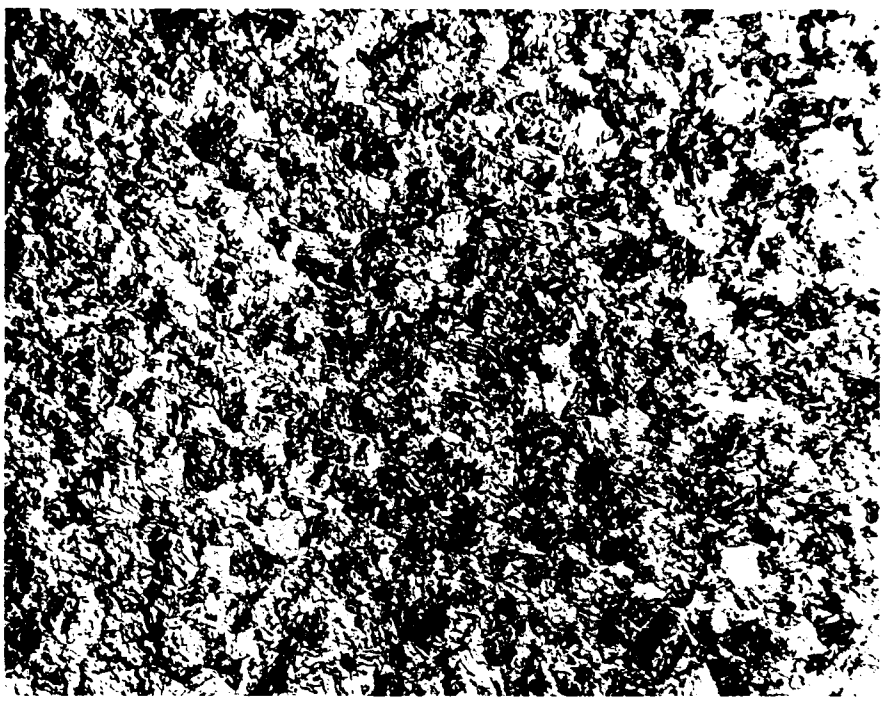


Figure 23. Sumitomo 9Cr-1Mo-V-Nb CCT specimen, 150KJ/in. Modified Wazu's etch, OLM 200X.

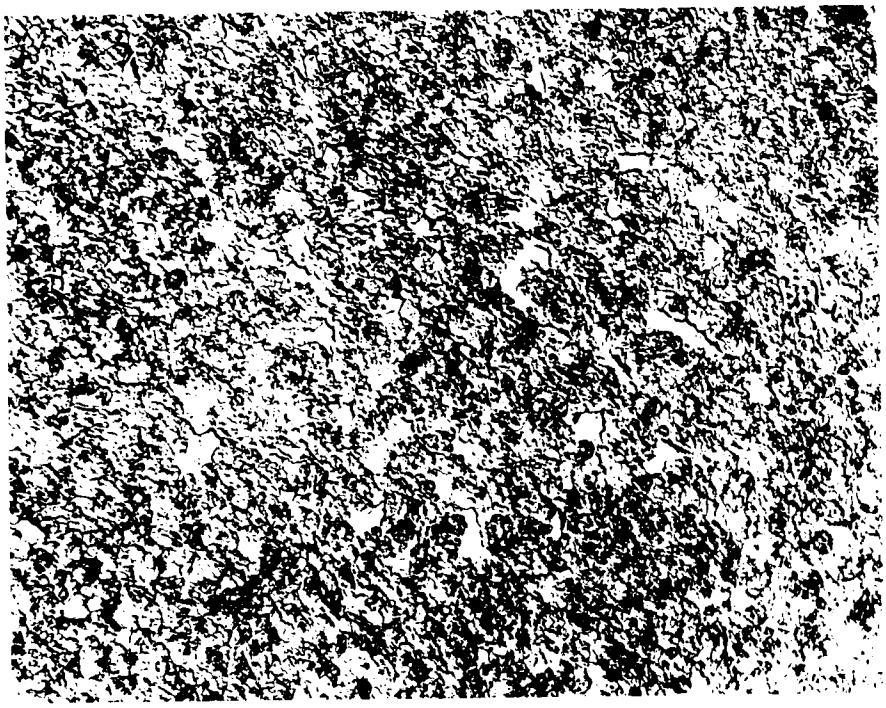


Figure 24. Timken 9Cr-1Mo-V-Nb CCT specimen, 18KJ/in. Modified Wazu's etch, OLM 200X.

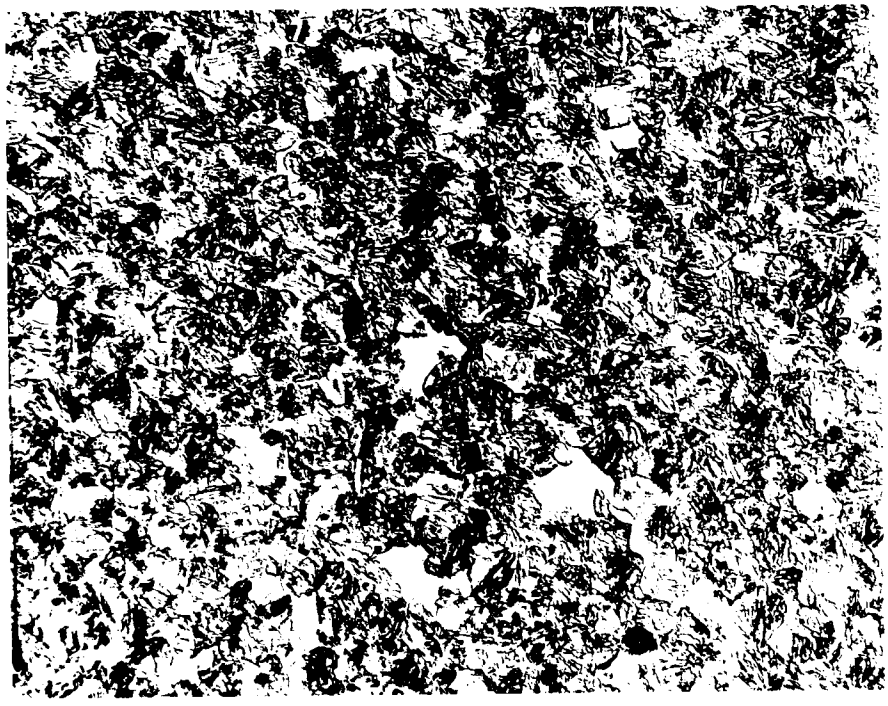
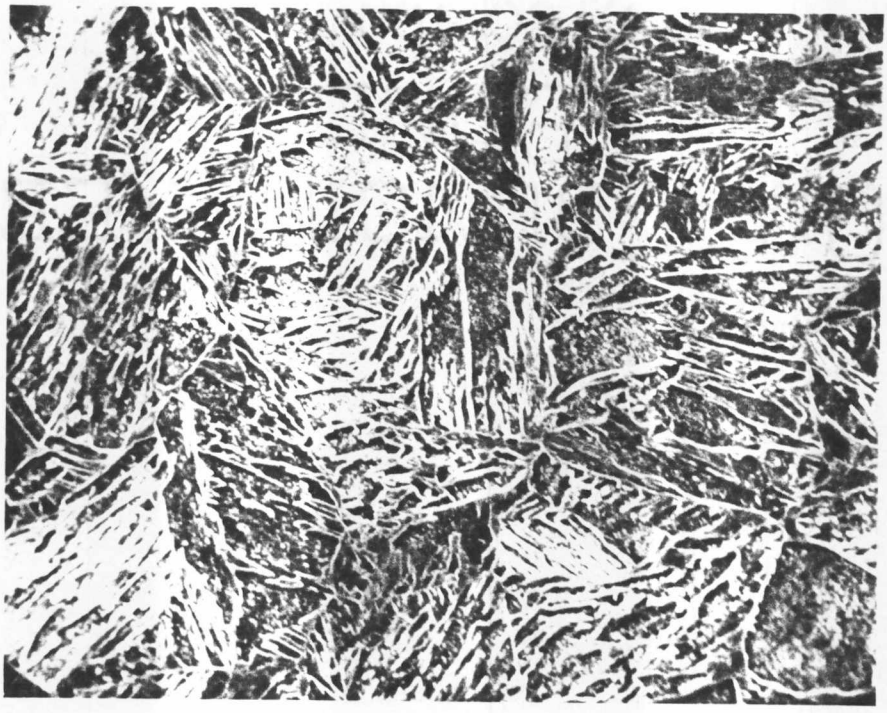


Figure 25. Timken 9Cr-1Mo-V-Nb CCT specimen 150KJ/in. Modified Wazu's etch, OLM 200X.



A



B

Figure 26. NKK 9Cr-1Mo-V-Nb CCT specimen, 150KJ/in. Modified Wazu's etch, SEM. a) 2,000X, b) 10,000X.

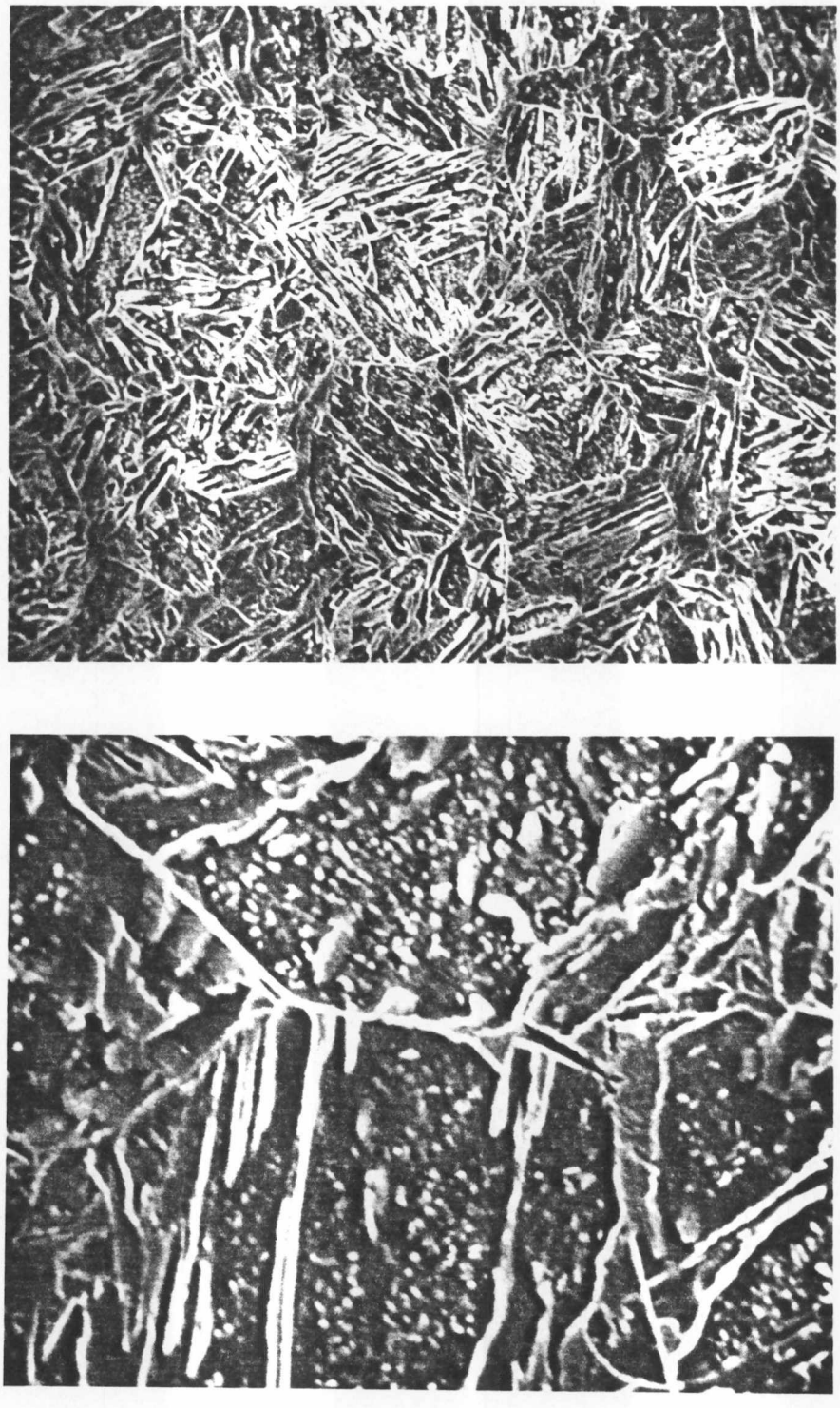


Figure 27. Sumitomo 9Cr-1Mo-V-Nb CCT specimen, 150KJ/in. Modified Wazu's etch, SEM. a) 2,000X, b) 10,000X.

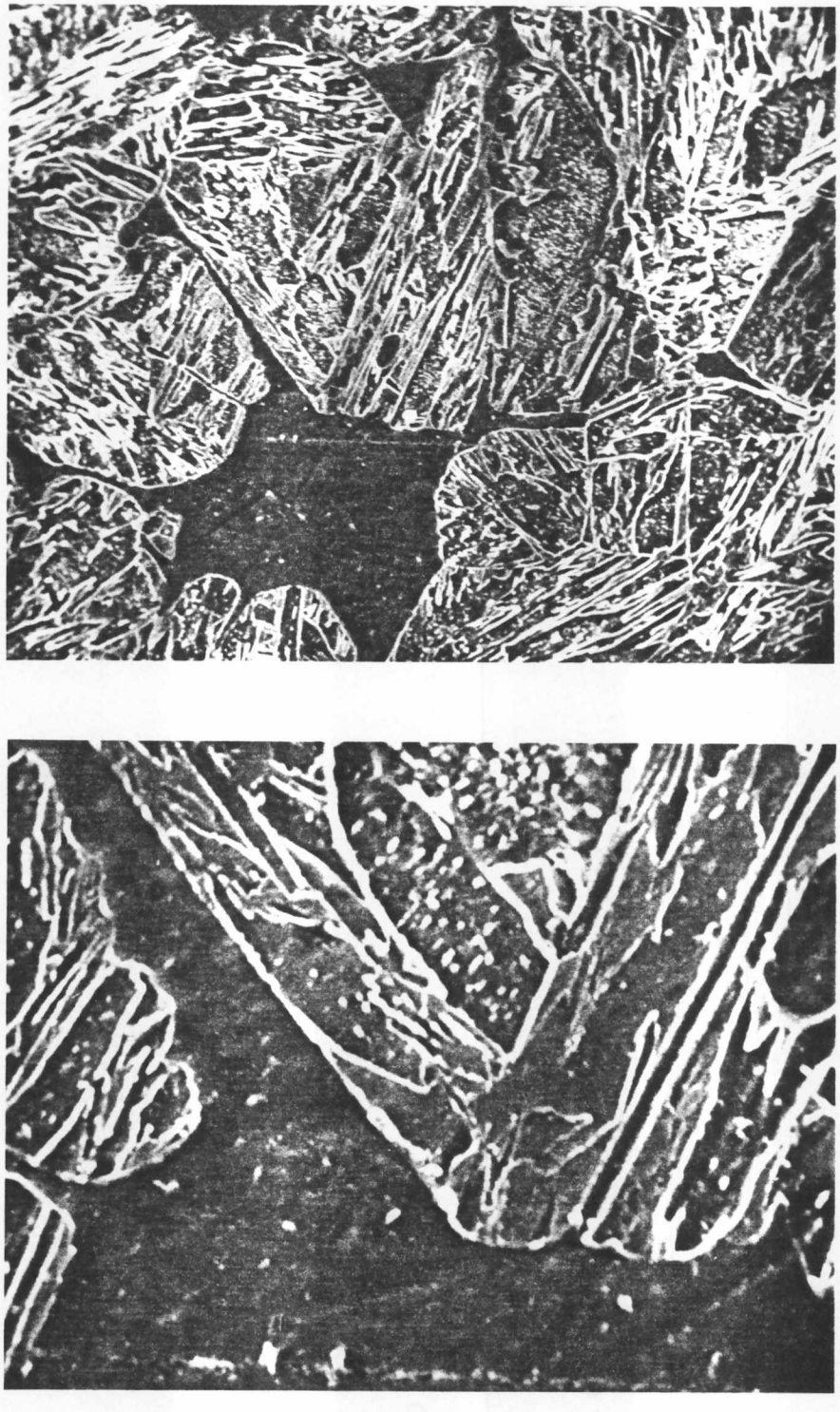


Figure 28. Timken 9Cr-1Mo-V-Nb CCT Specimen, 150KJ/in. Modified Wazu's etch SEM. a) 2,000X, b) 10,000X.

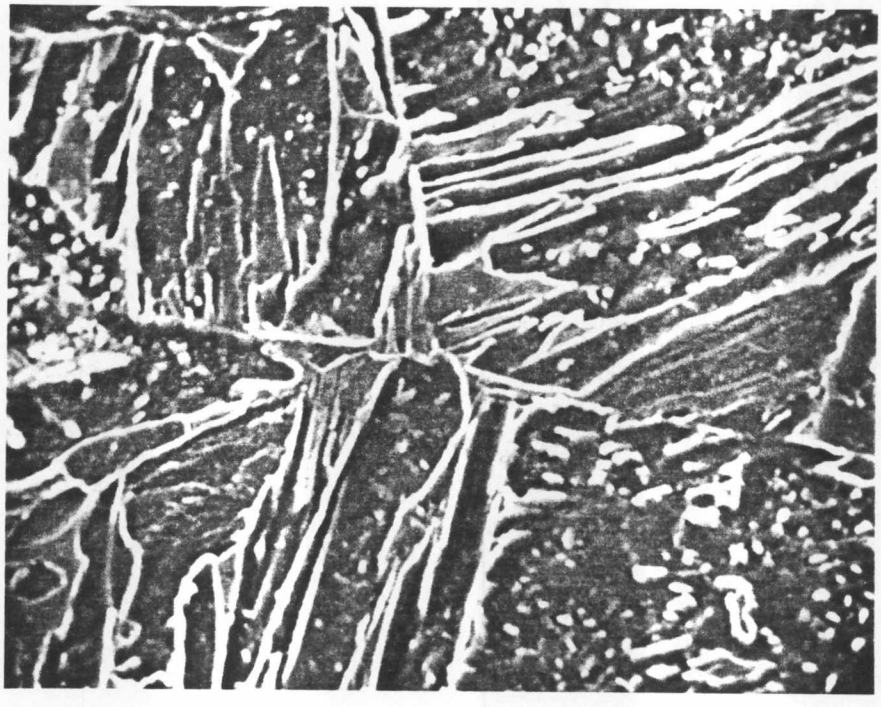


Figure 29. Timken 9Cr-1Mo-V-Nb CCT specimen, 150KJ/in. Modified Wazu's etch. SEM 10,000X.

time above the grain coarsening temperature associated with the higher energy input thermal cycle. Delta ferrite is present in both of the Timken 9Cr-1Mo-V-Nb optical micrographs (Figures 24 and 25) with the delta ferrite in the 150KJ/in (5.9KJ/mm) specimen present in larger and more widely spaced pools.

The scanning electron micrographs of the NKK 9Cr-1Mo-V-Nb (Figure 26)and Sumitomo 9Cr-1Mo-V-Nb (Figure 27) materials show microstructures consisting of acicular martensite and autotempered martensite. The autotempered martensite appears more clearly at the lower magnification, 2000X, (Figures 26a and 27a) as irregular, roughened, lenticular structures. Similar microstructures are shown in De Ferri Metallographia[110] for quenched 2 1/4Cr-1Mo (900°C to 500°C in 0.7sec) and 5Cr-1Mo (oil quenched from 950°C) with the lenticular, roughened structures described as being due to autotempering of the first martensite formed from the austenite. The roughening of the plate like structures is said to result from the formation of carbides during autotempering. At higher magnification, 10,000X, (Figures 26b and 27b) the roughening in the plate like structures observed at lower magnification can clearly be seen to be due to the formation of carbides within the autotempered martensite.

The scanning electron micrographs of the Timken 9Cr-1Mo-V-Nb material (Figures 28 and 29) show the microstructure to consist of martensite, autotempered martensite and delta ferrite. The large pool of delta ferrite shown in Figure 28 was located at a triple point in the prior austenite microstructure. The narrow regions of delta ferrite extending from the main pool are disposed along the

prior austenite grain boundaries. The presence of residual scratches, from polishing, within the pool may be used as additional evidence that this structure consists of ferrite, as ferrite is an inherently softer constituent than martensite.

The retention of delta ferrite, the elevated temperature body centered cubic phase, is a result of stabilization of the high temperature ferrite phase. 9Cr-1Mo alloys have a composition near the austenite-ferrite phase boundary of the iron-chromium equilibrium phase diagram. The addition of ferrite stabilizing elements such as silicon, molybdenum, vanadium and niobium may result in an alloy that exists in the two phase region over a large temperature range. Since the decomposition of ferrite to austenite is a diffusion controlled process, rapid cooling and a low ferrite to austenite transformation temperature combine to result in retention of delta ferrite in the ambient temperature microstructure.[25] Work performed at ORNL has shown that for normalizing heat treatments, the chromium equivalent equation (equation 3.1, page 62) can be utilized to predict the retention of delta ferrite in the microstructure.[117] For chromium equivalents in excess of 12 normalizing was found to result in the retention of substantial amounts of delta ferrite. The Timken 9Cr-1Mo-V-Nb alloy, with a chromium equivalent of 13.4, had delta ferrite retained in the Gleeble simulation microstructures as would be anticipated from the work performed at ORNL. The NKK and Sumitomo heats, with chromium equivalents of 11.7 and 10.6, did not exhibit delta ferrite retention in the optical or scanning electron micrographs although the work at ORNL indicated that delta ferrite

might be present for 9Cr-1Mo-V-Nb alloys with chromium equivalents between 10 and 12.

Figure 29 is a scanning electron micrograph of a region well removed from the delta ferrite in the Timken 9Cr-1Mo-V-Nb material. The microstructure is similar to that of the NKK 9Cr-1Mo-V-Nb and the Sumitomo 9Cr-1Mo-V-Nb (Figures 26b and 27b). The microstructure consists of both acicular martensite and autotempered martensite. Figure 29 again shows that the roughening of the auto tempered martensite is due to the formation of carbides within the plate like structures.

Summary of the 9Cr-1Mo-V-Nb Transformation Studies. The on-heating and on-cooling transformation temperatures for the NKK 9Cr-1Mo-V-Nb, Sumitomo 9Cr-1Mo-V-Nb, and Timken 9Cr-1Mo-V-Nb alloys were found to be approximately the same as would be expected from their similar chemical compositions. The A_{C1} and A_{C3} temperatures were found to be higher under the rapid heating of the simulated welding thermal cycle in comparison to those determined by Wada et al. (Figure 7, page 14). This elevation of the on-heating temperatures was expected as the formation of austenite is diffusion controlled. The on-cooling transformation temperatures are in substantial agreement with those shown on the continuous cooling transformation diagram (Figure 7, page 14). The formation of martensite occurs by a diffusionless, shear process and therefore depression of the transformation temperature would not be expected to be significant. With the exception of the Timken material the

microstructures of the weld simulated specimens were martensitic as was predicted by the continuous cooling transformation diagram. The microstructure of the Timken alloy contained retained delta ferrite due to the increased amount of ferrite stabilizing elements which was reflected in the higher value of the chromium equivalent in comparison to the NKK and Sumitomo materials. The presence of delta ferrite in the Timken material was in agreement with work performed at ORNL with normalized 9Cr-1Mo-V-Nb alloys.

Transformation Results for the Modified 2 1/4Cr and 3Cr Alloys.

The on-heating transformation temperatures for the AMAX (Climax) 3Cr-1 1/2Mo-0.1V (heat A9349), Berkeley composition 3Cr-1 1/2Mo-1/2Ni, JSW 3Cr-1Mo-V-Ti-B, and JSW 2 1/4Cr-1Mo-V-Ti-B alloys appear in Table 5. The on-cooling transformation temperatures determined for the modified 2 1/4Cr and 3Cr materials appear in Table 6. Figures 30 through 33 are continuous cooling transformation diagrams determined under simulated welding conditions for the AMAX (Climax) 3Cr-1 1/2Mo-0.1V, Berkeley 3Cr-1 1/2Mo-1/2Ni, JSW 3Cr-1Mo-V-Ti-B, and JSW 2 1/4Cr-1Mo-V-Ti-B materials.

The A_{C1} and A_{C3} temperatures for the Berkeley 3Cr-1 1/2Mo-1/2Ni material (Table 5) are dramatically increased by the additional heat treatment given to the as received material. The as received material, which had been given only a short time, low temperature stress-relief heat treatment, exhibited A_{C1} and A_{C3} temperatures of 1325°F (720°C) and 1570°F (850°C) respectively. After heat treatment to obtain a strength level concomitant with the proposed class III

Table 5. Summary of the on-heating transformation temperatures for the modified 3Cr and 2 1/4Cr alloys.

Material	A_{C1}		A_{C3}	
	°F	(°C)	°F	(°C)
Amax (Climax) 3 Cr-1½Mo-0.1	1490	(810)	1660	(905)
Berkeley 3 Cr-1½Mo-½Ni	1325	(720)	1570	(850)
Berkeley heat treated to Class III	1515	(825)	1630	(890)
JSW 3 Cr-1Mo-V-Ti-B	1480	(805)	1620	(880)
JSW 2¼ Cr-1Mo-V-Ti-B	1500	(815)	1670	(910)

Table 6. Summary of the on-cooling transformation temperatures for the modified 3Cr and 2 1/4Cr alloys.

Thermal Cycle (KJ/in)		Climax (A9349) 3 Cr-1½ Mo-0.1V		Berkeley 3 Cr-1½ Mo - ½ Ni		Berkeley Heat Treated to Class III		JSW 3Cr-1Mo-V-Ti-B		JSW 2¼ Cr-1Mo-V-Ti-B	
		°F	(°C)	°F	(°C)	°F	(°C)	°F	(°C)	°F	(°C)
18	S	820	(435)	790	(420)	790	(420)	830	(440)	880	(470)
	F	620	(325)	620	(325)	575	(300)	640	(340)	640	(340)
35	S	820	(435)	770	(410)	780	(415)	800	(425)	880	(470)
	F	680	(360)	650	(345)	650	(345)	660	(350)	670	(355)
60	S	820	(435)	770	(410)	775	(415)	810	(430)	890	(475)
	F	710	(375)	630	(330)	630	(330)	690	(365)	680	(360)
80	S	810	(430)	790	(420)	-	-	800	(425)	900	(480)
	F	720	(380)	710	(375)	-	-	690	(365)	700	(370)
127	S	840	(450)	820	(435)	-	-	840	(450)	900	(480)
	F	730	(385)	710	(375)	-	-	750	(400)	740	(395)
150	S	850	(455)	830	(445)	840	(450)	860	(460)	940	(505)
	F	740	(395)	730	(385)	715	(300)	760	(405)	770	(410)

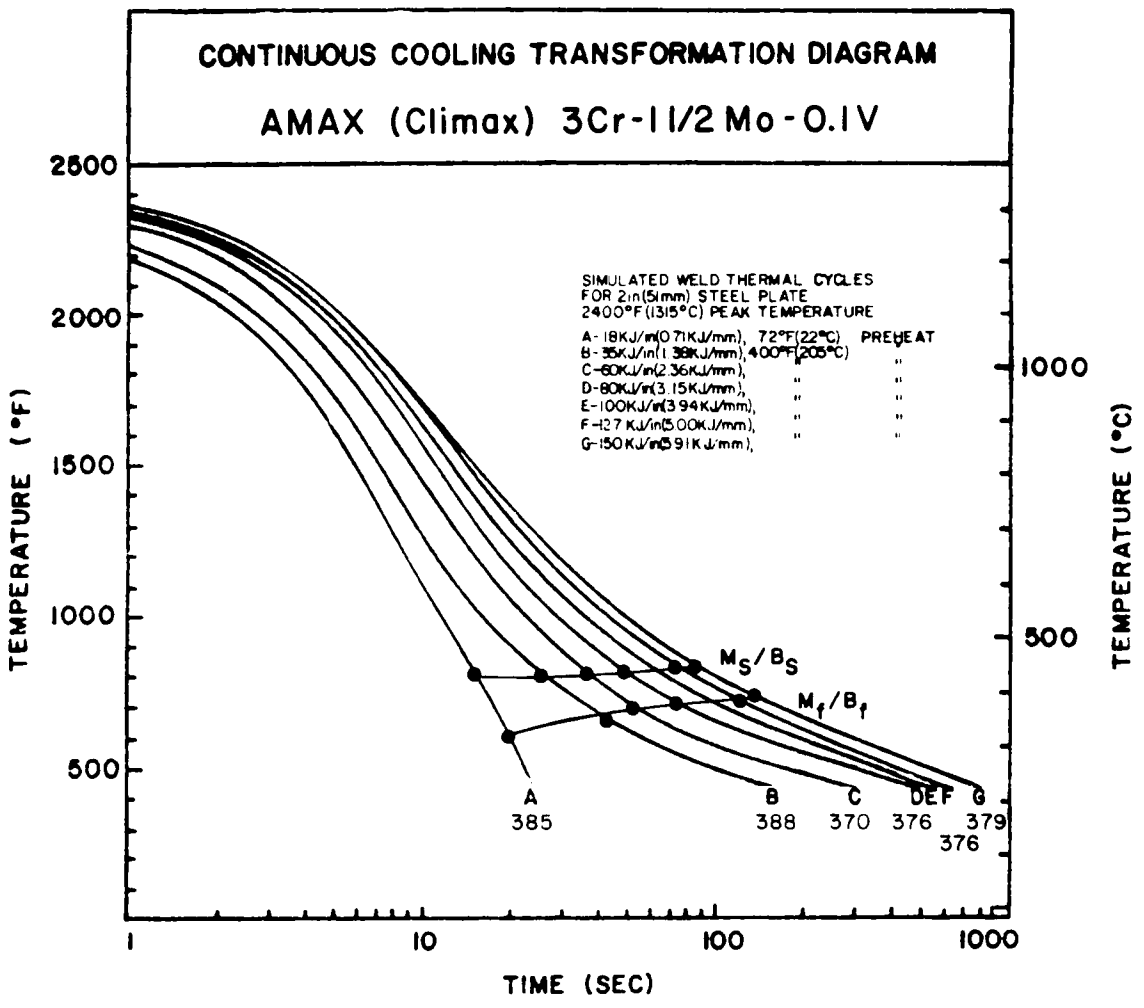


Figure 30. CCT diagram for AMAX (climax) 3Cr-1 1/2Mo-0.1V, determined for welding conditions.

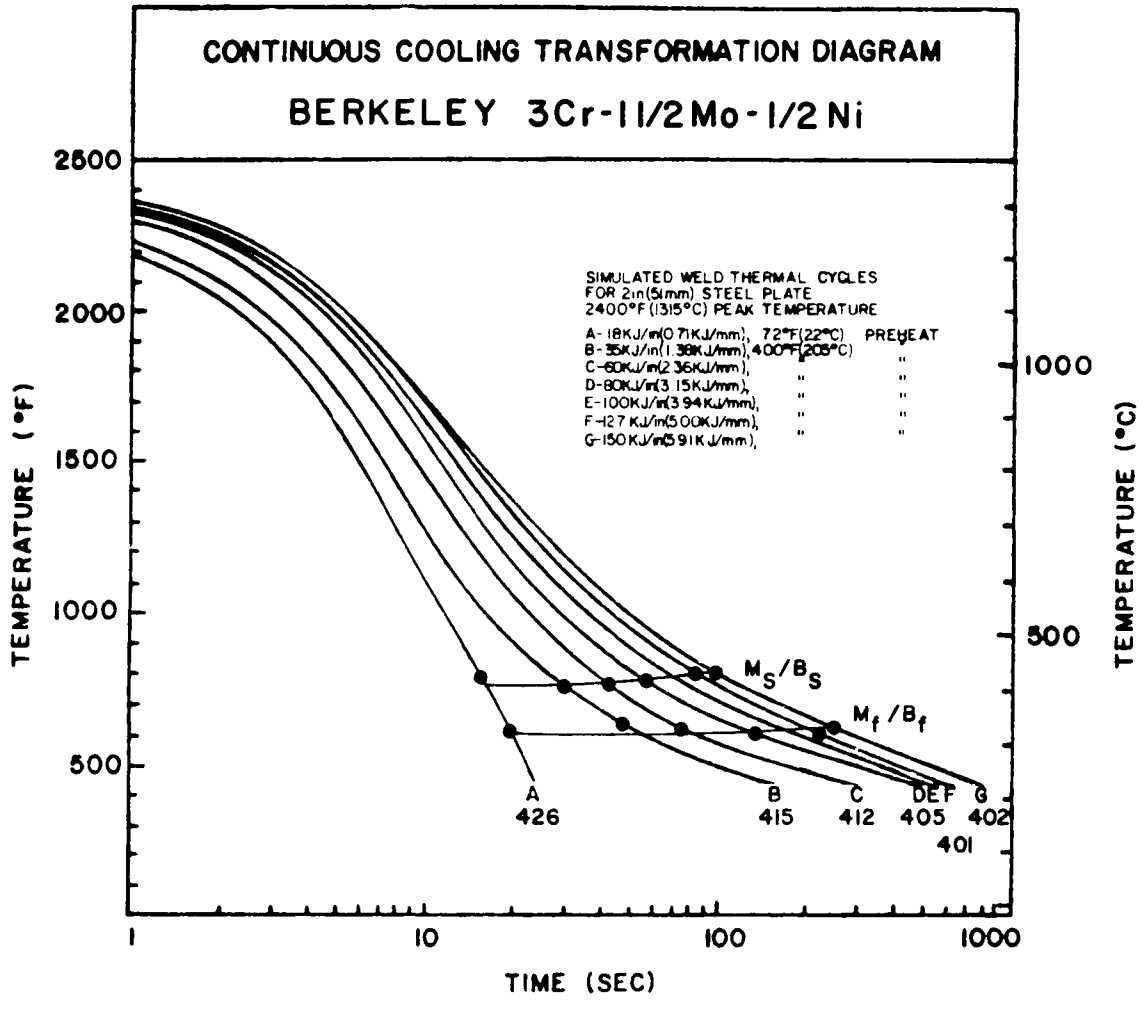


Figure 31. CCT diagram for Berkeley composition 3Cr-1 1/2Mo-1/2Ni, determined for welding conditions.

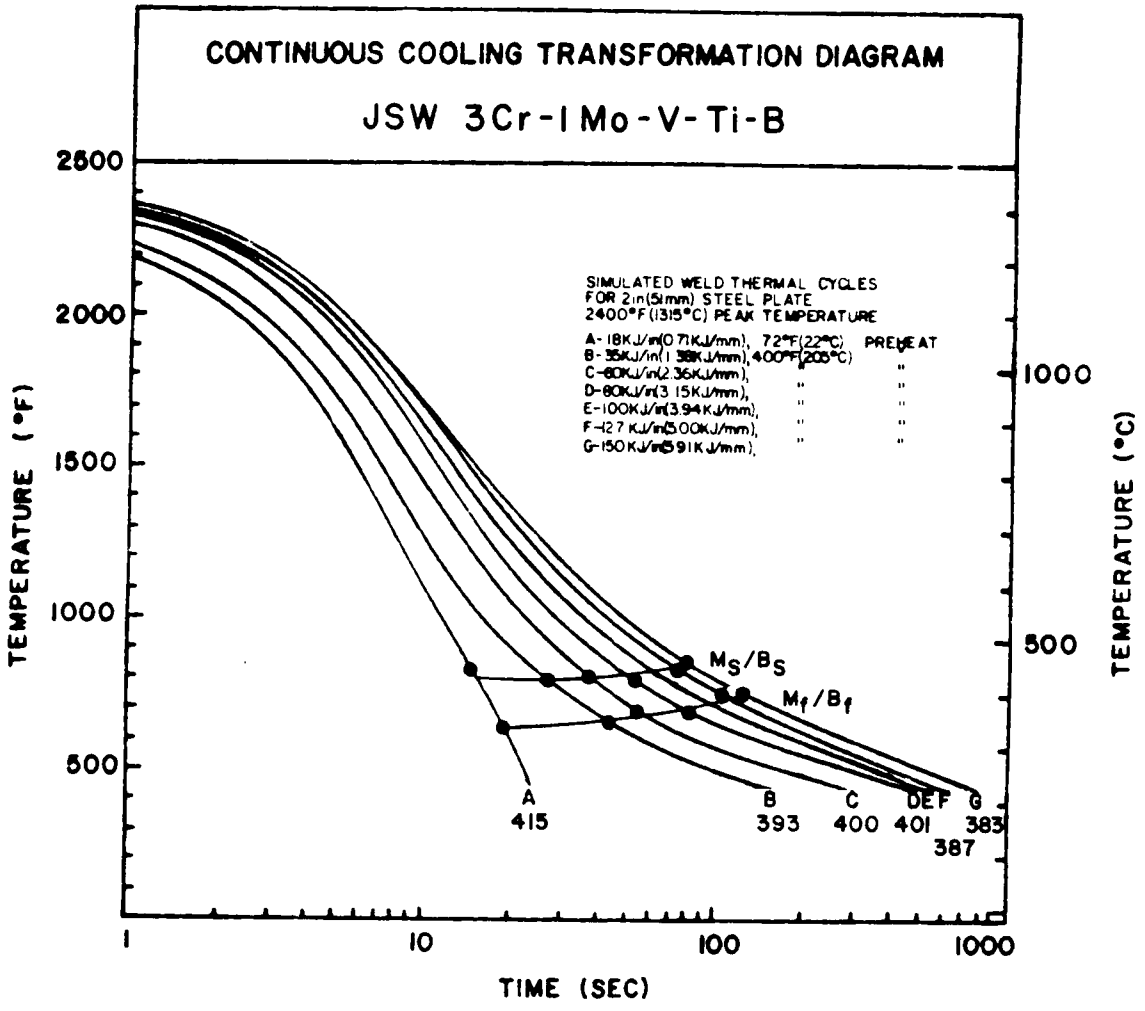


Figure 32. CCT diagram for JSW 3Cr-1Mo-V-Ti-B, determined for welding conditions.

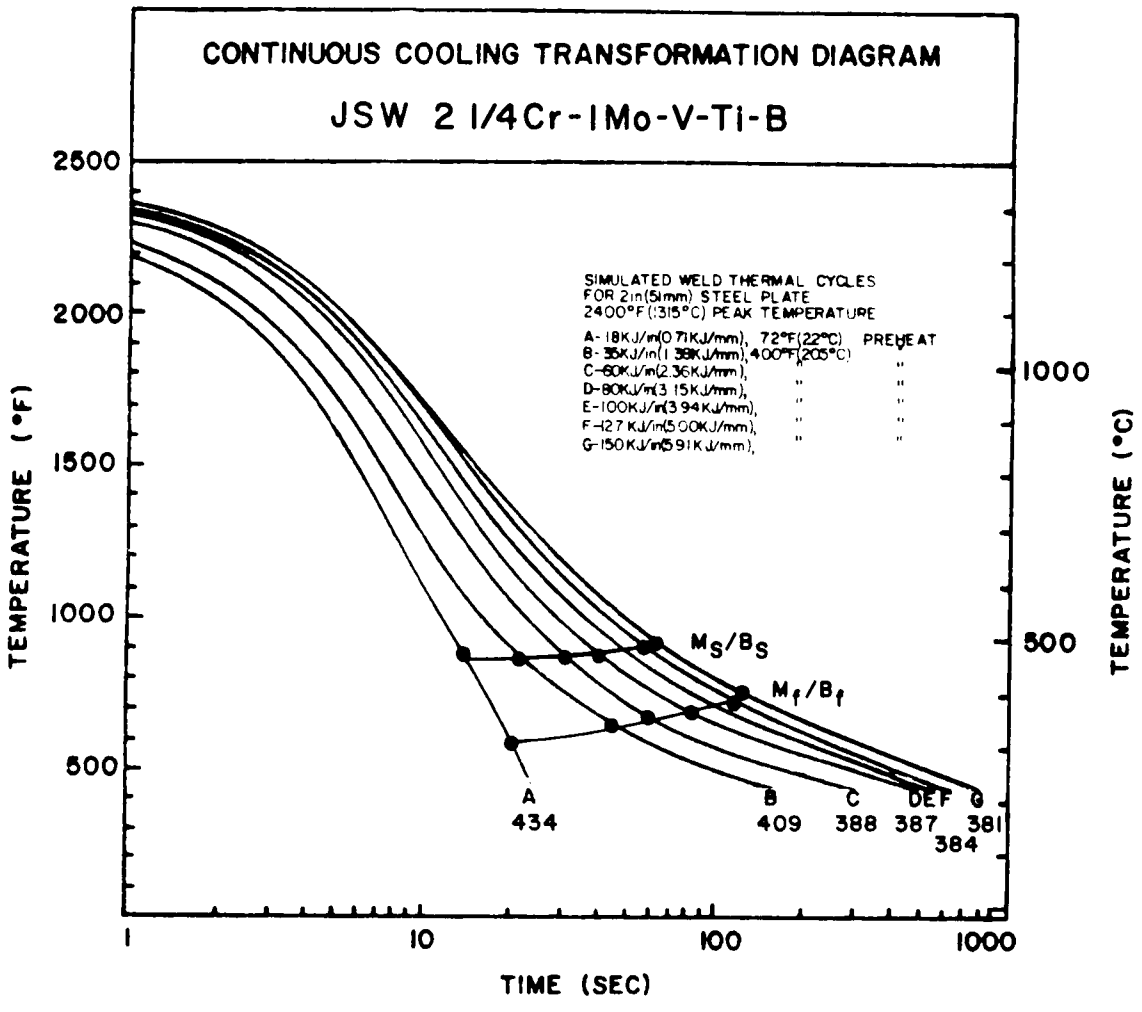


Figure 33. CCT diagram for JSW 2 1/4Cr-1Mo-V-Ti-B, determined for welding conditions.

strength level, the A_{C1} and A_{C3} temperatures were determined to be 1515°F (825°C) and 1630°F (890°C).

Higher heat treatment temperatures and longer times at the heat treatment temperature result in carbide coarsening. Coarser carbides dissolve more slowly and therefore inhibit the transformation to austenite by limiting the amount of carbon available. Under welding conditions, where the rate of heating is rapid, the sluggish dissolution of carbides results the in elevation of the transformation temperatures.

The A_{C1} temperatures for the AMAX (Climax) 3Cr-1 1/2Mo-0.1V, heat treated Berkeley 3Cr-1 1/2Mo-1/2Ni, and JSW 2 1/4Cr-1Mo-V-Ti-B materials range from 1490 to 1515°F (810 to 825°C) and A_{C3} temperatures range from 1620 to 1670°F (880 to 910°C). The A_{C1} and A_{C3} temperatures obtained from the Gleeble weld simulation studies for the AMAX (Climax) 3Cr-1 1/2Mo-0.1V, JSW 3Cr-1Mo-V-Ti-B, and JSW 2 1/4Cr-1Mo-V-Ti-B materials (Table 5) are higher than those reported on the continuous cooling transformation diagrams (Figures 4-6, pages 11 and 13) between 22 and 45F° (12 and 25C°) and 18 and 54F° (10 and 28C°) respectively. The increase in the transformation temperature is the result of the carbide dissolution kinetics and diffusion control of austenite formation and the rapid heating rate associated with welding conditions.

The on-cooling transformation temperatures in Table 6 are reported as start (S) and finish (F) and in Figures 30-33 as M_s/B_s and M_f/B_f as no discernible separate finish for the bainite transformation (B_f) or start for the martensite transformation (M_s)

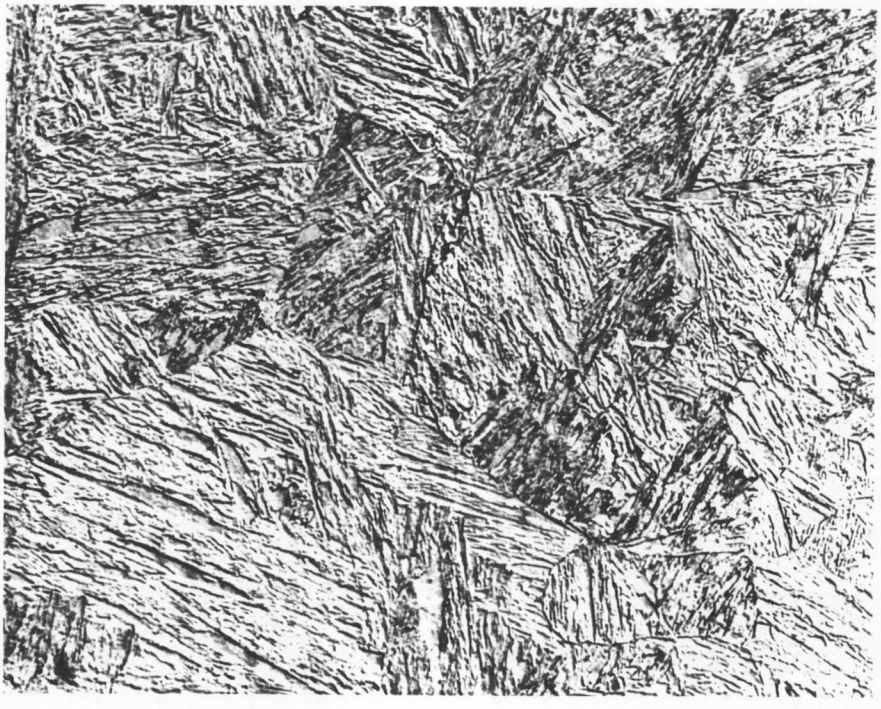
could be detected on the dilation versus temperature traces. For the Berkeley 3Cr-1 1/2Mo-1/2Ni no significant difference in the on-cooling transformation temperatures was observed between the as received or heat treated material with the exception of the 18KJ/in transformation finish temperature.

A comparison of the transformation start temperatures for the AMAX (Climax) 3Cr-1 1/2Mo-0.1V, JSW 3Cr-1Mo-V-Ti-B, and JSW 2 1/4Cr-1Mo-V-Ti-B under simulated welding conditions with the continuous cooling transformation diagrams for these materials (Figures 4-6, pages 11 and 13) show, in general, a lowering of the transformation start by approximately 45F° (25C°) due to the fast cooling rate under welding conditions. Table 5 and Figures 30 through 33 show that the highest on-cooling transformation start temperatures were exhibited by the JSW 2 1/4Cr-1Mo-V-Ti-B material and the lowest on-cooling transformation start temperatures were exhibited by the Berkeley 3Cr-1 1/2Mo-1/2Ni material. The higher transformation temperatures of the JSW 2 1/4Cr-1Mo-V-Ti-B material is due to the lower carbon (0.12%) and overall lower alloying element content of this material. The lower transformation start temperatures of the Berkeley 3Cr-1 1/2Mo-1/2Ni material is due to the relatively high carbon (0.16%) and nickel (0.51%) content compared to the other three modified alloys.

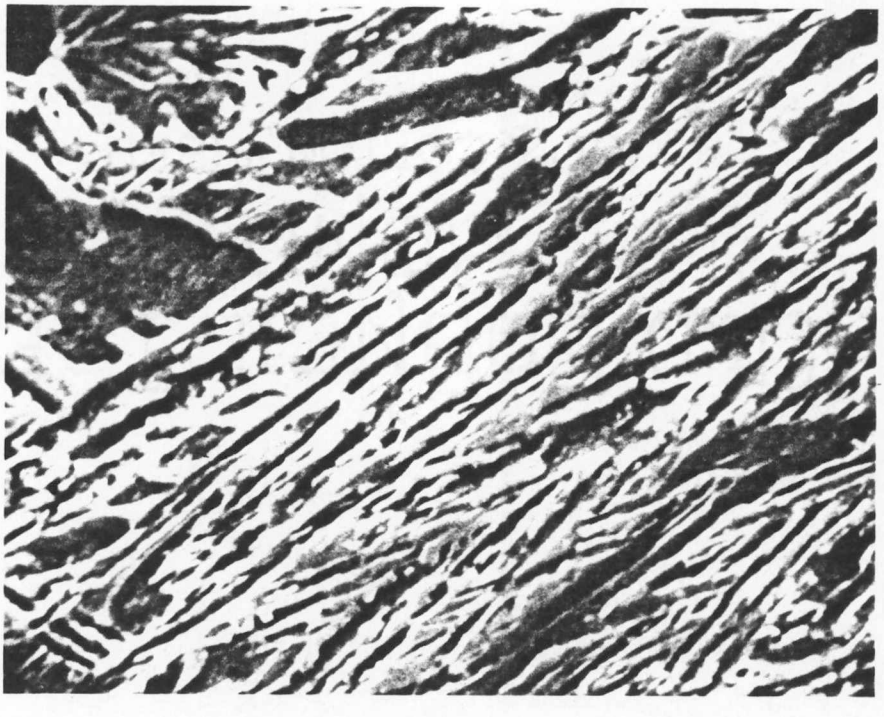
A comparison of the transformation finish temperatures obtained for the AMAX (Climax) 3Cr-1 1/2Mo-0.1V material and the continuous cooling transformation diagram for the same material (Figure 6, page 13) shows a general agreement between the finish temperatures

obtained under Gleeble simulated weld conditions and transformation temperatures corresponding to 90% completion of the austenite to martensite or bainite transformation. The transformation finish temperatures obtained under Gleeble simulated welding conditions range from 620 to 740°F (324 to 395°C) and M_{f90}-B_{f90} temperatures range from 617 to 740°F (325 to 393°C). As was the case with the 9Cr-1Mo materials, the last 10% of transformation occurs over a large temperature range (approximately 225°F (125°C)) and therefore was not detectable. Similarly, the finish transformation finish temperatures for the JSW 3Cr-1Mo-V-Ti-B and JSW 2 1/4Cr-1Mo-V-Ti-B shown in table 5 are higher than the transformation finish temperatures shown in Figures 4 and 5 (pages 11 and 13), continuous cooling transformation diagrams for materials of similar composition.

Modified 2 1/4Cr-1Mo and 3Cr-Mo Microstructures. Optical and scanning electron micrographs of the JSW 3Cr-1Mo-V-Ti-B alloy for the helium quench, 35 KJ/in (1.38 KJ/mm), 60 KJ/in (2.36 KJ/mm), and 150 KJ/in (5.91 KJ/mm) heat input simulated weld thermal cycles are shown in Figures 34 through 37. Since the microstructures for all the materials; AMAX (Climax) 3Cr-1 1/2Mo-0.1V, Berkeley 3Cr-1 1/2Mo-1/2Ni, JSW 3Cr-1Mo-V-Ti-B, and JSW 2 1/4Cr-1Mo-V-Ti-B, are similar only one representative set of microstructures for the range of thermal cycles employed is shown. Figures 38 through 40 are optical and scanning electron micrographs of the AMAX (Climax) 3Cr-1 1/2Mo-0.1V, Berkeley 3Cr-1 1/2Mo-1/2Ni, and JSW 2 1/4Cr-1Mo-V-Ti-B for the 60 KJ/in (2.36 KJ/mm) heat input weld

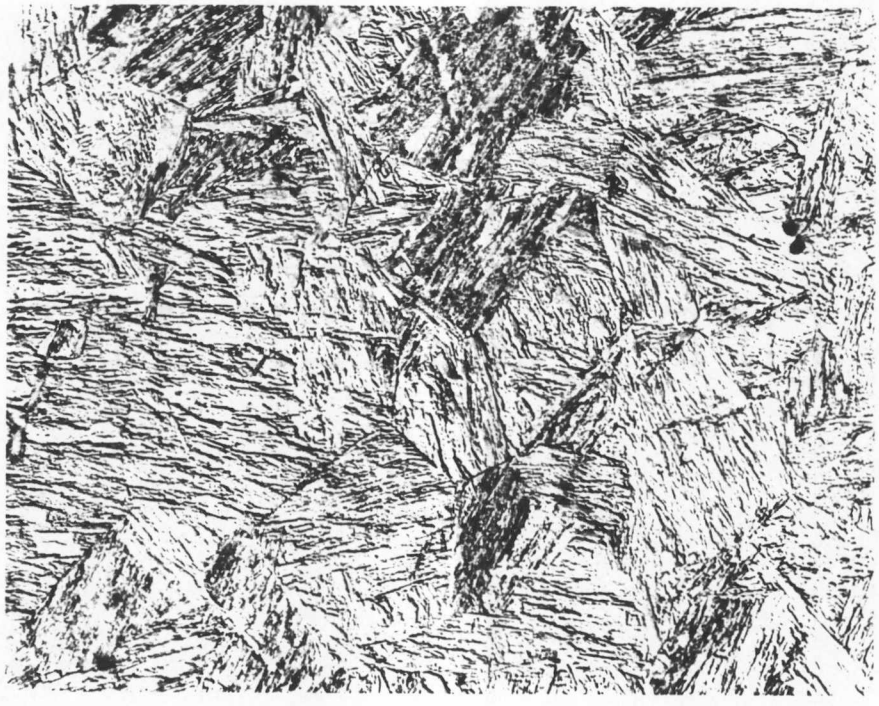


A

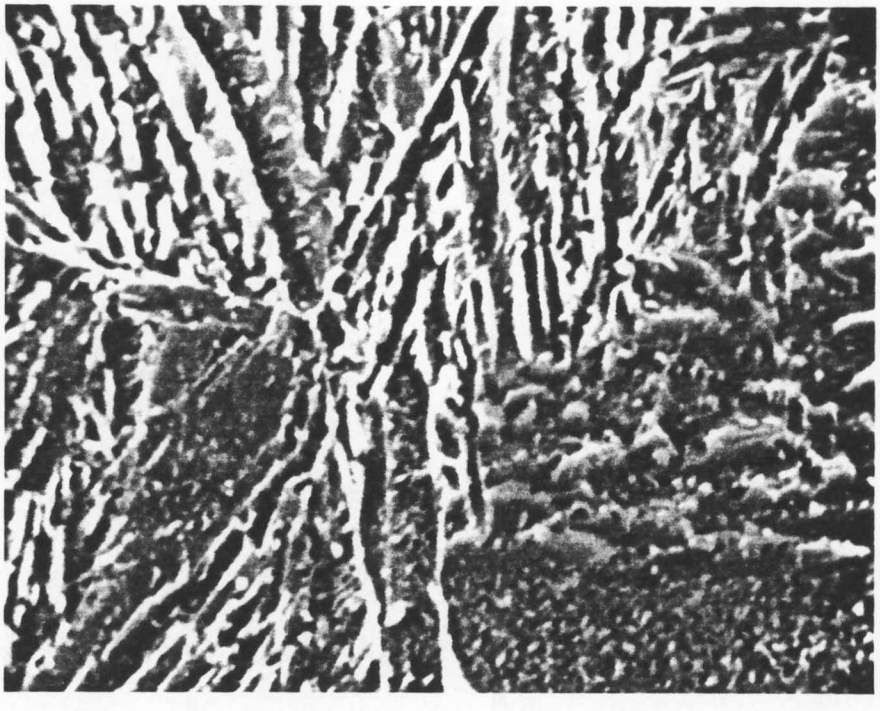


B

Figure 34. JSW 3Cr-1Mo-V-Ti-B, CCT specimen, helium quenched. Nital-Picral, a) 500X OLM, b) 10,000X SEM.

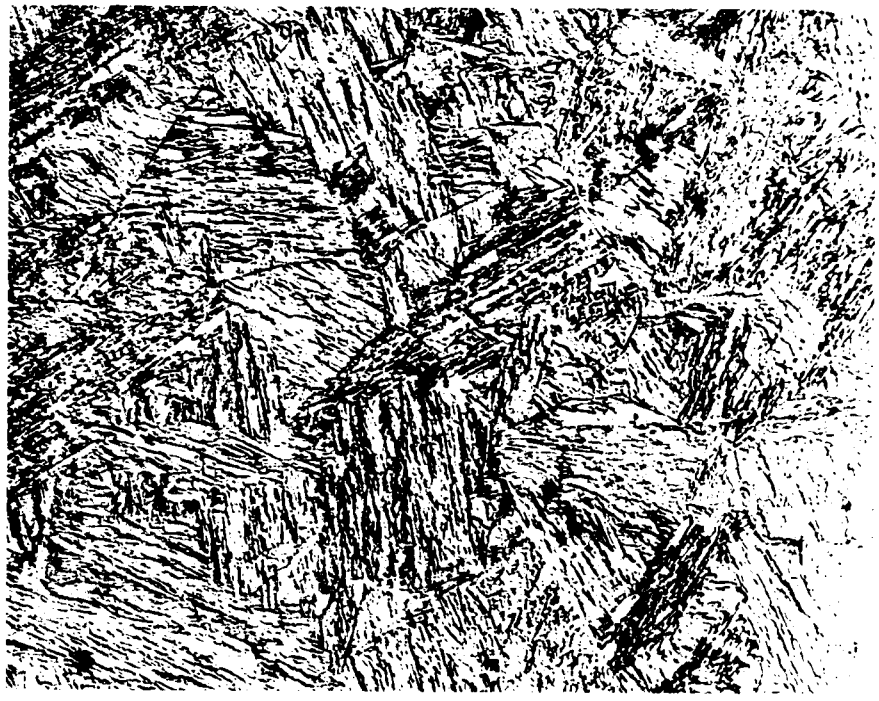


A



B

Figure 35. JSW 3Cr-1Mo-V-Ti-B, CCT specimen, 35KJ/in. Nital-Picral, a) 500X OLM, b) 10,000X SEM.

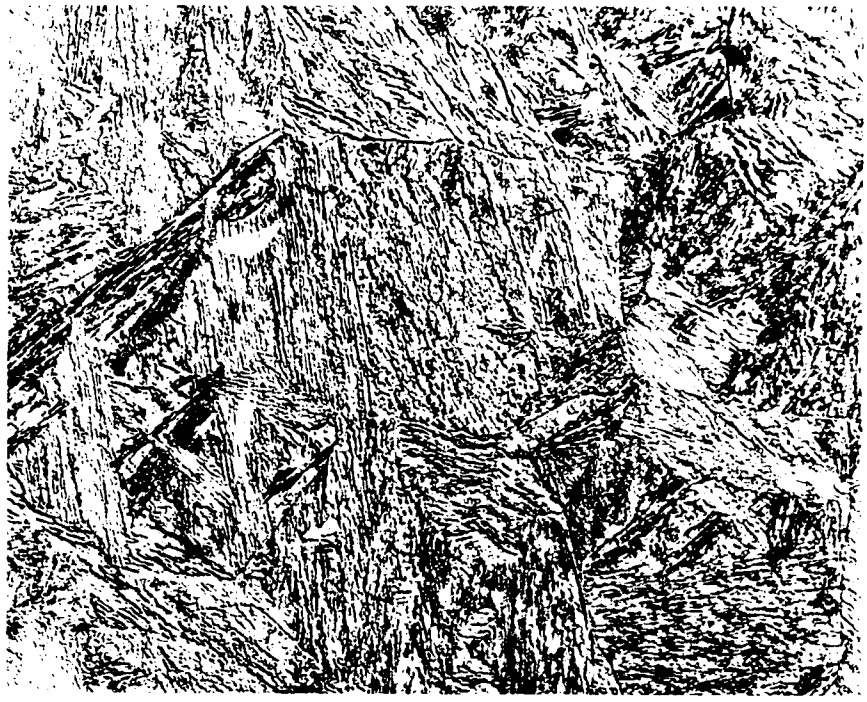


A

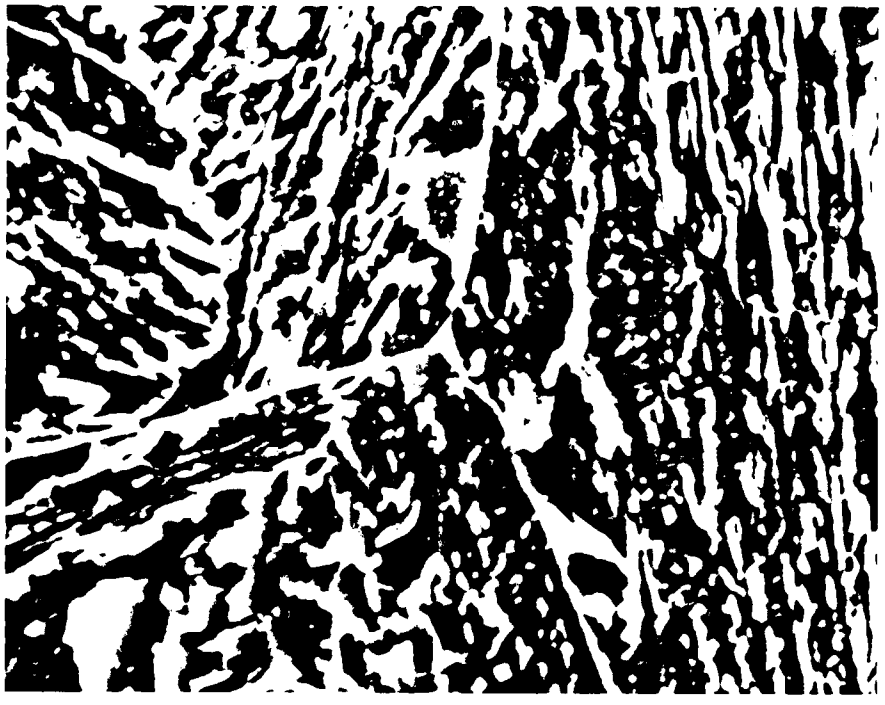


B

Figure 36. JSW 3Cr-1Mo-V-Ti-B, CCT specimen 60KJ/in. Nital-Picral, a) 500X OLM, b) 10,000X SEM.

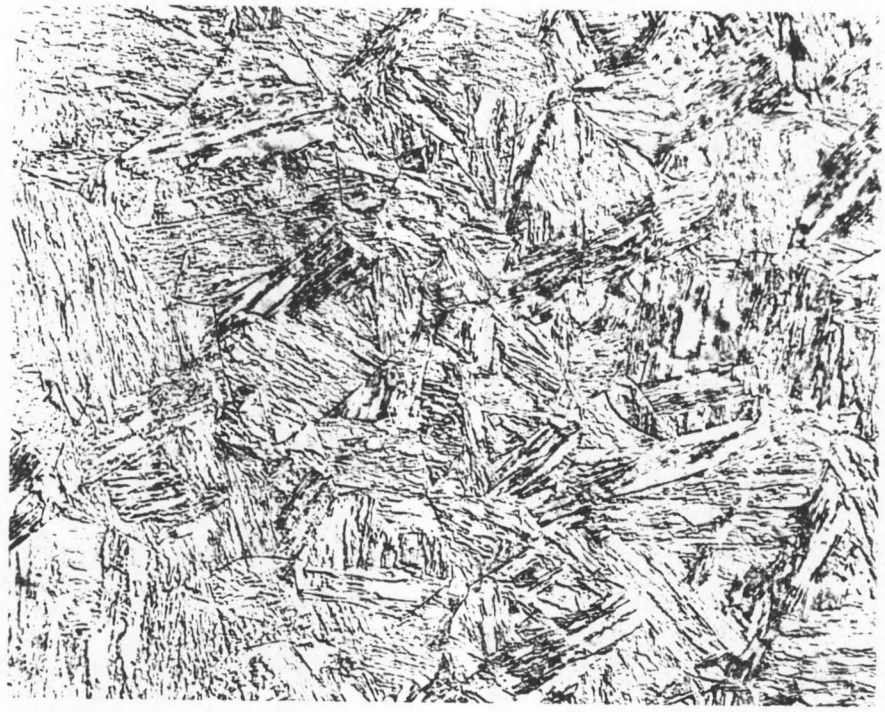


A

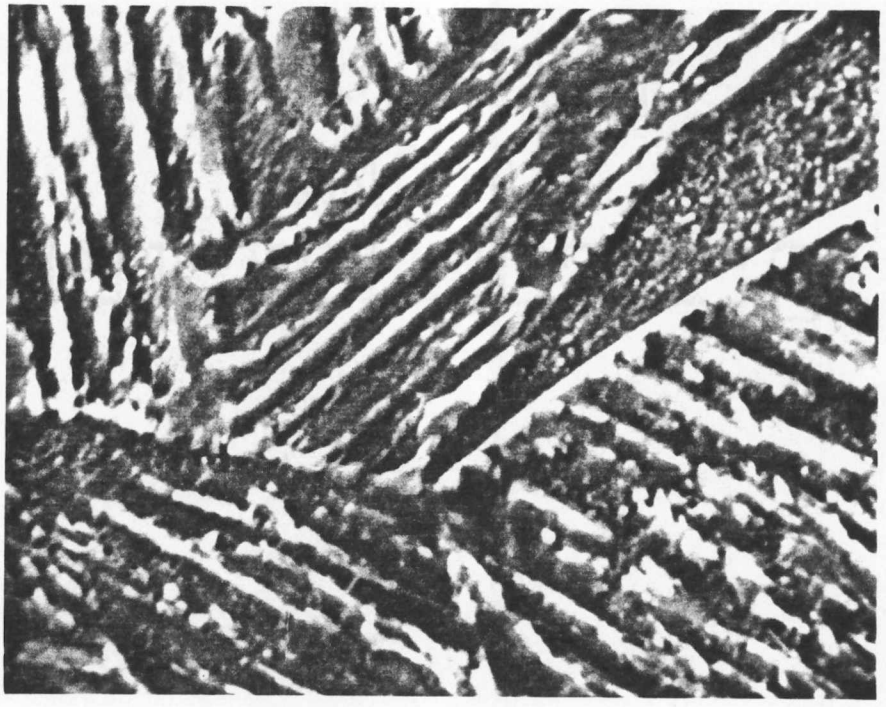


B

Figure 37. JSW 3Cr-1Mo-V-Ti-B, CCT specimen, 150KJ/in. Nital-Picral, a) 500X OLM, b) 10,000X SEM.

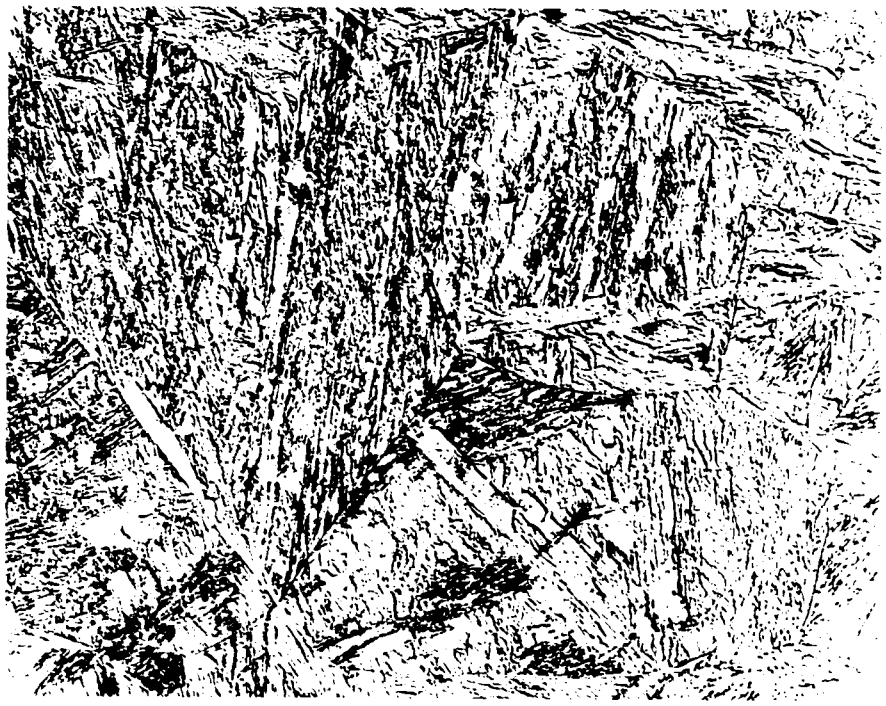


A

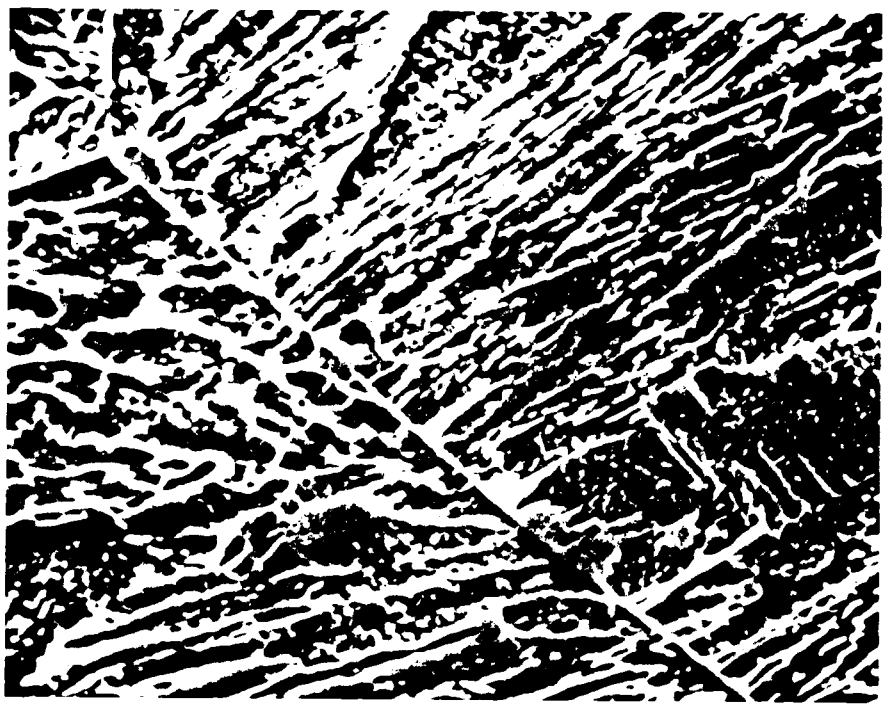


B

Figure 38. AMAX (Climax) 3Cr-1 1/2Mo-0.1V, CCT specimen, 60KJ/in. Nital-Picral, a) 500X OLM, b) 10,000X SEM.



A



B

Figure 39. Berkeley 3Cr-1 1/2Mo-1/2Ni CCT Specimen, 60KJ/in. Nital-Picral, a) 500X OLM, b) 10,000X SEM.

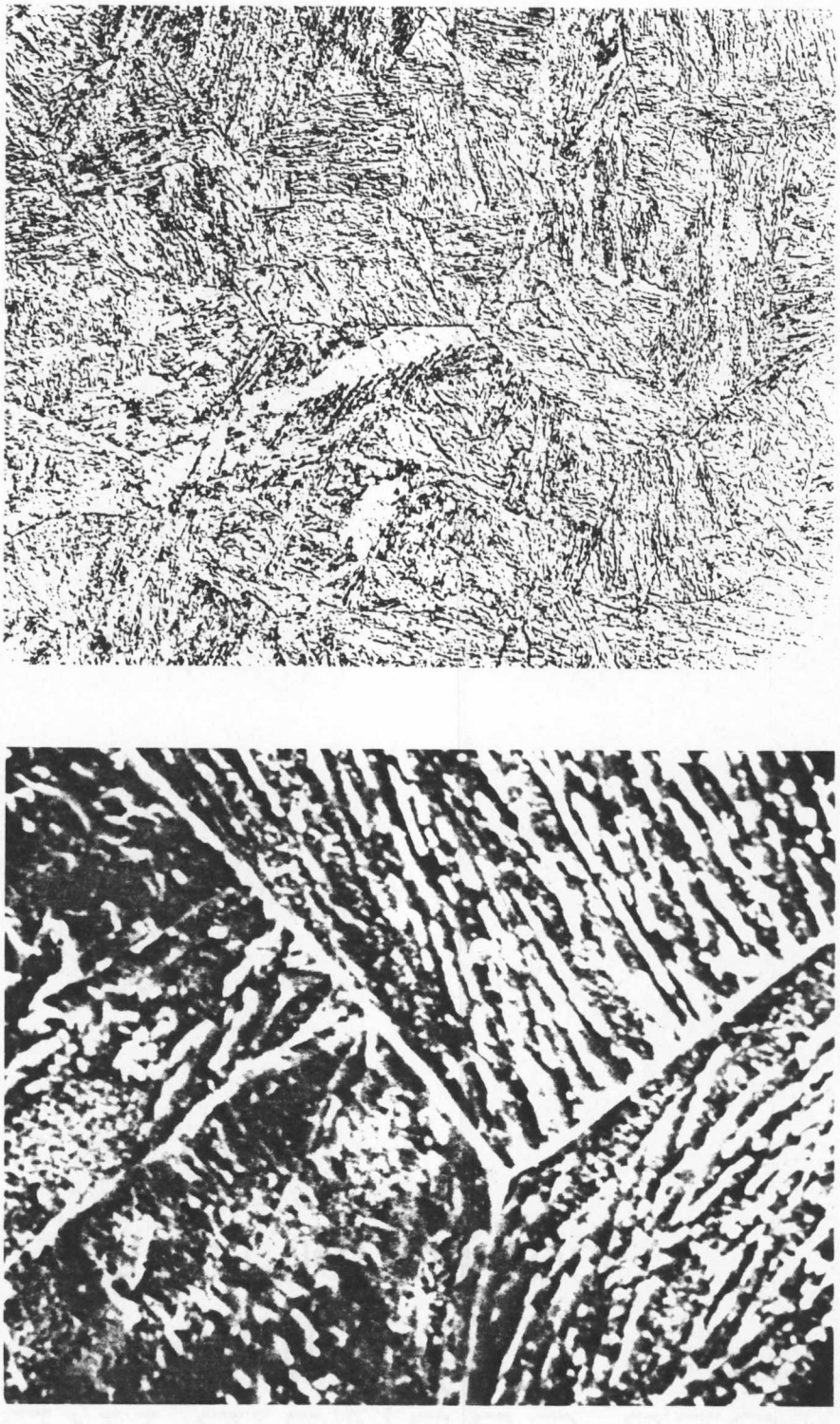


Figure 40. JSW 2 1/4Cr-1Mo-V-Ti-B, CCT specimen, 60KJ/in. Nital-Picrl, a) 500X OLM, b) 10,000X SEM.

simulation samples. The similarity of the microstructures obtained from the same heat input thermal cycle may be seen in the micrographs of the 60 KJ/in (2.36 KJ/mm) specimens.

As was the case with the modified 9Cr-1Mo continuous cooling transformation specimens, the optical micrographs (Figures 34a-40a) of the modified 2 1/4Cr and 3Cr materials reveal little information about the microstructures. A modest amount of coarsening of the prior austenite grains with increasing heat input (longer times above the grain coarsening temperature) is evident in Figures 34a through 37a. The acicular aspect of the microstructure also becomes less marked with increasing energy input.

The scanning electron micrographs (Figures 34b through 37b) for the JSW 3Cr-1Mo-V-Ti-B specimens show a change in the microstructure with increasing energy input from autotempered martensite and martensite, to lower bainite and autotempered martensite and, finally, to a transition microstructure consisting of lower bainite and granular bainite. Figure 34b, the helium quenched JSW 3Cr-1Mo-V-Ti-B specimen, shows a microstructure that consists of autotempered martensite and martensite. Figures 35b, the JSW 3Cr-1Mo-V-Ti-B 35 KJ/in (1.38 KJ/mm) specimen, and Figures 36b, and 38b through 40b, the 60 KJ/in (2.36 KJ/mm) specimens of the JSW 3Cr-1Mo-V-Ti-B, AMAX (Climax) 3Cr-1 1/2Mo-0.1V, Berkeley 3Cr-1 1/2Mo-1/2Ni, and JSW 2 1/4Cr-1Mo-V-Ti-B show microstructures that consist of lower bainite and autotempered martensite. The 150 KJ/in (5.91 KJ/mm), JSW 3Cr-1Mo-V-Ti-B specimen (Figure 37b) exhibits a breaking up of the lower bainite, lath like microstructure into

granular bainite and, since both structures are present, this is termed a transitional bainitic microstructure. The sequence of microstructures with increasing energy input is consistent with that determined by Richey[25] for 2 1/4Cr-1Mo alloys.

The presence of mixed microstructures consisting of bainite and martensite in alloy steels has been observed previously. Brown et al.[111] have predicted from the continuous cooling transformation diagram for 2 1/4Cr-1Mo that fast cooling rates would result in martensitic or mixed martensitic-bainitic microstructures. Autotempered martensite present with bainite has been reported in 2 1/4Cr-1Mo simulated weld HAZ's by Smith et al.[112] and in quenched 2 1/4Cr-1Mo and 5Cr-1Mo in De Ferri Metallographia.[110] Ishigiro et al.[105] have observed microstructures consisting of martensite, mixed martensite and bainite, and bainite in JSW 2 1/4Cr-1Mo-V-Ti-B simulated weld HAZ's. Bonizewski et al.[113] have reported mixed martensite and bainite in both actual and simulated weld HAZ's for 5Cr-1/2Mo, 9%Ni, 2%Mn and 3%Mn steels. The microstructures containing martensite or autotempered martensite reported in the literature are similar in appearance to the roughened, lenticular structures observed in the helium quenched, 35 KJ/in (1.38 KJ/mm), and 60 KJ/in (2.36 KJ/mm) microstructures (Figures 34-36, 38-40). These structures are also similar to those observed in the 9Cr-1Mo-V-Nb microstructures (Figures 26-29, pages 89-92) shown previously. Therefore, there is little question that these lenticular structures are auto tempered martensite.

Summary of the Modified 2 1/4Cr-1Mo and 3Cr-Mo Transformation Studies. As was expected with the rapid heating rate employed and the diffusion controlled nature of austenite formation, the on heating transformation temperatures of the AMAX (Climax) 3Cr-1 1/2Mo-0.1V, JSW 3Cr-1Mo-V-Ti-B, and JSW 2 1/4Cr-1Mo-V-Ti-B materials were higher than those shown on the continuous cooling transformation diagrams for these materials. The on cooling transformation temperatures were found to be depressed by approximately 45F° (25C°) with respect to the transformation temperatures shown on the continuous cooling transformation diagrams. The depression of the on-cooling transformation temperatures is due to the rapid cooling and limited amount of diffusion that must occur during the lower bainite bainite transformation. The JSW 2 1/4Cr-1Mo-V-Ti-B had the highest transformation start temperatures which is a result of the lower alloy and carbon content. The Berkeley 3Cr-1 1/2Mo-1/2Ni material had the lowest transformation start temperatures due to this alloys high carbon and nickel content.

The microstructures which were observed in the AMAX (Climax) 3Cr-1 1/2Mo-0.1V, Berkeley 3Cr-1 1/2Mo-1/2Ni, JSW 3Cr-1Mo-V-Ti-B, and JSW 2 1/4Cr-1Mo-V-Ti-B materials over the range of thermal cycles employed were consistent with those found by Richey[25] for 2 1/4Cr-1Mo. As the energy input increased, the microstructures changed from martensite and autotempered martensite to bainite and autotempered martensite and, at the highest energy input employed, to a transitional microstructure consisting of lower bainite and granular bainite. No retained austenite was observed in any of the

microstructures in the modified 2 1/4Cr-1Mo and 3Cr-Mo materials as is expected with the fast cooling rates in welding.

Postweld Heat Treatment Cracking Behavior

PWHT cracking is defined as intergranular cracking in the weld HAZ or weld metal that occurs during heat treatment or high temperature service.[40] This type of cracking is of particular concern for fabricators of Cr-Mo steels since no adequate predictor of susceptibility exists. To compound the difficulty, heat to heat variations in susceptibility may result in cracking of alloys with nominally equivalent compositions to those previously successfully welded.[38,40,41]

PWHT cracking involves a synergistic interaction of many metallurgical changes coupled with the high residual tensile stresses in the coarse grained HAZ.[18] A primary factor is the precipitation of M_2C, MC and M_4C_3 type carbides within the matrix resulting in an increase of the matrix flow stress relative to the grain boundary flow stress. The difference in relative flow stress between the grain matrix and grain boundaries prevents plastic deformation from occurring in the grain matrix during stress relaxation and gives rise to strain accumulation in the grain boundaries. If the strain accumulation exceeds the grain boundary ductility, cavitation and subsequent rupture occur.[37,39-43]

Grain boundary ductility may be decreased by the segregation of residual embrittling elements, particularly phosphorous, during PWHT.[42,53-56] Carbides, nitrides or sulphides located at the grain

boundaries may have poor interfacial bonding with the matrix and therefore may be initiation sites for grain boundary cavitation.[15,58,64,112,161] The rapid growth of grain boundary carbides may result in the formation of a weak, carbide denuded, zone immediately adjacent to the grain boundary in which strains may accumulate and thus initiate rupture.[30,52] Grain coarsening, associated with the high peak temperature regions closest to the weld, exacerbates the foregoing effects by limiting the grain boundary area available to accommodate slip and for accommodating segregation of residual elements.[3,19] In general, any mechanism which results in an increase in the grain matrix to grain boundary strength ratio or decreases grain boundary ductility during PWHT may be contributory to PWHT cracking.

The 9Cr-1Mo, 3Cr-Mo, and 2 1/4Cr-1Mo modified alloys are designed to have high strength, high hardenability and good resistance to loss in strength during tempering or elevated temperature service. In general, these attributes have been conferred by the addition of strong carbide forming elements, vanadium and/or niobium, which form highly stable MC or M_4C_3 type carbides. (Hardenability has been increased by boron, manganese and/or nickel additions in the 3Cr and 2 1/4Cr modified alloys.) However, the addition of strong carbide forming elements is known to increase PWHT cracking susceptibility and therefore the present work was undertaken to assess the susceptibility of the modified Cr-Mo alloys to this type of cracking.

Postweld Heat Treatment Cracking Susceptibility Evaluation of the 9Cr-1Mo-V-Nb Commercial Heats.

Susceptibility of the NKK 9Cr-1Mo-V-Nb, Timken 9Cr-1Mo-V-Nb, and Sumitomo 9Cr-1Mo-V-Nb materials was determined by Gleeble simulation. Cylindrical specimens, 1/4in diameter by 4in long (6mm diameter by 102mm long), were subjected to a 60KJ/in (2.36KJ/mm) heat input thermal cycle (2in (51mm) thick plate, 400°F (205°C) preheat) with a peak temperature of 2400°F (1315°C) followed by simultaneous heating to the PWHT temperature, 1350°F (732°C), and loading to a predetermined stress. Samples were held at the PWHT temperature under load until fracture occurred. While the stress is held constant for an individual specimen, a range of stress levels is employed during the testing of a material in order to obtain various times to fracture. The reduction in area (RA) was determined and a scanning electron microscopy examination of the fracture surfaces was conducted.

Figure 41 shows the RA as a function of the time to fracture for the three commercial heats of the modified 9Cr-1Mo-V-Nb material. The RA for the NKK 9Cr-1Mo-V-Nb material range between 30 and 37%, for the Timken 9Cr-1Mo-V-Nb material between 35 and 46%, and for the Sumitomo 9Cr-1Mo-V-Nb between 15 and 31%. In comparison, the RA obtained by Richey[25] for the experimental 9Cr-1Mo-V-Nb heat, ORNL 176, a forerunner to the commercial heats, was between 35 and 56% and for the unmodified 9Cr-1Mo-0.11C material was in excess of 70% under the same test conditions.

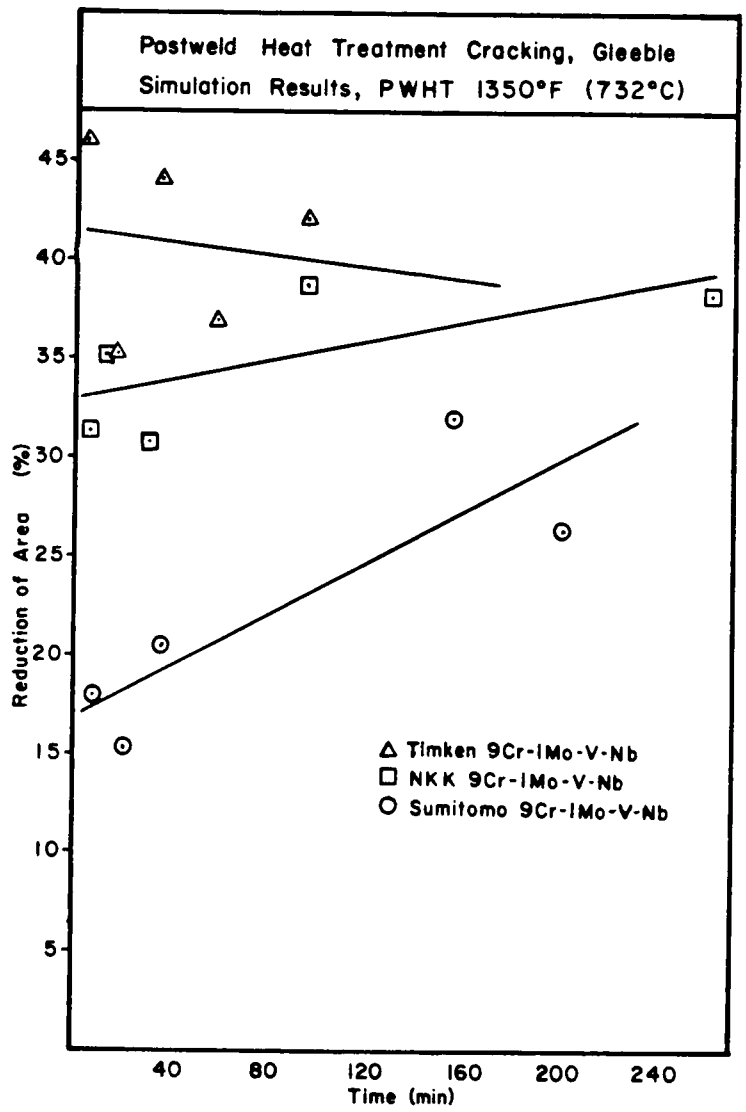


Figure 41. 9Cr-1Mo-V-Nb alloys' Gleeble stress-rupture behavior for simulated PWHT at 1350°F (732°C). Reduction in area vs. time to rupture at different stress levels.

The lower ductility of the V-Nb modified 9Cr-1Mo in relation to the unmodified 9Cr-1Mo material is the result of differences in carbide evolution. Vitek and Klueh[32] found that the addition of niobium and vanadium to 9Cr-1Mo provides a fine dispersion of Nb/Vcarbo-nitrides. These fine, dispersed MC type carbides act as nucleating sites for $M_{23}C_6$ resulting in more finely dispersed $M_{23}C_6$ carbides than exist in the unmodified 9Cr-1Mo material which does not have the fine precursor distribution.[33] Further, the addition of vanadium alters the mobility of chromium, slowing the growth of $M_{23}C_6$ carbides.[34] The presence of fine, dispersed carbides results in increased rupture strength and lower ductility compared to the unmodified 9Cr-1Mo material.

The generally lower rupture ductility of the Sumitomo 9Cr modified alloy may be the result of the higher phosphorous content compared to the NKK and Timken materials. The Sumitomo material has a phosphorous content of 0.014% while the NKK and Timken materials have phosphorous contents of 0.004 and 0.010% respectively. The increase in rupture ductility with increasing time to rupture exhibited by the Sumitomo material may be the result of carbide evolution (overaging affects).

Assuming that the Vinckier and Pense criteria (page 51) can be extended to the PWHT temperature employed for the 9Cr-1Mo materials, the NKK 9Cr-1Mo-V-Nb and Timken 9Cr-1Mo-V-Nb materials, having rupture ductilities in excess of 30%, would not be considered susceptible to PWHT cracking. The Sumitomo 9Cr-1Mo-V-Nb, which exhibits lower rupture ductilities compared to the NKK and Timken

materials, has a minimum ductility of 15% and may be considered marginally susceptible to PWHT cracking by the Vinckier and Pense criteria.

Fractography of the 9Cr-1Mo-V-Nb Materials. Figures 42, 43 and 44 are scanning electron fractographs of NKK 9Cr-1Mo-V-Nb, Timken 9Cr-1Mo-V-Nb, and Sumitomo 9Cr-1Mo-V-Nb Gleeble simulated PWHT specimens. The primary mode of fracture of the 9Cr-1Mo-V-Nb materials is microvoid coalescence. The Sumitomo alloy, which exhibited the lowest ductilities, clearly shows an underlying intergranular character to the fracture. The extent of microductility in these alloys is concomitant with the measured macroductility and indicates that PWHT cracking should not be a problem.

Summary of the 9Cr-1Mo-V-Nb PWHT cracking behavior. The addition of vanadium and niobium lowers the rupture ductility of 9Cr-1Mo from over 70% to between 15 and 56% in gleeble simulated PWHT testing. The decrease in ductility is a result of the precipitation of fine, dispersed V/Nb-carbo-nitrides, the nucleation of $M_{23}C_6$ on the V/Nb precipitates resulting in a fine, dispersed precipitation of $M_{23}C_6$, and reduction in the rate of growth of the $M_{23}C_6$ precipitates due to the lowering of chromium mobility by vanadium. However, both macroscopic and microscopic ductility are sufficient to preclude PWHT cracking as a significant fabrication problem in these materials. The relatively high phosphorous of the Sumitomo heat may be the primary causal factor for the lower rupture ductilities observed for

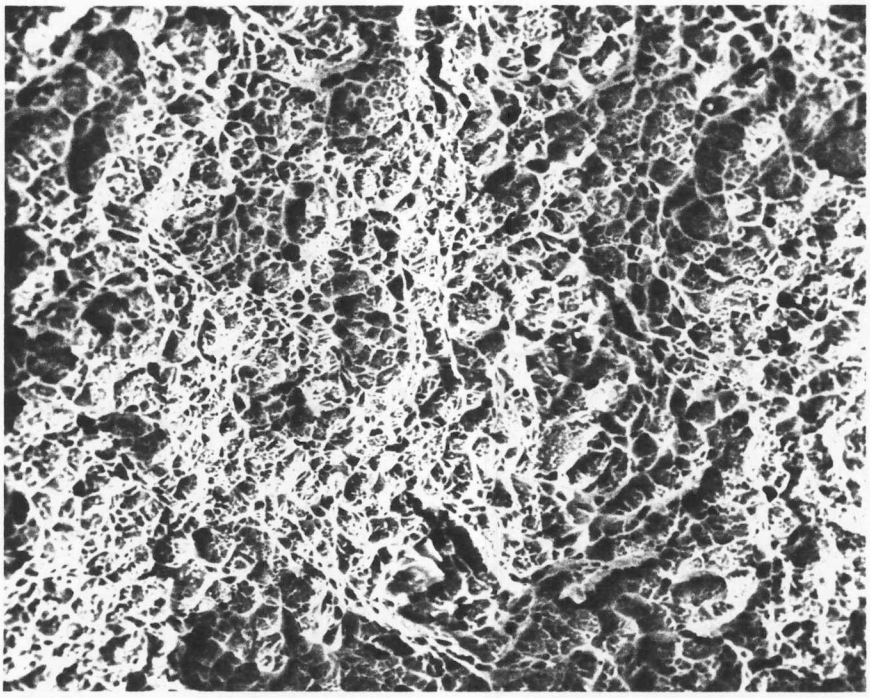


Figure 42. Fractograph of NKK 9Cr-1Mo-V-Nb. 34.2 KSI, 12.8 min. to fracture, 35.3% R/A, SEM 200X.

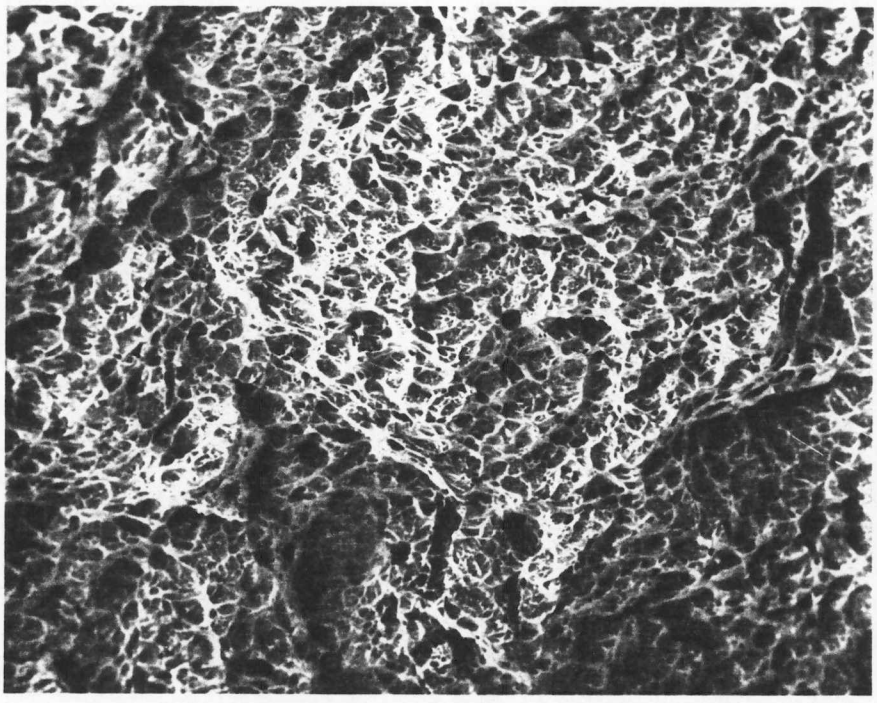


Figure 43. Fractograph of Timken 9Cr-1Mo-V-Nb. 35.0 KSI, 16.7 min. to fracture, 35.3% R/A, SEM 200X.

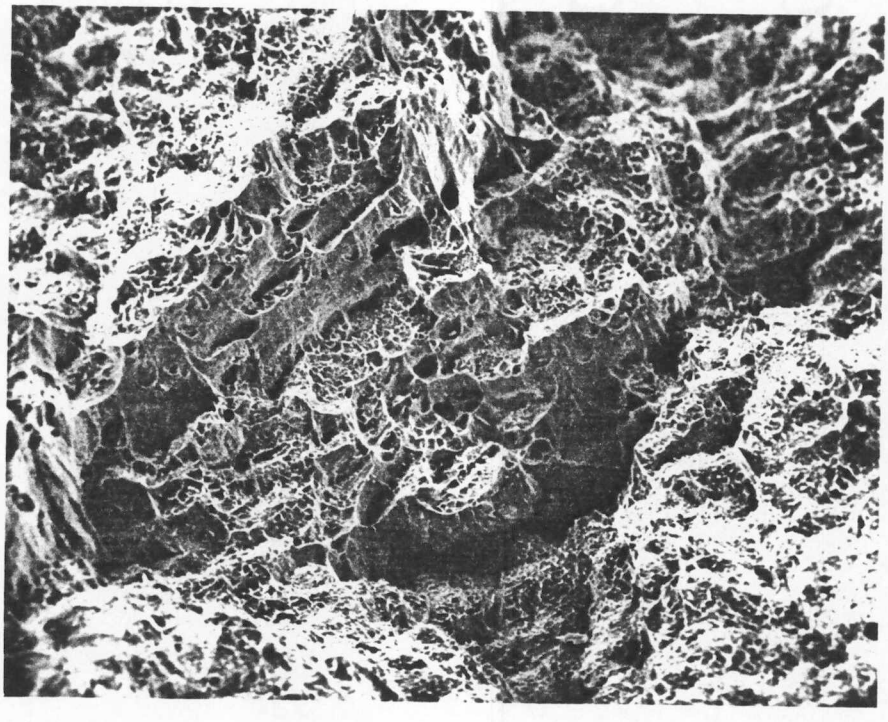


Figure 44. Fractograph of Sumitomo 9Cr-1Mo-V-Nb. 22KSI, 20.9 min. to fracture, 15.4% R/A, SEM 200X.

this alloy and may indicate a need to carefully control residuals in the modified 9Cr-1Mo alloys.

Postweld Heat Treatment Cracking Results for the Modified 3Cr-Mo and 2 1/4Cr-1Mo Materials by Gleeble Simulation.

The PWHT cracking susceptibility of the AMAX (Climax) 3Cr-1 1/2Mo-0.1V, Berkeley 3Cr-1 1/2Mo-1/2Ni, JSW 3Cr-1Mo-V-Ti-B, and JSW 2 1/4Cr-1Mo-V-Ti-B alloys was determined by Gleeble simulation in the same manner as that used with the modified 9Cr-1Mo materials. Two PWHT temperatures were employed, 1250°F (680°C) and 1150°F (620°C) for evaluation of cracking susceptibility of the modified 2 1/4Cr and 3Cr materials. The lower temperature was utilized to be representative of the trend toward lower PWHT temperatures and thus higher strength levels.

Figures 45 and 46 present the RA of the fractured Gleeble specimens as a function of time to fracture at the 1250°F (680°C) and 1150°F (620°C) PWHT temperatures respectively. At 1250°F (680°C) the RA ranges from 0.3 to 1.4% for AMAX (Climax) 3Cr-1 1/2Mo-0.1V, from 21 to 29% for Berkeley 3Cr-1 1/2Mo-1/2Ni, from 4 to 14% for JSW 3Cr-1Mo-V-Ti-B and from 2.3 to 10% for JSW 2 1/4Cr-1Mo-V-Ti-B. At 1150°F (620°C) the RA ranges from 0.1 to 1.3% for the AMAX (Climax) 3Cr-1 1/2Mo-0.1V, from 10 to 20% for Berkeley 3Cr-1 1/2Mo-1/2Ni, from 1.6 to 7.0% for JSW 3Cr-1Mo-V-Ti-B and from 1.8 to 3.9% for JSW 2 1/4Cr-1Mo-V-Ti-B.

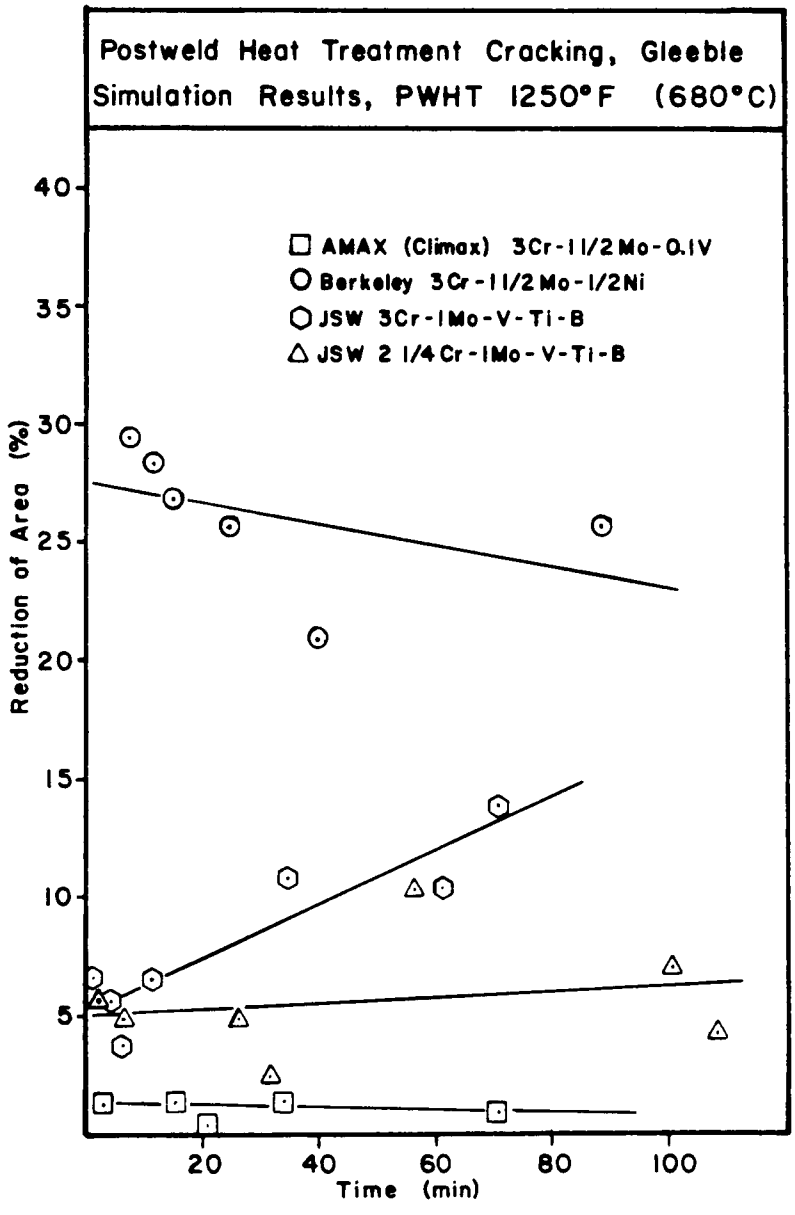


Figure 45. Modified 3Cr and 2 1/4Cr alloys' Gleeble stress-rupture behavior for simulated PWHT at 1250°F (680°C). Reduction in area vs. time to rupture at different stress levels.

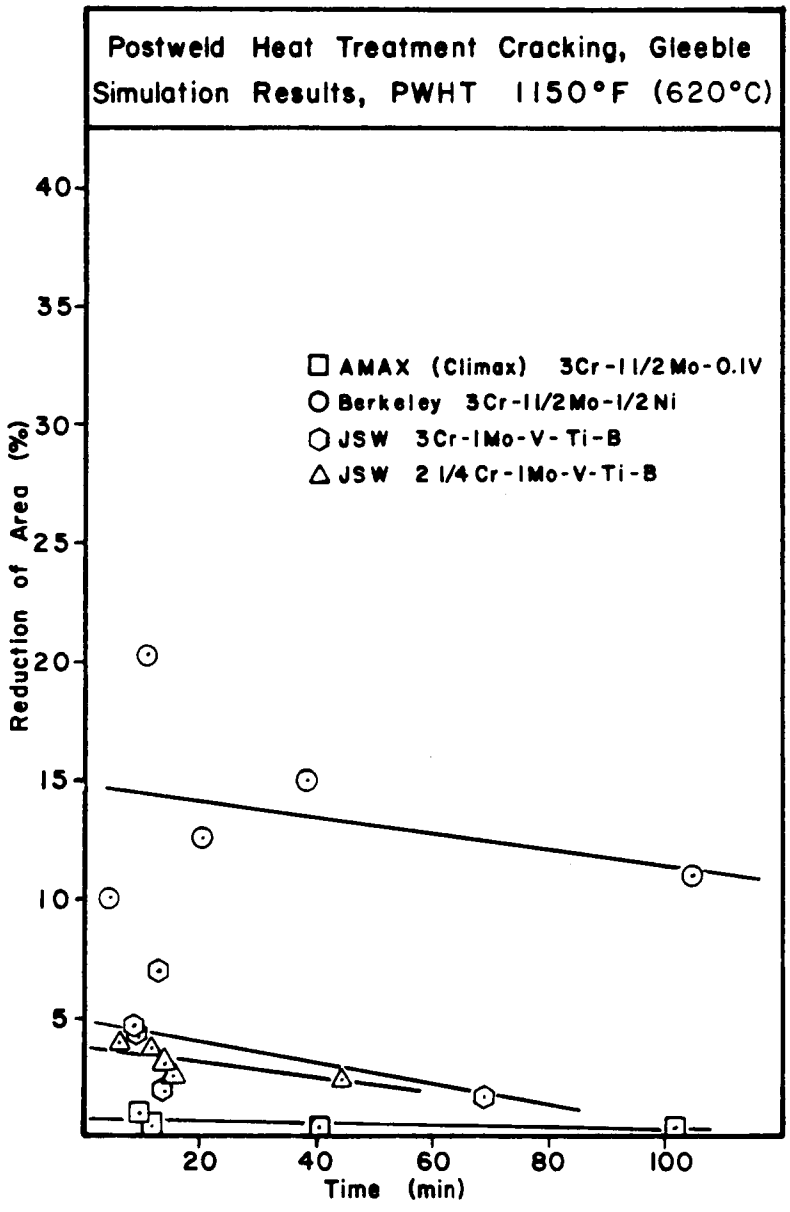


Figure 46. Modified 3Cr and 2 1/4Cr alloys' Gleeble stress-rupture behavior for simulated PWHT at 1150°F (620°C). Reduction in area vs. time to rupture at different stress levels.

Clearly there is a marked decrease in ductility for all four modified materials tested at 1150°F (620°C) compared to 1250°F (680°C). The decrease in ductility may be due to the increased duration of coherency of Mo_2C, slower growth and the increased time for the formation of the higher order carbides ($M_{23}C_6$, M_7C_3, M_6C) atthe lower PWHT temperature. These changes reduce plastic flow especially in the grain matrix as opposed to the grain boundaries.

Figures 45 and 46 clearly show a separation in the response of the Berkeley 3Cr-1 1/2Mo-1/2Ni and the three vanadium modified alloys. The RA of the Berkeley alloy, which has no vanadium addition, is significantly higher than the RA of the AMAX (Climax), JSW 3Cr or JSW 2 1/4Cr alloys. This is consistent with the literature which indicates that the addition of vanadium to the Cr-Mo alloys is detrimental with respect to PWHT cracking susceptibility.[18,46,49,59,73]

The Berkeley 3Cr-1 1/2Mo-1/2Ni material exhibits relatively high ductility at both 1150°F (620°C) and 1250°F (680°C) which probably is the result of the high nickel (0.52%) content and the absence of strong carbide formers (vanadium, niobium). Increased nickel has been shown to increase the rate of dissolution of Fe_3C and Mo_2C and speed the precipitation of $M_{23}C_6$, M_7C_3 and M_6C.[10] The rapid formation of carbides at lower temperatures and the concomitant very short times of coherency would result in the greatest strengthening of the matrix while the overall strength of the grain boundaries is high and before significant embrittlement could occur in accordance with Tamaki's model.[70] It is to be noted that although the Berkeley

3Cr-1 1/2Mo-1/2Ni material has the highest carbon (0.16%) and silicon (0.28%) and relative high phosphorous (0.010%), this material appears to be significantly resistant to PWHT cracking.

The relatively low rupture ductilities exhibited by the JSW 3Cr-1Mo-V-Ti-B and JSW 2 1/4Cr-1Mo-V-Ti-B is probably due to the high vanadium content (0.28 and 0.26%) of these materials. Both materials have particularly low phosphorous (0.007%) and silicon (0.06%) and therefore these elements would not significantly affect susceptibility. Although the aluminum content of the JSW 2 1/4Cr-1Mo-V-Ti-B material (0.016%) is at least three times greater than the other modified alloys investigated, the similarity in response of the JSW 3Cr-1Mo-V-Ti-B would appear to rule out aluminum as being significant in regard to the low ductility of the JSW 2 1/4Cr-1Mo-V-Ti-B material. The increase in rupture ductility with increasing time to fracture at 1250°F (680°C) for the JSW 3Cr-1Mo-V-Ti-B alloy may be the result of carbide coarsening which, in turn, may be related to the higher Cr to Mo ratio for this material compared to the other modified 2 1/4Cr-1Mo and 3Cr-Mo alloys.

The limited rupture ductility of the AMAX (Climax) 3Cr-1 1/2Mo-0.1V material (in comparison to the other V-Ti-B modified materials) was not anticipated. A nominally similar composition experimental heat of the AMAX (Climax) material (P2904), tested previously by Richey[25], exhibited higher rupture ductility (from 27 to 36% RA at 1250°F (680°C) and from 8.5 to 10% RA at 1150°F (620°C)). It should be noted that the composition of the AMAX

(Climax) 3Cr-1 1/2Mo-0.1V material is higher in phosphorous (0.012%) and silicon (0.26%) and lower in nickel (0.11%) than the other vanadium modified alloys including the experimental AMAX (Climax) heat, P2904. (Heat P2904 has phosphorous, silicon and nickel contents of 0.006%, 0.016% and 0.21% respectively.) As discussed in the literature review, phosphorous can cause grain boundary embrittlement, lower rupture ductility and increase susceptibility to PWHT cracking,[57,64,89,92] silicon can enhance the formation of Mo_2C[74,79,80] and aid phosphorous segregation,[79,91] and increasing nickel appears to accelerate the kinetics of carbide formation.[10] Thus, the high susceptibility of the AMAX (Climax) 3Cr-1 1/2Mo-0.1V material may be due to a combination of embrittlement, enhanced formation of Mo_2C and a slower rate of formation of more stable (and less detrimental) carbides such as $M_{23}C_6$, M_7C_3 and M_6C (due to the lower nickel content). Tamaki's[57,71] work has shown that the formation and persistence of Mo_2C at high temperatures combined with embrittlement due to elevated phosphorous levels is extremely detrimental with respect to cracking susceptibility.

Overall susceptibility of the modified 3Cr-Mo and 2 1/4Cr-1Mo alloys may be made using the Vinckier and Pense Criteria[53,78] (page 51). According to this criteria, an alloy that exhibits a RA of less than 5% is "extremely" susceptible, between 5 and 10% is "highly" susceptible, between 10 and 15% is "slightly" susceptible, and above 20% is "not" susceptible. The AMAX (Climax) 3Cr-1 1/2Mo-0.1V material would be considered "extremely" susceptible at both PWHT temperatures. The JSW 2 1/4Cr-1Mo-V-Ti-B and JSW 3Cr-1Mo-V-Ti-B

materials would both be considered "highly" susceptible at 1250°F (680°C) and "extremely" susceptible at 1150°F (620°C). The Berkeley 3Cr-1 1/2Mo-1/2Ni material would be considered "not" susceptible at 1250°F (680°C) and only "slightly" susceptible at 1150°F (620°C).

An alternative approach used by Spaeder and Plodder[83] is to multiply the RA by the stress to cause fracture for a time to fracture of ten minutes. This value, called the stress rupture parameter (SRP) indicates susceptibility to PWHT cracking when less than $15(10^4)$. The values of the SRP and the stress rupture index (SRI), a normalized value of the SRP with the highest SRP being equal to 100, are presented in Table 7. The SRP values indicate that only the AMAX (Climax) 3Cr-1 1/2Mo-0.1V at 1250°F (680°C) and 1150°F (620°C) and the JSW 2 1/4Cr-1Mo-V-Ti-B at 1150°F (620°C) are susceptible to PWHT cracking. However, the SRI shows the great difference in the response of the V and V-Ti-B modified alloys compared to the Berkeley 3Cr-1 1/2Mo-1/2Ni material with no addition of strong carbide forming elements. The Berkeley 3Cr-1 1/2Mo-1/2Ni has a SRI value at least four times the SRI value of the modified alloys containing deliberate additions of vanadium.

In order to ascertain that the grain coarsened region of the HAZ exhibited the lowest ductility during PWHT samples were subjected to several different thermal cycles and simulated PWHT. Further, grain refinement of the coarse grained HAZ by overlapping HAZ's in multiple pass welds has been proposed as one method of preventing PWHT cracking[39,65] and this also was evaluated. Samples of the AMAX (Climax) 3Cr-1 1/2Mo-0.1V, JSW 3Cr-1Mo-V-Ti-B, and JSW

Table 7. Stress-rupture parameter and stress rupture index for the modified 3Cr and 2 1/4Cr alloys.

Material	PWHT Temperature		Stress		Reduction in Area %	SRP (x10^4)	SRI
	°F	(°C)	KSI	(MPa)			
AMAX 3Cr-1½Mo-0.1V (Climax)	1250 1150	(680) (620)	42 64	(289) (441)	1.5 0.8	6.4 4.8	6 4
Berkeley 3 Cr-1½Mo-½Ni	1250 1150	(680) (620)	36 61	(248) (420)	31.0 16.0	110.0 97.0	100 88
JSW 3 Cr-1Mo-V-Ti-B	1250 1150	(680) (620)	44 55	(303) (379)	5.7 3.9	25.0 21.0	23 19
JSW 2¼ Cr-1Mo-V-Ti-B	1250 1150	(680) (620)	47 49	(324) (338)	6.0 3.0	28.0 14.0	25 13

2 1/4Cr-1Mo-V-Ti-B materials were subjected to two consecutive thermal cycles; the first to 2400°F (1315°C) to produce a coarse grained HAZ, the second to 1700°F (927°C) to produce a grain refined HAZ from the coarse grained material, and then subjected to simulated PWHT at 1150°F (620°C). With only a grain coarsening thermal cycle prior to PWHT all three materials exhibited severe embrittlement with rupture ductilities less than 5%. However, when a grain refining thermal cycle was superposed on the material after a grain coarsening cycle, rupture ductilities were found to be 12% for the JSW 3Cr-1Mo-V-Ti-B and JSW 2 1/4Cr-1Mo-V-Ti-B materials and 15% for the AMAX (Climax) 3Cr-1 1/2Mo-0.1V material after PWHT at 1150°F (620°C). By the Vinckier and Pense criteria,[53,78] the grain refining has resulted in change in ranking to "slightly" susceptible from the "extreme" susceptibility of the coarse grained regions. Therefore, the small bead, half bead technique[65] or temper beading[39] methods, which result in refinement of the coarse grained HAZ, may prove successful in preventing PWHT cracking in these alloys.

The cracking susceptibility of the grain refined region was determined for comparison with the results obtained from the multiple pass simulation (grain coarsening followed by grain refinement) for the JSW 2 1/4Cr-1Mo-V-Ti-B alloy. This material was thermal cycled to 1700°F (927°C) and then PWHT at 1150°F (620°C) with an applied stress of 62ksi (430MPa). The RA was found to be 54%, significantly higher than the 12% RA obtained for the multiple thermal cycle sample.

The stress to cause fracture was higher for the multiple thermal cycle specimens, 84ksi (580MPa), than for the grain refined specimens, 62ksi (430MPa), or the grain coarsened specimen, 52ksi (360MPa). This result indicates that that load shedding to the grain refined region or fusion zone may occur if the coarse grained region is fully refined by subsequent passes. However, if some coarse grained material remains in the HAZ after the use of welding techniques to refine the coarse grained region of the HAZ, strain accumulation may occur in the coarse grained material, due to it's lower strength, resulting in an increase in PWHT cracking susceptibility.

In addition, samples of the modified 2 1/4Cr-1Mo and 3Cr-Mo materials were subjected to simulated PWHT in the Gleeble with no prior thermal cycle. The JSW 3Cr-1Mo-V-Ti-B and Berkeley 3Cr-1 1/2Mo-1/2Ni materials were were PWHT at 1250°F (680°C) with applied stresses of 39ksi (270MPa) and 37ksi (260MPa) respectively and a sample of the JSW 2 1/4Cr-1Mo-V-Ti-B was PWHT at 1150°F (620°C) with an applied stress of 52ksi (360MPa). The RA values obtained were 91% for the JSW 3Cr-1Mo-V-Ti-B, 86% for the Berkeley 3Cr-1 1/2Mo-1/2Ni, and 74% for the JSW 2 1/4Cr-1Mo-V-Ti-B. Thus, these studies show that the grain coarsening thermal cycle is indeed a precursor to the metallurgical events which result in the embrittlement of the modified Cr-Mo steels observed at both PWHT temperatures.

Fractography of the Modified 3Cr-Mo and 2 1/4Cr-1Mo Alloys.

Fractographs of representative Gleeble simulated PWHT cracking specimens are shown in Figures 47 through 54 for the AMAX (Climax) 3Cr-1 1/2Mo-0.1V, Berkeley 3Cr-1 1/2Mo-1/2Ni, JSW 2 1/4Cr-1Mo-V-Ti-B, and JSW 3Cr-1Mo-V-Ti-B materials. The samples for the fractographic examination were thermal cycled and PWHT in an argon atmosphere chamber mounted in the Gleeble. The specimens were essentially free of oxidation on the fracture face.

Two modes of fracture are clearly evident in Figures 47 through 54 and are similar to those described by Hippsley[64] as low ductility intergranular fracture (LDIGF) and intergranular microvoid coalescence (IGMVC). LDIGF is characterized by intergranular fracture along the prior austenite grain boundaries that is smooth and free of any microductility. However, IGMVC is characterized by fracture along the prior austenite grain boundaries that exhibits extensive microductility.

The AMAX (Climax) 3Cr-1 1/2Mo-0.1V material (Figures 47 and 48) and the JSW 2 1/4Cr-1Mo-V-Ti-B material (Figures 51 and 52) exhibit LDIGF at both PWHT temperatures, 1250°F (680°C) and 1150°F (620°C). The low macroductility, 3.8 and 1.3% respectively for the AMAX material and 5.1 and 1.8% respectively for the JSW 2 1/4Cr material, correlates with the lack of microductility in the fractographs.

The Berkeley 3Cr-1 1/2Mo-1/2Ni material (Figures 49 and 50) primarily shows the IGMVC mode of fracture at both PWHT temperatures. Figure 50, the 1150°F (620°C) PWHT specimen fractograph, shows a lesser amount of microvoid formation with several grain faces devoid

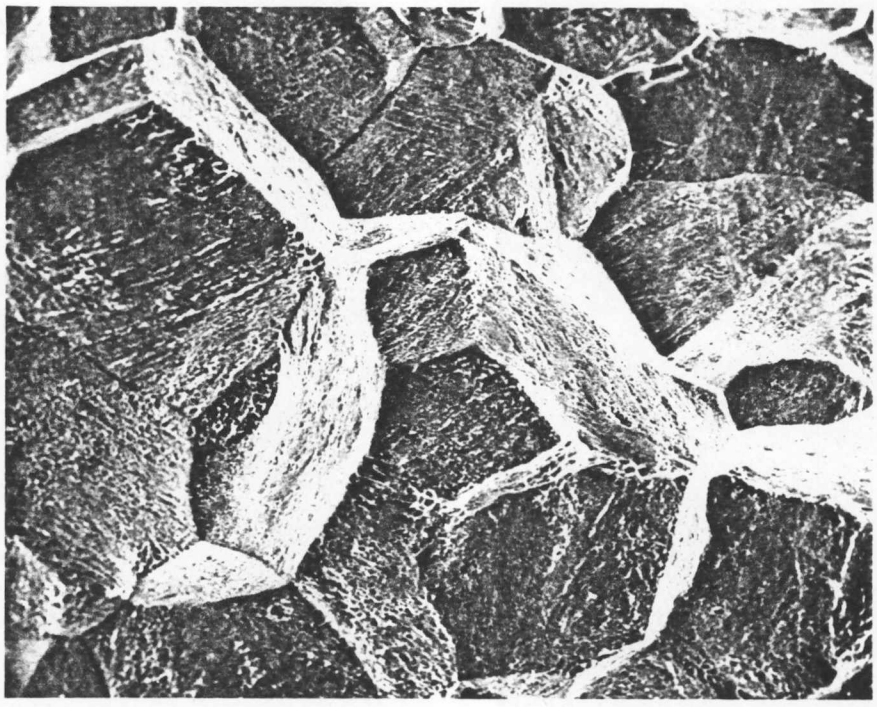


Figure 47. Fractograph of AMAX (Climax) 3Cr-1 1/2Mo-0.1V, 1250°F (680°C) PWHT. 43.4KSI (229MPa), 7.9min. to fracture, 3.8% RA, SEM 500X.

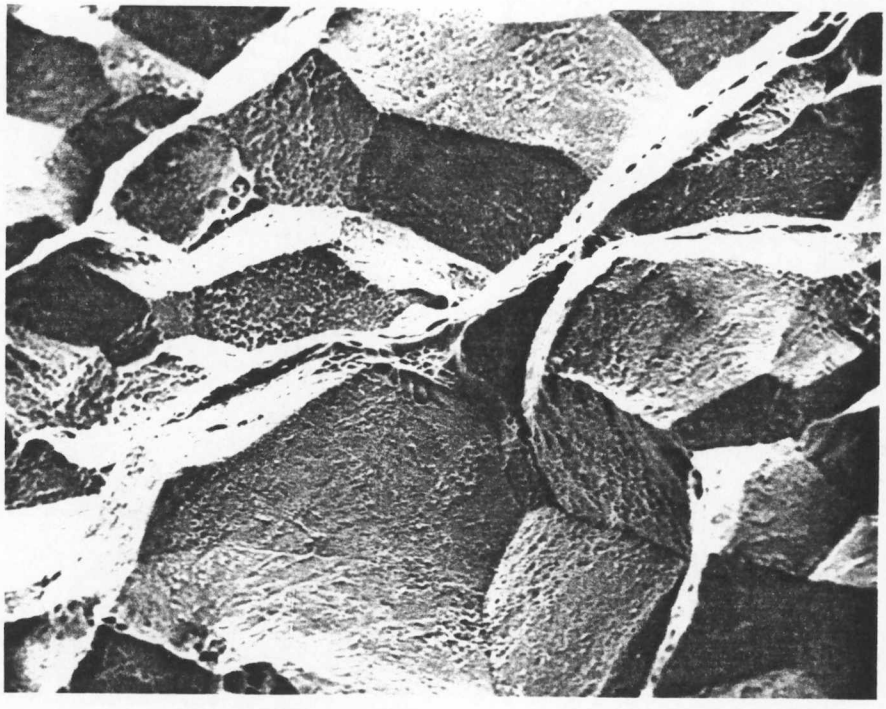


Figure 48. Fractograph of AMAX (Climax) 3Cr-1 1/2Mo-0.1V, 1150°F (620°C) PWHT. 65.1KSI (449MPa), 8.9min. to fracture, 1.3% RA, SEM 500X.

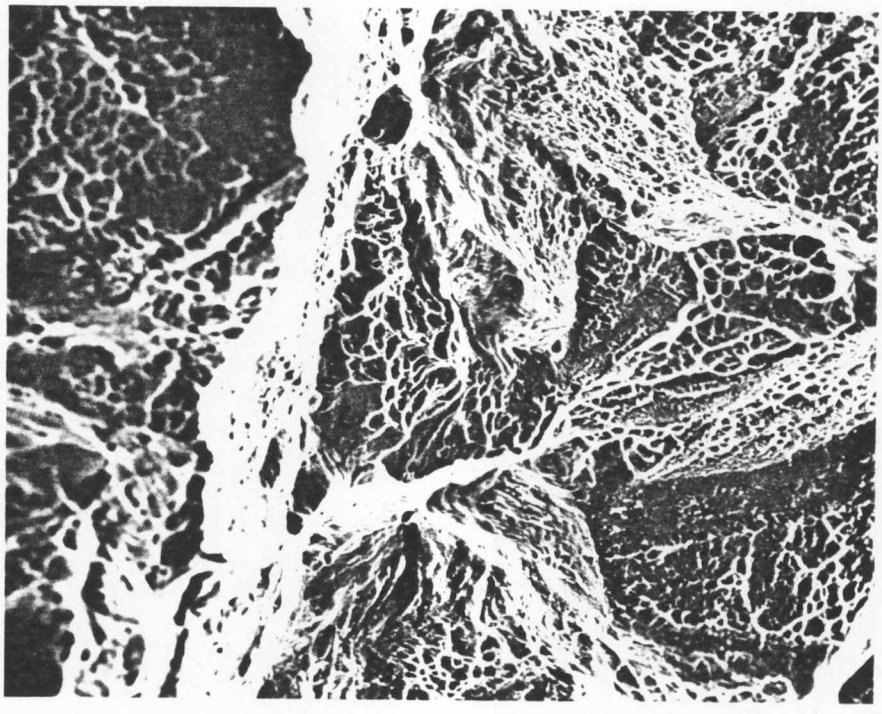


Figure 49. Fractograph of Berkeley 3Cr-1 1/2Mo-1/2Ni, 1250°F (680°C) PWHT. 39.3KSI (271MPa), 9.9min. to fracture, 21% RA, SEM 500X.

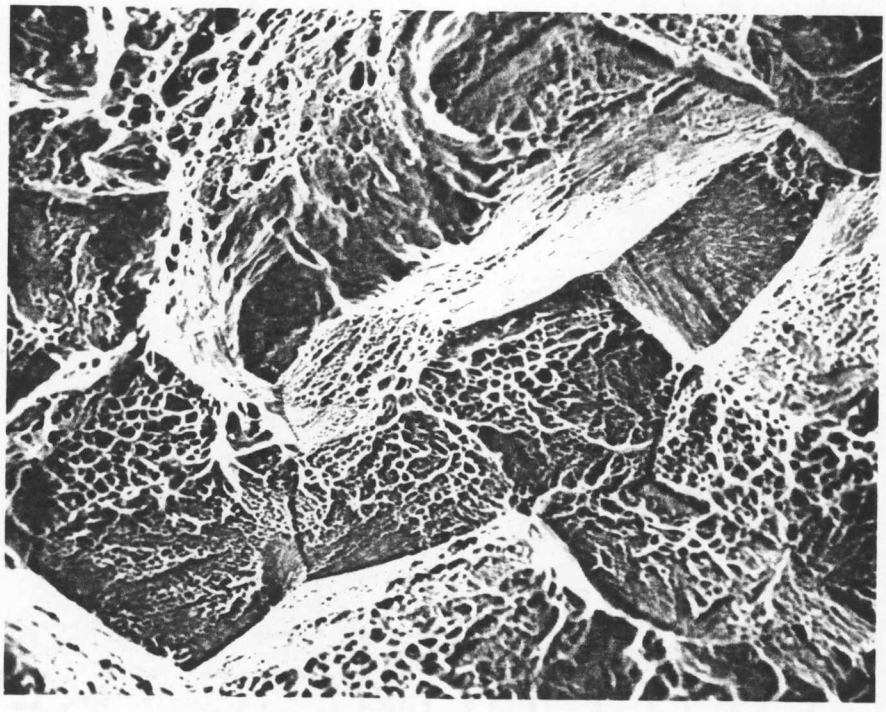


Figure 50. Fractograph of Berkeley 3Cr-1 1/2Mo-1/2Ni, 1150°F (620°C) PWHT. 64.2KSI (442MPa), 2.7 min. to fracture, 11% RA, SEM 500X.

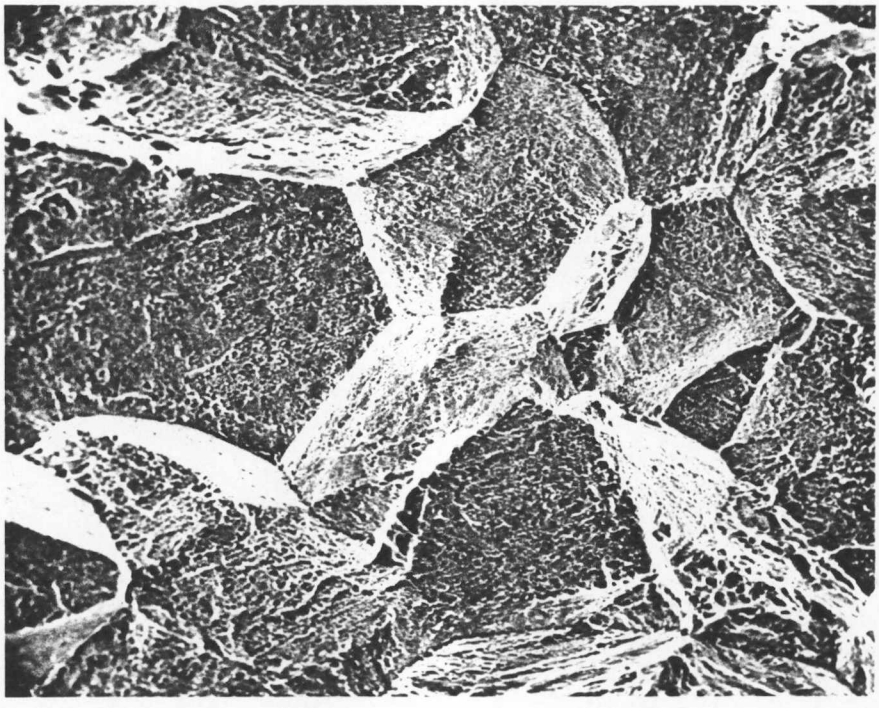


Figure 51. Fractograph of JSW 2 1/4Cr-1Mo-V-Ti-B, 1250°F (680°C) PWHT. 51.9ksi (358MPa), 5.5 min. to fracture, 5.1% RA, SEM 500X.

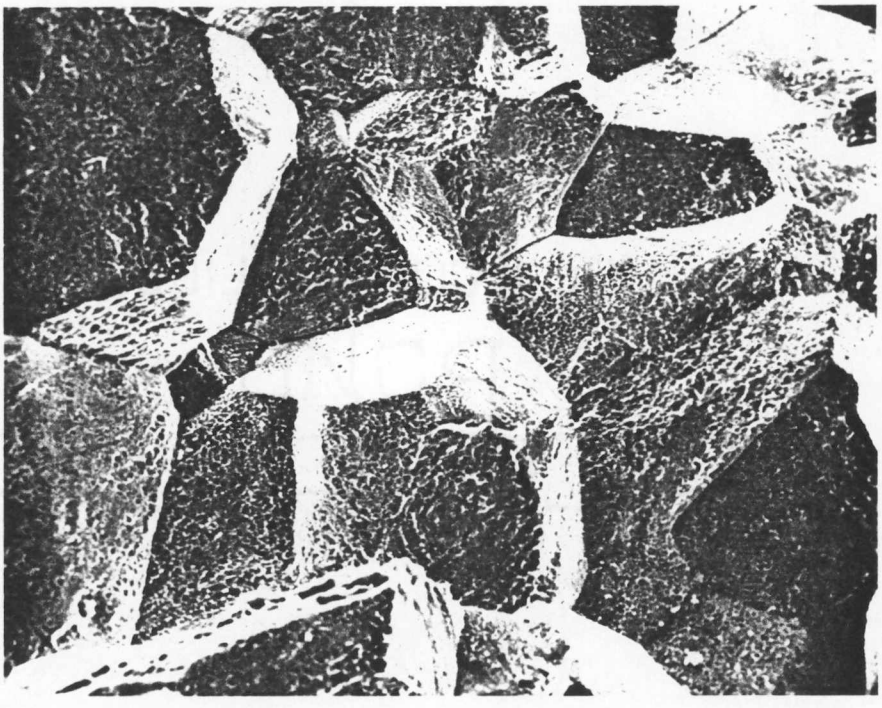
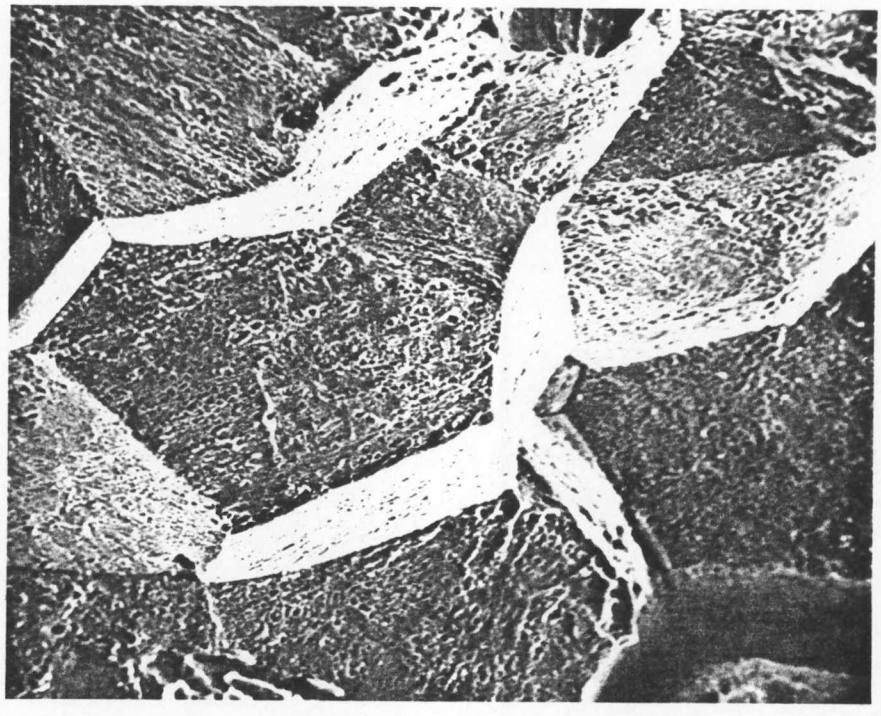
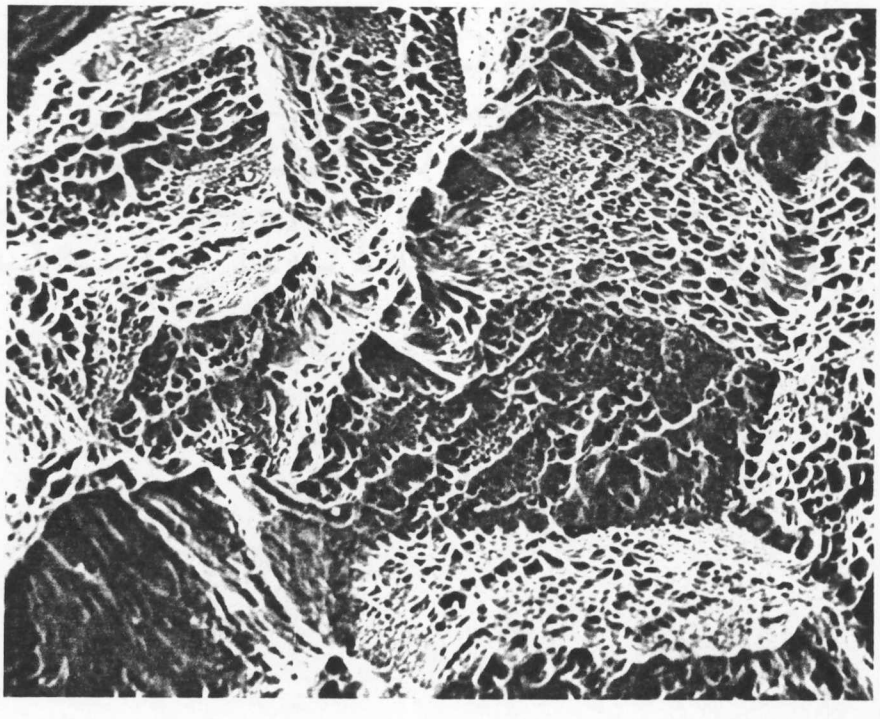


Figure 52. Fractograph of JSW 2 1/4Cr-1Mo-V-Ti-B, 1150°F (620°C) PWHT. 47.2ksi (325MPa), 44.6 min. to fracture, 1.8% RA, SEM 500X.

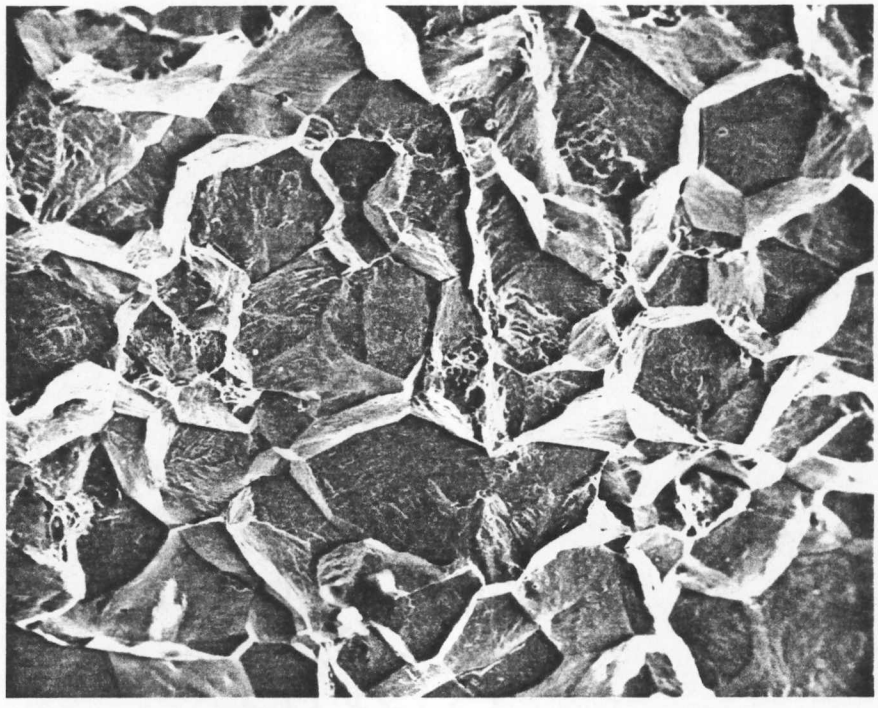


A

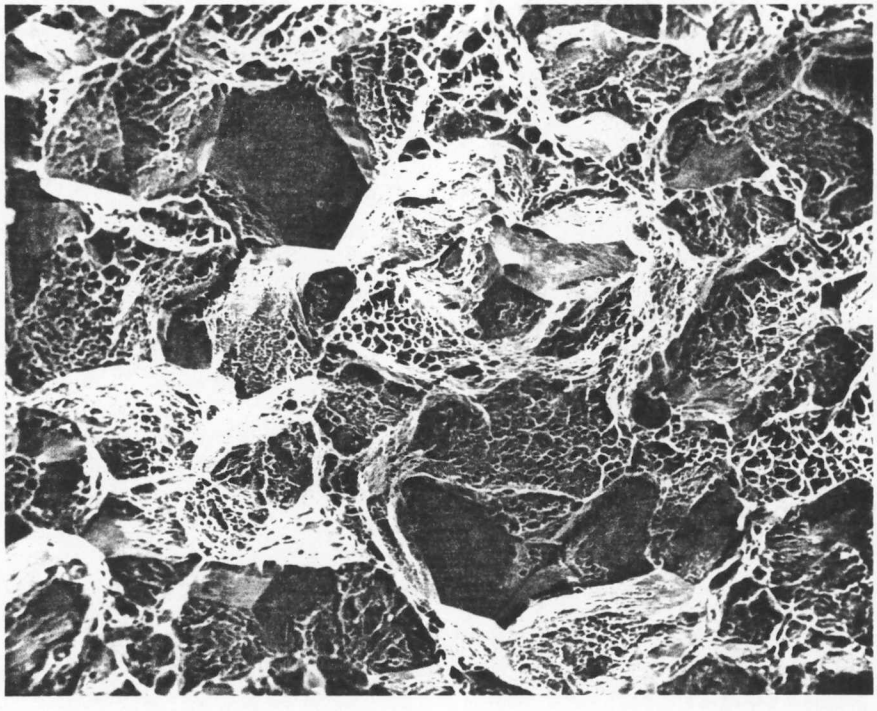


B

Figure 53. Fractographs of JSW 3Cr-1Mo-V-Ti-B, 1250°F (680°C) PWHT. 34.6ksi (239MPa), 16.3 min. to fracture, 7.7%RA, SEM 500X, a) LDIGF region, b) IGMVC region.



A



B

Figure 54. Fractographs of JSW 3Cr-1Mo-V-Ti-B, 1150°F (620°C) PWHT. 64.8ksi (446MPa), 8.6 min. to fracture, 1.8%RA, SEM 200X, a) LDIGF region, b) IGMVC region.

of any microductility. This corresponds with a decrease in macroductility, RA, from 21% at 1250°F (680°C) to 11% at 1150°F (620°C).

The JSW 3Cr-1Mo-V-Ti-B material exhibited a dual fracture mode at both PWHT temperatures. Figures 53a and 53b show the LDIGF and IGMVC regions observed on the sample PWHT at 1250°F (680°C). Comparison of Figure 53b and Figure 49, the Berkeley 3Cr-1 1/2Mo-1/2Ni, 1250°F (680°C) PWHT specimen, shows that the IGMVC regions of the JSW 3Cr-1Mo-V-Ti-B material exhibit less microvoid formation than the Berkeley type. The presence of the LDIGF region and the lesser extent of microvoid formation correspond to a lower ductility, 7.7% RA, compared to the Berkeley alloy, 20% RA.

Figures 54a and 54b show the LDIGF and IGMVC regions of the JSW 3Cr-1Mo-V-Ti-B type PWHT at 1150°F (620°C). (Note, the magnification has been reduced in Figure 54 to 200X) The IGMVC region, Figure 54b, contains some smooth grain faces, free of any microductility. The increase in the amount of LDIGF surface is seen in the reduction of the observed macroductility to 1.8% RA compared to 7.7% RA for the 1250°F (680°C) PWHT JSW 3Cr-1Mo-V-Ti-B specimen.

The dual mode of fracture has been observed by Granjon[59] in PWHT cracking susceptibility determinations employing the implant testing technique. Granjon found that at lower temperatures or higher stresses the LDIGF mode predominates on the fracture surface while at higher temperatures or lower stresses IGMVC is the mode of fracture. In Gleeble testing, where a constant load is maintained, it is possible that the fracture may initiate by IGMVC when the

stress is lowest and change to LDIGF as microvoid formation occurs. The formation of microvoids would decrease the load bearing cross sectional area effectively increasing the stress, driving the change in fracture mode to LDIGF.

Figure 55 shows a region of LDIGF on the Berkeley 3Cr-1 1/2Mo-1/2Ni, 1150°F (620°C) PWHT sample. Energy dispersivex-ray analysis (EDAX) for the small inclusion, the region immediately adjacent to the inclusion (region A in Figure 55b) and the smooth grain boundary well removed from the inclusion (region B in Figure 55a) are shown in Figures 56a through 56c. (Figure 56c superposes the EDAX spectrum for region B, the lower spectrum, and the EDAX spectrum for the inclusion.) The EDAX spectra show the presence of aluminum in the inclusion and on the grain boundaries. Although the aluminum content on the fracture surface well removed from the inclusion (region B, Figure 55a) is greatly reduced, the presence of aluminum in the EDAX spectrum can still be discerned in Figure 56c. The literature review indicated that aluminum has been found to increase PWHT cracking susceptibility in several studies.[54,80-82] The presence of aluminum on the LDIGF surfaces in the Berkeley 3Cr-1 1/2Mo-1/2Ni alloy, for which the predominant fracture mode is IGMVC, indicates that aluminum segregation to the prior austenite grain boundaries or partial dissolution of aluminum rich particles during the weld thermal cycle may be a factor in the loss of ductility during PWHT.

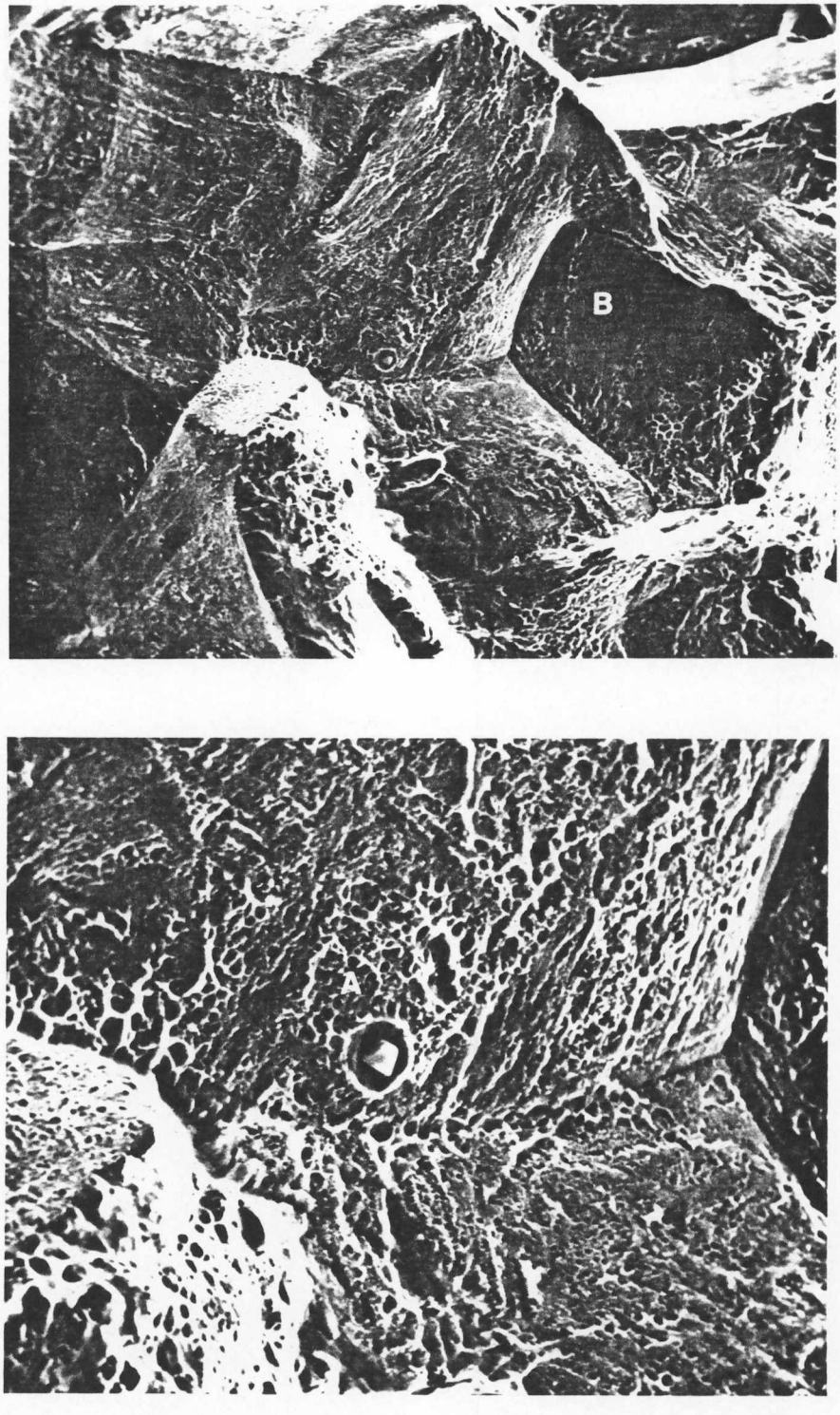
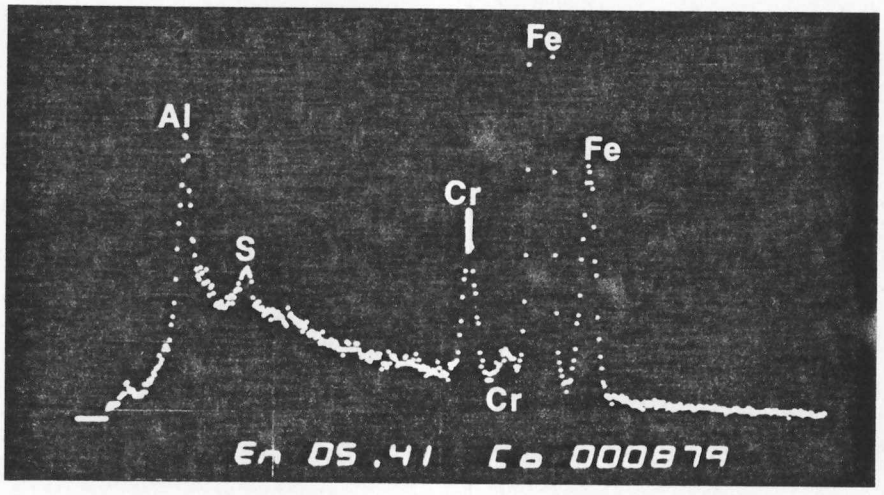
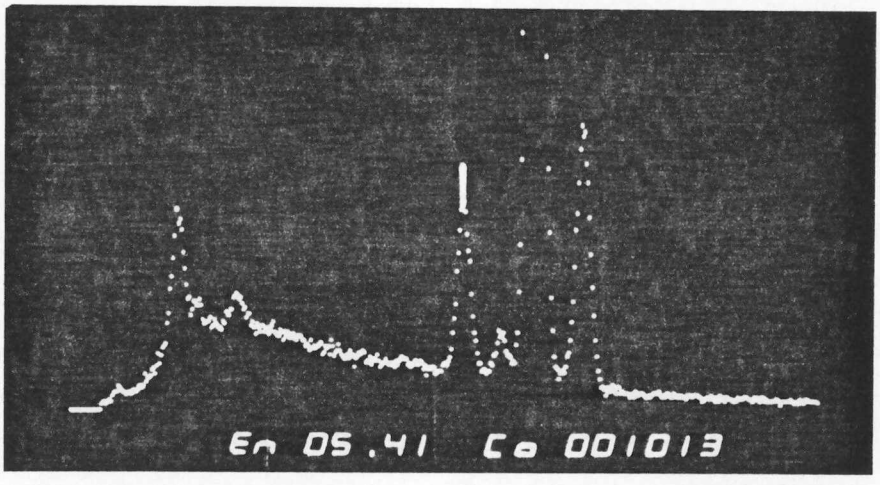


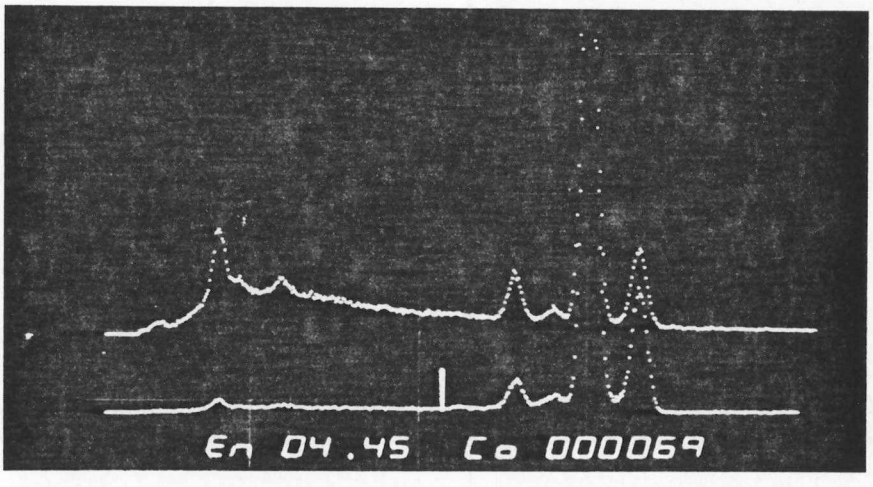
Figure 55. Fractographs of Berkeley 3Cr-1 1/2Mo-1/2Ni, 1150°F (620°C) PWHT. 64.2ksi (442MPa), 2.7 min. to fracture, 11% RA, a) SEM 500X, b) SEM 2000X.



A



B



C

Figure 56. Energy dispersive X-ray analysis (EDAX) of; a) inclusion, b) region A, c) region B vs. inclusion shown in Figure 58.

Aluminum bearing grain boundary particles were also found in the JSW 3Cr-1Mo-V-Ti-B material (Figure 57a). (Figure 57 is a fractograph of an IGMVC region taken from the same sample as shown in Figure 53.) The EDAX spectra for the particle and region immediately adjacent to the particle are shown in Figures 57b and 57c respectively. The limited ductility of the area immediately adjacent to the particle, which also showed aluminum in the EDAX spectrum, is evident in Figure 57a. However, unlike the Berkeley material shownin Figure 55, the region devoid of significant microvoid formation is limited to the area immediately adjacent to the particle. To some extent this may be the result of the lower PWHT temperature, 1150°F (620°C), of the Berkeley 3Cr-1 1/2Mo-1/2Ni sample as opposed to the 1250°F (680°C) PWHT temperature of the JSW 3Cr-1Mo-V-Ti-B sample as the ductility is greater at the higher temperature microvoid formation is enhanced.

Grain boundary particles in the JSW 3Cr-1Mo-V-Ti-B material were found to be present in greater number and were most often found to be initiation sites for the formation of microvoids (Figure 58). The EDAX spectra for the three typical particle compositions are shown in Figure 59. The particles labeled 1 on Figure 58a and 58b consist primarily of chromium, manganese and iron (Figure 59a) and are probably carbides. The particles labeled 2 and 3 both contain sulphur with type 2 being rich in manganese and iron with lesser amounts of titanium and chromium while type 3 particles are rich in titanium with lesser amounts of manganese, chromium, and iron.

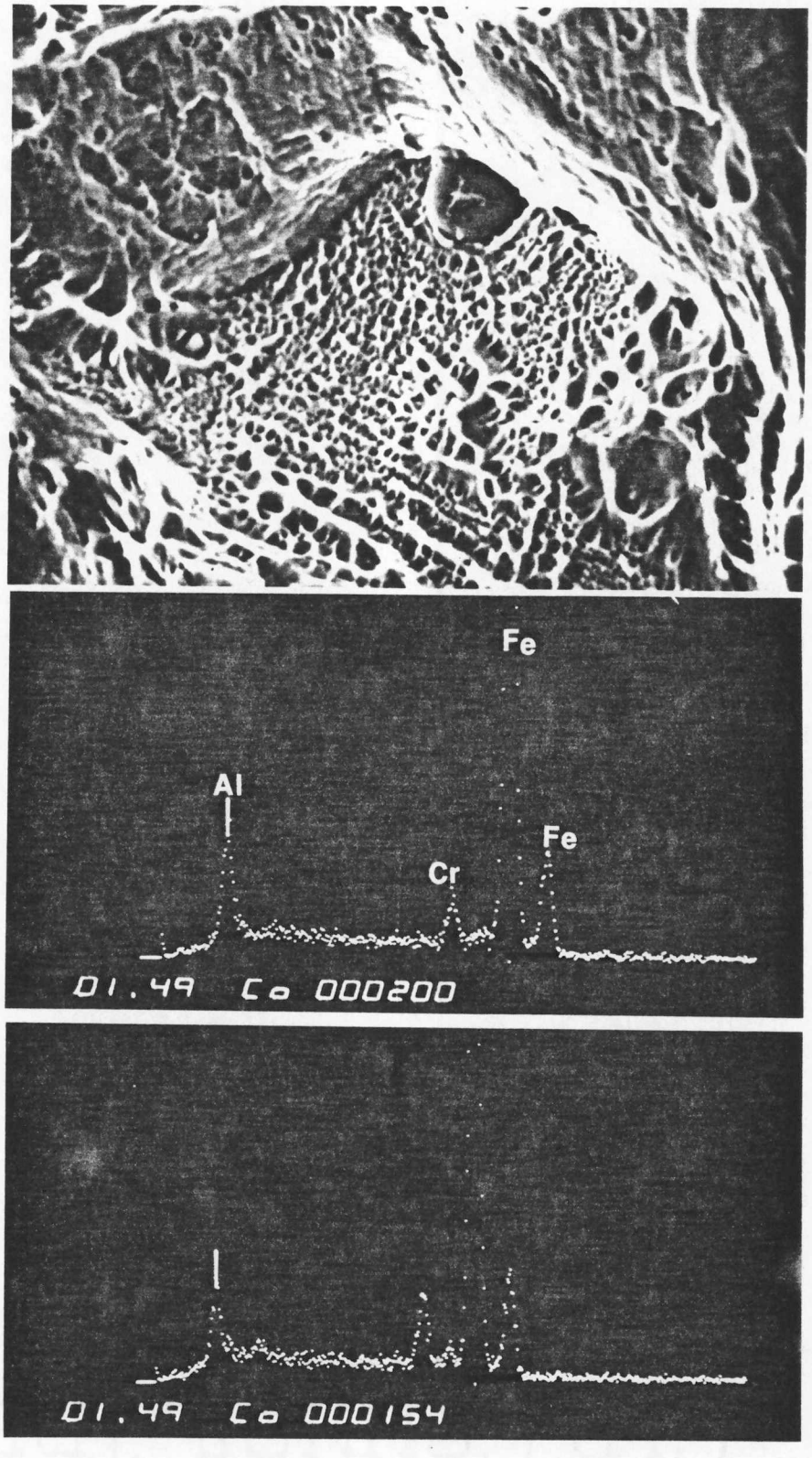


Figure 57. Fractographs of JSW 3Cr-1Mo-V-Ti-B, 1250°F (680°C) PWHT. 34.6ksi (239MPa), 16.3 min. to fracture, 7.7% RA, a) SEM 2000X, b) EDAX of grain boundary particle, c) EDAX of area immediately adjacent to the particle.

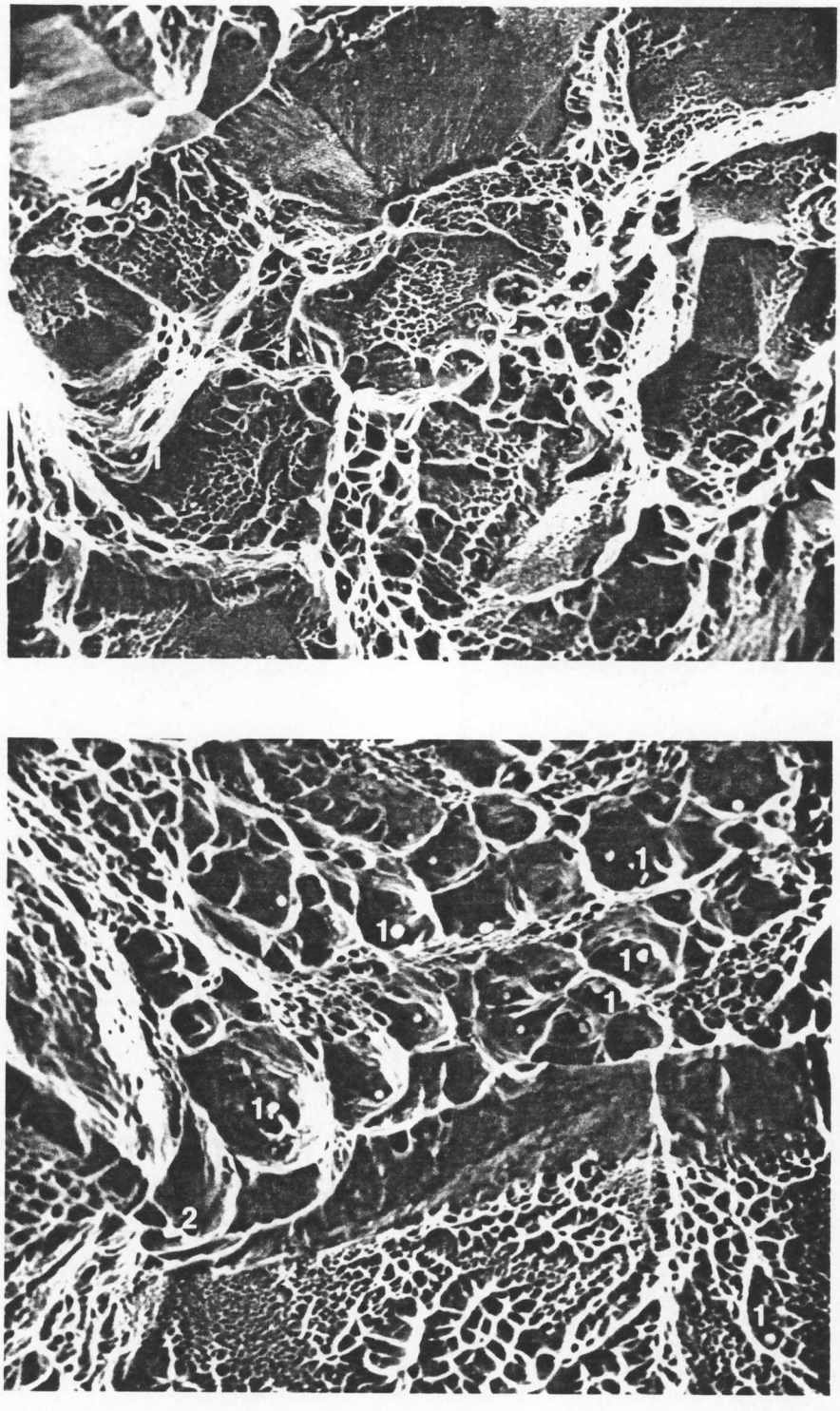
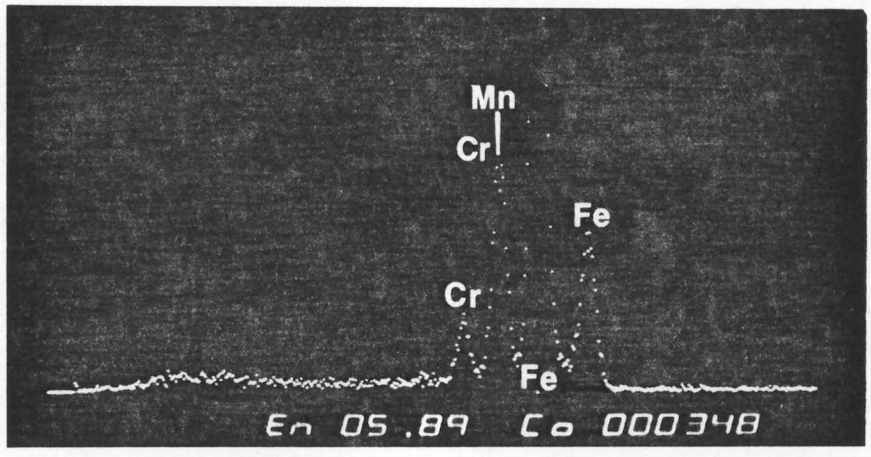
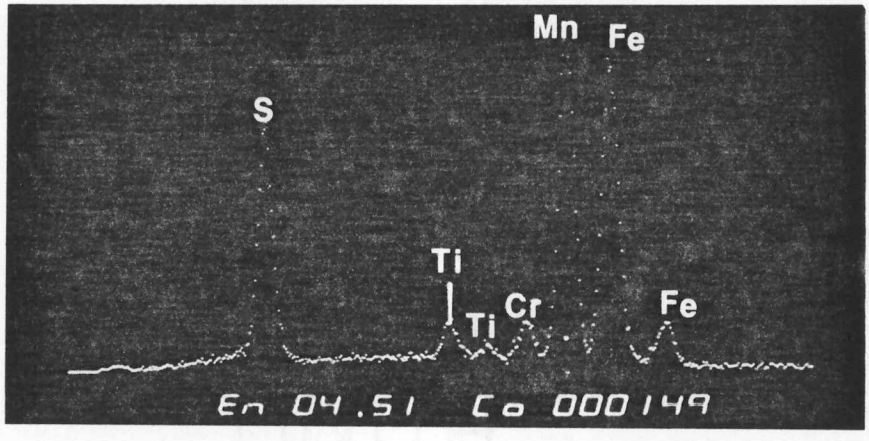


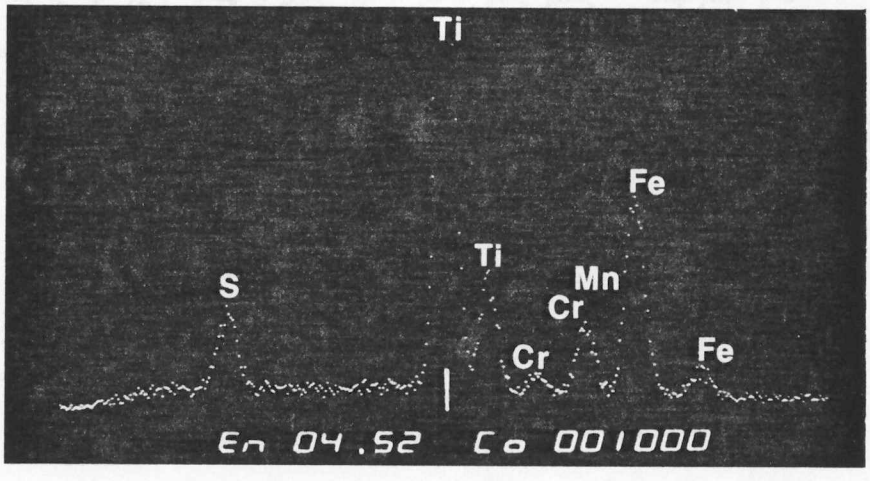
Figure 58. Fractographs of JSW 3Cr-1Mo-V-Ti-B, 1150°F (620°C) PWHT. 64.8ksi (446MPa), 8.6 min. to fracture, 1.8% RA, a)SEM 500X, b)SEM 1000X.



A



B



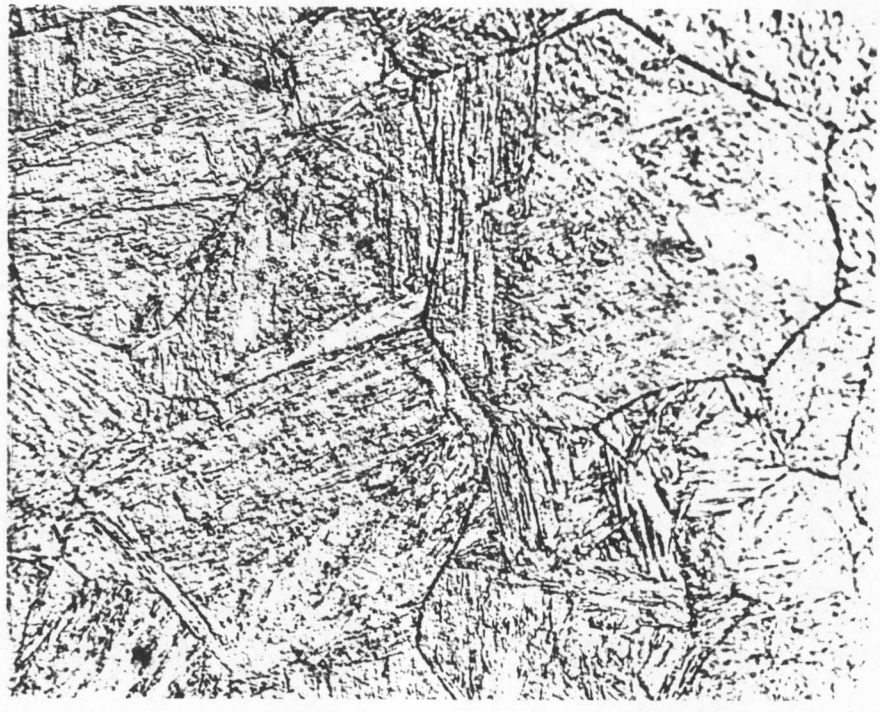
C

Figure 59. EDAX analysis of grain boundary particles initiating cavitation in JSW 3Cr-1Mo-V-Ti-B (Figure 58), a) type 1, b) type 2, c) type 3.

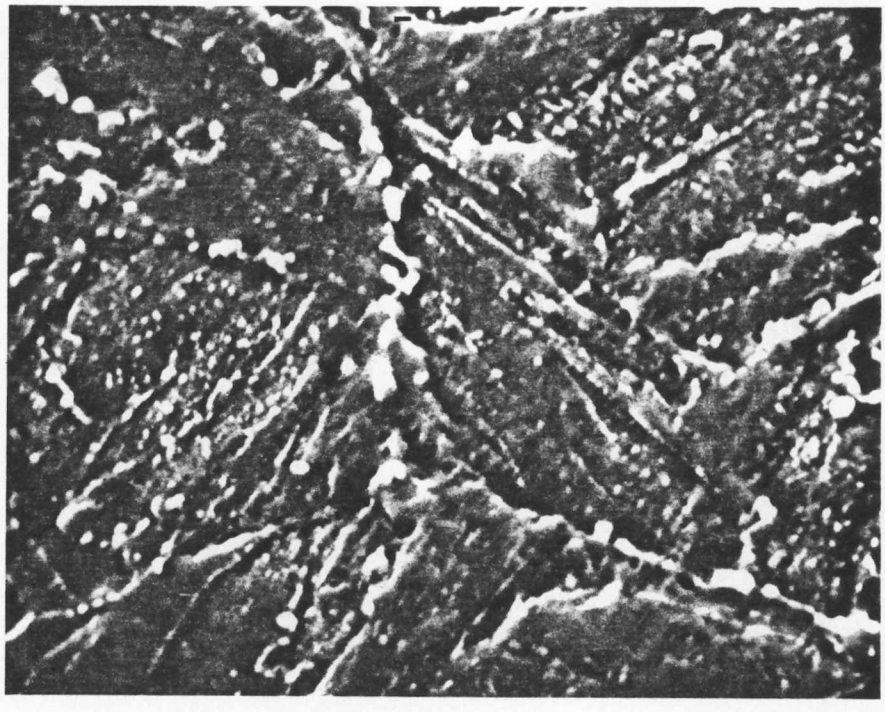
(The aluminum bearing particles discussed previously were found only rarely.) The nucleation of microvoids on sulphides, nitrides and carbides has been observed by several researchers.[15,56,64,96,114] Hippsley[64] has stated that low interfacial strength may be the cause of cavitation or microvoid formation about grain boundary particles.

The fractographic study therefore shows that the two fracture modes reported in the literature[59,64,96], LDIGF and IGMVC, are observed in the present study and, in agreement with Granjon[59], may in fact be present on a single specimen. The presence of aluminum and aluminum bearing particles in the prior austenite grain boundaries has been shown to be a possible factor contributing to LDIGF. However, in the JSW 3Cr-1Mo-V-Ti-B, where an abundance of grain boundary particles are present, cavitation initiating on the grain boundary particles may have a greater overall effect on rupture mode than the presence of a limited number of aluminum rich particles per se.

Optical, Scanning Electron and Transmission Electron Microscopy of Gleeble Simulated Postweld Heat Treatment Specimens. Figures 60 through 63 are optical and scanning electron micrographs of the region near the fracture surface of AMAX (Climax) 3Cr-1 1/2Mo-0.1V, Berkeley 3Cr-1 1/2Mo-1/2Ni, JSW 3Cr-1Mo-V-Ti-B, and JSW 2 1/4Cr-1Mo-V-Ti-B Gleeble simulated PWHT cracking specimens. The specimens employed for study were the longest time to fracture (88, 88.5, 71, and 100.9 minutes respectively), lowest stress, 1250°F (680°C) PWHT specimens for each alloy.

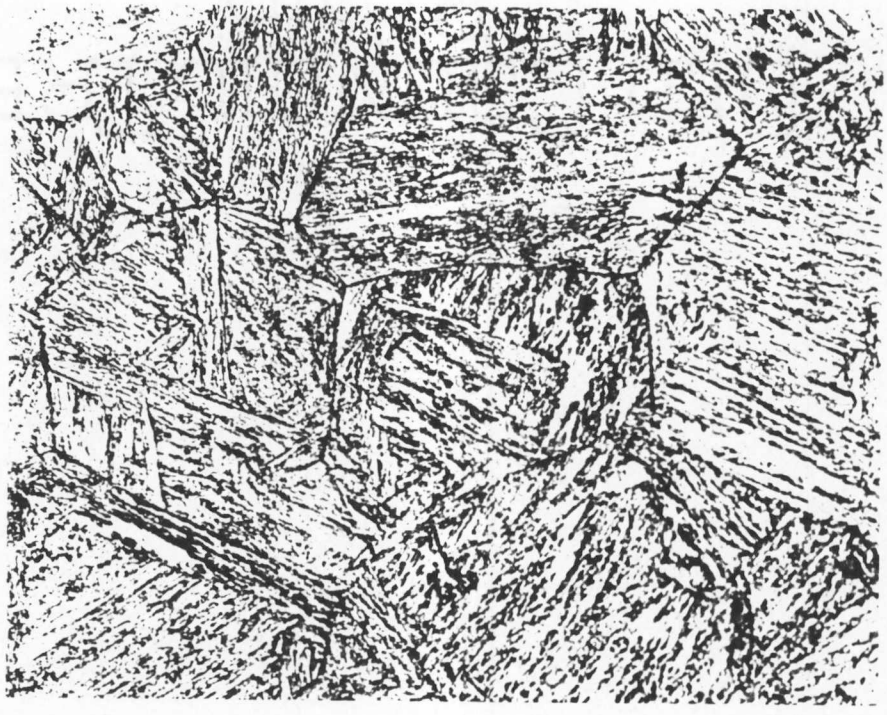


A

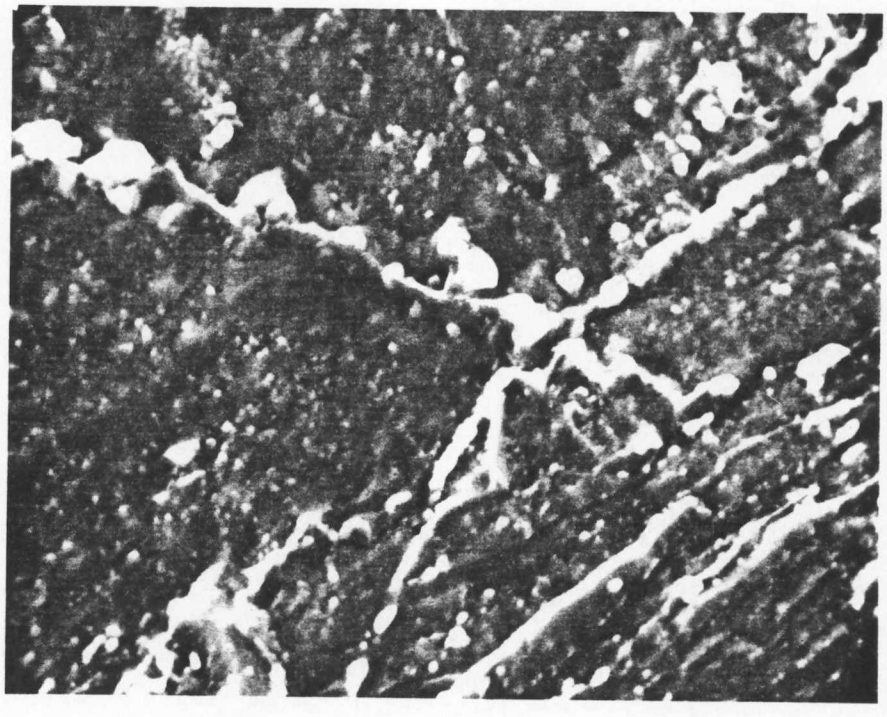


B

Figure 60. AMAX (Climax) 3Cr-1 1/2Mo-0.1V Gleeble simulated PWHT cracking specimen, 1250°F (680°C) PWHT. 25.5ksi (176MPa), 5% RA, 88 min. to fracture, a)500X OLM, b) 10,000X SEM.

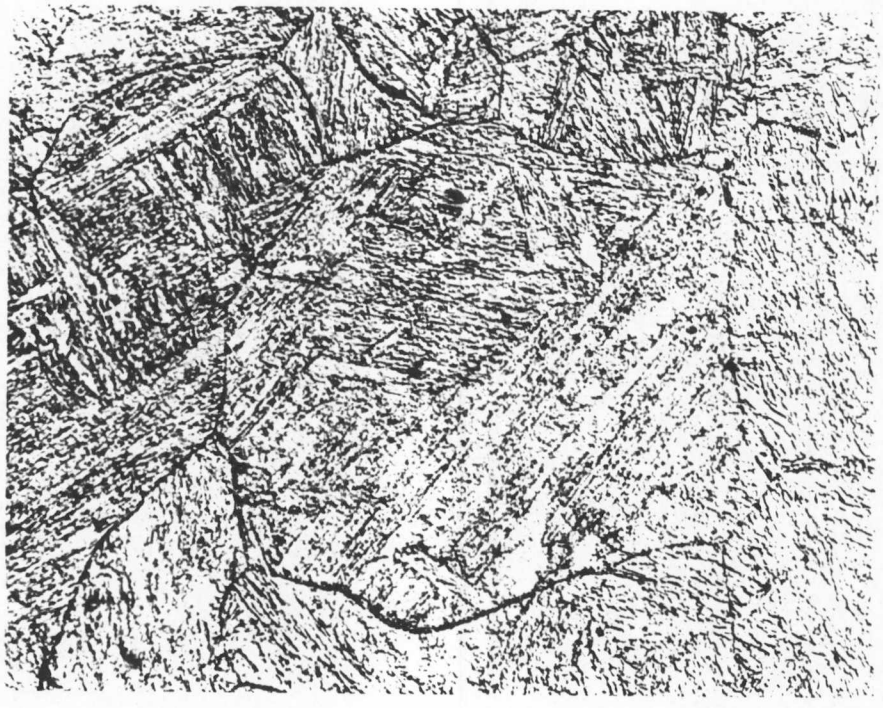


A

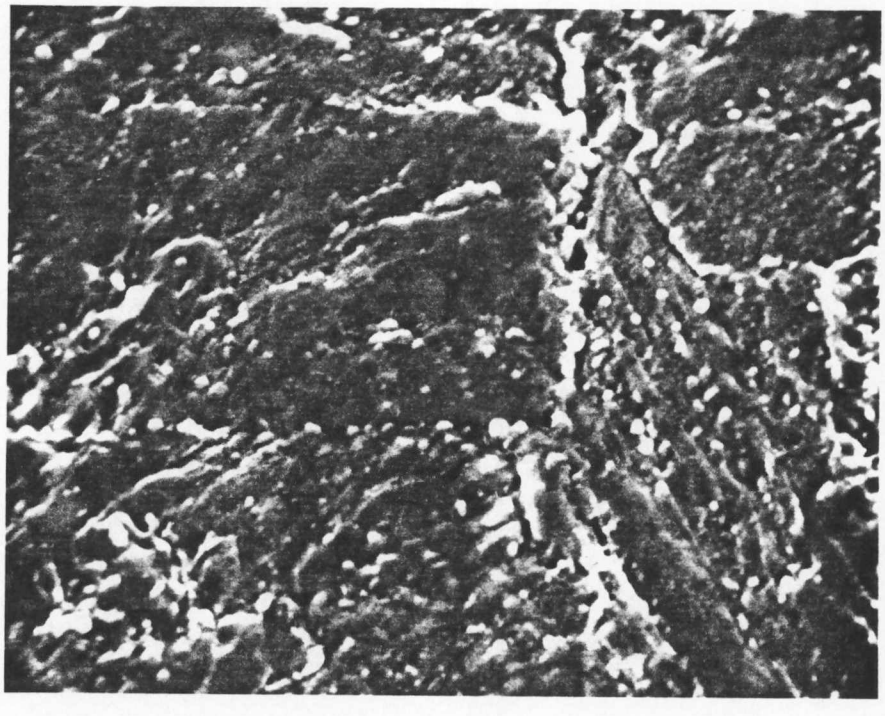


B

Figure 61. Berkeley 3Cr-1 1/2Mo-1/2Ni Gleeble simulated PWHT cracking specimen, 1250°F (680°C) PWHT. 21.4ksi (147MPa) 88.5 min. to fracture, 26% RA, a) 500X OLM, b) 10,000X SEM.

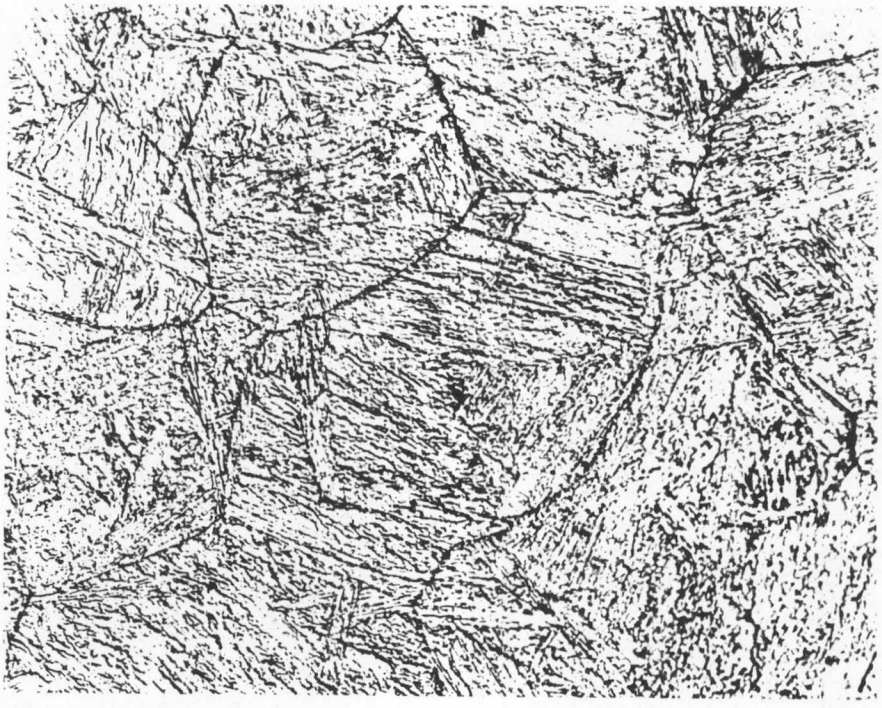


A

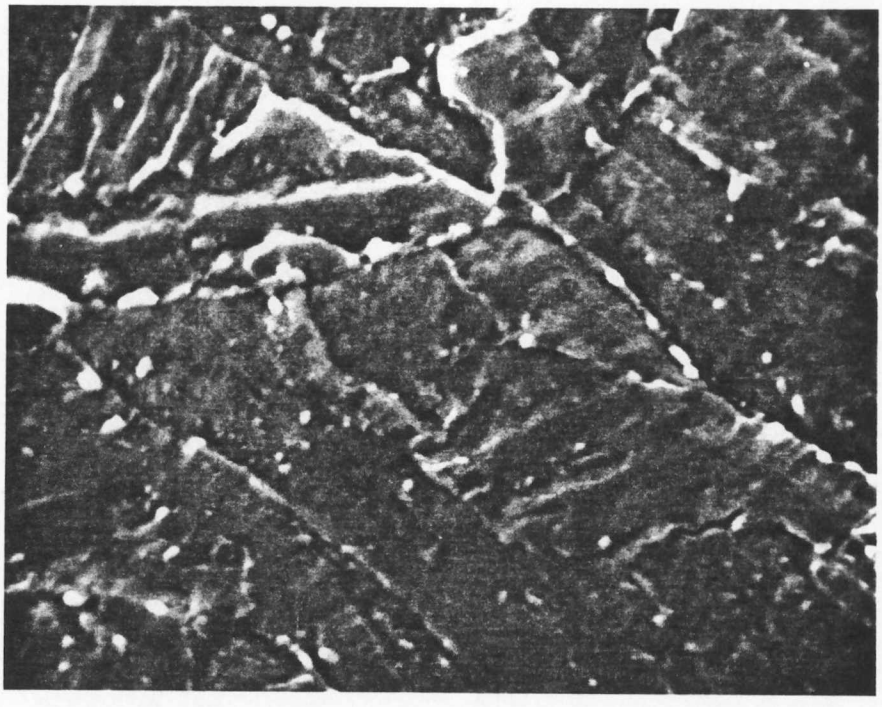


B

Figure 62. JSW 3Cr-1Mo-V-Ti-B Gleeble simulated PWHT cracking specimen, 1250°F (680°C) PWHT. 39.1ksi (269MPa), 14% RA, 71 min. to fracture, a) 500X OLM, b) 10,000X SEM.



A



B

Figure 63. JSW 2 1/4Cr-1Mo-V-Ti-B Gleeble simulated PWHT cracking specimen, 1250°F (680°C) PWHT. 34.3ksi (236MPa), 7.1% RA, 101 min. to fracture, a) 500X OLM, b) 10,000X SEM.

The microstructure, shown by both optical and scanning electron microscopy, has changed substantially from the as-cycled (as welded and no PWHT) microstructure shown in the transformation section (Figures 36 and 38 through 40, pages 108 and 110 through 112). The optical microstructures (Figures 60a through 63a) show that after PWHT the prior austenite grain boundaries are more clearly delineated and the acicular aspect of the microconstituents are less well defined in comparison to the as cycled microstructures. The scanning electron micrographs (Figures 60b through 63b) show an almost complete break down of the lath type constituents observed in the as cycled condition with extensive carbide precipitation along the prior austenite grain boundaries. Fine carbide precipitation has occurred within the grain matrix with the carbides in the Berkeley 3Cr-1 1/2Mo-1/2Ni material coarser than in the AMAX (Climax) 3Cr-1 1/2Mo-0.1V, JSW 3Cr-1Mo-V-Ti-B, or JSW 2 1/4Cr-1Mo-V-Ti-B alloys.

The presence of observable carbides in the matrix and extensive precipitation along the grain boundaries is concomitant with a loss in hardness or strength. The as cycled hardnesses, shown in Figures 30 through 33 (pages 99 through 102), were 370, 412, 400, and 388DPH for the AMAX (Climax) 3Cr-1 1/2Mo-0.1V, Berkeley 3Cr-1 1/2Mo-1/2Ni, JSW 3Cr-1Mo-V-Ti-B, and JSW 2 1/4Cr-1Mo-V-Ti-B materials respectively. After Gleeble simulated PWHT at 1250°F (680°C), the hardnesses were 253, 227, 268, and 256DPH for the AMAX (Climax), Berkeley, JSW 3Cr, and JSW 2 1/4Cr alloys respectively. The Berkeley 3Cr-1 1/2Mo-1/2Ni material exhibited the greatest change in hardness,

a 185DPH decrease, and the lowest hardness value, 227DPH, after PWHT which is indicative of a greater progression of carbides toward the end of the evolutionary chain.

Figures 64 through 67 show the transmission electron micrographs of the carbide extraction replicas of the AMAX (Climax) 3Cr-1 1/2Mo-0.1V, Berkeley 3Cr-1 1/2Mo-1/2Ni, JSW 3Cr-1Mo-V-Ti-B, and JSW 2 1/4Cr-1Mo-V-Ti-B from a cooperative effort undertaken at the University of Southern California, Los Angeles.[115] Table 8 summarizes the results of the carbide identification performed on extraction replicas for specimens thermal cycled on the Gleeble and PWHT at 1250°F (680°C) for 100 minutes (with applied stress). Table 8 also shows the approximate width of a carbide denuded zone observed adjacent to the prior austenite grain boundaries for the AMAX (Climax) 3Cr-1 1/2Mo-0.1V, Berkeley 3Cr-1 1/2Mo-1/2Ni, JSW 3Cr-1Mo-V-Ti-B, and JSW 2 1/4Cr-1Mo-V-Ti-B specimens. The width of the carbide denuded zone in the Berkeley 3Cr-1 1/2Mo-1/2Ni material was not determined.

The precipitates found within the grain matrix for all four materials was primarily M_2C with some MC type carbides in the vanadium modified alloys. The matrix precipitates in the AMAX (Climax) 3Cr-1 1/2Mo-0.1V, JSW 3Cr-1Mo-V-Ti-B, and JSW 2 1/4Cr-1Mo-V-Ti-B materials (Figures 64a, 66a and 67a) appear to be finer than in the Berkeley 3Cr-1 1/2Mo-1/2Ni material (Figure 65a). It is also apparent that the AMAX (Climax) 3Cr-1 1/2Mo-0.1V alloy had a higher volume fraction of precipitates in comparison to the Berkeley 3Cr-1 1/2Mo-1/2Ni material. The smaller size and greater

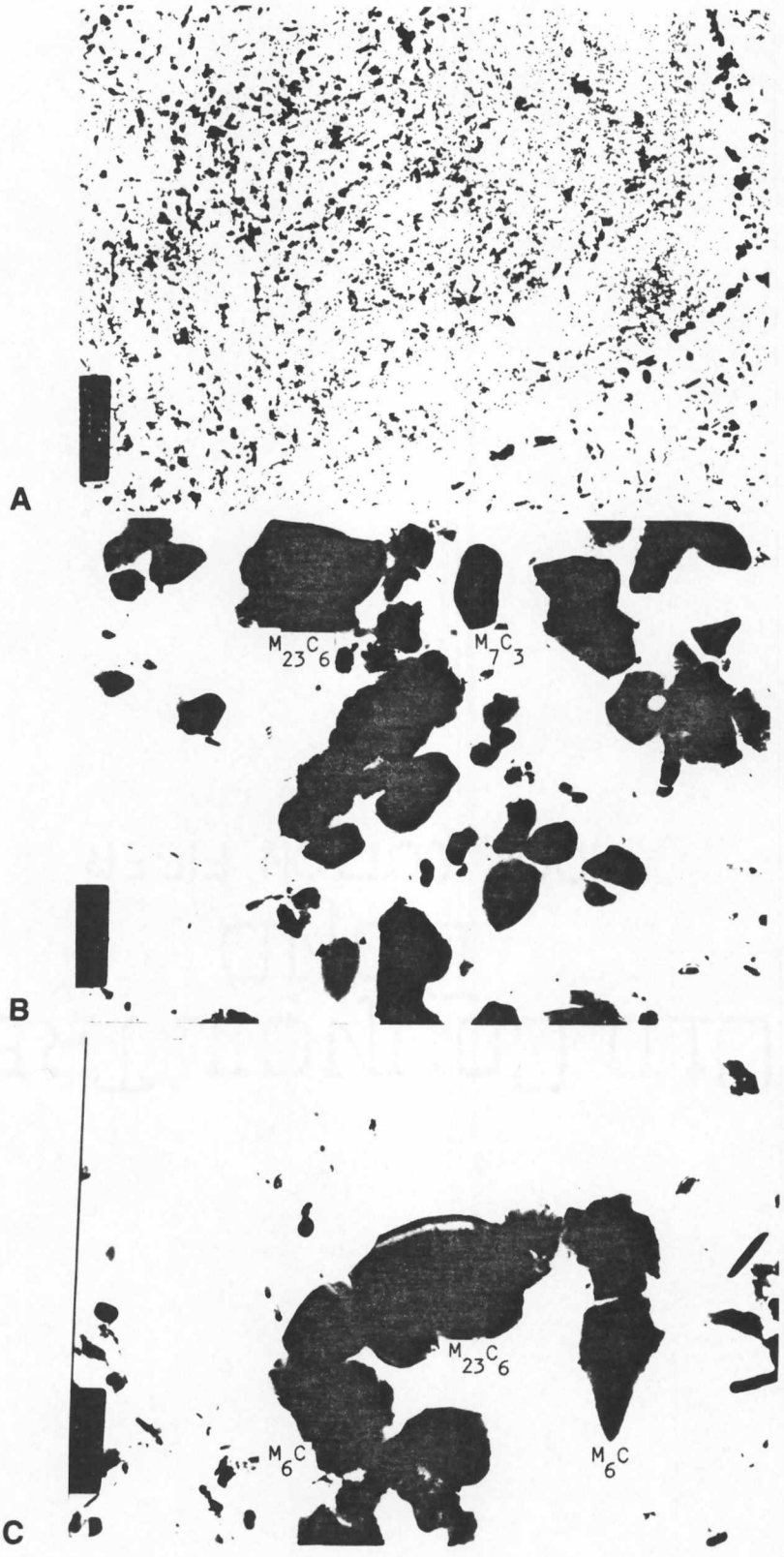


Figure 64. Transmission electron micrographs of AMAX (Climax) 3Cr-1 1/2Mo-0.1V, thermal cycled and PWHT at 1250°F (680°C) for 100 min. a) 3,300X, b) 36,000X, c) 49,000X.

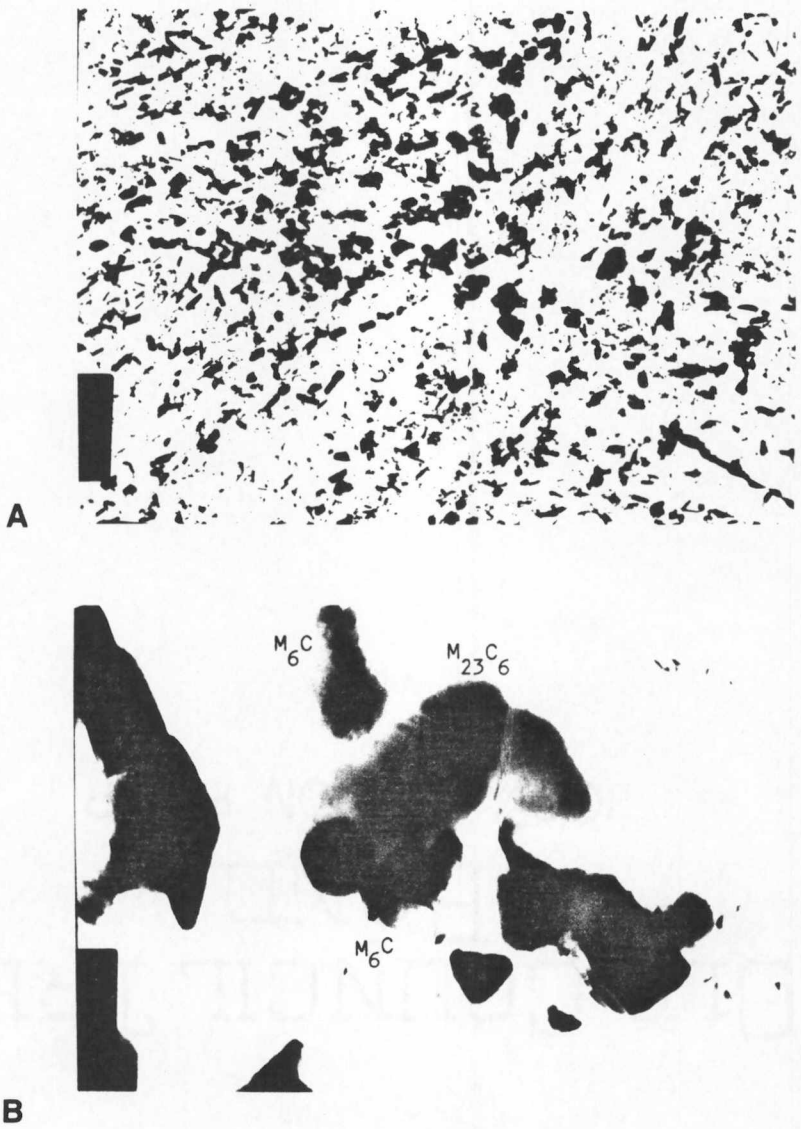


Figure 65. Transmission electron micrographs of Berkeley 3Cr-1 1/2Mo-1/2Ni , thermal cycled and PWHT at 1250°F (680°C) for 100 min. a) 6,350X, b) 82,000X.

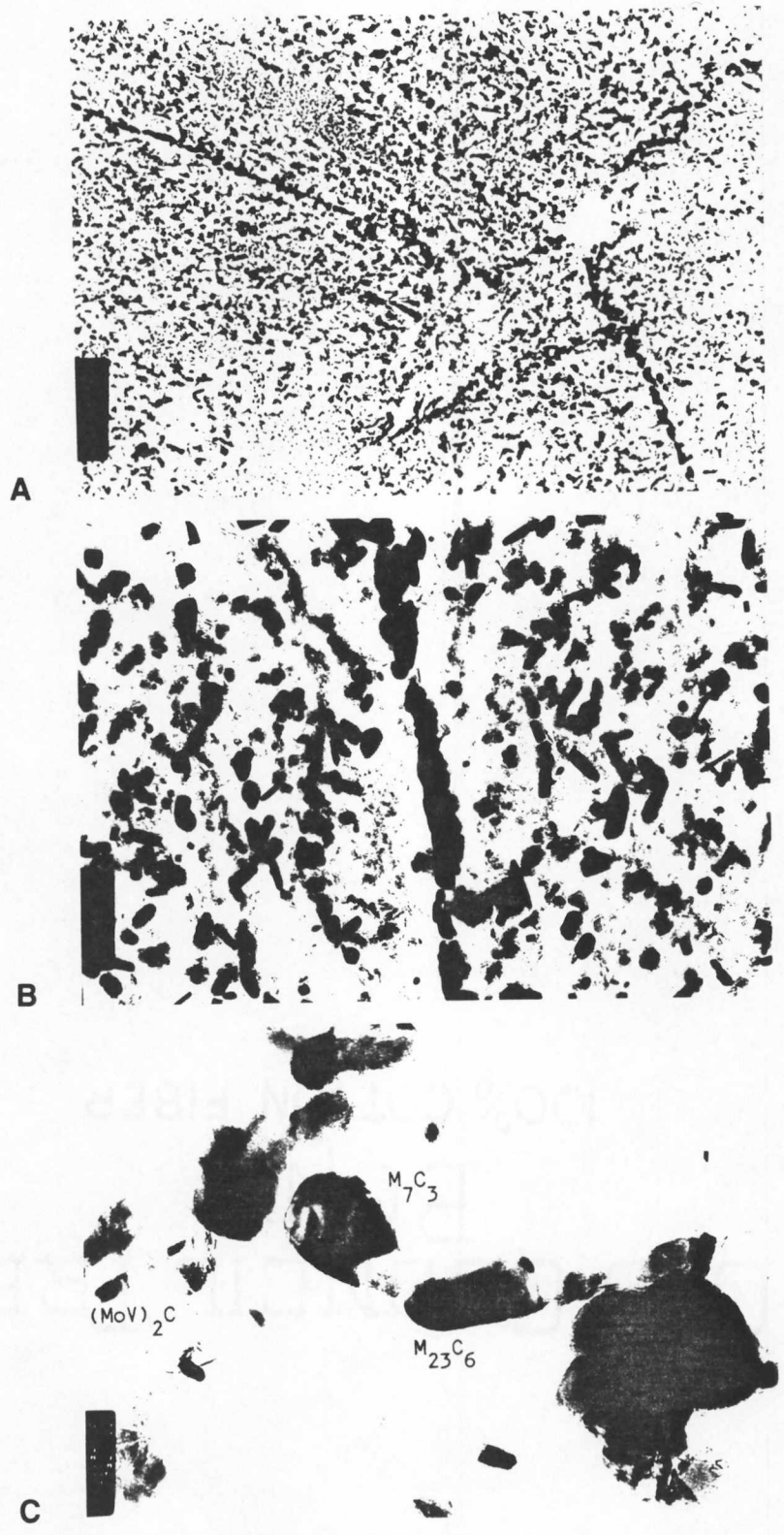


Figure 66. Transmission electron micrographs of JSW 3Cr-1Mo-V-Ti-B, thermal cycled and PWHT at 1250°F (680°C) for 100 min. a) 3,300X, b) 18,500X, c) 175,000X.

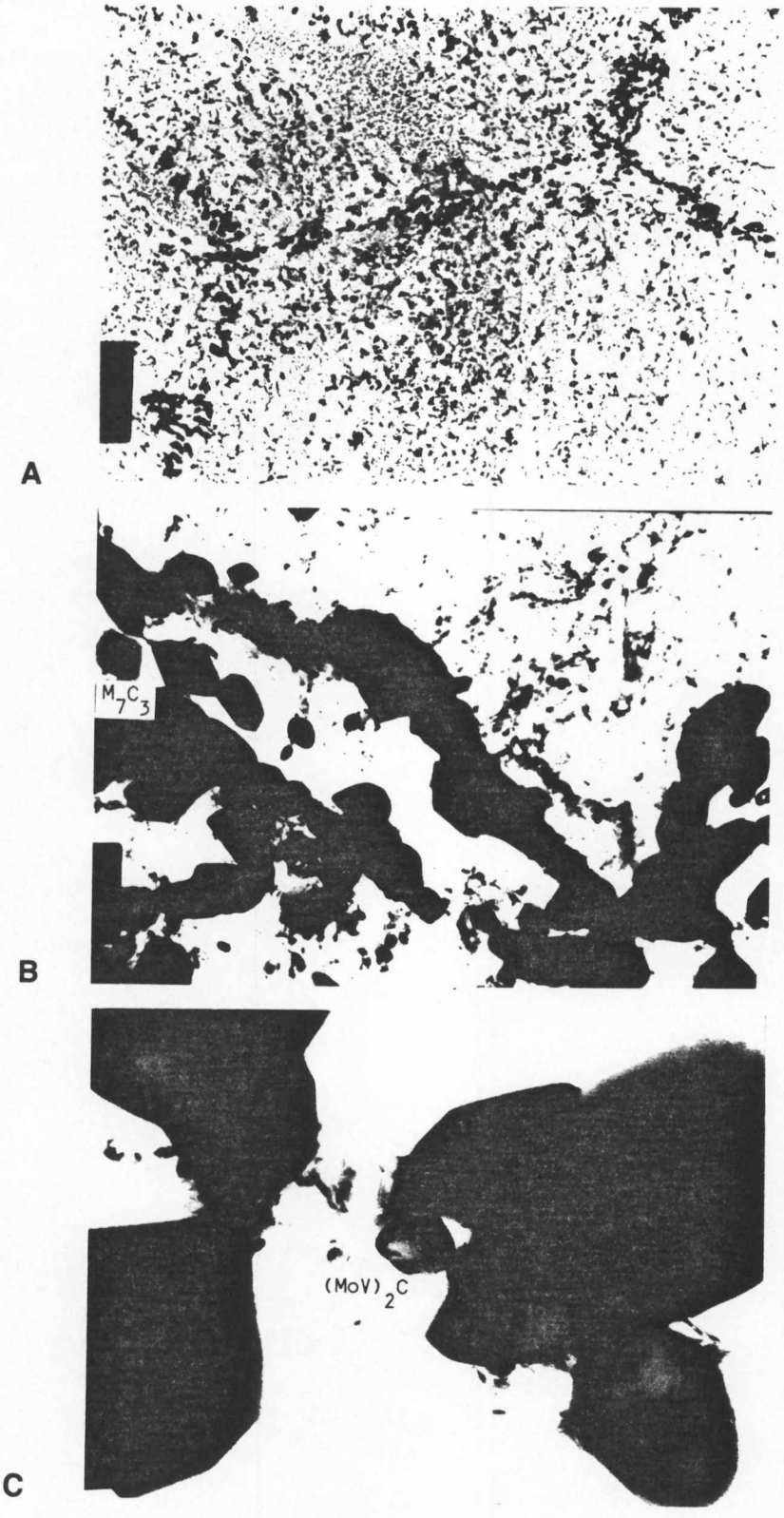


Figure 67. Transmission electron micrographs of JSW 2 1/4Cr-1Mo-V-Ti-B, thermal cycled and PWHT at 1250°F (680°C) for 100 min. a) 3,300X, b) 49,000X, c) 230,000X.

Table 8. Carbide analysis for the modified 3Cr and 2 1/4Cr alloys; Gleeble simulated PWHT at 1250°F (680°C) for 100 minutes.

Carbide	Berkeley 3 Cr-1½Mo-0.1V	AMAX (Climax) 3 Cr-1½Mo-0.1V	JSW 3 Cr-1Mo-V-Ti-B	JSW 2¼ Cr-1Mo-V-Ti-B
M_3C	NF	NF	NF	NF
M_2C	M	M	M	M
M_7C_3	NF	B (0.3-0.6μm)	B* (0.3-0.6μm)	B (0.3-0.6μm)
$M_{23}C_6$	B,LB (0.3-0.6μm)	B (0.3-0.6μm)	B (0.3-0.6μm)	B* (0.3-0.6μm)
M_6C	B (0.3-0.6μm)	B (0.3-0.6μm)	NF	NF
Denuded zone width	NR	~0.3μm	~0.1μm	<0.1μm

M - Matrix
B - boundary
LB - Lath boundary

* - predominate species
NF - not found
NR - not reported

amount of precipitates in the vanadium modified materials would result in a generally higher matrix strength than that of the Berkeley 3Cr-1 1/2Mo-1/2Ni alloy. The slower growth of the precipitates in the vanadium modified alloys also indicates that the duration of the period of coherency during PWHT is also probably longer. The combined effect of the delayed carbide evolution and the carbide morphology for the vanadium modified materials is to extend the period of maximum matrix strengthening to longer times and higher temperatures which is considered a major factor in PWHT cracking susceptibility as discussed by Tamaki.[70]

The TEM micrographs (Figures 64 through 67) show clearly the presence of coarse grain boundary carbides in all four alloys (approximately 0.3 to 0.6 μm in size). However, the scanning electron micrographs (Figures 60 through 63) show that the grain boundary carbides in the Berkeley 3Cr-1 1/2Mo-1/2Ni material tend to be larger in size than the grain boundary carbides in the AMAX (Climax) 3Cr-1 1/2Mo-0.1V, JSW 3Cr-1Mo-V-Ti-B, or JSW 2 1/4Cr-1Mo-V-Ti-B materials.The presence of only $M_{23}C_6$ and M_6C carbides in the grain boundaries (Table 8) of the Berkeley 3Cr-1 1/2Mo-1/2Ni material clearly demonstrates the accelerated kinetics of carbide precipitation in this alloy with respect to the other vanadium modified alloys. In the AMAX (Climax) 3Cr-1 1/2Mo-0.1V material, the presence of M_7C_3 in addition to $M_{23}C_6$ and M_6C indicates that carbide evolution is somewhat more sluggish in this alloy compared to the Berkeley alloy. However, the lack of any M_6C in the JSW 3Cr-1Mo-V-Ti-B or the JSW 2 1/4Cr-1Mo-V-Ti-B

materials, with 0.28% and 0.26% vanadium respectively, shows the significant retardation of carbide evolution in these alloys with respect to the Berkeley alloy. The effect of vanadium in stabilizing carbides[31] and restricting diffusion of chromium in ferrite[34] was discussed in the literature review. The retardation of carbide evolution and growth with the increased vanadium content is clearly evident from the data in Table 8.

The formation of the grain boundary carbides is accompanied with the formation of carbide denuded zones in the AMAX (Climax) 3Cr-1 1/2Mo-0.1V, JSW 3Cr-1Mo-V-Ti-B, and JSW 2 1/4Cr-1Mo-V-Ti-B materials. (The presence of and extent of a carbide denuded zone in the Berkeley 3Cr-1 1/2Mo-1/2Ni material has not been defined.) The rapid formation and growth of carbides along the prior austenite grain boundaries depletes the surrounding material of carbon and alloying elements and results in the formation of a weak region devoid of carbides. Several researchers have considered this narrow, soft region to be the site of strain accumulation and, ultimately, the region in which fracture occurs.[30,52]

The denuded zone widths were reported to be approximately 0.3 μm in the AMAX (Climax) 3Cr-1 1/2Mo-0.1V, 0.1 μm in the JSW 3Cr-1Mo-V-Ti-B, and not as pronounced in the JSW 2 1/4Cr-1Mo-V-Ti-B as in the JSW 3Cr-1Mo-V-Ti-B. It has been stated in the literature that as the denuded zone width increases the zone should be more able to accommodate the strain associated with creep induced plastic flow and therefore more resistant to cavitation and rupture.[35,42,46] However, the Gleeble results for the PWHT cracking study show that

the AMAX (Climax) 3Cr-1 1/2Mo-0.1V material, with the greatest extent of the denuded zone, was more susceptible to cracking than the JSW 3Cr-1Mo-V-Ti-B or JSW 2 1/4Cr-1Mo-V-Ti-B materials. The higher phosphorous content (0.012%) in the AMAX (Climax) material than the JSW 3Cr or JSW 2 1/4Cr materials (0.007%) may result in embrittlement being more potent in increasing susceptibility than the increase in the denuded zone width is in decreasing susceptibility. It is important to remember at this point that the effect of the denuded zone is disputed in the literature with both Swift[46] and Meitzner and Pense[50] arguing that the denuded zone is not a factor in PWHT cracking.

Summary of the Gleeble Simulated Postweld Heat Treatment Cracking Results for the Modified 3Cr-Mo and 2 1/4Cr-1Mo Materials.

It is apparent that vanadium additions strongly influence susceptibility to PWHT cracking. At both PWHT temperatures, 1150°F (620°C) and 1250°F (680°C), the AMAX (Climax) 3Cr-1 1/2Mo-0.1V, JSW 3Cr-1Mo-V-Ti-B, and JSW 2 1/4Cr-1Mo-V-Ti-B materials exhibited significantly lower rupture ductilities than the Berkeley 3Cr-1 1/2Mo-1/2Ni material which does not have a vanadium addition. Both the scanning electron and transmission electron microscopy examinations showed that carbide growth and precipitation was accelerated in the Berkeley alloy compared to the vanadium modified alloys. Precipitation of carbides at lower temperatures, more rapid growth and short times of coherency are the probable factors in the

increased resistance to cracking exhibited by the Berkeley 3Cr-1 1/2Mo-1/2Ni material.

Carbide precipitation and growth (evolution to more stable carbides) in the vanadium modified alloys was clearly retarded as compared to the Berkeley alloy. Finer matrix precipitates with greater volume fractions than in the Berkeley alloy is indicative of longer times of coherency and greater matrix strengthening at higher temperatures. Since the relative difference in grain boundary strength with relation to grain matrix strength is the principal factor in PWHT cracking, the overall greater susceptibility, as shown by the lower rupture ductilities, of the three vanadium modified alloys may be explained on this basis.

Additional factors that may have an effect on susceptibility have also been presented. The presence of aluminum bearing particles and aluminum in the prior austenite grain boundaries was observed to be associated with region of LDIGF in the Berkeley alloy and associated with areas of decreased microvoid formation in the JSW 3Cr alloy. Extensive cavitation was observed to initiate on particles along the prior austenite grain boundaries in the JSW 3Cr-1Mo-V-Ti-B material. Initiation of cavitation on grain boundary particles is thought to be due to low interfacial strength with the matrix.[64,94,95] The linking up of cavities thus formed ultimately leads to rupture along the prior austenite grain boundaries.

As was discussed previously the extremely low ductilities observed with the AMAX (Climax) 3Cr-1 1/2Mo-0.1V material were not anticipated, particularly in light of the relatively good ductilities

previously obtained[25] with the the experimental heat, P2904, of the AMAX (Climax) alloy. Tamaki's[116] work on the effect of phosphorous on cracking susceptibility indicates that critical phosphorous levels exist for the Cr-Mo alloys beyond which small increments in phosphorous content (0.003 to 0.006%) can cause marked decreases in the stress to cause fracture during PWHT. The critical phosphorous level was found to vary from alloy to alloy being 0.008% for a 1Cr-1/2Mo alloy, 0.014% for a 1.3Cr-1/2Mo alloy, and lying between 0.004 and 0.010% for a 2Cr-1Mo alloy. The difference in the phosphorous content between the experimental heat, P2904, (0.006%) and the commercial heat, A9349, (0.012%) may be sufficient to result in heat P2904 being below the critical phosphorous content and heat A9349 being above the critical content. The effect of phosphorous was also seen to be the probable cause of the low ductility of the Sumitomo 9Cr-1Mo-V-Nb material where the principal difference in alloy content between the various 9Cr-1Mo-V-Nb materials was the phosphorous content. Phosphorous, therefore, appears to be a most potent variable in susceptibility to cracking and its control to the lowest possible levels may be a critical factor in reducing susceptibility of the Cr-Mo alloys.

The AMAX (Climax) 3Cr-1 1/2Mo-0.1V material also has the highest silicon content (0.26%) and lowest nickel content of the vanadium modified materials. The presence of silicon may enhance the formation of Mo_2C[74,79,80] while the lower nickel may retard the formation and growth of higher order carbides.[10] These effects may

be superposed on the grain boundary embrittlement due to phosphorous resulting in the "extreme" susceptibility of this material.

The Gleeble testing program has shown that refining the coarse grained heat affected zone by overlapping the HAZ's of subsequent passes may result in mitigation of PWHT cracking in susceptible alloys. Therefore, the use of small beads, half bead welding, buttering of the base metal and temper beading techniques may be a partial solution to the problem of PWHT cracking and should be employed wherever possible.

C-Ring Test Evaluation of Postweld Heat Treatment Cracking Susceptibility of the Modified 3Cr-Mo and 2 1/4Cr-1Mo Alloys.

No single test for evaluating PWHT cracking susceptibility has been universally accepted although a great number of tests have been used and the results reported in the literature.[53,40,41,78] An ideal test for evaluating PWHT cracking susceptibility should have the following characteristics:[84] the specimen should include a notch or defect in a microstructure representative of the actual HAZ, the HAZ should be strained in a manner similar to that experienced in an actual weld, and the specimen should experience stress relaxation analogous to that experienced in actual welds. To find a single test that incorporates all the factors involved in an actual weld into a small specimen has been said to be "difficult".[53]

The Gleeble test for determining susceptibility is certainly not an ideal test. A major objection is that a constant load is normally employed rather than a time dependent, decreasing load as is

actually experienced during PWHT. (A paper was presented at the 1986 American Welding Society Annual Convention on a new test method for evaluating PWHT cracking.[117] The method employs the new Gleeble 1500 which is capable of applying a preprogrammed load and incorporates feed back control for these parameters which makes possible a simulation of the variable stress state present during PWHT.) Since Gleeble simulation reproduces only a single portion of the HAZ the constraint effects of the surrounding base metal and weld metal are not included.[40,43] Also, since the specimens normally employed do not include a notch, the test does not simulate actual conditions, in that a notch or internal defect invariably is the initiation site for cracking.[40,18]

The C-ring test, normally employed for evaluating susceptibility to stress-corrosion cracking, was determined to be a suitable, small scale test to evaluate PWHT cracking susceptibility. This test incorporates all aspects of the ideal test outlined by Baker.[40] It is possible to incorporate an actual weld, to introduce a notch into the coarse grained HAZ, to load the coarse grained HAZ to any level of stress and, most importantly, since the C-ring is a constant strain type test, the stress decreases with time at temperature in a manner similar to that of an actual weldment.

The procedure employed in making the C-rings was presented in the experimental procedure section (pages 74 through 80), however several points deserve further discussion. The walls of the weld groove are made along radial lines from the center of the bar in order to obtain an HAZ which is oriented perpendicular to the walls

of the machined C-ring. Therefore, the plane of maximum stress will be aligned through the HAZ and, therefore, crack propagation will not be forced to deviate from the plane of maximum stress in order to remain in the coarse grained HAZ as is the case with the Y-groove test.

The shielded metal arc welds that were performed to fill the groove in the bar were made at heat inputs ranging from 55 to 84KJ/in (2.17 to 3.31KJ/mm) as shown in Table 9. The high heat input was employed so that the microstructures in the HAZ would be similar to that obtained with the 60KJ/in (2.36 KJ/mm) thermal cycle employed inthe Gleeble test and to obtain a HAZ with a reasonable width. A wide HAZ is desirable as more tolerance exists for placement of the notch in the coarse grained region. Although higher energy input welds may reduce cracking susceptibility[18,44,66,86,94] the ability to place the notch consistently in the coarse grained HAZ is a critical factor in the test.

Four test conditions were employed for C-ring testing, utilizing two PWHT temperatures, 1150°F (620°C) and 1250°F (680°C), and three stress levels, 100ksi (690MPa), 80ksi (550MPa) and 60ksi (410MPa). The amount of deflection to produce the nominal stress was determined using equations from ASTM standard G38.[120] The 100ksi (690MPa) stress was used at both PWHT temperatures in order to determine the effect of temperature on cracking. All three stress levels were used at the lower PWHT temperature, which was associated with greater susceptibility in the Gleeble test, in order to examine

Table 9. Weld parameters and heat input utilized in C-ring specimen preparation.

Material	Volts	Amps	Time (min)	Length of Weld		Heat Input	
				(in)	(mm)	KJ/m	(kJ/mm)
AMAX 3Cr-1½Mo-0.1V (Climax)	23	150	1.13	2 7/8	73	82	3.2
	23	150	1.30	3 3/4	95	72	2.8
	29	145	2.43	7 1/2	190	82	3.2
	30	165	1.07	3 3/4	95	84	3.3
	30	165	0.95	3 1/2	89	81	3.2
Berkeley 3 Cr-1½Mo-¼Ni	30	120	1.50	4	100	81	3.2
	30	120	1.38	4	100	74	2.9
	30	120	1.45	4	100	78	3.1
JSW 3Cr-1Mo-V-Ti-B	25	150	2.38	6 5/8	170	81	3.2
	30	165	0.83	4 1/4	110	58	2.3
	30	165	1.02	4 1/4	110	71	2.8
	30	165	1.00	4 1/4	110	70	2.8
	30	165	0.88	4 1/8	105	64	2.5
	30						
JSW 2¼ Cr-1Mo-V-Ti-B	25	150	2.12	5 5/8	140	85	3.3
	30	165	1.12	5	130	66	2.6
	30	165	0.92	4 7/8	125	56	2.2
	30	165	0.90	4 7/8	125	55	2.2
	30	165	1.03	4 3/4	120	65	2.5
	30	165	1.12	4 3/4	120	70	2.8
Lukens 2¼Cr-1Mo-0.10C	24	160	1.28	4 3/4	120	62	2.4
	24	160	1.32	4 3/4	120	64	2.5

the effects of stress level and also to try and develop a greater degree of accuracy in the ranking of the materials.

Evaluation of the C-ring test is based on the maximum extent of crack propagation through the ring thickness (the maximum depth of the crack). This parameter was chosen as the manually performed, shielded metal arc welds do not always produce linearly uniform HAZ's. Therefore, the notch does not always lie within the coarse grained HAZ along the entire specimen width with the result that cracking was not uniform within the section.

The maximum depth of the crack can be determined in a number of ways depending on how the sample was prepared and PWHT. Some C-rings were cut into six sections along the notch (approximately 1/8 inch (3mm) thick), and metallographically prepared. The crack length was measured in each of the six sections with the maximum crack length used for comparison. The remaining C-ring specimens, whether heat treated in air or vacuum, were cooled to liquid nitrogen temperatures and fractured. The extent of intergranular fracture through the section was determined with a low power microscope. The samples PWHT in air were the more easily evaluated than those PWHT in vacuum as the intergranular fracture surface was discolored due to oxidation as opposed to the bright cleavage fracture surface. The fracture surfaces of the samples PWHT in vacuum were examined in the scanning electron microscope for fracture characteristics .

Results of the C-ring Test for the Modified 3Cr-Mo and 2 1/4Cr-1Mo Materials. The Berkeley 3Cr-1 1/2Mo-1/2Ni and Lukens 2 1/4Cr-1Mo-0.10C materials did not crack when stressed to 100ksi (690MPa) and PWHT at 1150°F (620°C) or 1250°F (680°C). Both the Lukens 2 1/4Cr-1Mo-0.10C and Berkeley 3Cr-1 1/2Mo-1/2Ni were predicted to be "not" susceptible at 1250°F (680°C) and only "slightly" susceptible at 1150°F (620°C) using the Gleeble technique. However all three vanadium modified materials, predicted to be "highly susceptible" or "extremely" susceptible by the Gleeble test, cracked at both PWHT temperatures at all stress levels employed in the C-ring test. Thus, the C-ring test confirms the general ranking of materials as either susceptible or not susceptible.

One sample of the AMAX (Climax) 3Cr-1 1/2Mo-0.1V material was tested without a notch in the coarse grained HAZ but with the HAZ oriented in the same manner. The unnotched specimen was stressed to 100ksi (690MPa) and PWHT at 1150°F (620°C) for eight hours. No cracking was found in mounted and polished cross sections indicating the necessity of imperfections (stress concentrators) in initiating PWHT cracking.

The results of the C-ring test program appear in Figure 68 and Table 10. Figure 68 and Table 10 show the average value of the depth of section cracked as a percentage of the total section height for each vanadium modified alloy at each test condition. Table 10 also includes the maximum deviation (range) from the average value. The average deviation (ignoring the large deviations for the AMAX

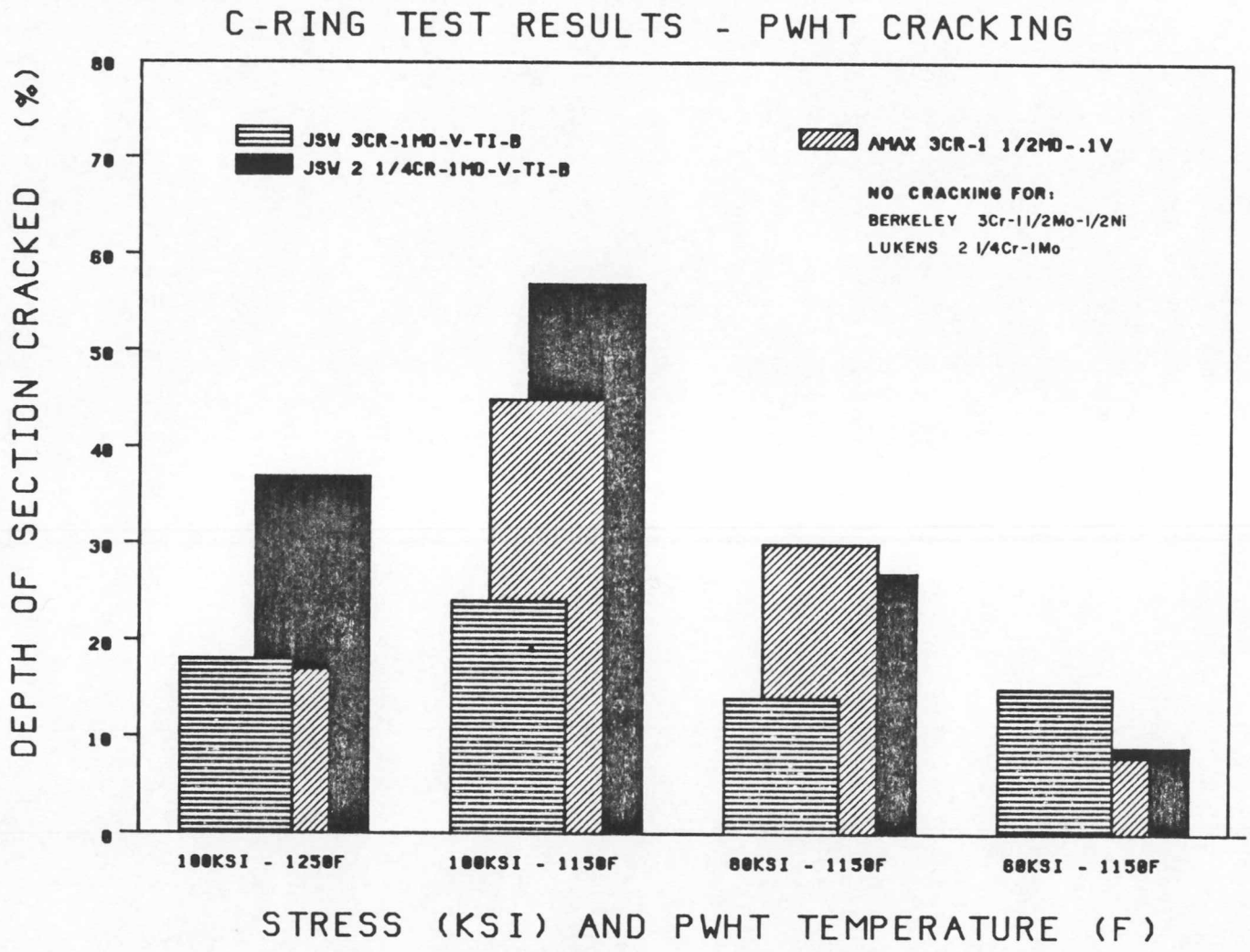


Figure 68. PWHT cracking results for the C-ring test.

Table 10. PWHT cracking results for the C-ring test.

PWHT Temperature		Stress		% Depth of Section Cracked		
°F	(°C)	KSI	(MPa)	AMAX (Climax) 3Cr	JSW 3Cr	JSW2¼Cr
1250	(680)	100	(690)	17 (Range +4,-2)	18 (± 3)	37 (± 13)
1150	(620)	100	(690)	45 (+34,-20)	24 (± 11)	53 (+15,-12)
1150	(620)	80	(550)	30 (± 1)	14 (± 1)	27 (± 12)
1150	(620)	60	(410)	8 (± 4)	15 (± 6)	9 (± 4)

(Climax) 3Cr-1 1/2Mo-0.1V material PWHT at 1150°F (620°C) and stress to 100ksi (690MPa)) is approximately ± 6%.

A comparison of results at 1250°F (680°C) and 1150°F (620°C) with an applied stress of 100ksi (690MPa)shows a decrease in the depth of section cracked for all three materials. The decrease in crack depth indicates a lower susceptibility to cracking at the higher PWHT. The Gleeble test results also showed a lower susceptibility to cracking at 1250°F (680°C) compared to 1150°F (620°C). Thus the general trend toward lower susceptibility with higher PWHT temperatures is confirmed by both the C-ring and Gleeble simulation tests.

As would be anticipated, cracking diminished as the applied stress was decreased. Since the stress is the driving force for crack propagation, as the stress decreases less cracking occurs. An apparent exception to this trend occurs with the JSW 3Cr-1Mo-V-Ti-B stressed to 80ksi (550MPa) and 60ksi (410MPa). However, with the average deviation in cracking being ±6%, the 1% increase in crack depth with a decrease in stress from 80ksi (550MPa) to 60ksi (410MPa) is not significant.

As the stress was decreased, at 1150°F (620°C), the magnitude of the difference in crack depth between the alloys decreased. At 60ksi (410MPa), considering the average deviation of ±6%, the difference in the response of the AMAX (Climax) 3Cr-1 1/2Mo-0.1V, JSW 3Cr-1Mo-V-Ti-B, and JSW 2 1/4Cr-1Mo-V-Ti-B alloys observed in Figure 68 and Table 10 has little significance. The same reasoning can be applied to the results for the AMAX (Climax) and JSW 2 1/4Cr

materials tested at 80ksi (550MPa) and 1150°F (620°C) where the difference in the depth of cracking is 3% and to the results for the AMAX (Climax) and JSW 3Cr materials tested at 1250°F (680°C) where the difference in the depth of section cracked is only 1%.

Based on the test results at 1150°F (620°C) and 1250°F (680°C) with an applied stress of 100ksi (690MPa) the JSW 2 1/4Cr-1Mo-V-Ti-B material may be ranked as the most susceptible of the three vanadium modified materials. Based on the test results at 1150°F (620°C) with applied stresses of 100ksi (690MPa) and 80ksi (550MPa) the next most susceptible material is the AMAX (Climax) 3Cr-1 1/2Mo-0.1V. The least susceptible material is the JSW 3Cr-1Mo-V-Ti-B alloy.

The greater susceptibility of the JSW 2 1/4Cr-1Mo-V-Ti-B material with respect to the JSW 3Cr-1Mo-V-Ti-B material may be the result of the smaller Cr:Mo and Cr:V ratios. The relatively higher Cr content of the the JSW 3Cr-1Mo-V-Ti-B alloy results in the preferential precipitation and growth of chromium rich M_7C_3 in the grain boundaries (which was found to be the predominate grain boundary species, Table 8, page 158) as opposed to the preferential precipitation and growth of molybdenum rich $M_{23}C_6$ in the grain boundaries of the JSW 2 1/4Cr-1Mo-V-Ti-B alloy. The growth of M_7C_3 in the grain boundaries would leave more molybdenum available in solution and may permit a relatively faster growth rate of Mo_2C during PWHT resulting in a shorter period of Mo_2C coherency.

The lower susceptibility of the JSW 3Cr-1Mo-V-Ti-B material with respect to the JSW 2 1/4Cr-1Mo-V-Ti-B material at both PWHT temperatures and with respect to the AMAX (Climax) 3Cr-1 1/2Mo-0.1V

material at 1150°F (620°C) are the points of agreement between the C-ring test and the Gleeble simulation test in the ranking of the individual vanadium modified alloys. The major discrepancy in ranking of materials for the two tests is in the rating of the AMAX (Climax) 3Cr-1 1/2Mo-0.1V material. In the Gleeble test the AMAX (Climax) material was ranked as the most susceptible material at both PWHT temperatures. However, in the C-ring test the AMAX (Climax) material is less susceptible to cracking than the JSW 2 1/4Cr-1Mo-V-Ti-B alloy at both PWHT temperatures and equivalent to the JSW 3Cr-1Mo-V-Ti-B alloy at 1250°F (680°C).

The improvement in the relative susceptibility of the AMAX (Climax) 3Cr-1 1/2Mo-0.1V material with respect to the JSW 3Cr-1Mo-V-Ti-B and JSW 2 1/4Cr-1Mo-V-Ti-B materials observed in the C-ring test may possibly be related to a lesser degree of segregation (and embrittlement) during the critical period when the residual stress (applied stress in the C-ring test) is high. Since stress relief and segregation occur simultaneously in the C-ring test, as the stress decreases the effect of grain boundary embrittlement on cracking susceptibility may be attenuated in comparison to the Gleeble simulation test where the stress is artificially maintained at high levels for the duration of the test. Additionally, if Hippsley's[57] model of stress induced transport of residual embrittling elements is considered, the constant stress employed in the Gleeble simulation test may result in a significant increase in the degree of embrittlement compared to the C-ring test in which the stress decreases with time at temperature.

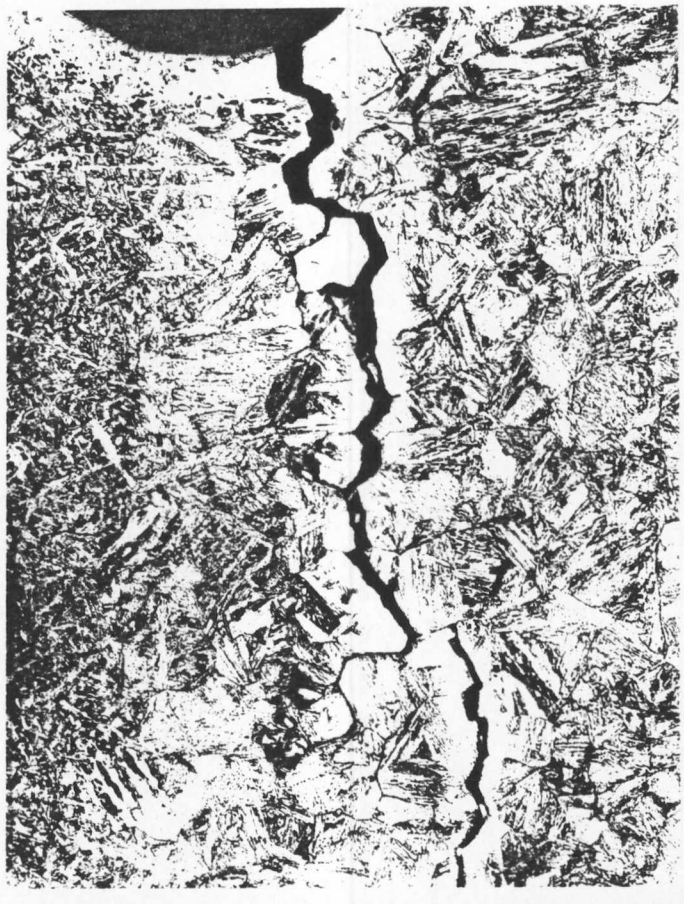
The difference in the 1250°F (680°C) and 1150°F (620°C) C-ring test results for the AMAX (Climax) 3Cr-1 1/2Mo-0.1V alloy appears to substantiate the foregoing argument. At 1150°F (620°C), when the persistence of coherent Mo_2C inhibits relaxation of stress, the stress level is maintained for longer times and the relative embrittlement, as shown by the extent of cracking, is high (Figure 68). However, at 1250°F (680°C), where stress relaxation may occur more rapidly due to the shorter coherency times of Mo_2C, the relative embrittlement of the AMAX (Climax) material is lower. The decrease in the extent of cracking from 1250°F (680°C) to 1150°F (620°C) is approximately twice the amount observed for the JSW 2 1/4Cr-1Mo-V-Ti-B material and four times the amount observed for the JSW 3Cr-1Mo-V-Ti-B material. This greater decrease in the extent of cracking in the AMAX (Climax) material would appear to be related to more than just a change in carbide morphology which would be expected to produce approximately equivalent decreases in the extent of cracking. Further, the Gleeble test results indicate that the AMAX (Climax) 3Cr-1 1/2Mo-0.1V material should be substantially more susceptible to cracking at 1250°F (680°C) than either the JSW 3Cr-1Mo-V-Ti-B or JSW 2 1/4Cr-1Mo-V-Ti-B. The time dependency of residual stress and embrittlement due to segregation, with high stress early in PWHT concomitant with limited embrittlement and lower stress (due to stress relaxation) later in PWHT concomitant with significant embrittlement, appears to be a plausible explanation of the AMAX (Climax) 3Cr-1 1/2Mo-0.1V material behavior.

Metallographic and Fractographic Examination of the Modified 2 1/4Cr-1Mo and 3Cr-Mo C-ring Specimens. Figures 69 through 71 show the optical light micrographs of the C-ring cross sections and scanning electron fractographs of the AMAX (Climax) 3Cr-1 1/2Mo-0.1V, JSW 3Cr-1Mo-V-Ti-B, and JSW 2 1/4Cr-1Mo-V-Ti-B C-rings stressed to 100ksi (690MPa) and PWHT at 1150°F (620°C). The optical light micrographs clearly show the intergranular morphology of cracking with the crack propagating along the prior austenite grain boundaries in the coarse grained region of the HAZ.The fractographs (Figures 69b through 71b) show the characteristic LDIGF along the prior austenite grain boundaries for these materials. No evidence of any microductility was observed on the grain faces in the fractographic examinations.

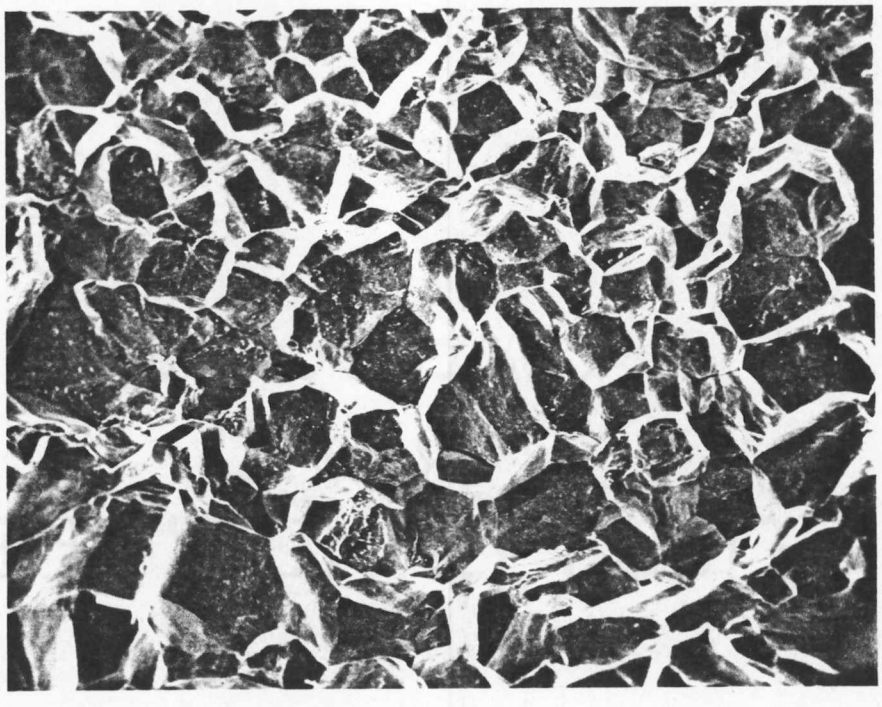
Figure 72 is a higher magnification (1000X) fractograph of the JSW 2 1/4Cr-1Mo-V-Ti-B C-ring specimen. Figure 72 is representative of the smooth fracture surface obtained with all three vanadium modified materials. Secondary cracking is exhibited in the lower right portion of fractograph.

Evidence of microductility was observed only at the crack tip or the boundary of the intergranular and cleavage fracture regions. Figure 73 is typical of that observed under creep conditions. Note that the cavitation does not appear to be associated with particles on the grain boundaries.

Problems Encountered with the C-ring Test. The problems encountered in making and using the C-ring specimens were, as



A



B

Figure 69. AMAX (Climax) 3Cr-1 1/2Mo-0.1V C-ring specimen. 1150°F (620°C) PWHT, 100ksi (690MPa), a) Noren's reagent, 100X OLM, b) 200X SEM.

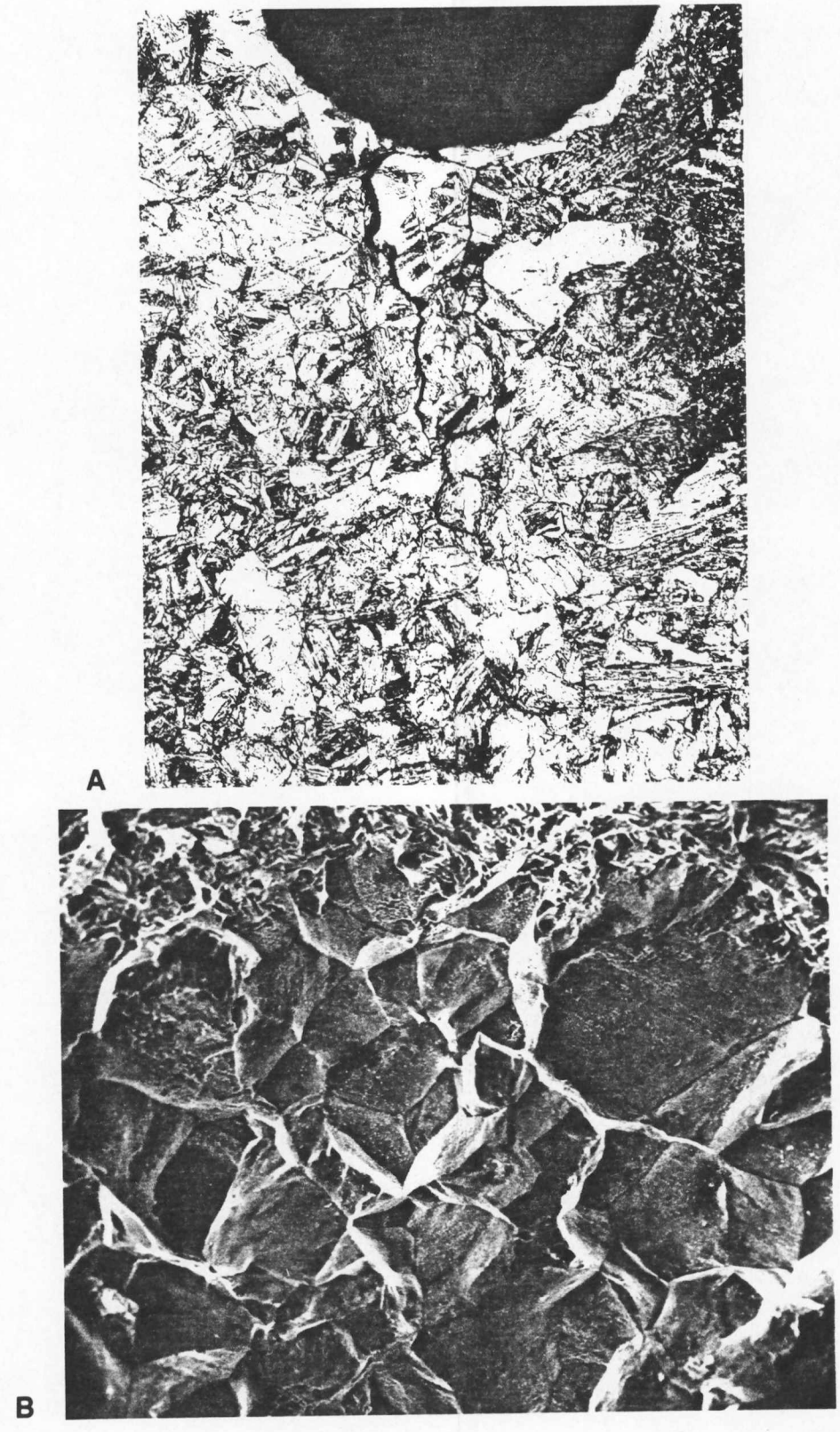
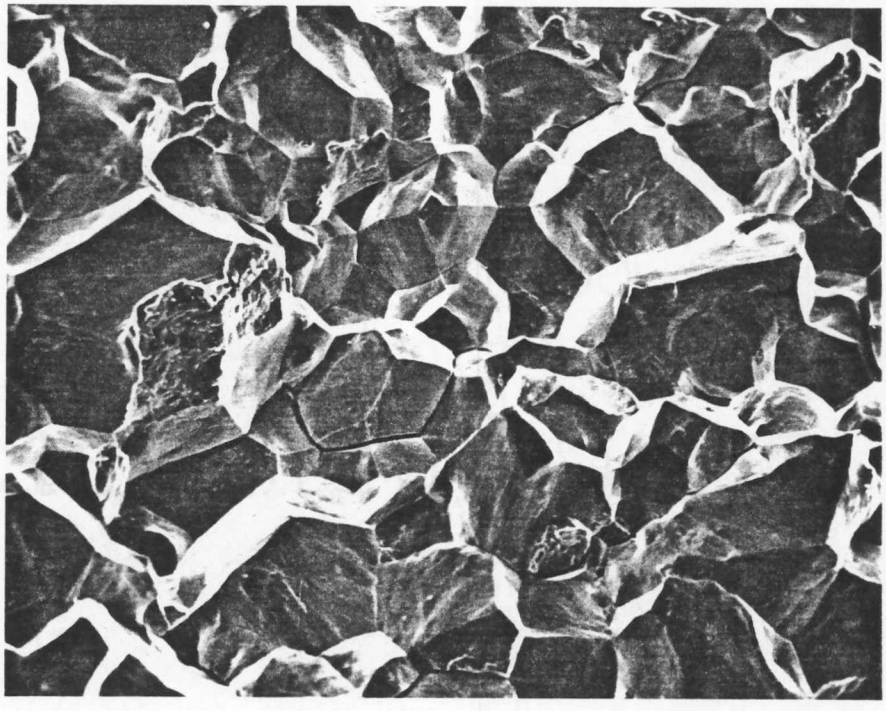


Figure 70. JSW 3Cr-1Mo-V-Ti-B C-ring specimen. 1150°F (620°C) PWHT, 100ksi (690MPa), a) Noren's reagent, 100X OLM, b) 200X SEM.



A



B

Figure 71. JSW 2 1/4Cr-1Mo-V-Ti-B C-ring specimen. 1150°F (620°C) PWHT, 100ksi (690MPa), a) Noren's reagent, 100X OLM, b) 200X SEM.

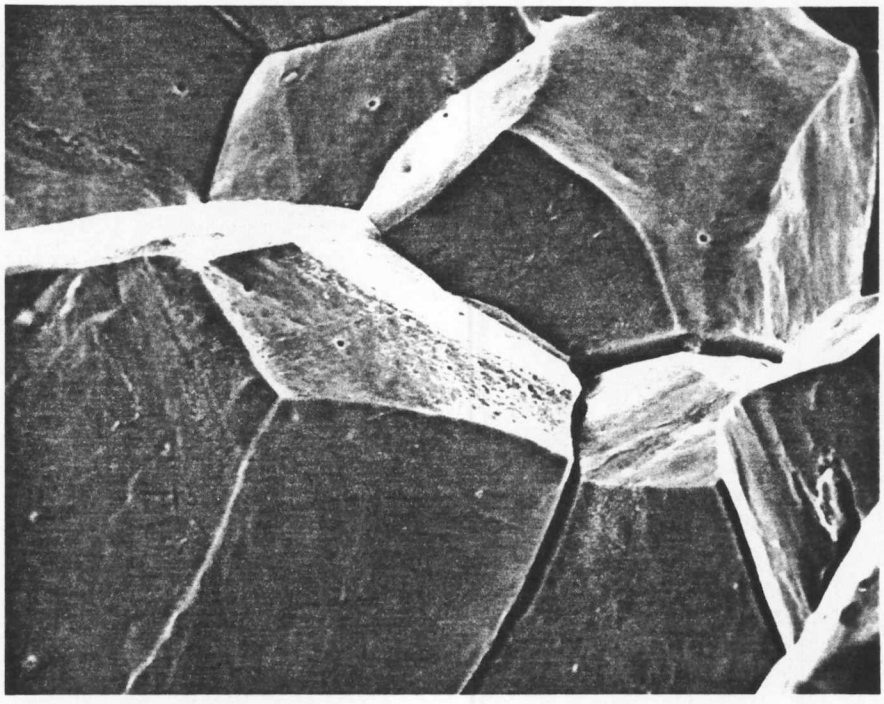


Figure 72. Higher magnification fractograph of the JSW 2 1/4Cr-1Mo-V-Ti-B C-ring specimen. 1150°F (620°C) PWHT, 100ksi (690MPa), 1,000X SEM.

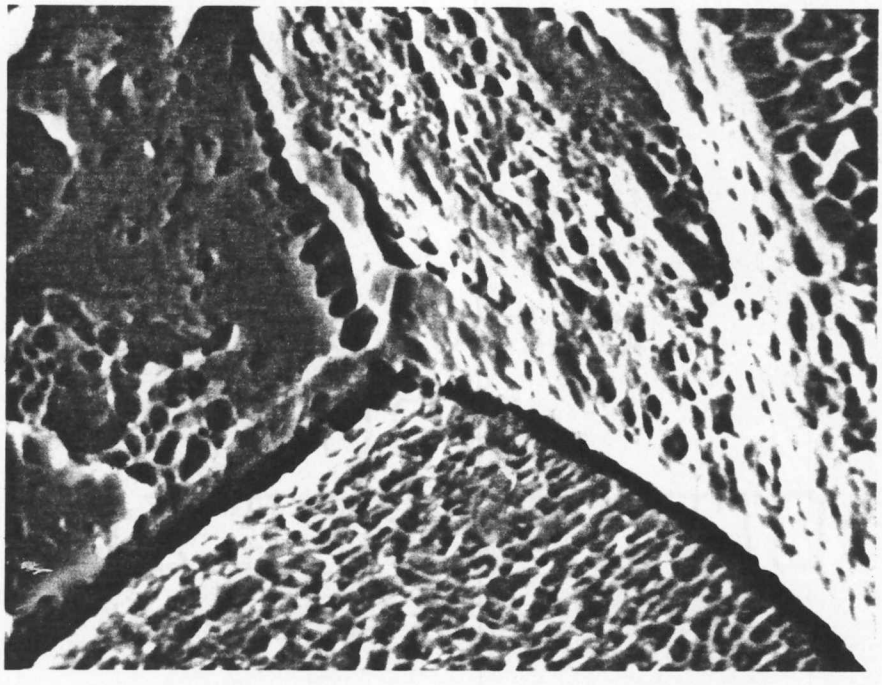


Figure 73. Grain boundary cavitation at the intergranular-cleavage fracture interface in the AMAX (Climax) 3Cr-1 1/2Mo-0.1V C-ring specimen. 1150°F (620°C) PWHT, 100ksi (690MPa), 5,000X SEM.

indicated previously, primarily the result of the irregular HAZ due to the manually performed shielded metal arc welds. Figure 74 shows a macrograph of a notched C-ring not employed in testing. Note the unequal HAZ width and the deviation of the notched HAZ from a perpendicular to the ring wall. The arc in this case clearly favored one side wall of the notch at this point which resulted in the HAZ distortion.

Figure 75 shows several notch positions in the HAZ that were encountered during testing. The correct placement of the notch, at the fusion line, is shown darkened in on the Figure. Displacement of the notch either into the fusion zone or towards the fine grained HAZ is shown in Figure 68 with the displacement being between 0.02 to 0.04 inches (0.5 to 1mm). If the notch is displaced into the fusion zone either no cracking occurs or, if the displacement is small, cracking may initiate at the root of the notch, traverse into the coarse grained region and propagate along the coarse grained HAZ as shown in Figure 76. If, on the other hand, the notch is displaced from the fusion line towards the fine grained HAZ, any cracking which initiates at the root of the notch propagates only a short distance before being stopped as shown in Figure 77. Several small cracks along the fusion zone may also be observed in Figure 77.

One improvement in the preparation of the C-rings would be to perform the welds automatically and thus obtain more uniform HAZ's. If the HAZ is linear over the sample width and perpendicular to the ring wall, an assessment of susceptibility based on the percentage of

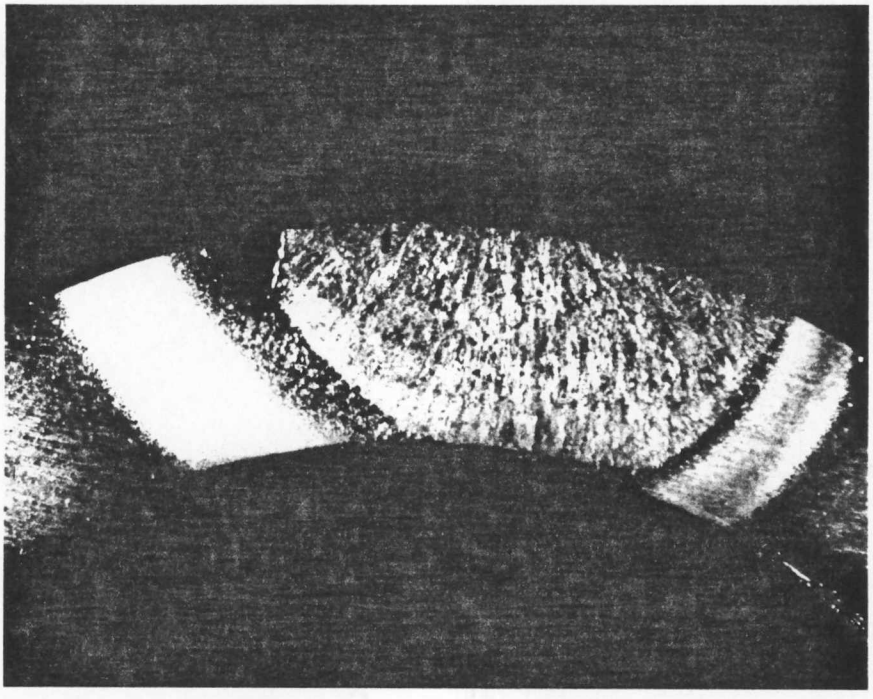


Figure 74. Unequal, non-linear HAZ's as a result of welding in a C-ring specimen.

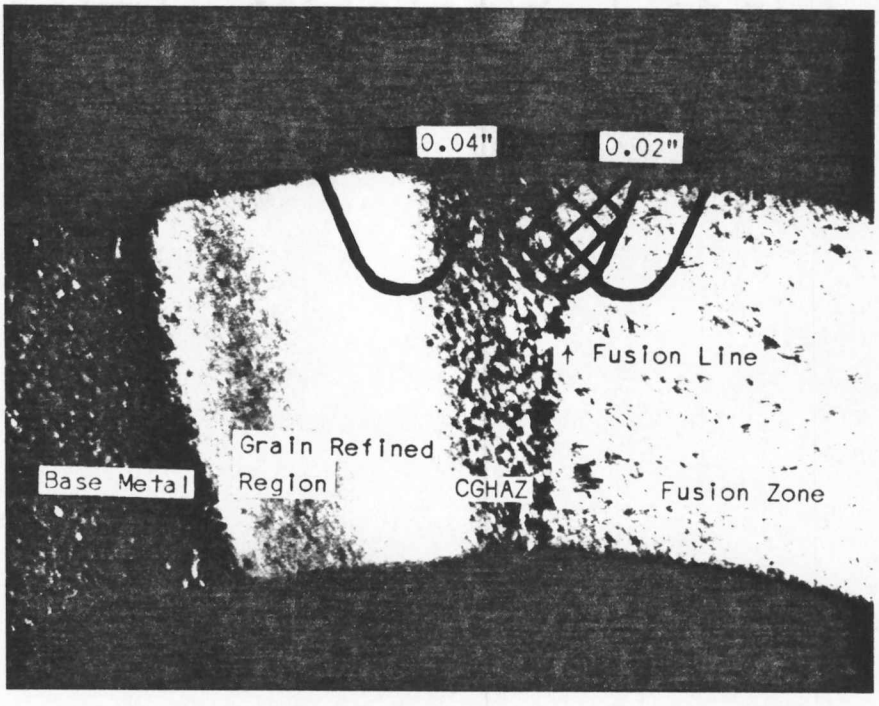


Figure 75. Schematic of ideal notch placement and two sites of notch misplacement in the C-ring test specimen.



Figure 76. Notch displaced into the fusion zone in a AMAX (Climax) 3Cr-1 1/2Mo-0.1V C-ring specimen. 1150°F (620°C) PWHT, 100ksi (690MPa), Noren's reagent, 100X OLM.

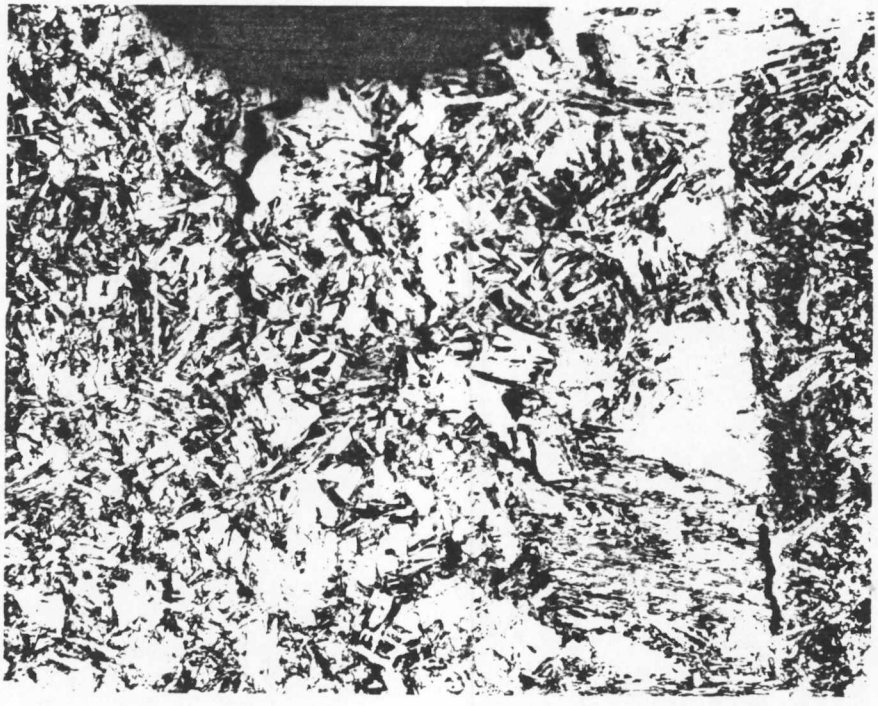


Figure 77. Notch displaced towards the fine grained HAZ in a JSW 2 1/4Cr-1Mo-V-Ti-B C-ring specimen. 1150°F (620°C) PWHT, 100ksi (690MPa), Noren's reagent, 100X OLM.

total area cracked might be employed and the scatter in the data reduced.

Summary of the C-ring Cracking Test Results. The C-ring test has achieved the same major separation, as susceptible or not susceptible, for the modified 2 1/4Cr-1Mo and 3Cr-Mo alloys as was obtained with the Gleeble test. The Berkeley 3Cr-1 1/2Mo-1/2Ni and unmodified Lukens 2 1/4Cr-1Mo-0.10C materials exhibited no cracking under the most severe loading conditions, 100ksi (690MPa), at both PWHT temperatures, 1150°F (620°C) and 1250°F (680°C). All three vanadium modified alloys cracked at both PWHT temperatures with all levels of stress employed. Thus, from the results of both the C-ring test and the Gleeble simulation test, the Berkeley 3Cr-1 1/2Mo-1/2Ni and Lukens 2 1/4Cr-1Mo-0.10C are not susceptible to PWHT cracking while the three vanadium modified alloys tested are susceptible to cracking.

The C-ring test also agrees with the general trend of decreased susceptibility with higher PWHT temperature obtained from the Gleeble test results. The three vanadium modified alloys exhibited lower depth of section cracked values when PWHT at 1250°F (680°C) than when PWHT at 1150°F (620°C).

The general ranking of the vanadium modified alloys by the C-ring test was determined to be: JSW 2 1/4Cr-1Mo-V-Ti-B (most susceptible), AMAX (Climax) 3Cr-1 1/2Mo-0.1V, and JSW 3Cr-1Mo-V-Ti-B (least susceptible). The presence of chromium rich M_7C_3 as the predominant grain boundary carbide in the JSW 3Cr material as opposed to molybdenum rich $M_{23}C_6$ as the predominant grain boundary carbide in

the JSW 2 1/4Cr-1Mo-V-Ti-B may result in more molybdenum in solution in the JSW 3Cr. With more molybdenum in solution the length of time Mo_2C remains coherent with the matrix may be reduced resulting in a lower overall susceptibility of JSW 3Cr-1Mo-V-Ti-B as compared to the JSW 2 1/4Cr-1Mo-V-Ti-B.

The relative decrease in susceptibility for the AMAX (Climax) 3Cr-1 1/2Mo-0.1V alloy in the C-ring test compared to the Gleeble simulation test may be related to the different stress states present in the two tests. In the C-ring test the rate of stress relaxation in competition with segregation induced embrittling effects may be the primary factor involved in the decreased relative susceptibility of the AMAX (Climax) material. The Gleeble test, performed with constant stress, removes the effect of stress relaxation and thus may measure the total embrittlement potential of a material. The constant stress may also cause embrittlement as a result of stress induced transport of embrittling elements. Auger analysis of fracture surfaces might be employed to determine the degree of phosphorous segregation in both types of test and resolve the question of the role of phosphorous segregation on the susceptibility of this alloy.

An important point to be remembered is that this is the first use of the C-ring test to evaluate PWHT cracking and a limited number of samples have been employed to determine the susceptibility of these materials. Although the general trends obtained from the Gleeble test results have been reproduced, the relative ranking of the individual alloys is tenuous. Refinement in both test techniques

and sample preparation are necessary to fully establish the viability of this test to accurately predict susceptibility between individual heats of alloys.

Summary of PWHT Cracking Results for the Modified 3Cr-Mo and 2 1/4Cr-1Mo Alloys. The vanadium modified alloys; AMAX (Climax) 3Cr-1 1/2Mo-0.1V, JSW 3Cr-1Mo-V-Ti-B, and JSW 2 1/4Cr-1Mo-V-Ti-B, have been found to more susceptible to PWHT cracking than the Berkeley 3Cr-1 1/2Mo-1/2Ni or the unmodified 2 1/4Cr-1Mo alloys. The vanadium modified alloys exhibited low rupture ductilities at PWHT temperatures of 1150°F (620°C) and 1250°F (680°C) in the Gleeble simulation test and would be considered as either "highly" susceptible or "extremely" susceptible to cracking by the Vinckier and Pense criteria.[53,78] In the C-ring test the vanadium modified alloys exhibited cracking at both PWHT temperatures and at all stress levels employed while the Berkeley 3Cr-1 1/2Mo-1/2Ni and the unmodified Lukens 2 1/4Cr-1Mo-0.10C materials did not crack at either PWHT temperature when stressed to 100ksi (690MPa), the highest stress utilized.

Both the Gleeble test and the C-ring test results show that a higher PWHT temperature results in a lower susceptibility to cracking. In the Gleeble simulation test the RA was greater at the higher PWHT temperature,1250°F (680°C), than at the 1150°F (620°C) PWHT temperature for all materials tested. In the C-ring test the depth of section cracked decreased at the higher PWHT in comparison to the lower PWHT temperature for the vanadium modified materials.

The greater susceptibility of the vanadium modified alloys with respect to the Berkeley 3Cr-1 1/2Mo-1/2Ni and unmodified 2 1/4Cr-1Mo alloys is primarily related to the retarded carbide evolution in the alloys with vanadium additions. Scanning transmission electron microscopy and scanning electron microscopy have shown that the Berkeley 3Cr-1 1/2Mo-1/2Ni alloy has large grain boundary carbides of the $M_{23}C_6$ and M_6C type after thermal cycling to 2400°F (1315°C) and a PWHT at 1150°F (620°C) for 100 minutes. However, the AMAX (Climax) 3Cr-1 1/2Mo-0.1V, JSW 3Cr-1Mo-V-Ti-B, and JSW 2 1/4Cr-1Mo-V-Ti-B specimens all have smaller grain boundary carbides than the Berkeley material for the same PWHT conditions with the Climax material having M_6C, $M_{23}C_6$, and M_7C_3 grain boundary carbides and the JSW 3Cr and 2 1/4Cr alloys having only $M_{23}C_6$ and M_7C_3 carbides in the grain boundaries. The matrix carbides have been identified by Todd[114] as $(CrMo)_2CN$ in the Berkeley and AMAX (Climax) alloys and as Mo_2C containing chromium, molybdenum, and vanadium in the JSW 3Cr and JSW 2 1/4Cr alloys. The delay in grain boundary carbide evolution and the lower order matrix carbides may be related to longer times of coherency and slower growth of Mo_2C or $(CrMo)_2CN$ in the matrix resulting in greater strengthening over longer times in comparison with the unmodified materials. As was shown in the literature review, the longer the duration of significant matrix strengthening the greater the susceptibility of the material to PWHT cracking.[36,69,70]

The greater susceptibility of the JSW 2 1/4Cr-1Mo-V-Ti-B material in comparison with the JSW 3Cr-1Mo-V-Ti-B alloy,

particularly in the C-ring test, may be related to the lower chromium to molybdenum ratio of the JSW 2 1/4Cr alloy. The predominant grain boundary carbide in the JSW 2 1/4Cr alloy was molybdenum rich $M_{23}C_6$ whereas the predominant grain boundary carbide in the JSW 3Cr alloy was chromium rich M_7C_3. The preferential formation of $M_{23}C_6$ in the JSW 2 1/4Cr alloy may lower the level of molybdenum in solution and increase the time of Mo_2C coherency as compared to the JSW 3Cr alloy. A longer period of coherency and slower growth of Mo_2C will result in an overall greater susceptibility to cracking.

The width of the carbide denuded zone may also be a factor in the greater susceptibility of the JSW 2 1/4Cr-1Mo-V-Ti-B alloy in comparison to the JSW 3Cr-1Mo-V-Ti-B alloy. Strain accumulation in the soft, denuded, zone has been cited as one of the factors in PWHT cracking.[30,52] The JSW 2 1/4Cr was found to have a smaller denuded zone width than the JSW 3Cr alloy with the result that strain accumulation will occur over a smaller "width" of boundary and thus, higher local strains will develop.[52]

The AMAX (Climax) 3Cr-1 1/2Mo-0.1V alloy was found to be "extremely" susceptible to PWHT cracking in the Gleeble simulation test and cracked in the C-ring test. The susceptibility to cracking in this material appears to be a synergistic combination of precipitation strengthening of the matrix and grain boundary embrittlement due to phosphorous segregation. (We have no direct evidence for the phosphorous segregation but the majority of the research literature shows that phosphorous is indeed a major contributor to PWHT cracking.) The Climax alloy had the highest

phosphorous content (0.012%) of the vanadium modified alloys tested (0.007%) and twice the phosphorous content of an experimental heat, P2904, (0.006%) of similar composition which exhibited significantly higher rupture ductilities.[25] This material exhibited the most extensive denuded zone and only a moderate retardation in precipitate evolution (some M_6C was found along the grain boundaries) in comparison to the JSW 3Cr-1Mo-V-Ti-B and JSW 2 1/4Cr-1Mo-V-Ti-B alloys which would suggest that the Climax material should be less susceptible to cracking than the other vanadium modified alloys. Thus, the susceptibility of this material is probably due to a combined precipitation and segregation effect exacerbated by the relatively high phosphorous content.

Gleeble simulation has also shown that susceptibility to cracking may be lowered by refinement of structure in the grain coarsened region through the overlapping effect of the HAZ's of subsequent passes in a multiple pass weld. Thermal cycling samples to 1700°F (927°C) after a grain coarsening thermal cycle increased the rupture ductility to above 12% from less than 5% for the vanadium modified alloys. Thus, the small bead, half bead technique[65] or temper beading[39] methods may prove to be successful in preventing PWHT cracking. However, due to the higher elevated temperature rupture strength of both the multiple thermal cycled and the grain refined region (experiencing only a single thermal cycle to 1700°F), complete refinement of all coarse grained HAZ regions must be accomplished in order to prevent strain accumulation in any lower strength coarse grained material left unrefined.

CHAPTER VI

CONCLUSIONS

The purpose of this study was to determine the transformation characteristics and susceptibility to post weld heat treatment cracking of alloys representative of the new generation of modified 9Cr-1Mo, 3Cr-Mo and 2 1/4Cr-1Mo alloys. The conclusions derived from this study may be summarized as follows:

I. Transformation Characteristics.

A. Transformation characteristics of the 9Cr-1Mo-V-Nb commercial commercial heats.

1. The rapid heating rates associated with the welding thermal cycle resulted in the A_{C1} and A_{C3} temperatures being higher than those reported in the literature for a similar composition material by 94 to 124F° (50 to 65C°) and 89 to 109F° (35 to 45C°) respectively.

2. The M_s temperatures range from 710 to 755°F (375 to 400°F) and are in substantial agreement with those obtained under CCT conditions.

3. The minor variations in chemical composition of the three commercial heats had no observable effect on the M_s or M_f temperatures.

4. The M_s and M_f temperatures were independent of cooling rate over the range of simulated weld thermal cycles employed.

5. The primary microstructural constituents were martensite and autotempered martensite.
6. The Timken 9Cr-1Mo-V-Nb material, with a chromium equivalent of 13.4, contained delta ferrite in the simulated coarse grained HAZ as anticipated.

B. Transformation characteristics of the modified 3Cr-Mo and 2 1/4Cr-1Mo alloys.

1. The rapid heating rates associated with the welding thermal cycle resulted in the A_{C1} and A_{C3} temperatures being higher than those reported in the literature for AMAX (Climax) 3Cr-1 1/2Mo-0.1V, Berkeley 3Cr-1 1/2Mo-1/2Ni, JSW 3Cr-1Mo-V-Ti-B, JSW 2 1/4Cr-1Mo-V-Ti-B by 22 to 45F° (12 to 25C°) and 18 to 54F° (10 to 28C°) respectively.
2. No discernible separate M_f or B_S temperature could be detected for any of the materials.
3. The M_s temperatures obtained under simulated welding conditions were approximately 45F° (25C°) lower than those determined under standard CCT conditions.
4. The JSW 2 1/4Cr-1Mo-V-Ti-B material exhibited the highest on-cooling transformation temperatures of the modified alloys due to the lower carbon content (0.12%) and overall lower alloying element content.
5. The Berkeley 3Cr-1 1/2Mo-1/2Ni material exhibited the lowest transformation temperatures of the modified

materials due to the higher carbon content (0.16%) and nickel content (0.51%).

6. The microstructures obtained under simulated welding conditions depend on the energy input (cooling rate). With low energy inputs (fast cooling rates), the microstructures consisted of martensite and autotempered martensite. With intermediate energy inputs, the microstructures consisted of autotempered martensite and lower bainite. With the highest energy input (slowest cooling rate) employed, 150KJ/in (5.9 KJ/mm), the microstructure consisted of lower bainite and granular bainite.

II. Postweld heat treatment cracking susceptibility.

A. Gleeble simulation evaluation of the 9Cr-1Mo-V-Nb commercial heats.

1. The 9Cr-1Mo-V-Nb alloys exhibit lower rupture ductilities (RA 15 to 56%) than unmodified 9Cr-1Mo (70% minimum RA). The lower rupture ductility of the modified materials is most likely the result of precipitation of fine V/Nb carbo-nitrides, nucleation of $M_{23}C_6$ on the V/Nb carbo-nitrides in a fine dispersed form, and a reduction in the the rate of growth of $M_{23}C_6$ due to a lowering of chromium mobility by vanadium.

2. The primary mode of fracture was microvoid coalescence.

3. The higher phosphorous content of the Sumitomo alloy (0.014%) may be the primary factor in the lower relative rupture ductility (RA 15 to 31%) of this material.
4. Macroscopic and microscopic ductility of the 9Cr-1Mo-V-Nb alloys is sufficient to preclude PWHT cracking as a problem in fabrication.

B. Gleeble simulation evaluation of the modified 3Cr-Mo and 2 1/4Cr-1Mo alloys.

1. The Berkeley 3Cr-1 1/2Mo-1/2Ni alloy with no vanadium addition exhibited significantly higher rupture ductility at both PWHT temperatures than the vanadium modified alloys; AMAX (Climax) 3Cr-1 1/2Mo-0.1V, JSW 3Cr-1Mo-V-Ti-B, and JSW 2 1/4Cr-1Mo-V-Ti-B.
2. By the Vinckier and Pense criteria[53,78] the Berkeley 3Cr-1 1/2Mo-1/2Ni alloy would be considered "not" susceptible to cracking when PWHT at 1250°F (680°C) and "slightly" susceptible at 1150°F (620°C), the JSW 3Cr-1Mo-V-Ti-B and JSW 2 1/4Cr-1Mo-V-Ti-B alloys would be considered "highly" susceptible to cracking at 1250°F (680°C) and "extremely" susceptible at 1150°F, and the AMAX (Climax) 3Cr-1 1/2Mo-0.1V alloy would be considered "extremely" susceptible to cracking at both PWHT temperatures.
3. Rupture ductility was lower for all materials PWHT at 1150°F (620°C) than when PWHT at 1250°F (680°C). At the lower PWHT temperature longer duration of coherency and

slower growth of Mo_2C or $(CrMo)_2CN$ in the matrix would result in increased susceptibility to cracking.

4. Rupture ductility for the base material subjected to simulated PWHT was in excess of 70% RA and for the simulated fine grained HAZ was in excess of 54% and thus shows that the grain coarsening thermal cycle is the precursor to metallurgical events which result in embrittlement.

5. The primary fracture mode for the Berkeley 3Cr-1 1/2Mo-1/2Ni alloy was IGMVC, for the JSW 3Cr-1Mo-V-Ti-B was mixed IGMVC and LDIGF with microvoids initiating on grain boundary particles, and for the AMAX (Climax) 3Cr-1 1/2Mo-0.1V and JSW 2 1/4Cr-1Mo-V-Ti-B was LDIGF.

6. The scanning electron microscopy examination of samples PWHT at 1250°F (680°C) for 70 to 100 minutes revealed almost complete break down of the lath type morphology and extensive carbide formation at the grain boundaries. The grain boundary carbides in the Berkeley 3Cr-1 1/2Mo-1/2Ni material were coarser than the grain boundary carbides in the other modified materials.

7. The scanning transmission electron microscopy of carbide extraction replicas showed that the precipitation of grain boundary carbides was retarded in the vanadium modified materials in comparison to the Berkeley 3Cr-1 1/2Mo-1/2Ni alloy. Grain boundary carbides in the

Berkeley alloy were $M_{23}C_6$ and M_6C, in the AMAX (Climax) 3Cr-1 1/2Mo-0.1V were M_7C_3, $M_{23}C_6$, and M_6C and in the JSW 3Cr-1Mo-V-Ti-B and JSW 2 1/4Cr-1Mo-V-Ti-B were $M_{23}C_6$ and M_7C_3. The predominant grain boundary carbide in the JSW 3Cr was chromium rich M_7C_3 and in the JSW 2 1/4Cr was molybdenum rich $M_{23}C_6$. Precipitation of the grain boundary carbides was accompanied with the formation of denuded zones in the AMAX (Climax), JSW 3Cr and JSW 2 1/4Cr alloys being 0.3 μm , 0.1 μm and less than 0.1 μm in width respectively.

8. The scanning transmission electron microscopy of carbide extraction replicas identified the matrix carbides in the Berkeley 3Cr-1 1/2Mo-1/2Ni and AMAX (Climax) 3Cr-1 1/2Mo-0.1V alloys as $(CrMo)_2CN$ and in the JSW 2 1/4Cr-1Mo-V-Ti-B and JSW 3Cr-1Mo-V-Ti-B alloys as Mo_2C containing molybdenum, chromium and vanadium.

9. The retarded evolution of the grain boundary carbides is probably accompanied by a concomittant slow growth of Mo_2C or $(CrMo)_2CN$ in the grain matrix. Slower growth of Mo_2C or $(CrMo)_2CN$ in the matrix will be associated with longer times of coherency and matrix strengthening resulting in greater susceptibility to PWHT cracking. The transmission microscopy examination showed a greater volume fraction of matrix precipitates in the vanadium modified alloys and the scanning electron microscopy examination showed the carbides to be coarser in the

Berkeley alloy thus supporting the hypothesis of slower development of the matrix carbides in the vanadium modified alloys.

10. The formation of chromium rich $M_{23}C_6$ as the predominant grain boundary carbide may be the result of the higher chromium to molybdenum ratio of the JSW 3Cr-1Mo-V-Ti-B alloy in comparison to the other vanadium modified alloys. Due to the preferential formation of chromium rich M_7C_3, more molybdenum may remain in solution promoting the growth and loss of coherency of Mo_2C in the matrix. This may be the cause of the increasing ductility with time to fracture observed in the 1250°F (680°C) PWHT results.
11. The low rupture ductility of the AMAX (Climax) 3Cr-1 1/2Mo-0.1V material may be the result of embrittlement due to higher phosphorous content (0.012%) compared to the other modified materials (0.006 to 0.007%) combined with precipitation strengthening. Further, the relatively high silicon content (0.26%) may enhance the formation of Mo_2C, lowering molybdenum in solution and promoting phosphorous segregation.
12. The presence of aluminum and aluminum bearing particles was found to be associated with regions of LDIGF in the Berkeley material and limited microductility in the JSW 3Cr material. Thus, aluminum may play a minor role in increasing cracking susceptibility.

13. Superposition of a grain refining thermal cycle on a grain coarsening thermal cycle improves rupture ductility of the vanadium modified materials from less than 5% to more than 12% and therefore suggests that welding techniques which result in refinement of the coarse grained HAZ may prevent PWHT cracking in susceptible materials.

C. C-ring evaluation of the modified 3Cr-Mo and 2 1/4Cr-1Mo alloys.

1. The Berkeley 3Cr-1 1/2Mo-1/2Ni and unmodified Lukens 2 1/4Cr-1Mo-0.10C materials did not crack in the C-ring test while the AMAX (Climax) 3Cr-1 1/2Mo-0.1V, JSW 3Cr-1Mo-V-Ti-B, and JSW 2 1/4Cr-1Mo-V-Ti-B cracked at both 1250°F (680°C) and 1150°F (620°C) and at all stress levels employed. Thus, the C-ring test confirms the general ranking of materials as either susceptible or not susceptible to cracking determined from Gleeble simulation.
2. The depth of section cracked decreased in the vanadium modified alloys at the higher PWHT temperature, 1250°F (680°C), indicating decreasing susceptibility with increasing PWHT temperature. This agrees with the results for the two PWHT temperatures obtained in Gleeble simulation testing.
3. An unnotched C-ring of the AMAX (Climax) 3Cr-1 1/2Mo-0.1V material did not crack when PWHT at 1150°F (620°C) and

stressed to 100ksi (690MPa) indicating the necessity of stress concentrators in initiating PWHT cracking.

4. The depth of section cracked for the vanadium modified alloys decreased as the stress was decreased.
5. Ranking of the vanadium modified alloys was determined to be JSW 3Cr-1Mo-V-Ti-B (least susceptible), AMAX (Climax) 3Cr-1 1/2Mo-0.1V, and JSW 2 1/4Cr-1Mo-V-Ti-B (most susceptible).
6. The greater susceptibility of the JSW 2 1/4Cr-1Mo-V-Ti-B alloy in comparison to the JSW 3Cr-1Mo-V-Ti-B alloy may be the result of the lower chromium to molybdenum ratio.
7. The C-ring test results for the AMAX (Climax) 3Cr-1 1/2Mo-0.1V alloy indicates that effect of embrittlement due to phosphorous segregation, which occurs simultaneously with decreasing stress due to stress relief, may be attenuated in comparison to the Gleeble simulation test performed with constant load.
8. Fracture morphology for the vanadium modified alloys was intergranular along the prior austenite grain boundaries with the fracture surface showing characteristic LDIGF.
9. The C-ring test incorporates all the factors for an ideal test to evaluate PWHT cracking and appears to be a simple, valid test for determining susceptibility to cracking based on the substantial agreement with results obtained from Gleeble simulation.

CHAPTER VII

FUTURE WORK

(1) Additional testing of another heat of the AMAX (Climax) composition material with lower phosphorous content than in heat A9349 in order to determine whether the severe embrittlement in this heat is due to the relatively high phosphorous or is related to the general alloy chemistry.

(2) Auger spectroscopy analysis of fracture surfaces of the AMAX (Climax) material to determine the extent of segregation to the grain boundaries and provide direct evidence as to the role of phosphorous in embrittlement of this alloy.

(3) Auger analysis of fracture surfaces of the Sumitomo 9Cr-1Mo-V-Nb material to determine whether phosphorous segregation is the cause of the relatively low ductility of this material.

(4) Extensive STEM analysis of as cycled specimens, short time (5 minute) specimens PWHT at both 1250°F (680°C) and 1150°F (620°C), and long time (100 minute) specimens PWHT at 1150°F (620°C) in order to fully determine the precipitation kinetics, precipitate morphology and effect of PWHT temperature on precipitation in the modified 3Cr-Mo and 2 1/4Cr-1Mo alloys.

(5) Determination of optimum groove configuration and welding method to obtain more uniform weld HAZ's in the C-ring specimen.

(6) Additional testing of C-ring specimens with varying postweld heat treatment temperature and stress level to develop a

sufficiently large data base for statistical analysis of the test results.

(7) Testing of C-rings containing two welds with overlapping HAZ's to determine whether grain refinement of the coarse grained HAZ is effective in lowering susceptibility to PWHT cracking.

(8) Testing of susceptible material with C-rings with different notch depths and sharpness to determine the effect of notch accuity on the initiation of cracking.

(9) Determination of the stress state at the root of the notch by the finite element method.

(10) Determination of PWHT cracking susceptibility with the full scale, Y-groove test in order to compare results obtained from Gleeble simulation and the small scale, C-ring test with those obtained with an actual weldment.

LIST OF REFERENCES

LIST OF REFERENCES

1 Patriarca, P., Hoffman, E. and Cunningham, G., "Ferritic Steels as Alternate Structural Materials for High Temperature Applications," P. Patriarca (ed.), Modified 9Cr-1Mo Steel Techmical Program Data Package for Use in Design Analysis, ORNL Technology Transfer Meeting, April 7, 1982, Oak Ridge National Laboratory, Oak Ridge, TN, 1982, pp. 11 - 17.

2 Sikka, V., "National Program Plan for Commercialization of Modified 9Cr-1Mo Alloy," Oak Ridge National Laboratory, Oak Ridge, TN, 1980.

3 Swindeman, R., Thomas, R., Nanstad, R. and Long, C., "Assessment of the Need for an Advanced Chromium-Molybdenum Steel for Construction of Third Generation Gasifier Pressure Vessels," Oak Ridge National Laboratory, Oak Ridge, TN, 1980.

4 Ishiguro, T., Ohnishi, K., Murakami, Y., Mima, S. and Watanabe, J., "Development of a 3Cr-1Mo-1/4V-Ti-B Pressure Vessel Steel for the Enhanced Design Stress," R.A. Swift (ed.), Research on Cr-Mo Steels, American Society of Mechanical Engineers, New York, 1984, pp. 43 - 53.

5 Tagawa, H. and Tsuyama, S., "Modified 3Cr-1Mo Steel with Improved Toughness and Elevated Temperature Strength," Compilation of Recent Technical Information for the Program - Materials for Service with Hydrogen at High Temperatures and Pressures, Metals Property Council, New York, 1983, pp. 15 - 26.

6 Klueh, R.L. and Nasreldin, A.M., "Microstructure and Mechanical Properties of a 3Cr-1.5Mo Steel," Oak Ridge National Laboratory, Oak Ridge, TN, 1985.

7 Swindeman, R.W., Nasreldin, A.M., Klueh, R.L. and King, J.F., "Metallographic Examination of Response of 3Cr-1.5Mo Steel to Heat Treatment," ORNL/TM-9691, Oak Ridge National Laboratory, Oak Ridge, TN, 1985.

8 Wada, T. and Cox, T.B., "3Cr-1.5Mo Steel for Pressure Vessels in Hydrogen Service," Climax Molybodenum Co., Ann Arbor, MI, 1982.

9 Wada, T. and Cox, T.B., "A New 3Cr-1.5Mo Steel For Pressure Vessel Applications," R.A. Swift (ed.), Research on Cr-Mo Steels, American Society of Mechanical Engineers, New York, 1984, pp. 77 - 94.

10 Ritchie, R.O., Parker, E.R., Spencer, P.N. and Todd, J.A., "Topical Report: A New Series of Advanced 3Cr-Mo-Ni Steels For Thick Section Pressure Vessels In High Temperature and Pressure Hydrogen Service," UCB/RP/84/D1020, Oak Ridge National Laboratory, Oak Ridge, TN., 1984.

11 Mima, S., "Technical Data Sheet of 3Cr-1Mo-1/4V-Ti-B Steel for Elevated Temperature Applications," The Japan Steel Works, Muroran, Japan, 1983.

12 "Modified 2 1/4Cr-1Mo and 3Cr-1Mo Steels - Mechanical Properties, Hydrogen Resistance and Weldability," Nippon Kolan K.K., Kawasaki, Japan, 1985.

13 "Development of Advanced 2 1/4Cr-1Mo and 3Cr-1Mo Steels," Kawasaki Steel Corporation, Kawasaki, Japan, 1985.

14 Yukitoshi, T., Nishida, K., Oda, T. and Daikoku, T., "Low-Alloy High-Strength Steel for Boiler Tubes (Low C-9Cr-2Mo)," Transactions of the American Society of Mechanical Engineers, 98(1), 1976, pp. 173 - 178.

15 Yukitoshi, T., Yoshikawa, K., Tokimasa, K., Shida, Y. and Imaba, Y., "Application of 9Cr-2Mo Steel (HCM9M) for Fast Breeder Reactor Steam Generators," The Sumitomo Search, 23, 1980, pp. 45 - 58.

16 Devletian, J.H. and Wood, W.E., "Principles of Joining Metallurgy," E.F. Nippes (ed.), Welding, Brazing, and Soldering - Metals Handbook Ninth Edition, American Society for Metals, Metals Park, OH, 1984, pp. 21 - 49.

17 Linnert, G.E., Welding Metallurgy, American Welding Society, Miami, FL, 1983.

18 Ito, Y. and Nakanishi, M., "Study of Stress Relief Cracking in Welded Low Alloy Steels," The Sumitomo Search, 7, 1972, pp. 27 - 36.

19 Eyre, B.L., Edwards, B.C. and Titchmarsh, J.M., "Physical Metallurgy of Reversible Temper Embrittlement," Proc. of Conf. Advances in the Physical Metallurgy and Applications of Steels, University of Liverpool, 21-24 September, 1981, Metals Society, London, 1981, pp. 246 - 258.

20 Viswanathan, R. and Joshi, A., "Effect of Microstructure on the Temper Embrittlement of Cr-Mo-V Steels," Metallurgical Transactions A, 6A, 1975, pp. 2289 - 2295.

21 Easterling, K., Introduction to the Physical Metallurgy of Welding, Butterworths, Boston, 1983.

22 Udin, H., Funk, E.R. and Wulf, J., Welding for Engineers, John Wiley and Sons, New York, 1954.

23 Torok, T.E. and Stout, R.D., "Relation of dilatometric Characteristics of Steels to Delayed Cracking in Welds," Welding Journal, 44(12), 1965, pp. 592s - 544s.

24 Nippes, E.F., "The Weld Heat Affected Zone," Welding Journal, 38(1), 1955, pp. 1s - 18s.

25 Richey, M.W., The Weldability of Cr-Mo Steels for Fossil Energy Applications, M.S. Thesis University of Tennessee, Knoxville, TN, 1984.

26 Habraken, C.J. and Economopoulos, M., "Bainitic Microstructures in Low-Carbon Alloy Steels and Their Mechanical Properties," Transformation and Hardenability in Steels, Climax Molybdenum Company, Ann Arbor, 1967, pp. 69 - 108.

27 Biss, V. and Cryderman, R.L., "Martensite and Retained Austenite in Hot Rolled Low Carbon Bainitic Steels," Metallurgical Transactions, 2(8), 1971, pp. 2267 - 2276.

28 Thomas, G., Sarikaga, M., Smith, G.D.W. and Barnard, S.J., "Microstructure, Retained Austenite, and Mechanical Properties of Experimental 0.3%C Steels," Proc. of Conf. Advances in the Physical Metallurgy and Applications of Steel, University of Liverpool, 21-24 September, 1981, Metals Society, London, 1981, pp. 259 - 265.

29 Baker, R.G. and Nutting, J., "The Tempering of 2 1/4%Cr-1%Mo Steel After Quenching and Tempering," Journal of the Iron and Steel Institute, 192, 1959, pp. 257 - 267.

30 Stone, P.G. and Murray, J.D., "Creep Ductility of Cr-Mo-V Steels," Journal of the Iron and Steel Institute, 203, 1965, pp. 1094 - 1107.

31 Woodhead, J.H. and Quarrell, A.G., "The Role of Carbides in Low-Alloy Creep-Resisting Steels," Climax Molybdenum Co. Ltd., London, 1965.

32 Vitek, J.M. and Klueh, R.H., "Precipitation Reactions During the Heat Treatment of Ferritic Steels," Metallurgical Transactions A, 14A(6), 1983, pp. 1047 - 1055.

33 Sikka, V., Personal Communication, 2/14/1985.

34 Seal, A.K. and Honeycombe, R.W.K., "Carbide Precipitation in Several Steels Containing Chromium and Vanadium," Journal of The Iron and Steel Institute, January, 1958, pp. 9 - 15.

35 Murray, J.D., "Stress-Relief Cracking in Carbon and Low Alloy Steels," British Welding Journal, 14(8), 1967, pp. 447 - 456.

36 Tamaki, K. and Suzuki, J., "Effect of Chromium and Molybdenum on Reheat Cracking Sensitivity of Steels (Study of Reheat Cracking of Cr-Mo Steels, Report 2)," Transactions of the Japan Welding Society, 14(2), 1983, pp. 39 - 43.

37 Erwin, W.E. and Kerr, J.G., "WRC Bulletin 275 - The Use of Quenched and Tempered 2 1/4Cr-1Mo Steel for Thick Wall Reactor Vessels in Petroleum Refining Processes: An Interpretive Review of 25 Years of Research and Application," Welding Research Council, 1982.

38 McPherson, R., "Compositional Effects on Reheat Cracking of Low Alloy Ferritic Steels," Metals Forum, 2(3), 1980, pp. 175 - 186.

39 Vinckier, A., "Use of Weld Simulation Tests to Study Susceptibility to Reheat Cracking," Proc. of Conf. Welding Research Related to Power Plant, University of Southampton, 17 - 21 September, 1972, Central Electric Generating Boar, London, 1972, pp. 336 - 355.

40 Meitzner, C.F., "WRC Bulletin 211 - Stress Relief Cracking in Steel Weldments," Welding Research Council, 1975.

41 Vinckier, A.G. and Pense, A.W., "WRC Bulletin 197 - Review of Underclad Cracking in Pressure-Vessel Components," Welding Research Council, 1974, pp. 1 - 35.

42 Swift, R.A. and Rogers, H.C., "A Critical Review of Weld Metal Embrittlement," Welding Journal, 60(7), 1971, pp. 357s - 363s.

43 Nichols, R.W., "Reheat Cracking in Welded Structures," Welding in the World, 7(4), 1969, pp. 36 - 44.

44 Swift, R.A., "The Mechanism of Stress Relief Cracking in 2 1/4Cr-1Mo Steel," Welding Journal, 50(5), 1971, pp. 195s - 200s.

45 Swift, R.A. and Rogers, H.C., "Embrittlement of 2 1/4Cr-1Mo Steel Weld Metal by Postweld Heat Treatment," Welding Journal, 52(4), 1973, pp. 145s - 153s.

46 Swift, R.A., "Creep-Rupture Tests on 2 1/4Cr-1Mo Simulated Heat Affected Zone," Lukens Steel Company Research Report RDR 69-11 Lukens Steel Company, Coatesville, Pa, 1969.

47 Orr, J., Beckitt, F.R. and Fawkes, G.D., "Paper 16: The Physical Metallurgy of Chromium-Molybdenum Steels for Fast Reactor Boilers," Proceedings of the International Conference on Ferritic Steels for Fast Reactor Steam Generators, British Nuclear Energy Society, London, 1978, pp. 91 - 109.

48 Bentley, K.P., "Precipitation During Stress Relief of Welds in Cr-Mo-V Steels," British Welding Journal, 11(10), 1964, pp. 507 - 515.

49 Mullery, F. and Cadman, R., "Cracking of Welded Joints in Ferritic Heat Resisting Steels," British Welding Journal, 9(4), 1962, pp. 212 - 220.

50 Vinckier, A. and Dhooge, A., "Reheat Cracking in Welded Structures During Stress Relief Heat Treatments," Journal of Heat Treating, 1(1), 1979, pp. 72 - 80.

51 Meitzner, C.F. and Pense, A.W., "Stress Relief Cracking in Low-Alloy Steel Weldments," Welding Journal, 48(10), 1969, pp. 431s - 440s.

52 Edwards, R.H., Barbaro, F.J. and Gunn, K.W., "Stress Relief Cracking in Cr-Mo-V Steels," Metals Forum, 5(2), 1982, pp. 119 - 129.

53 Dhooge, A., Dolby, R.E., Sebile, J., Steinmetz, R. and Vinckier, A.G., "A Review of Work Related to Reheat Cracking in Nuclear Reactor Pressure Vessel Steels," International Journal of Pressure Vessels and Piping, 6, 1978.

54 Presser, R.I. and McPherson, R., "The Role of Trace Elements in Reheat Cracking," Proc. of Conf. Residual Stresses in Welded Construction and Their Effects, London, 15-17 November, 1977, Welding Institute, Cambridge, 1978, pp. 387 - 398.

55 Vinckier, A. and Dhooge, A., "Paper 36: Reheat Cracking in Welded Structures During Stress Relief Heat Treatments," Proc. of Conf. Residual Stresses in Welded Construction and Their Effects, London, 15-17 November, 1977, The Welding Institute, Cambridge, 1978, pp. 375 - 385.

56 Hippsley, C.A., King, J.E. and Knott, J.F., "Toughness Variations and Intergranular Fracture During the Tempering of Simulated HAZ Structures in a Mn-Mo-Ni Stel," Proc. of Conf. Advances in the Physical Metallurgy and Applications of Steel, University of Liverpool, 21-24 September 1981, Metals Society, London, 1981, pp. 147 - 155.

57 Hippsley, C.A., Knott, J.F. and Edwards, B.C., "A Study of Stress-Relief Cracking in 2 1/4Cr-1Mo Steel - II. The Effects of Multicomponent Segregation," Acta Metallurgica, 30, 1982, pp. 641 - 652.

58 Troiano, A.R., "The Role of Hydrogen and Other Interstitials in the Mechanical Behavior of Metals," Transactions of the American Society for Metals, 52, 1960, pp. 54 - 80.

59 Debiez, S. and Granjon, H., "Work Carried Out by the Institut de Soudure on Reheat Cracking," Proc. of Conf. Resiudual Stresses in Welded Construction and Their Effects, London, 15-17 November, 1977, Welding Institute, Cambridge, 1978, pp. 231 - 239.

60 Nakamura, H., Naiki, T. and Okabayashi, H., "Fracture in the Process of Stress-Relaxation Under Constant Strain," Proceedings of the First International Conference on Fracture, Sendai, Japan, September, 1965, Japan Welding Society, 1965, pp. 863 - 878.

61 Pense, A.W., Galda, E.J. and Powell, G.T., "Stress Relief Cracking in Pressure Vessel Steels," Welding Journal, 50(8), 1971, pp. 374s - 378s.

62 McMahon, C.J., Jr., Dobbs, R.J. and Gentner, D.H., "Stress-Relief Cracking in MnMoNi and MnMoNiCr Pressure Vessel Steels," Materials Science and Engineering, 37, 1979, pp. 179 - 186.

63 Wada, T., Grobner, P.J. and Vineberg, E.J., "Duplex Structure 12Cr-2Mo Steels With Improved Weldability," Proc. of Conf. Production, Fabrication, Properties, and Applications of Ferritic Steels for High Temperature Applications, American Society for Metals, Warren, Pa, 1981.

64 Hippsley, C.A., Knott, J.F. and Edwards, B.C., "A Study of Stress-Relief Cracking in 2 1/4Cr-1Mo Steel - The Effects of P Segregation," Acta Metallurgica, 28, 1980, pp. 869 - 885.

65 Miller, R.C. and Batte, R.D., "Reheat Cracking in 1/2CrMoV/2 1/4CrMo Welded Joints," Metal Construction, 7(11), 1975, pp. 550 - 558.

66 Muraki, T., Jahaco, J. and Watanabe, J., "Reheat Cracking of 2 1/4Cr-Mo Pressure Vessel Steel," Research Report, Japan Steel Works, Muroran Plant Research Laboratory, PV76-78, 1975, pp. 1 - 17.

67 Imanaka, T., Sato, S., Shimomura, J. and Aso, K., "Improvements in the Susceptibility to Hydrogen Attack and Stress-Relief Cracking of 2 1/4Cr-1Mo Steels," Kawasaki Steel Corporation, Mizushima, Japan, 1985.

68 Boniszewski, T., "Reheat Cracking in 2 1/4Cr-1Mo Submerged Arc Weld Metal," Metal Construction, 14(9), 1982, pp. 495 - 496.

69 Tamaki, K. and Suzuki, J., "Reheat Cracking Test on High Strength Steels by a Modified Implant Test," Transactions of The Japan Welding Society, 14(2), 1983, pp. 33 - 38.

70 Tamaki, K., Suzuki, J., Nakaseko, Y. and Tajiri, M., "Effect of Carbides on Reheat Cracking Sensitivity (Study of Reheat Cracking of Cr-Mo Steels, Report 3)," Transactions of The Japan Welding Society, 15(1), 1984, pp. 8 - 16.

71 Tamaki, K. and Suzuki, T., "Assessment of Reheat Cracking Sensitivity of Steels from their Chemical Compositions," Proc. of Conf. 1985 American Ssociety for Metals' International Welding Congress/JDC University Research, Toronto, Canada, 14-17 October 1985.

72 "Discussion Session 4, Part 1 - Heat Treatment Cracking Paper 11 (Reheat Cracking in Cr-Mo-V steel Weldments)," Metal Construction and British Welding Journal, 1(2), 1969, pp. 125 - 128.

73 Chu, C., Yue-Chang, Z., Shou-Shan, Y., Lu-Hai, W., Miao-Tao, L. and Xi-Zhen, L., "Study of Reheat Cracking Mechanism in 15CrMoV Steel," The Fourth International Symposium of the Japan Welding Society, November, 1982, Japan Welding Society, Osaka, Japan, pp. 461 - 466.

74 "Improvement in High Temperature Properties of Heavy Section 2 1/4Cr -1Mo Steel," Kawasaki Steel Corporation, 1982.

75 Meyers, J., "Influence of Alloy and Impurity Content on Stress-Relief Cracking in Cr-Mo-V Steels," Metals Technology, 5(pt.2), 1978, pp. 391 - 396.

76 Jones, K.E., "Paper 5: Stress-Relief Cracking of Welded Pipe/Casting Joints in Cr-Mo-V Steel," Proc. of Conf. Welding of Creep Resisting Steels, The Welding Institute, Cambridge, England, 1970, pp. 66 - 78.

77 Stone, P.G. and Murray, J.D., "Creep Ductility of Cr-Mo-V Steels," Journal of the Iron and Steel Institute, 203, 1965, pp. 1094 - 1107.

78 Vinckier, A., (chrmn.), "Testing Techniques to Study the Susceptibility to Reheat Cracking of Carbon-Manbganese and Low Alloy Steels," Welding in the World, 12, 1974, pp. 1 - 22.

79 Yu, J. and McMahon, C.J., Jr., "The Effects of Composition and Carbide Precipitation on Temper Embrittlement of 2.25Cr-1Mo Steel: Part II - Effects of Mn & Si," Metallurgical Transactions A, 11A(2), 1980, pp. 291 - 300.

80 Ratliff, J.L. and Brown, R.M., "The Deleterious Effect of Small Quantities of Aluminium on the Stress Rupture Propperties of a Cr-Mo-V Steel," Transactions of the American Society for Metals, 60, 1967, pp. 176 - 186.

81 Meyers, J., "Effects of Deoxidants and Impurities on Simulated Stress Relief Cracking of 1/2Cr 1/2Mo 1/4V Steel," Proc. of Conf. Welding Research Related to Power Plant, University of Southampton, 17-21 September, 1972., Central Electric Generating Board, London, 1972, pp. 356 - 368.

82 Harris, P. and Jones, K.E., "The Effect of Composition and Deoxidation Practice on the Reheat Cracking Tendencies of 1/2Cr 1/2Mo 1/4V Steel," Proc. of Conf. Welding Research Related to Power Plant, University of Southampton, 17-21 Sept. 1972, Central Electric Generating Board, London, 1972, pp. 369 - 380.

83 Spaeder, G.J. and Ploder, G., "Technical Report: Stress Rupture Properties of the Simulated Heat-Affected Zone of USS "T-1" Steel," Applied Research Laboratory, US Steel, Monroeville, Pa., 1963.

84 Wyatt, L.M., (chrmn.) and Edmondson, B., (rapporteur), "Rapporteur's Remarks and Discussion (Discussion of Papers 24-31)," Proc. of Conf. Welding Research Related to Power Plant, University of Southampton, 17-21 Sept. 1972, Central Electric Generating Board, London, 1972, pp. 435 - 448.

85 Presser, R.I. and McPherson, R., "Boron Segregation and Elevated Temperature Embittlement of Ferritic Steel," Scripta Mtallurgica, 11(9), 1977, pp. 745 - 749.

86 Hunter, A.N.R., "Reheat Cracking in 2 1/4Cr-1Mo Submerged Arc Weld Metal - Part 1 Materials, Welding and Testing," Metal Construction, 14(4), 1982, pp. 198 - 201.

87 Hunter, A.N.R., "Reheat cracking in 2 1/4Cr-1Mo Submerged Arc Weld Metal - Part 2 Results and Discussion," Metal Construction, 14(5), 1982, pp. 266 - 270.

88 Wittig, J.E., Sinclair, R. and Viswanathan, R., "Precipitation of Phosphorous and Tin in Temper Embrittled Low Alloy Steel," Scripta Metallurgica, 19(1), 1985, pp. 111 - 117.

89 Kikuchi, T. and Nakao, Y., "Effects of Impurity Elements on the Reheat Cracking in Weld Zones of Steels," The Fourth International Symposium of The Japan Welding Society, November, 1982, Japan Welding Society, Osaka, Japan, pp. 455 - 460.

90 Horn, H. and Kunze, H.D., "Reheat Cracking Studies by Weld Simulation and Scanning Auger Investigation," The Fourth International Symposium of the Japan Welding Society, November 1982, Japan Welding Society, Osaka, Japan, pp. 449 - 454.

91 Yu, J. and McMahon, C.J., Jr, "The Effects of Composition and Carbide Precipitation on Temper Embrittlement of 2.25Cr-1Mo Steel: Part 1. Effects of P and Sn," Metallurgical Transactions A, 11A, 1980, pp. 277 - 289.

92 Hippsley, C.A., "Precipitation Sequences in Heat Affected Zone of 2.25Cr-1Mo Steel During Stress-Relief Heat Treatment," Metal Science, 15(4), 1981, pp. 137 - 147.

93 Muhammad, A.B., Szkopiak, Z.C. and Waldron, M.B., "Effect of Types of Carbides on Temper Embrittlement in Commercial 2.25Cr-1Mo Steel," Proc. of Conf. Advances in the Physical Metallurgy and Applications of Steel, University of Liverpool, 21-24 September, 1981, Metals Society, London, 1981, pp. 340 - 348.

94 You, C.P., Hippsley, C.A. and Knott, J.F., "Stress Relief Cracking Phenomena in High Strength Structural Steel," Metal Science, 18(8), 1984, pp. 387 - 394.

95 Dolby, R.E., "Advances in the Welding Metallurgy of Steel," Proc. of Conf. Advances in the Physical Metallurgy and Applications of Steels, University of Liverpool, 21-24 September, 1981, Metals Society, London, 1981, pp. 111 - 125.

96 Colombe, G., Debiez, S., Donati, J.R., Petrequin, P. and Zacharie, G., "Paper 75: Metallurgical Aspects of the Weldability of Cr-Mo Ferritic Steels," Proceedings of the International Conference on Ferritic Steels for Fast Reactor Steam Generators, British Nuclear Energy Society, London, England, 1978, pp. 447 - 458.

97 Meyers, J. and Price, A.T., "Stress-Relief Cracking Studies of 0.5Cr-Mo-V and 2Cr-Mo Steels Using HAZ Simulation," Metals Technology, 4(8), 1977, pp. 406 - 410.

98 Stout, R.D., "WRC Bulletin 302 - Post Weld Heat Treatment of Pressure Vessel Steels," Welding Research Council, 1985, pp. 1 - 14.

99 Price, A.T. and Siverns, M.J., "Stress Relief Cracking In Low Alloy Ferritic Steels," Metal Construction and British Welding Journal, 2(6), 1970, pp. 239 - 245.

100 Glossop, B.A., Eaton, N.F. and Boniszewski, T., "Reheat Cracking in Cr-Mo-V Steel Weldments," Metal Construction and British Welding Journal, 16(2), 1969, pp. 68 - 73.

101 Hippsley, C.A., "The Influence of Heating Rate on Reheat-Cracking in a Commercial 2 1/4Cr-1Mo Steel," Report #AERE-R-10840 (DE 83911013), UKAEA Atomic Energy Research Establishment, Metallurgy Division, United Kingdom, Harwell, Oxfordshire, 1983.

102 Ishiguro, T., Murakami, Y., Ohnishi, K. and Watanabe, J., "Interim Reports of the R&D Program for Coal Liquefaction Reactor Materials," Compilation of Recent Tech. Information for the Program Materials for Service with Hydrogen at High Temperatures and Pressures, Metals Property Council, New York, 1983, pp. 1 - 29.

103 George, T., Parker, E.R. and Ritichie, R.O., "Susceptibility to Hydrogen Attack of a Thick Section 3Cr-1Mo-1Ni Pressure Vessel Steel - Role of Cooling Rate," Materials Science and Technology, 1, 1985, pp. 198 - 208.

104 Kar, R.J. and Todd, J.A., "Alloy Modification of Thick-Section 2 1/4Cr-1Mo Steel," G.S. Sangdahl and M. Semchyshen (eds.), ASTM STP 755 The Symposium on Applications of 2 1/4Cr-1Mo Steel for Thick-Wall Pressure Vessels, Metals Property Council - American Society for Testing and Materials, Denver, 1980, pp. 228 - 252.

105 Ishiguro, T., Murakami, Y., Ohnishi, K. and Watatnabe, J., "A 2 1/4Cr-1Mo Pressure Vessel Steel with Improved Creep Rupture Strength," G.S. Sangdahl and M. Semchyshen (eds.), ASTM STP 755 The Symposium on Applications of 2 1/4Cr-1Mo Steel for Thick-Wall Pressure Vessels, Metals Property Council - American Society for Testing and Materials, Denver, 1980, pp. 129 - 147.

106 Bodine, G.C., Jr., Chakravarti, B., Owens, C.M., Roberts, B.W., Vandergriff, D.M. and Ward, C.T., "A Program for the Development of Advanced Ferritic Alloys for LMFBR Structural Applications," Topical Report. ORNL/SUB-4291/1, 1977.

107 Savage, W.F., "Apparatus for Studying the Effects of Rapid Thermal Cycles and High Strain Rates on the Elevated Temperature Behavior of Materials," Journal of Applied Polymer Science, 6(21), 1962, pp. 303 - 315.

108 "Standard Recommended Practice for Making and Using C-Ring Stress-Corrosion Test Specimens - Designation G38-73 (Reapproved 1979)," R.P. Lukens, J.L. Cornillot, R.A. Priemon, and D.F. Savini (eds.), 1982 Annual Book of ASTM Standards, Metals - Physical, Mechanical, Corrosion Testing, American Society for Testing and Materials, Philadelphia, PA, 1982, pp. 1003 - 1011.

109 Peterson, R.E., Stress Concentation Factors, John Wiley & Sons, New York, 1974.

110 Schrader, A. and Rose, A., De Ferri Metallographia (Metallograpic Atlas of Iron, Steels, and Cast Irons) - Structure of Steels, W. B. Saunders Company, Philadelphia, PA, 1966.

111 Brown, R.M., Rege, R.A. and Spaeder, C.E., "The Properties of Normalized and Tempered and Quenched and Tempered 6 1/4 inch Thick Plates of 2 1/4Cr-1Mo Steel," Symposium of Heat Treated Steels for Elevated Temperature Service, American Society of Mechanical Engineers, New York, 1966, pp. 27 - 44.

112 Smith, E., Blanchard, B.E. and Apps, R.L., "The Weld HAZ in 2 1/4%Cr-1%Mo Steels," Proc. of Conf. Welding Creep-Resistant Steels, The Welding Institute, Cambridge, 1970, pp. 79 - 89.

113 Boniszewski, T., Watkinson, F., Baker, R.G. and Tremlett, H.F., "Hydrogen Embrittlement and Heat-Affected Zone Cracking in Low-Carbon Alloy Syeels with Acicular Microstructures," British Welding Journal, 34, 1965, pp. 14 - 36.

114 Todd, J.A., Lundin, C.D. and Henning, J.A., "Microstructural Characterization of Weld Heat Affected Zones in Modified Cr-Mo Steels," (unpublished paper), (1986).

115 Tamaki, K. and Suzuki, J., "Effect of Phosphorous on Reheat Cracking of Cr-Mo Steels," Research Reports of the Faculty of Engineering, Mie University, 9, 1984.

116 Dickinson, D.W. and Liu, J.H., "A New Test Method to Study Reheat Cracking in Low Alloy Steel," unpublished paper presented at the 67th Annual American Welding Society Convention, April 13-18,1986.

VITA

John A. Henning was born in Milwaukee, Wisconsin, on February 19, 1950. He attended high school in Milwaukee, Wisconsin and graduated from Concordia High School in June, 1968. After entering the Milwaukee School of Engineering in September of 1979, he received a B.S. degree in Mechanial Engineering in June of 1983. In the Summer of 1983 he accepted a teaching assistantship at the University of Tennessee, Knoxville, and began his study towards a Master's degree in Metallurgical Engineering. This degree was awarded in June, 1986.

The author is a member of the American Welding Society, the American Society for Metals, the American Society of Mechanical Engineers and Tau Omega Mu.